PERFORMANCE-BASED PLASTIC DESIGN OF SEISMIC RESISTANT SPECIAL TRUSS MOMENT FRAMES

by

Shih-Ho Chao
Subhash C. Goel

Department of Civil and Environmental Engineering
The University of Michigan
College of Engineering

Ann Arbor, MI 48109-2125

May 2006 **Research Report UMCEE 06-03**

PERFORMANCE-BASED PLASTIC DESIGN OF SEISMIC RESISTANT SPECIAL TRUSS MOMENT FRAMES

by

Shih-Ho Chao
Subhash C. Goel

A report on research sponsored by
Nabih Youssef & Associates Structural Engineers,
and NUCOR Research and Development

Department of Civil and Environmental Engineering
The University of Michigan
College of Engineering

Ann Arbor, MI 48109-2125

ACKNOWLEDGEMENT

This study was made possible by a generous financial support provided by Nabih Youssef & Associates Structural Engineers, and NUCOR Research and Development. The senior author also received a stipend from the G. S. Agarwal Fellowship Fund at the Department of Civil & Environmental Engineering while working on this project. The authors acknowledge the contribution of Dr. Gustavo Parra-Montesinos and Dr. K.Y. Kim to the experimental phase of this study (Chapter 3). The opinions and views expressed in the report are solely those of the authors and do not necessarily reflect those of the sponsors.

PERFORMANCE-BASED PLASTIC DESIGN OF SEISMIC RESISTANT SPECIAL TRUSS MOMENT FRAMES

EXECUTIVE SUMMARY

Special Truss Moment Frame (STMF) is a relatively new type of steel structural system that was developed for resisting forces and deformations induced by severe earthquake ground motions. The system dissipates earthquake energy through ductile special segments located near the mid-span of truss girders. STMFs generally have higher structural redundancy compared to other systems because four plastic hinges can form in the chords of one truss girder. The redundancy can be further enhanced if web members are used in the special segments. Simple connection details are adequate for girder-to-column moment connections. Another advantage of using STMF system is that the truss girders can be efficiently used over longer spans and higher overall structural stiffness can be achieved by using deeper girders. In addition, the open-webs can easily accommodate mechanical and electrical ductwork. As a consequence, this system is gaining popularity in the U.S., especially for hospital and commercial buildings. Research work carried out during the Nineties led to the formulation of design code provisions. However, current design practice generally follows elastic analysis procedures to proportion the frame members. Therefore, it is possible that story drifts and yielding in the special segments may not be uniformly distributed along the height of the structure and may be concentrated in a few floors causing excessive inelastic deformations at those levels. Thus, the intended deformation limits and yield mechanism may not be achieved when an STMF is subjected to strong earthquakes.

In the first phase of the study an experimental program was conducted to investigate the ductility and plastic rotation capacity of chord members consisting of double channel sections for the special segments. A total of seven specimens were tested under reversed

cyclic bending. These specimens represent half length of a chord member of open Vierendeel segment of an STMF. The testing was undertaken to determine the influence of some detailing parameters, such as compactness, stitch spacing, lateral supports and end connections, on the ductility and hysteretic behavior.

In the second phase of the study a Performance-Based Plastic Design (PBPD) procedure based on energy and plastic design concepts was applied to STMFs. The design approach was originally developed and successfully applied to steel moment frames. The procedure begins by selecting a desired yield mechanism for the structure. The design base shear and lateral forces are determined from spectral energy for a given hazard level needed to push the structure in the yielded state up to a selected target drift. The frame members are then designed by following the plastic design method in order to develop the needed strength and the intended yield mechanism.

Two 9-story STMFs, representing the class of essential facilities (i.e., hospital buildings) as well as ordinary office/residential occupancy type, were designed by using the proposed procedure. For ordinary building type the target drifts of 2% and 3% for 10% in 50 years and 2% in 50 years design hazard levels, respectively, were chosen. The corresponding numbers for essential building were 1.5% and 2.25%. Design spectral values were based on NEHRP Provisions for the San Francisco site. After the final design work was completed, inelastic pushover and dynamic analyses were conducted to study the response and ductility demands of the frames. Nine 10% in 50 years and five 2% in 50 years SAC Los Angeles region ground motions representing the two design hazard levels were used for the nonlinear dynamic analyses. The results of the analyses were studied to validate the design procedure, and to compare the chord member ductility demands with the capacities as determined from the testing work on built-up double channel specimens. The study parameters included: location of yielding, maximum plastic rotation in chord members, maximum relative story shear distribution, maximum interstory drift, and peak floor accelerations.

TABLE OF CONTENTS

LIST OF TABLES

Table

LIST OF FIGURES

<u>Figure</u>

CHAPTER 1

Introduction

1.1 Background

Seismic behavior of STMF system has been studied both analytically and experimentally by Goel et al. (Itani and Goel, 1991; Basha and Goel, 1994) at the University of Michigan during the past fifteen years and has been incorporated into the AISC Seismic Provisions for Structural Steel Buildings (AISC, 2005). This frame consists of truss frames with special segment designed to behave inelastically under severe earthquakes while the other members, including girder-to-column connections, outside the special segment remain essentially elastic. The special segment can be made with or without (Vierendeel) X-diagonal web members, as shown in Figure 1.1. When a STMF is subjected to seismic motions, the induced shear force in the middle of the joist girder is resisted primarily by the chord members and the web diagonals in the special segment. After yielding and buckling of the diagonal members, plastic hinges will form at the ends of the chord members. The yield mechanism of this structural system is the combination of yielding of all special segments in the frame plus the plastic hinges at the column bases, as shown in Figure 1.2. Comparison between STMF and frames with conventional truss girders as well as solid web beams has shown that STMF outperforms the others in terms of the energy-dissipation capacity, story drifts, and hysteretic behavior. The lateral design forces may also be smaller for STMF system (Itani and Goel, 1991).

The first STMF system with X-diagonal special segment was first developed by Itani and Goel (Itani and Goel, 1991). Design of STMFs starts with designing the special segment. Based on capacity design approach, other elements are then designed to remain elastic under the shear forces in the middle of the joist girder generated by fully yielded and strain hardened special segments, along with other external forces.

A similar concept was employed in reinforced concrete frames by Paulay and Priestley (1992), where they used a weak segment near the mid-span of beams, as shown in Figure 1.3. When the frame is subjected to reversed cyclic inelastic displacement, the central diagonally reinforced portion will behave like a coupling beam which is used to transfer shear between to walls. Because the shear in a coupling beam is transferred primarily by the diagonal concrete strut across the beam, the added diagonal reinforcement will be subjected to large inelastic tensile or compressive strains during a major earthquake. As a result, a very ductile behavior with excellent energy-dissipation capacity could be expected.

Due to excellent behavior of STMFs observed from both experimental and analytic results, Basha and Goel (1994) developed another type of special segment by using a ductile Vierendeel segment without the diagonal members. A mathematical expression for the ultimate expected shear capacity of the special segment was derived by Basha (1994). Tests on subassemblages showed no pinching in the hysteretic loops with very stable and ductile behavior. All the inelastic deformations were confined to the special segments only, thus eliminating the possibility of damage in the other elements, such as girder-to-column connections. As a consequence, simple detailing without the need for ductility is used for the connections.

Ireland (1997) studied the STMF system for low to moderate seismic regions where wind can be a significant design factor. STMFs were compared with conventional systems in those areas. The results of that study also showed superior performance of STMFs compared to the conventional truss system.

Aslani (1998) studied the seismic behavior of STMFs under combined gravity and lateral loads. The results showed that STMF system designed for combined loads was able to perform satisfactorily in the event of a severe ground motion. Moreover, the overall seismic behavior with floor deck (not designed for composite action) was also investigated. Based on experimental and nonlinear dynamic analytical results, he suggested that the effect of composite action could be neglected in the dynamic analysis. That is because the composite action deteriorates rapidly under cyclic loading and after a few cycles the effect of composite action almost vanishes. If proper amount of shear connectors were used in the region of special segment, the composite action would lead to increased flexural capacity of the chord members. In that situation, Aslani suggested that, the effect of composite action between the chord member and floor deck should be accounted for the design of the members outside the special segments in order to ensure elastic behavior. Since the design of members outside the special segment is governed by the expected shear strength of the special segment, any increase in strength of the special segment also affects the design strength of members outside the special segments. Aslani suggested an increased chord strength equal to $0.65M_p^*$, where M_p^* is the ultimate flexural strength of the composite section.

Aslani also examined the reparability of STMF system by testing a repaired specimen. The results confirmed that, under the same loading history, the STMF can be retrofitted to the original strength and hysteretic response with minimum cost.

Other advantages of using STMF system include: (1) The open-web floor framing can have longer span length and overall structural stiffness due to greater girder depth; (2) The open-webs can accommodate electrical conduits, plumbing and heating, and air-conditioning ductwork through the openings, which in turn results in greater ceiling height (Viest et al., 1997). Figure 1.4 shows the ductwork through openings in an STMF building and a typical STMF building structure is shown in Figure 1.5.

1.2 Design Criteria for STMFs

The key points for designing an STMF as summarized in this section are based on the past research (Itani and Goel, 1991; Basha anf Goel, 1994; Leelataviwat and Goel, 1998a; Rai, Basha and Goel, 1998) and the AISC Seismic Provisions (AISC, 2005).

1) Special segment design criteria:

- The size of X-diagonal members and chord members in the special segment are selected based on the maximum vertical force resulting from the appropriate design earthquake load combination.

- The shear contribution from the X-diagonals is limited to 75% of the required shear V_{req}.
- Chord members of the special segment are designed for the remaining 25% of the required shear which is resisted through the end plastic hinges.
- X-diagonal members are interconnected at point of crossing.
- X-diagonal members are flat bars with $\frac{b}{t} \leq 2.5$
- Chord angle sections must have $\frac{b}{t} \leq \frac{52}{\sqrt{F_y}}$
- The length of the special segment is limited within 0.1 and 0.5 times the span length (AISC 12.2).
- The length-to-depth ratio of any panel in the special segment is to neither exceed 1.5 nor be less than 0.67 (AISC 12.2)
- The axial force in the chord members is not to exceed 0.45 times $\phi F_y A_g$ ($\phi = 0.9$).
- Design of an STMF can be quite sensitive to the strength of elements in the special segments resulting in oversizing of the elements outside the special segment. For optimizing the chord members, built-up sections composed of double angles and plate should be used.

2) Design of members outside the special segment:

- Determine the expected vertical nominal shear strength, V_{ne}, in the special segment according to AISC Seismic Provisions Eq. (12-1) for design of members outside the special segment:

$$V_{ne} = \frac{3.75 R_y M_{nc}}{L_s} + 0.075 E_s I \frac{\left(L - L_s\right)}{L_s^3} + R_y \left(P_{nt} + 0.3 P_{nc}\right) sin\alpha \tag{1.1}$$

where

R_y = yield stress modification factor

M_{nc} = nominal flexural strength of the chord member of the special segment

$E_s I$ = flexural elastic stiffness of the chord members of the special segment

L = span length of the truss

L_s = length of the special segment

P_{nt} = nominal axial tension strength of diagonal members of the special segment

P_{nc} = nominal axial compression strength of diagonal members of the special segment

α = angle of diagonal members with the horizontal

The first two terms of Eq. (1.1) were derived based on Vierendeel special segment without web diagonals (Basha and Goel, 1994). The third term is needed only when the X-diagonal members are present.

- Design members outside the special segments using the gravity loads, expected vertical nominal shear strength in the special segments, V_{ne}, and lateral forces needed to maintain equilibrium.

1.3 Remarks on STMF Design and Research Scope

As mentioned earlier, the reason for using the maximum expected vertical shear strength, V_{ne}, to design members outside special segment is to prevent other members from yielding. Experimental results have shown that well-detailed special segment members can sustain large inelastic deformation reversals without losing strength and stiffness. Therefore global structural stability and performance will not be compromised if inelastic activity is confined only to special segments. Unintended yielding or buckling of diagonal members or columns can result in undesirable response. As a matter of fact, testing on weak-column strong-beam steel frames has shown that columns exhibit poor hysteretic behavior with rapid strength and stiffness deterioration if the axial load exceeds 25% of the nominal axial yield strength (Schneider and Roeder, 1993). Unfortunately, such unintended poor seismic behavior cannot be effectively predicted and prevented by conventional seismic design methods. In particular, although the column design follows capacity design approach in an indirect way, the calculated design moments may not give actual distribution of moments when the yield mechanism is reached. In this regard, the design lateral forces acting on the frames should be increased appropriately to account for the fully yielded and strain hardened special segments at all floor levels. By using this treatment, the resulting distribution of moments in the columns will be more realistic and, in conjunction with the applicable gravity axial loads, the capacity design can be achieved. This approach was used in the PBPD design procedure for STMFs in this study.

In recent years, seismic design has been gradually moving towards performance-based design approach, which is intended to produce structures with predictable and controlled seismic performance. To achieve this goal, knowledge of the ultimate structural behavior, such as nonlinear relations between forces and deformations, and yield mechanism of structural system are essential. Therefore, the desired global yield mechanism needs to be built into the design process.

Recently, various performance-based design methods have been developed such as capacity spectrum approach for determining the design lateral loads, displacement-based design procedure, and energy-based design procedure (Rai, 2000). The energy-based design procedure uses the balance relation between the required elastic and inelastic work and the energy dissipated by structures to predict the drift level a structure may undergo when subjected to a specified seismic hazard level. If the drift can be accurately determined at the design stage, then damage can be controlled, thus intended performance is achieved. This approach, together with the plastic design procedure, has been successfully developed and validated using steel moment frames (Leelataviwat, Goel, and Stojadinović, 1999, Lee and Goel, 2001). In this report, the same procedure was employed to design STMFs with Vierendeel special segments, one with seven stories, and another with nine stories. Nonlinear static pushover and dynamic time history analyses were carried out. Performance evaluation of the frame responses was made in terms of interstory drift, chord member deformation, energy dissipation, absolute floor acceleration, and global performance.

Chord members of STMFs tested previously were built-up sections made of double angles and a plate. These build-up sections generally have limited strength capacity. However, larger strength capacity may be needed for STMFs used for larger and taller buildings, such as for hospitals. Chord members made of double channel sections may be more suitable for use. In order to check the feasibility of using double channels for chord members, component tests were also carried out with various detailing configurations. The results were used to develop details to achieve adequate ductility. As a consequence, the STMFs studied in this report used double channel sections for chord members.

1.4 Organization of the Report

This report is organized into six chapters. Details of each chapter are briefly described in the following.

The overall proposed performance-based design procedure is presented in Chapter 2. A brief background regarding the design philosophy based on energy concept is also given, along with two design flowcharts.

Chapter 3 describes the experimental results for double channel component tests under cyclic displacement reversals. Suggested detailing is given as derived from the test results.

Chapter 4 presents the details of the design of a seven-story STMF. A preliminary design based on an earlier study of SMRF was examined using non-linear dynamic analyses and a refinement was made for this study. A revised equation for calculating the maximum expected vertical shear strength, V_{ne}, is proposed. The modeling details used in the Perform-2D program, as well as the ground motion records (10 % in 50 years and 2 % in 50 years SAC LA region ground motion) and the design spectra are given.

Chapter 5 describes the design and performance evaluation of an ordinary and an essential nine-story STMF building based on non-linear pushover and dynamic analyses using some SAC LA region ground motions with 10% and 2% probability of exceedence in 50 years. The study parameters included: location of yield activity, maximum plastic hinge rotation in chord members, maximum relative story shear distribution, maximum interstory drifts, and peak floor accelerations.

Chapter 6 presents a brief summary of the study and important conclusions and recommendations based on the results.

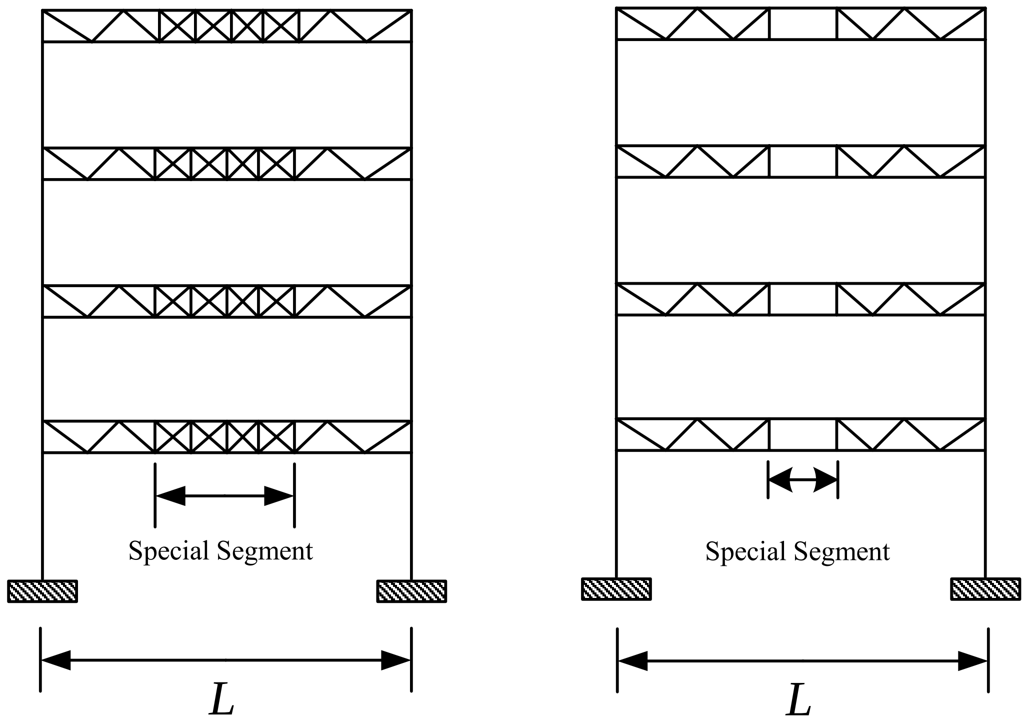

Figure 1.1 STMF with different configurations of Special Segment (Basha, 1994)

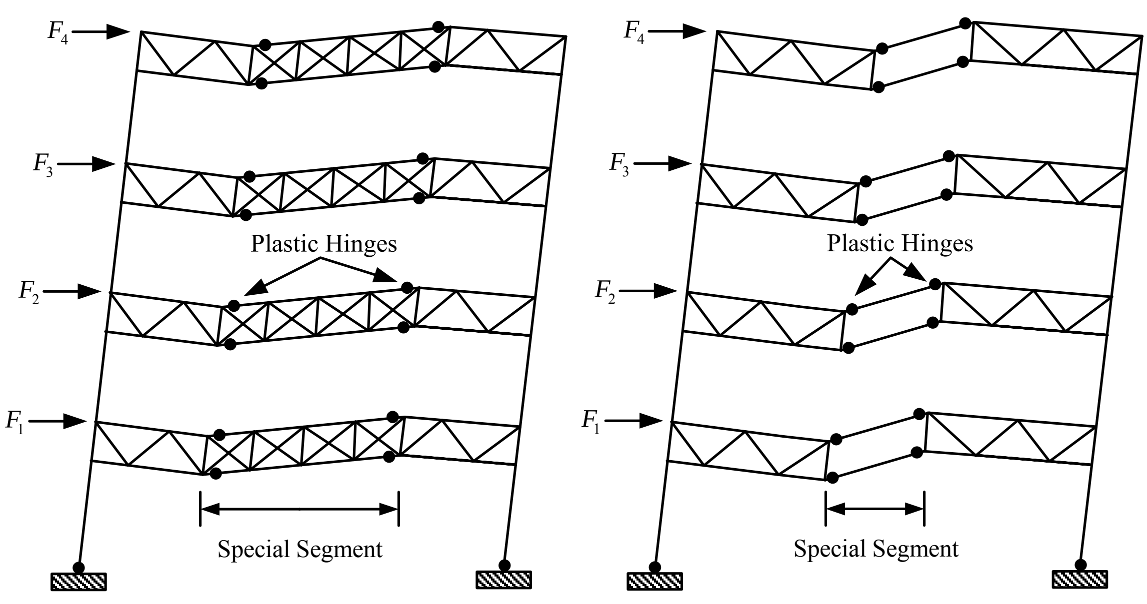

Figure 1.2 Mechanism of STMF with different Special Segment (Basha, 1994)

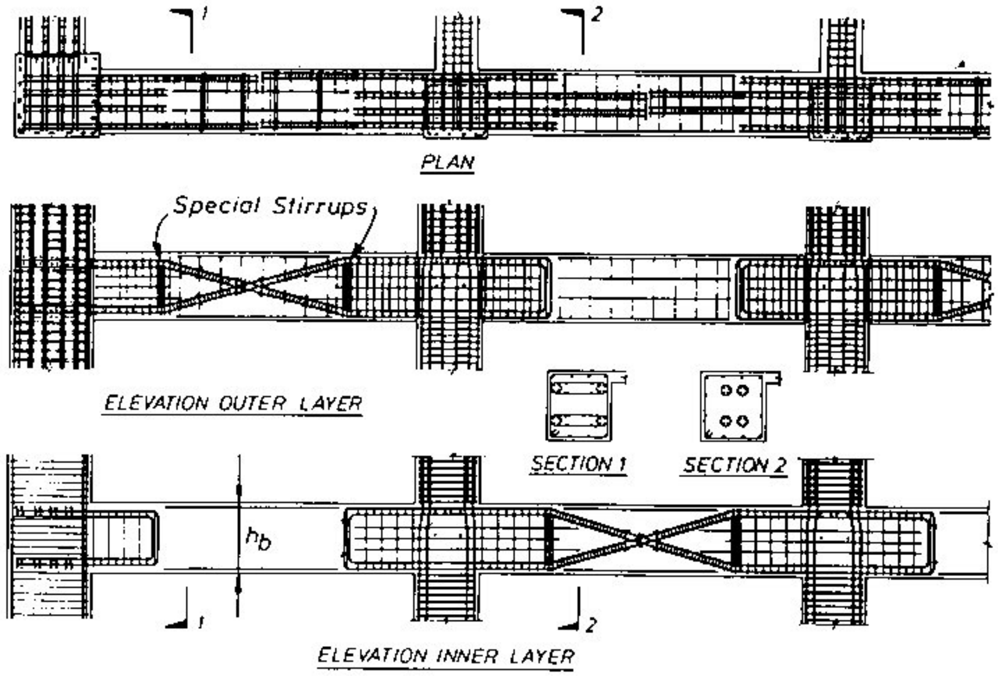

Figure 1.3 Details of diagonally reinforced central portion to relocate the inelastic deformation away from column faces (Paulay and Priestley, 1992)

(a)

(b)

Figure 1.4 Ductwork through a Vierendeel special segment opening of an STMF (Courtesy of John Hooper)

Figure 1.5 A typical STMF with 2-panel Vierendeel special segments under construction (Courtesy of John Hooper)

CHAPTER 2

Performance-Based Plastic Design Procedure for STMF Using Pre-Selected Target Drift

2.1 Introduction

It is most desirable that structures are proportioned to yield at locations which are most capable of deforming into inelastic range and sustaining large cyclic deformations. Yielding in columns should be avoided or minimized because of the difficulty in detailing for ductile response in the presence of high axial loads and because of the possibility that excessive column yielding may result in formation of story mechanism which may lead to cause collapse. Hence, for conventional special moment frames, capacity-design approach (strong column weak-beam) is usually employed to force plastic hinges to form at the beam ends. The strong column-weak beam design requirements in the current codes, however, do not guarantee that plastic hinging would not occur in the columns during major earthquake events (Paulay and Priestley, 1992; Lee 1996). Yielding in the columns may also be caused due to higher modes of vibration, particularly in the upper stories, as well as due to commonly used design methods which are based on elastic analysis and response results.

The performance-based design procedure, as briefly described herein, is aimed at achieving predictable and controlled behavior of structures during design level seismic events. Three major factors are important in achieving this goal:

1) A design lateral force distribution which reflects realistic story shear distribution along the height of the structure when subjected to severe earthquakes. The triangular force distribution used in most design codes is derived from elastic analysis and may not be valid in the inelastic state. Therefore, a design lateral force distribution derived from nonlinear dynamic analysis results and calibrated by representative ground motion records is more appropriate for performance-based design procedure.

2) A predictable global yield mechanism so that the damage could be confined in pre-selected locations of the frame. In this regard, elastic design procedure cannot guarantee a predicable mechanism due to the predominantly inelastic nature of the structural response during severe earthquakes. Therefore, plastic design procedure is more suitable for purposes of performance-based seismic design because desirable yield mechanism is preselected. This design procedure was developed and successfully validated through nonlinear dynamic analyses for steel moment resistant frames (Leelataviwat, Goel and Stojadinović, 1999; Lee and Goel, 2001; Lee, Goel, and Chao, 2004).

3) A pre-selected target drift limit which can be incorporated at the design stage. To achieve the target building performance levels (such as immediate occupancy, collapse prevention, etc.) for selected earthquake hazard levels the story drift is a good design parameter. Therefore, a design base shear based on selected target drift level, ductility reduction factor, and structural ductility factor was used in this study. This design base shear was derived from modified energy equation and the proposed lateral force distribution (Leelataviwat, Goel and Stojadinović, 1999; Lee and Goel, 2001; Lee, Goel,

and Chao, 2004).

The performance-based plastic design methodology which integrates the above factors is briefly presented in the following section for STMF with Vierendeel special segments.

2.2 Performance-Based Plastic Design Procedure

2.2.1 Design Lateral Forces

The design lateral forces are determined by using the shear distribution factor β_i (Lee and Goel, 2001) obtained by nonlinear time-history analyses. However, the shear distribution factor was previously derived for moment frames. Therefore, β_i was re-calibrated through nonlinear dynamic analyses for STMFs in this study (see Figure 2.1 as well as Chapter 4 for details) and can be expressed as:

$$\beta_i = \frac{V_i}{V_n} = \left(\frac{\sum_{i}^{n} w_i h_i}{w_n h_n} \right)^{0.75T^{-0.2}} \tag{2.1}$$

$$F_n = V \left(\frac{w_n h_n}{\sum_{j=1}^{n} w_j h_j} \right)^{0.75T^{-0.2}} \tag{2.2}$$

$$F_i = (\beta_i - \beta_{i+1})F_n \quad \text{when } i = n,\ \beta_{n+1} = 0 \tag{2.3}$$

where β_i is the shear distribution factor at level i; V_i and V_n respectively are the story shear forces at level i and at the top (nth) level; w_i and w_j are the weights of the structure at level i and j, respectively; h_i and h_j are the heights of story level i and j from ground, respectively; w_n is the weight of the structure at top level; h_n is the height of top story level from ground; T is the fundamental period; F_i and F_n are the lateral forces applied at level i and top level n, respectively; V is the design base shear (see next step).

2.2.2 Design Base Shear

2.2.2.1 Conventional Method

Design base shear in current seismic codes is commonly calculated by reducing the elastic strength demands to the inelastic strength demands using the response modification factors. These inelastic strength demands are further increased according to the importance of specific structures using occupancy importance factor. Generally, the design base shear is determined from the code prescribed design acceleration spectrum and can be expressed in the following form:

$$V = C_s W = C_e \left(\frac{I}{R} \right) W \qquad (2.4)$$

where C_s is the seismic response coefficient calculated based on specific design code; C_e is the design pseudo-acceleration coefficient; I is the occupancy importance factor; R is the response modification factor (= 7.0 for STMF; NEHRP, 2001); and W is the total seismic weight.

After selecting the member sizes for required strengths (which is generally done by elastic analysis) the calculated drift using elastic analysis is multiplied by deflection amplification factor, such as C_d given in the codes, and kept within specified drift limits (in the order of 2%).

2.2.2.2 Proposed Energy-Based Procedure

The response modification factors, *R*, listed in design codes for various structural systems are determined primarily based on engineering judgment and have little throretical basis. Moreover, as stated earlier, the conventional design procedures in the codes are based on elastic force-based analysis methods rather than displacement-based methods, thus the inelastic response beyond the elastic limit for a structure cannot be predicted with good precision. A more rational design approach to overcome the shortcomings in the conventional approach was proposed by Leelataviwat (1998b) and modified by Lee and Goel (2001), which uses energy equation as the design basis with the structure pushed monotonically up to a target drift beyond the formation of a selected yield mechanism. The amount of external work needed to do that is assumed as a factor γ times the elastic input energy $E\left(=\frac{1}{2}MS_v^2\right)$ for an equivalent SDOF. The modification factor γ is dependent on the natural period of the structure which has significant influence on the earthquake input energy, as observed by many investigators (Uang and Bertero, 1988) Thus, the energy equation can be written as:

$$\gamma E = (E_e + E_p) \tag{2.5}$$

where E_e and E_p are, respectively, the elastic and plastic components of the energy going into the structure as it is pushed up to the target drift. S_v is the design pseudo-velocity; M is the total mass of the system. The modification factor, γ, depends on the structural ductility factor (μ_s) and the ductility reduction factor (R_μ). Figure 2.2 shows the relationship between the base shear (CW) and the corresponding drift (Δ) of the elastic and corresponding elastic-plastic SDOF systems. From the geometric relationship the following relationship can be obtained based on Eq. (2.5):

$$\gamma\left(\frac{1}{2}C_{eu}W\Delta_{eu}\right) = \frac{1}{2}C_yW\left(2\Delta_{\max} - \Delta_y\right) \tag{2.6}$$

Using the expression for drifts (Δ), Eq. (2.6) can be rewritten as:

$$\gamma\frac{\Delta_{eu}}{\Delta_y} = \frac{\left(2\Delta_{\max} - \Delta_y\right)}{\Delta_{eu}} \tag{2.7}$$

where Δ_{eu} and $\Delta_{\max}$ from Figure 2.2 are equal to $R_\mu\ \Delta_y$ and $\mu_s\Delta_y$, respectively. Substituting these terms in Eq. (2.7), the energy modification factor γ can be expressed as:

$$\gamma = \frac{2\mu_s - 1}{R_\mu^2} \tag{2.8}$$

where μ_s is the ductility factor equal to $\Delta_{\max}/\Delta_y$; R_μ is the ductility reduction factor equal to C_{eu}/C_y. It can be seen in Eq. (2.8) that the modification factor γ is a function of the ductility reduction factor (R_μ) and the ductility factor (μ_s). Using different approaches, many investigators have attempted to relate the ductility reduction factor and structural ductility factor (Miranda and Bertero 1994). In this study, the method proposed by Newmark and Hall (1982) is adopted to relate the ductility reduction factor and the structural ductility factor as shown in Figures 2.3 and Table 2.1 (Miranda and Bertero, 1994; Lee and Goel, 2001). The energy modification factor γ calculated based on Eq. (2.8) is shown in Figure 2.4.

The elastic input energy demand (E) can be determined from the elastic design pseudo acceleration spectra as given in the building codes (CBC, IBC, UBC, or NEHRP). The design pseudo-acceleration based on the selected design spectrum for elastic systems can be specified as:

$$A = C_e g \tag{2.9}$$

where A is the design pseudo-acceleration, g is the acceleration due to gravity, and C_e is the normalized design pseudo-acceleration as defined in Eq. (2.4). Note that no occupancy importance factor is included in the design pseudo-acceleration for the approach proposed in this study. The occupancy importance factor, I, increases the design force level in an attempt to lower the drift and ductility demands for the structure at a given level of ground shaking (SEAOC, 1999; NEHRP, 2001). However, that cannot be considered as a direct method to achieve the intended purpose such as damage control. The reduction of potential damage should better be handled by using appropriate drift limitations. In this regard, the approach of calculating the design base shear proposed in this study uses the target drift as an important parameter. It is assumed that the selected target drift will have the occupancy importance factor built into it. However, C_e can be further increased if other effects such as Spectral Ratio (CBC 1631A.5.4), near-fault effect, redundancy consideration, or possible torsion in the global structural system need to be considered. Pending further research on these issues, guidance given in current codes can be used.

The energy equation can be re-written as:

$$(E_e + E_p) = \gamma\left(\frac{1}{2}MS_v^2\right) = \frac{1}{2}\gamma M\left(\frac{T}{2\pi}C_e g\right)^2 \tag{2.10}$$

Akiyama (1985) showed that the elastic vibrational energy (E_e) can be calculated by assuming that the structure can be reduced into a single-degree-of-freedom system, *i.e.*:

$$E_e = \frac{1}{2} M \left(\frac{T}{2\pi} \cdot \frac{V}{W} \cdot g \right)^2 \tag{2.11}$$

where V is the yield base shear and W is the total seismic weight of the structure (W=Mg). Substituting Eq. (2.11) into Eq. (2.10) and rearranging the terms gives:

$$E_p = \frac{WT^2 g}{8\pi^2} \left(\gamma C_e^{\,2} - \left(\frac{V}{W} \right)^2 \right) \tag{2.12}$$

By using a pre-selected yield mechanism as shown in Figures 2.5 or 2.6 and equating the plastic energy term E_p to the external work done by the lateral forces shown in Eq. (2.3) gives:

$$E_p = \sum_{i=1}^{n} F_i h_i \theta_p \tag{2.13}$$

where θ_p is the inelastic drift of the global structure, which is the difference between the pre-selected target drift (θ_u) and yield drift (θ_y). Based on nonlinear analysis in this study, the yield drift of a STMF can be taken as 0.75% for design purposes.

Substituting Eqs. (2.3) and (2.12) into Eq. (2.13), and solving for V/W gives:

$$\frac{V}{W} = \frac{-\alpha + \sqrt{\alpha^2 + 4\gamma C_e^2}}{2} \tag{2.14}$$

where V is the design base shear and α is a dimensionless parameter, which depends on the stiffness of the structure, the modal properties and the selected drift level, and is given by:

$$\alpha = \left(\sum_{i=1}^{n} (\beta_i - \beta_{i+1}) h_i \right) \cdot \left(\frac{w_n h_n}{\sum_{j=1}^{n} w_j h_j} \right)^{0.75T^{-0.2}} \cdot \left(\frac{\theta_p 8\pi^2}{T^2 g} \right) \tag{2.15}$$

It should be noted that the design base shear in Eq. (2.14) is related to the lateral force distribution, the target plastic drift, θ_p, and pre-selected yield mechanism. Also note that in Eq. (2.15) when $i = n$, $\beta_{n+1} = 0$.

It can be seen that the proposed method for determining lateral design forces is based on principles of structural dynamics, while ensuring formation of selected yield mechanism and drift control at the same time. There is no need for using a response modification factor, R, occupancy importance factor, I, or a displacement amplification factor (such as C_d), which are required in current practice and are largely based on engineering judgment. It should also be noted that the design base shear in the proposed method as given by Eq. 2.14 represents the ultimate yield force level (i.e., $C_y W$ in Figure 2.1) at which complete mechanism is expected to form. In contrast, the code design base shear as given by Eq. 2.4 represents the required strength at first significant yield point for use in design by elastic methods.

2.3 Proposed Design Procedure

2.3.1 Pre-Selected Yield Mechanism

Figure 2.5 shows a STMF subjected to design lateral forces and pushed to its target drift state. All the inelastic deformations are intended to be confined within the special segment in the form of plastic hinges in the chord members. Since the plastic hinges developed at the column bases are almost inevitable in a major earthquake, the desired global yield mechanism of STMF is formed by yielding (due to shear force) of the special segments plus the plastic hinges at the column bases. The gravity loads (dead load and live load) are assumed uniformly distributed and no pattern loading is considered for live loads.

2.3.2 Proportioning of Chord Members of the Special Segments

2.3.2.1 Vierendeel Special Segments

The primary aim of using plastic design procedure is to ensure the formation of intended yield mechanism. For STMFs, the plastic hinges are intended to occur only in the special segments and column bases. Earlier studies have shown that it is desirable to have the distribution of chord member strength along the building height closely follow the distribution of story shears derived by using shear distribution factor (β_i) which is obtained and calibrated by nonlinear dynamic time-history analyses (namely, the lateral force distribution proposed in this study). This helps to distribute the yielding more evenly along the height, thereby, preventing excessive yielding from concentrating at a few levels. Referring to Figure 2.6, only one bay of the frame is shown for illustration of the design procedure. It should be noted that using all the bays gives the same required chord strength.

By using the principle of virtual work and equating the external work to the internal work, as is commonly done in plastic analysis by mechanism method, the required chord member strength at each level can be determined as:

$$\sum_{i=1}^{n} F_i h_i \theta_p = 2M_{pc}\theta_p + 4\sum_{i=1}^{n} \beta_i M_{pbr} \frac{L}{L_p}\theta_p \tag{2.16}$$

where L is the span length of truss girders; L_s is the length of special segment (see Figure 2.6); L_p is the distance between the plastic hinges at the ends of the special segments, which is taken as $0.85L_s$ in this study. However, using L_s to replace L_p in Eq. (2.16) is conservative when designing the chord members of the special segment. It is assumed herein that L_s is the same for all truss girders. M_{pbr} is the required plastic moment of chord members at the top level and the only unknown variable in Eq. (2.16). The required chord member strength (plastic moment capacity) at level i can be determined by multiplying M_{pbr} by the shear distribution factor β_i at level i, namely, $\beta_i M_{pbr}$. M_{pc}

is the required plastic moment of columns in the first story as shown in Figure 2.6. Note that due to the deformation of truss girder (as shown in Figures 2.5 and 2.6) and uniformly distributed gravity loads as assumed earlier, the external work done by the gravity loads is zero, thus not included in Eq. (2.16).

The required plastic moment of columns in the first story, M_{pc}, needs to be determined before using Eq. (2.16). Leelataviwat et al. (1999) suggested that M_{pc} can be selected in such a way that no soft story mechanism would occur when 1.1 times the design lateral forces are applied on the frame as shown in Figure 2.7. Thus, the plastic moment of the first-story columns can be computed as:

$$M_{pc} = \frac{1.1V'h_1}{4} \qquad (2.17)$$

where V' is the base shear (for one bay), which is equal to V divided by the number of bays; h_1 is the height of the first story; and the factor 1.1 is the overstrength factor accounting for possible overloading due to stain hardening and uncertainty in material strength. By using Eqs. (2.16) and (2.17), the required chord member strength at level i can be determined as:

$$\beta_i M_{pbr} = \beta_i \cdot \frac{\left(\sum_{i=1}^{n} F_i h_i - 2M_{pc}\right)}{4\frac{L}{L_p}\sum_{i=1}^{n}\beta_i} \qquad (2.18)$$

The design is performed using:

$$\phi M_{nci} = \phi Z_i F_y \geq \beta_i M_{pbr} \tag{2.19}$$

where ϕ is the resistance factor which is taken as 0.9; Z_i is the plastic section modulus; and F_y is the yield strength (taken equal to 50 ksi in this study). Chord members should also satisfy the width-thickness limitations listed in AISC Seismic Provisions Table I-8-1 (AISC, 2005).

2.3.2.2 Vierendeel Special Segments with intermediate vertical members

A special segment can contain multiple Vierendeel panels by adding intermediate vertical members, as shown in Figure 2.8. One benefit of using multiple Vierendeel panels is that the redundancy of seismic energy dissipation mechanism increases. It also has the advantages of allowing more flexibility in mechanical and architectural layout, as well as reducing the rotational ductility demands on special segment chords (Valley and Hooper, 2002). It is very likely that, during minor earthquake events, inelastic deformation would only occur in intermediate vertical members, which could be replaced easily. In addition, the size of chord members can be reduced because of additional strength due to those vertical members.

However, as illustrated in Figure 2.8, while the vertical members generally have smaller length than the chord members, the vertical members sustain the same plastic rotation with chord members when yield mechanism forms. As pointed out by Engelhardt at el. (Engelhardt and Popov, 1989), as member length decreases, flexural yielding tends to be confined to a smaller region at the ends of the member, leading to higher curvature and bending strain demands for the same plastic rotation. This higher demand on bending strains in turn result in higher possibility of fracture at welded connections at the member ends. In addition, reduced length of plastic region can cause problems of flange buckling and lateral torsion buckling in flexural yielding members. As a consequence, it is suggested that the vertical members should be designed as secondary members to prevent possible instability of the frame in case premature failure occurs in the vertical members.

Plastic hinges must be avoided in the chord members except at chord ends; therefore, the moment capacity of vertical members has to be limited so that the moment in the chord members at sections adjacent to the vertical members is less than the moment capacity of chord members after the vertical members yield. Assuming that the Vierendeel panels are of equal length, the moment next to the intermediate vertical members would be approximately half that of their moment capacity. Thus,

$$M_{pbr} > \frac{1}{2} M_{pvr} \tag{2.20}$$

where M_{pvr} is the required plastic moment capacity of the intermediate vertical members at the top floor level (see Section 2.3.2.1). Eq. (2.16) can be rewritten as:

$$\sum_{i=1}^{n} F_i h_i \theta_p = 2M_{pc}\theta_p + \left(4\sum_{i=1}^{n}\beta_i M_{pbr} + 2\sum_{i=1}^{n} m_i \beta_i M_{pvr}\right)\frac{L}{L_p}\theta_p \qquad (2.21)$$

where m_i is the number of intermediate vertical members at the *ith* level.

To design intermediate vertical members as secondary members, it is suggested at this time that at least 70% of the input energy be dissipated by the chord members and the remainder by intermediate vertical members unless further research can show that yielding of intermediate vertical members is not detrimental to the overall performance of an STMF. Therefore, at a given level:

$$\frac{4M_{pbr}}{70} = \frac{2m_i M_{pvr}}{30} \qquad (2.22)$$

$$M_{pvr} = \frac{6}{7}\frac{M_{pbr}}{m_i} \approx \frac{M_{pbr}}{m_i} \qquad (2.23)$$

It is noted that Eq. (2.23) complies with the requirement of Eq. (2.20).

From Eqs. (2.21) and (2.23), it can be shown that:

$$4M_{pbr} + 2m_i M_{pvr} = 4M_{pbr} + 2m_i \frac{M_{pbr}}{m_i} = 6M_{pbr} \qquad (2.24)$$

Thus, Eq. (2.21) can be rewritten as:

$$\sum_{i=1}^{n} F_i h_i \theta_p = 2M_{pc}\theta_p + 6\sum_{i=1}^{n} \beta_i M_{pbr} \frac{L}{L_p}\theta_p \tag{2.25}$$

The required chord member strength at a given level can be determined as:

$$\beta_i M_{pbr} = \beta_i \cdot \frac{\left(\sum_{i=1}^{n} F_i h_i - 2M_{pc}\right)}{6\frac{L}{L_p}\sum_{i=1}^{n}\beta_i} \tag{2.26}$$

By comparing Eqs. (2.18) and (2.26), it can be seen that chord member size/weight can be reduced by approximately 30% by adding intermediate vertical members. After the chord members are designed according to Eq. (2.19) the intermediate vertical members can be designed based on Eq. (2.23).

2.3.3 Design of Members outside the Special Segments

The design of elements outside the special segments, including truss members and columns, is performed based on the capacity design approach. That is, elements outside the special segments should have a design strength to resist the combination of factored gravity loads and the maximum expected vertical shear strength developed at the mid point of the special segments. The maximum expected vertical shear strength, V_{ne}, depends primarily on the length of the special segment, the moment of inertia of chord member, the maximum vertical translation and rotational deformation of the chord member, and the strain hardening and yield strength of the material (Basha and Goel, 1994). V_{ne} specified in AISC Seismic Provision (Eq. (1.1)) was originally derived based on somewhat conservative chord deformation assumption. When double channel sections are used as chord members, Eq. (1.1) generally leads to very conservative design for members outside the special segments. In view of this, a modification is proposed in this study (see Section 2.4 for details) and the revised V_{ne} can be calculated by using the following equation for STMF with Vierendeel configuration of the special segment:

$$V_{ne} = \frac{3.75 R_y M_{nc}}{L_s} + 0.036 E_s I \frac{L}{L_s^3} \tag{2.27}$$

where R_y is the yield stress modification factor (taken as 1.1 in this study); M_{nc} is the nominal flexural strength of the chord members of the special segment; E_s is the Young's modulus (= 29,000 ksi); I_s is the moment of inertia of the chord members of the special segment. Note that L_s is used in Eq. (2.27) instead of L_p. Once the maximum expected vertical shear strength is determined, the frame can be broken into free body diagrams of exterior and interior columns with associated truss girders as illustrated in Figures 2.9, 2.10, and 2.11. Only one half of the special segment of each truss girder is included because the maximum expected vertical shear is applied at the middle of the special segment. This is done so that the elements outside the special segment remain elastic as intended.

For STMF using multiple Vierendeel panels in the special segments, the maximum expected vertical shear strength, V_{ne}, is calculated as (see Section 2.4 for details):

$$V_{ne} = \left(\frac{3.75 R_y M_{nc}}{L_s} + 0.036 E_s I_c \frac{L}{L_s^3} \right) + \frac{m}{2} \left(\frac{3.75 R_y M_{nv}}{L_s} + 0.036 E_s I_v \frac{L}{L_s^3} \right) \tag{2.28}$$

where m is the number of intermediate vertical members, I_c is the moment of inertia of the chord member and I_v is the moment of inertia of the intermediate vertical member.

2.3.4 Exterior columns with associated truss girders

Referring to Figure 2.9a, when the frame reaches its target drift, the vertical shear force in the middle of the special segment at all levels is assumed to reach the maximum expected strength, $(V_{ne})_i$. The column at the base is also assumed to have reached its maximum capacity, M_{pc}. At this stage, the required balancing lateral forces applied on this free body are assumed to maintain the distribution as used earlier and can be easily calculated by using moment equilibrium of the free body. For the case when the lateral forces are acting to the right, the sum of those forces, $(F_R)_{ext}$, can be obtained as:

$$(F_R)_{ext} = \frac{\frac{L}{2} \cdot \sum_{i=1}^{n} (V_{ne})_i - \frac{L^2}{8} \sum_{i=1}^{n} w_{iu} + M_{pc}}{\sum_{i=1}^{n} \alpha_i h_i} \tag{2.29}$$

where w_{iu} is the factored uniformly distributed gravity load on the truss girders, taken as $1.2DL + 0.5LL$ in this study; and:

$$\alpha_i = \frac{(\beta_i - \beta_{i+1})}{\sum_{i=1}^{n} (\beta_i - \beta_{i+1})} \qquad \text{when } i = n, \beta_{n+1} = 0 \tag{2.30}$$

For the case when the lateral forces are directed to the left (Figure 2.9b), the sum of the applied lateral forces, $(F_L)_{ext}$, can be obtained as:

$$(F_L)_{ext} = \frac{\frac{L}{2} \cdot \sum_{i=1}^{n} (V_{ne})_i + \frac{L^2}{8} \sum_{i=1}^{n} w_{iu} + M_{pc}}{\sum_{i=1}^{n} \alpha_i h_i} \tag{2.31}$$

For the case where the gravity loading on truss girders consists of concentrated loads, Eq. (2.29) can be replaced by Eq. (2.32), see Figure 2.10:

$$(F_R)_{ext} = \frac{\frac{L}{2} \cdot \sum_{i=1}^{n} (V_{ne})_i - L_1 \cdot \sum_{i=1}^{n} p_{iu} + M_{pc}}{\sum_{i=1}^{n} \alpha_i h_i} \tag{2.32}$$

Also Eq. (2.31) can be replaced by:

$$(F_L)_{ext} = \frac{\frac{L}{2} \cdot \sum_{i=1}^{n} (V_{ne})_i + L_1 \cdot \sum_{i=1}^{n} p_{iu} + M_{pc}}{\sum_{i=1}^{n} \alpha_i h_i} \tag{2.33}$$

2.3.5 Interior columns with associated truss girders

For the case of interior columns with associated truss girders, both directions of lateral forces lead to the same result, hence only the lateral forces acting to the right are shown in Figure 2.11. The sum of lateral forces, $(F_R)_{\text{int}}$, can be calculated as:

$$(F_R)_{\text{int}} = \frac{L \cdot \sum_{i=1}^{n} (V_{ne})_i + M_{pc}}{\sum_{i=1}^{n} \alpha_i h_i} \tag{2.34}$$

After the lateral forces are calculated as described above, the required strength of individual members (diagonals, chord members, columns, and vertical members if any) can be easily computed by using an elastic structural analysis program such as RISA-3D (RISA, 2001). Preliminary sections can be assumed in the beginning and revised later. The terms $\alpha_i F_R$ ($\alpha_i F_L$), $(V_{ne})_i$, and w_{iu} represent and are applied as external loads. Design of these elements is performed in accordance with the AISC LRFD provisions (AISC, 2001) through conventional elastic design procedures. For STMF with hinged bases, the column-truss models may be structurally unstable when loaded since they are basically determinate cantilever beams. Nevertheless, the hinge support can be replaced with fixed support for computing the element forces without affecting the results because all the external forces are already balanced and moment at the column base will automatically be null (because of hinged supports).

The vertical members adjacent to the special segment are recommended to have the same section as the chord member in the special segment without performing any design calculations (Basha and Goel, 1994). However, a stronger section can be used, if needed.

Flowcharts are given in Figures 2.12 and 2.13 to illustrate the design procedure.

2.4 Proposed modification of the expected vertical nominal shear strength in special segment (V_{ne})

The expected maximum vertical nominal shear strength of the special segment V_{ne} is given in the current AISC Seismic Provision (AISC, 2005), Eq. (12-1), as:

$$V_{ne} = \frac{3.75 R_y M_{nc}}{L_s} + 0.075 E_s I \frac{(L - L_s)}{L_s^3} + R_y (P_{nt} + 0.3 P_{nc}) sin\alpha \qquad \text{AISC (12-1)}$$

where

R_y = yield stress modification factor

M_{nc} = nominal flexural strength of the chord members of the special segment

$E_s I$ = flexural elastic stiffness of the chord members of the special segment

L = span length of the truss

L_s = length of the special segment

P_{nt} = nominal axial tension strength of diagonal members of the special segment

P_{nc} = nominal axial compression strength of diagonal members of the special segment

α = angle of diagonal members with the horizontal

The first two terms of Eq. (12-1) were derived based on Vierendeel special segment without X-braces (Basha and Goel, 1994). One of the assumptions made in the derivation was that the elastic moment at the ends of chord members of the special segment results from vertical translation only, *i.e.*, the effect of end rotation is neglected, as shown in Figure 2.14a. This assumption leads to overestimation of the elastic stiffness of the chord members, which in turn gives higher coefficient, 0.075, in the second terms of Eq. (12-1). Nevertheless, this overestimation has little influence on the V_{ne} if moment of inertia of the chord member is small. However, for heavier chord members, the overestimation can be quite large because of their high value of moment of inertia. Since the members outside the special segment such as vertical members, diagonal members, connections, and columns are designed based on V_{ne}, any overestimation would result in overly conservative design of those members. Moreover, during a major earthquake, it is not likely that all the special segments along the height of the building would reach their maximum moment capacity simultaneously. Therefore, the overestimated V_{ne} as well as the assumption that all the special segments would develop their maximum strength simultaneously can lead to undue over design of the elements outside the special segments, especially for the columns.

A remedy to this problem is to use a more realistic flexural elastic stiffness of the chord members. This is done by the following approach:

If the chord member has no end rotation (fixed end condition), the elastic moment at chord end can be expressed as:

$$M = \frac{6E_s I\theta}{L_s} \tag{2.35}$$

where θ is defined as the relative vertical displacement at chord ends divided by the length of special segment. Hence, the elastic stiffness is:

$$\frac{M}{\theta} = \frac{6E_s I}{L_s} = k \tag{2.36}$$

This elastic stiffness will decrease by allowing the end rotation to occur. For the extreme case, *i.e.*, when the chord member has pinned ends as shown in Figure 2.14b, the elastic stiffness is equal to zero. True elastic stiffness is somewhere between these two extreme cases. It is assumed here that the true elastic stiffness can be approximated by:

$$k = \frac{3E_s I}{L_s} \tag{2.37}$$

By using this formulation, the maximum chord end moment is determined as follows:

Referring to Figure 2.15, the chord moment-rotation relation can be modeled by a bi-linear curve, in which the inelastic stiffness is ηk. From Eq. (2.37), the maximum elastic rotation is:

$$\theta_e = \frac{M_p L_s}{3E_s I} \tag{2.38}$$

The maximum rotation of the chord member can be obtained by using the geometrical relation. Thus,

$$\theta_u = \frac{L}{L_s}\left(\frac{\Delta}{h}\right) \tag{2.39}$$

where (Δ / h) is the story drift. Hence the plastic rotation is:

$$\theta_p = \theta_u - \theta_e = \frac{L}{L_s}\left(\frac{\Delta}{h}\right) - \frac{M_p L_s}{3E_s I} \tag{2.40}$$

The expression for maximum moment can be written as (see Figure 2.15):

$$\begin{aligned} M_{\max} &= M_p + \eta k \theta_p \\ &= (1-\eta) R_y M_{nc} + 3E_s I \eta \left(\frac{L}{L_s^2}\right)\left(\frac{\Delta}{h}\right) \end{aligned} \tag{2.41}$$

The expected maximum nominal shear strength of the special segment V_{ne} is then calculated as:

$$V_{ne} = \frac{4M_{\max}}{L_s} \tag{2.42}$$

By using $\eta = 0.1$ (Basha and Goel, 1994; Kim et al., 2003) and $\Delta / h = 0.03$, it can be found that:

$$V_{ne} = \frac{3.6 R_y M_{nc}}{L_s} + 0.036 E_s I \frac{L}{L_s^3} \tag{2.43}$$

Since the first term is close to the one shown in AISC Eq. (12-1), Eq. (2.43) is rewritten as:

$$V_{ne} = \frac{3.75 R_y M_{nc}}{L_s} + 0.036 E_s I \frac{L}{L_s^3} \tag{2.44}$$

Eq. (2.44) was first verified by the test results (presented in Chapter 3) on double channel ($2C10\times25$, $I=182.2in^4$), in which the maximum shear capacity was 150 kips when the corresponding story drift reached 3%. The V_{ne} calculated by Eq. (2.44) gave the same exact value, *i.e.*, 150 kips.

Eq. (2.44) was also verified by investigating the maximum developed shear in the Vierendeel special segment of a 7-story STMF (see Chapter 4). The chord member at 5-th floor of this frame is made of $2C10\times25$. Pushover analysis was performed until the inter-story drift of the 5-th floor reached 3%. It was found that the average V_{ne} was about 143 kips, which is close to the predicted value, 150 kips. While the proposed equation gives good agreement with the test and analysis results, the V_{ne} calculated by the AISC Eq. (12-1) is 177.3 kips, about 20% higher than that obtained from Eq. (2.44). It should be noted that both the AISC Eq. (12-1) and Eq. (2.44) are based on a story drift equal to 3%. If the expected maximum story drift is well below 3%, the AISC Eq. (12-1) would be even more conservative.

It should also be noted that, the L_s used in Eq. (2.44) is taken as center-to-center distance of the vertical members at the ends of the special segment. In reality, the distance between the plastic hinges, L_p, will be smaller that L_s. L_p in the UM double channel tests was formed to be about $0.82L_s$ and the V_{ne} in the 7-story STMF analysis was calculated based on $0.85L_s$. Both of them have almost the same V_{ne} as that obtained from Eq. (2.44). This suggests that Eq. (2.44) is still on the safe side even though L_s is used (using L_p instead of L_s in denominator of Eq. (2.44) leads to higher V_{ne}).

Eq. (2.44) was further verified using the test results of a subassemblage STMF (Basha and Goel, 1994), in which the chord members of the Vierendeel special segment was a built-up section composed of double angles and plate ($2L3\times3\times\frac{1}{2}$ and $PL1\times2\frac{1}{4}$). The built-up section has a very small moment of inertia ($I = 5.87in^4$). The maximum end moment occurred when the story drift reached 3% was 440 kip-in, which corresponds to V_{ne}= 26.2 kips. The estimated value from Eq. (2.44) is 24.4 kips, about 7.3% lower than the experimental value. On the other hand, the AISC equation gives a value of 28.4 kips, about 8.5% higher than the testing data. As noted earlier, the value from proposed equation may still be conservative if the maximum story drift is below 3%.

As a consequence, it is suggested that the AISC Eq. (12-1) being modified as:

$$V_{ne} = \frac{3.75R_y M_{nc}}{L_s} + 0.036E_s I \frac{L}{L_s^3} + R_y\left(P_{nt} + 0.3P_{nc}\right)sin\alpha \tag{2.45}$$

In the case where multiple Vierendeel panels are present as shown in Figure 2.8, the calculation of V_{ne} should include the contribution from intermediate vertical members. It can be shown that both the chord member and intermediate vertical member have the same plastic rotation when yield mechanism is reached. Thus the maximum moment developed in chord members and intermediate vertical members can be obtained from Eq. (2.41):

$$\left(M_c\right)_{\max} = \left(1-\eta\right)R_y M_{nc} + 3E_s I_c \eta\left(\frac{L}{L_s^2}\right)\left(\frac{\Delta}{h}\right) \tag{2.46}$$

$$\left(M_v\right)_{\max} = \left(1-\eta\right) R_y M_{nv} + 3 E_s I_v \eta \left(\frac{L}{L_s^2}\right)\left(\frac{\Delta}{h}\right) \tag{2.47}$$

where $(M_c)_{\max}$ and $(M_v)_{\max}$ are the maximum expected developed moments in the chord member and intermediate vertical member, respectively. I_c is the moment of inertia of the chord member and I_v is the moment of inertia of the intermediate vertical member. It should be noted that the strain-hardening ratio tends to increase when the member length decreases (Engelhardt and Popov, 1989). For a regular chord member, a 10% strain-hardening ratio is reasonable but the strain-hardening ratio for the vertical member might be actually higher due to its much short length. In this study, both chord and intermediate vertical members are assumed having the same strain-hardening ratio.

The expected maximum vertical nominal shear strength of the special segment with one intermediate vertical member is then calculated as (See Figure 2.16):

$$V_{ne} = \frac{4\left(M_c\right)_{\max}}{L_s} + \frac{2\left(M_v\right)_{\max}}{L_s} \tag{2.48}$$

For special segment with two intermediate vertical members is (See Figure 2.17):

$$V_{ne} = \frac{4\left(M_c\right)_{\max}}{L_s} + \frac{4\left(M_v\right)_{\max}}{L_s} \tag{2.49}$$

In general, the expected maximum vertical nominal shear strength for special segment with intermediate vertical members can be expressed as:

$$V_{ne} = \frac{4\left(M_c\right)_{\max}}{L_s} + \left(\frac{m}{2}\right) \cdot \frac{4\left(M_v\right)_{\max}}{L_s} \tag{2.50}$$

where m is the number of intermediate vertical members.

By using $\eta = 0.1$ and $\Delta / h = 0.03$, V_{ne} will be given by:

$$V_{ne} = \left(\frac{3.75 R_y M_{nc}}{L_s} + 0.036 E_s I_c \frac{L}{L_s^3} \right) + \frac{m}{2} \left(\frac{3.75 R_y M_{nv}}{L_s} + 0.036 E_s I_v \frac{L}{L_s^3} \right) \tag{2.51}$$

Table 2.1 Ductility reduction factor ($R_\mu = \dfrac{C_{eu}}{C_y}$) and its corresponding structural period range

Period Range	Ductility Reduction Factor
$0 \le T < \dfrac{T_1}{10}$	$R_\mu = 1$
$\dfrac{T_1}{10} \le T < \dfrac{T_1}{4}$	$R_\mu = \sqrt{2\mu_s - 1} \cdot \left(\dfrac{T_1}{4T}\right)^{2.513 \cdot \log\left(\frac{1}{\sqrt{2\mu_s - 1}}\right)}$
$\dfrac{T_1}{4} \le T < T_1'$	$R_\mu = \sqrt{2\mu_s - 1}$
$T_1' \le T < T_1$	$R_\mu = \dfrac{T\mu_s}{T_1}$
$T_1 \le T$	$R_\mu = \mu_s$

where

$$T_1 = 0.57 \text{ sec}$$

$$T_1' = T_1 \cdot \frac{\sqrt{2\mu_s - 1}}{\mu_s} \text{ sec}$$

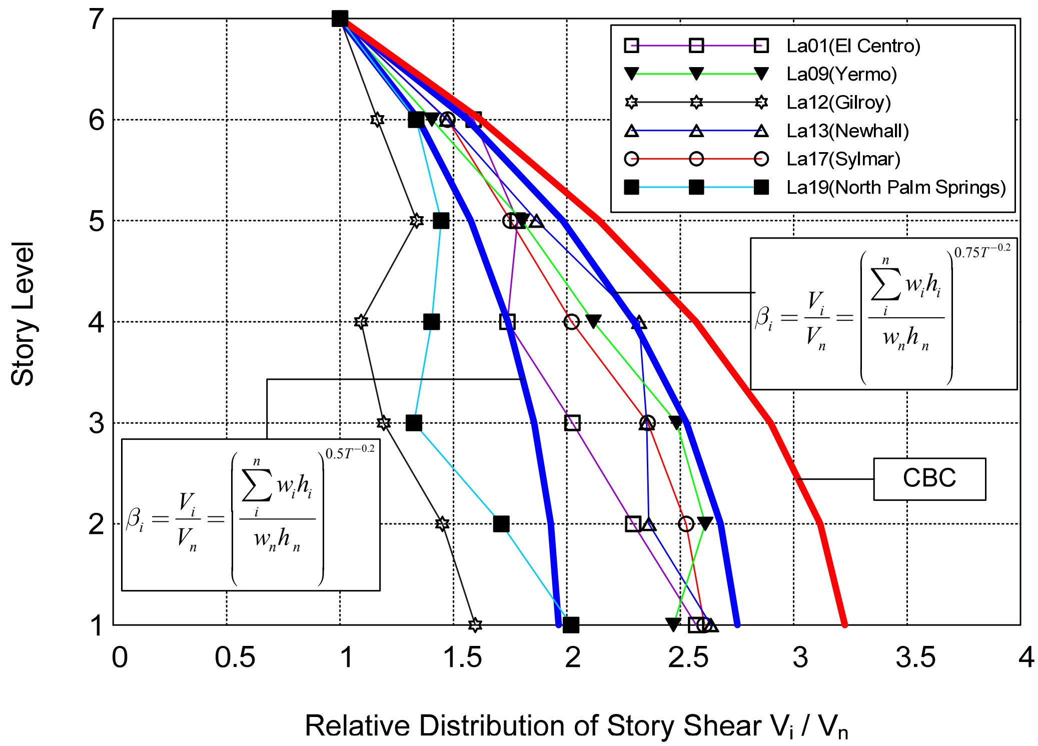

Figure 2.1 Three selected story shear distributions in the first phase of study

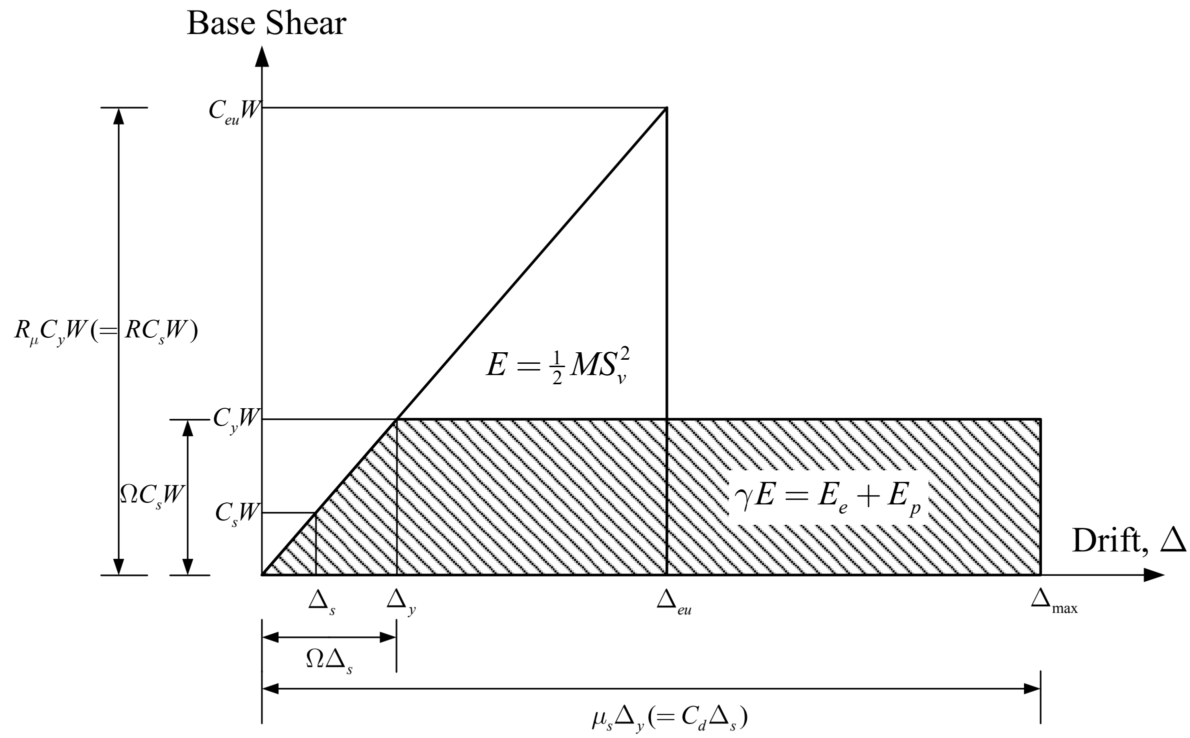

Figure 2.2 Structural idealized response—application of principle of energy conservation

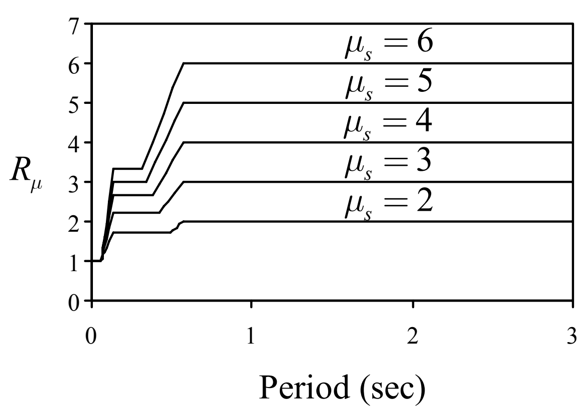

Figure 2.3 Ductility reduction factors proposed by Newmark and Hall (1982)

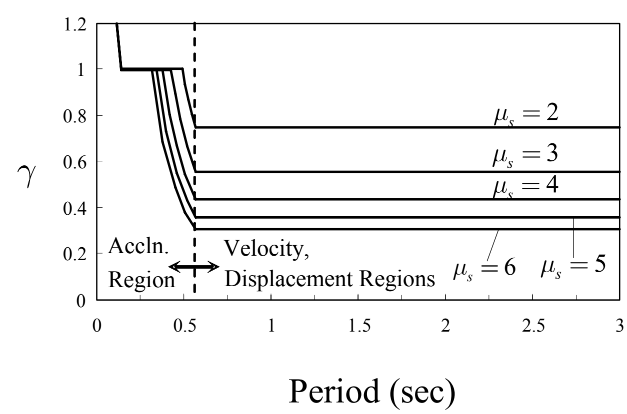

Figure 2.4 Modification factors for energy equation versus period

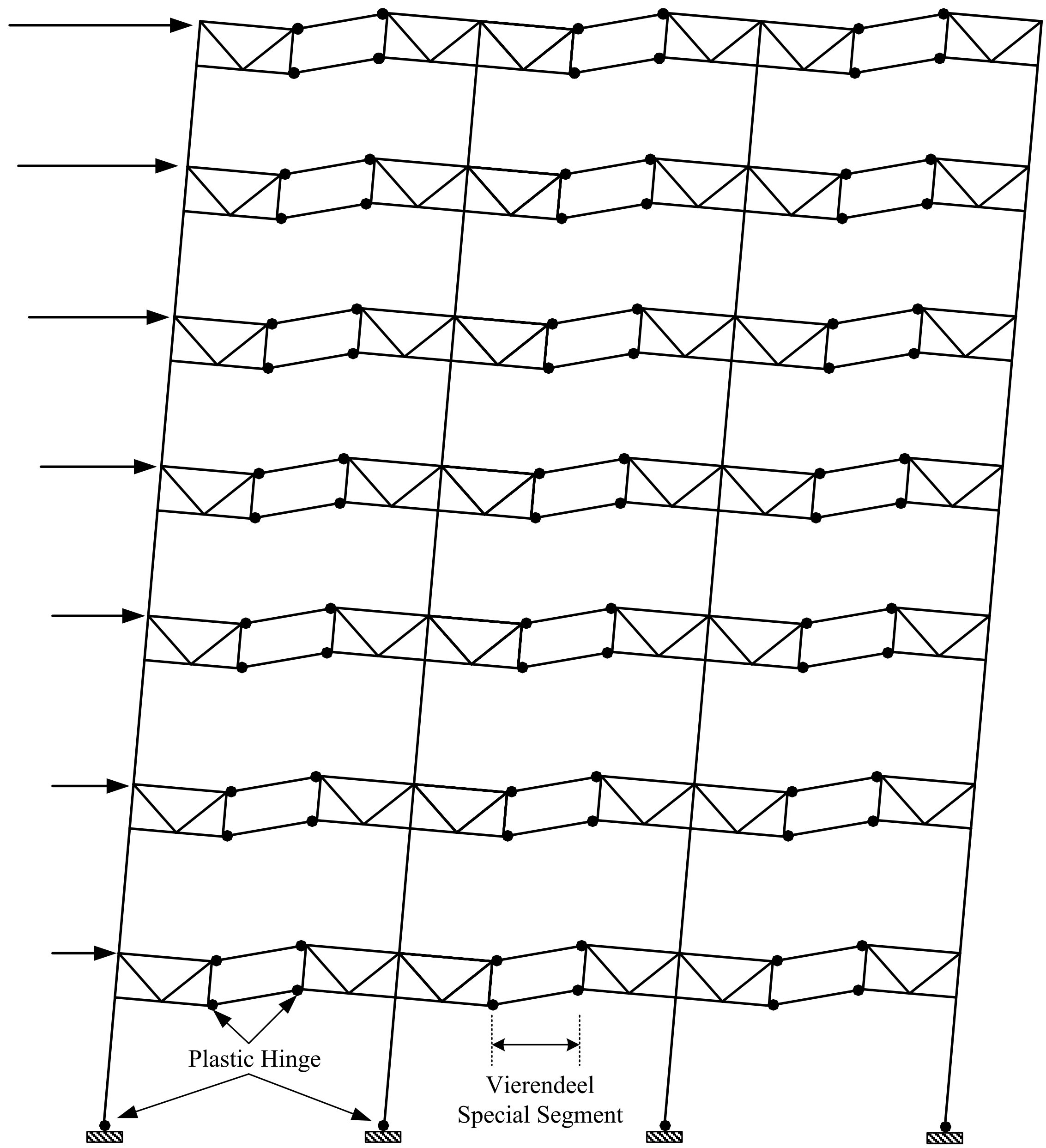

Figure 2.5 Pre-selected yield mechanism of STMF with Vierendeel configuration of Special Segment

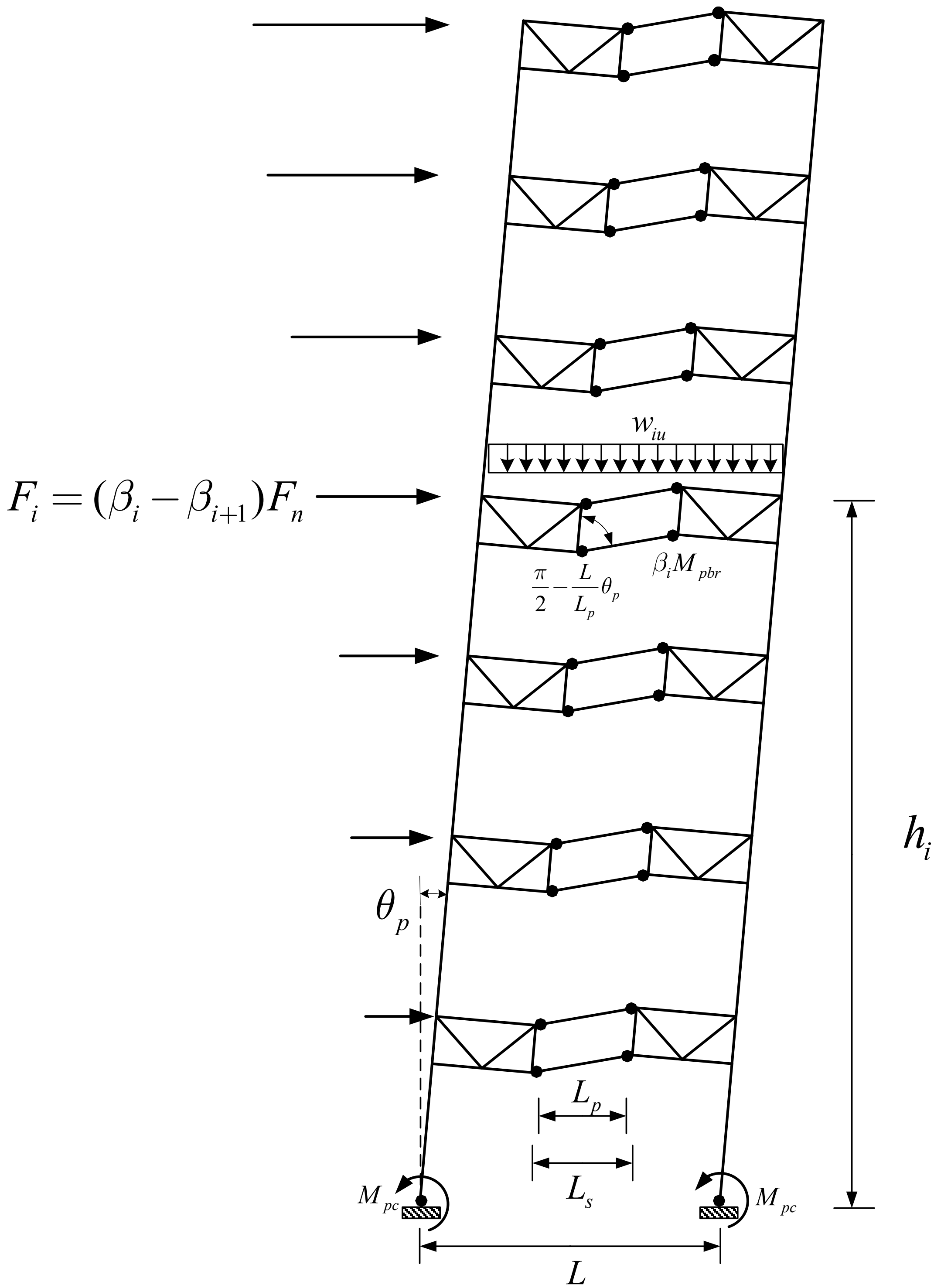

Figure 2.6 One-bay frame with pre-selected yield mechanism for calculating required strength of chord members; note that the values of F_i and F_n are for one bay only

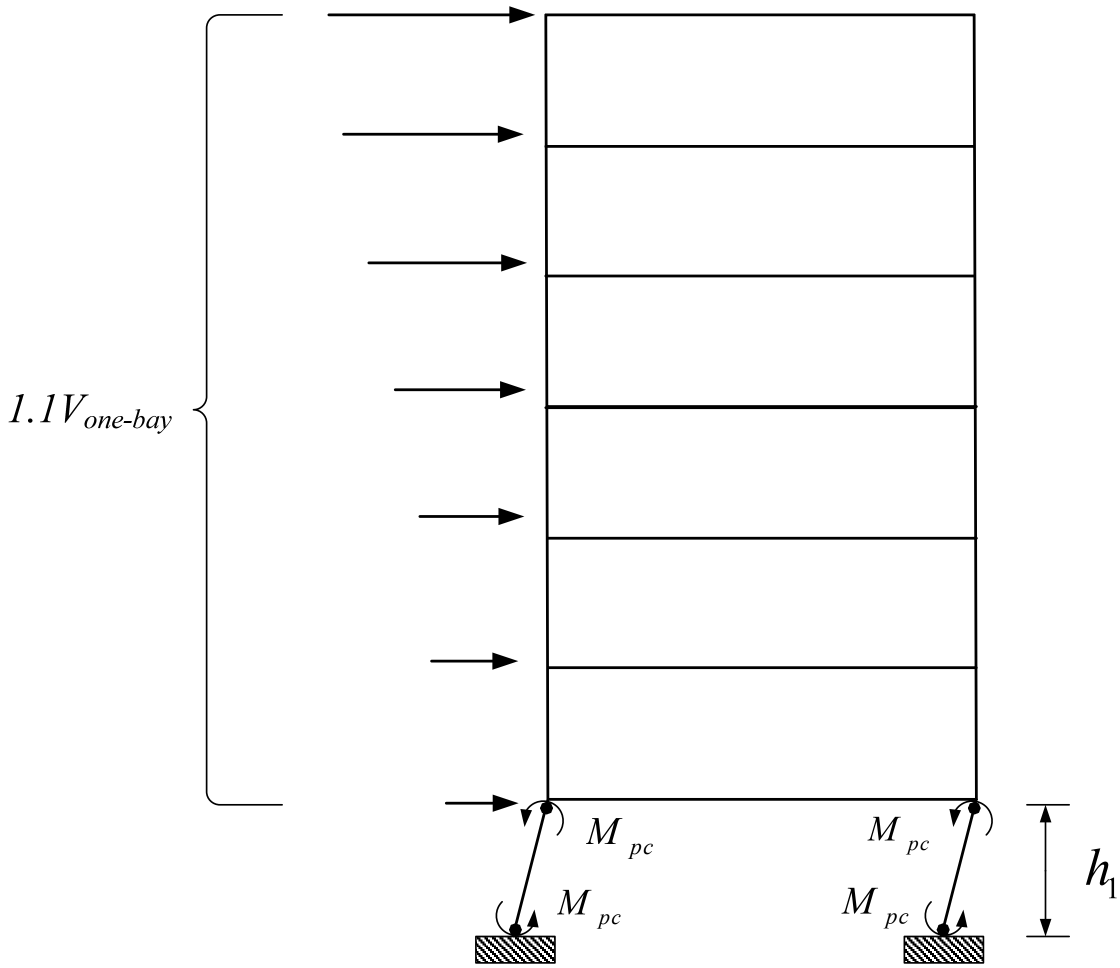

Figure 2.7 One-bay frame with soft-story mechanism (Leelataviwat et al., 1999)

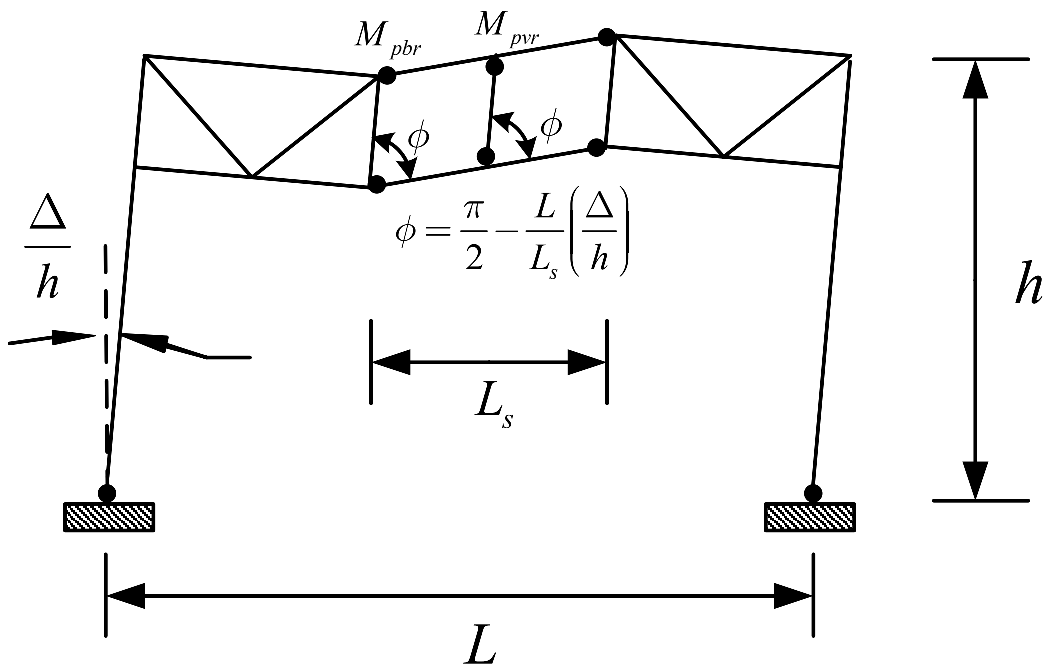

Figure 2.8 Yield mechanism of STMF with multiple Vierendeel panels

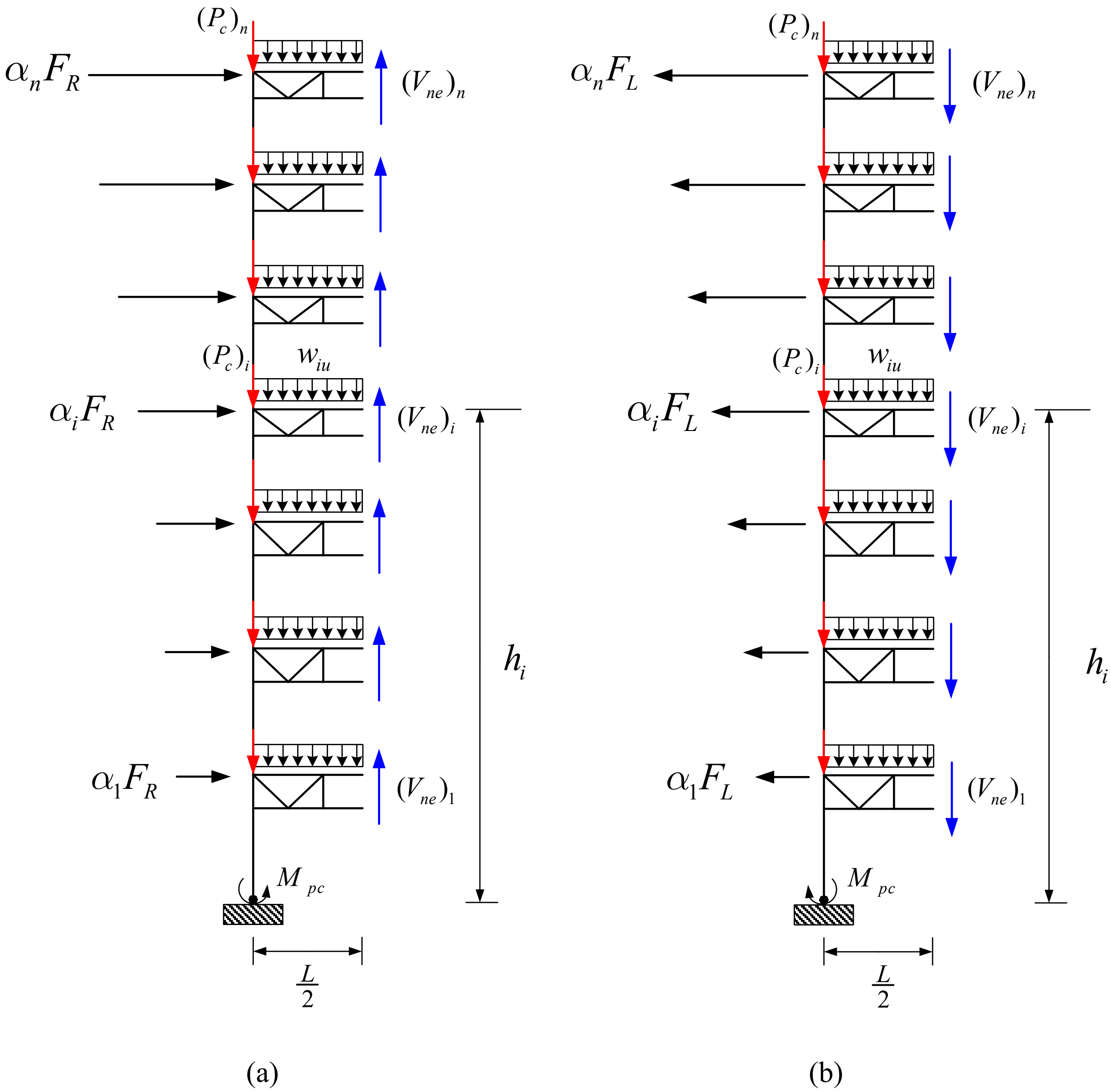

Figure 2.9 Free body diagram of an exterior columns and associated truss girder branches: (a) lateral forces acting to right side; (b) lateral force acting forces to left side

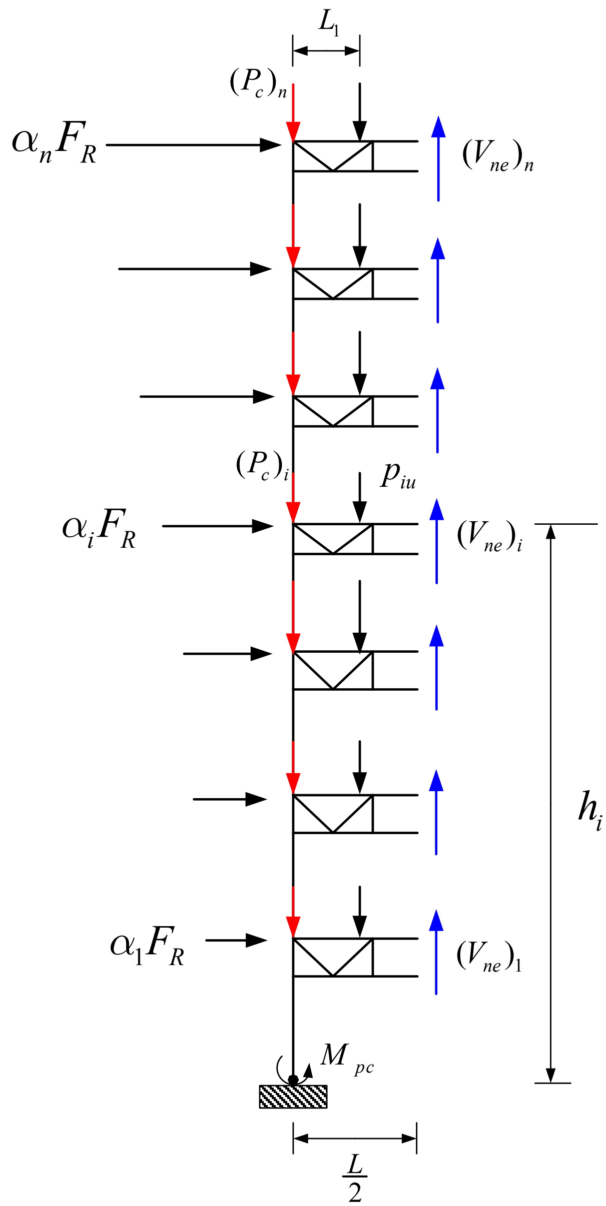

Figure 2.10 Free body diagram of an exterior columns and associated truss girder branches with concentrated gravity loadings on truss girders (lateral forces acting to right side)

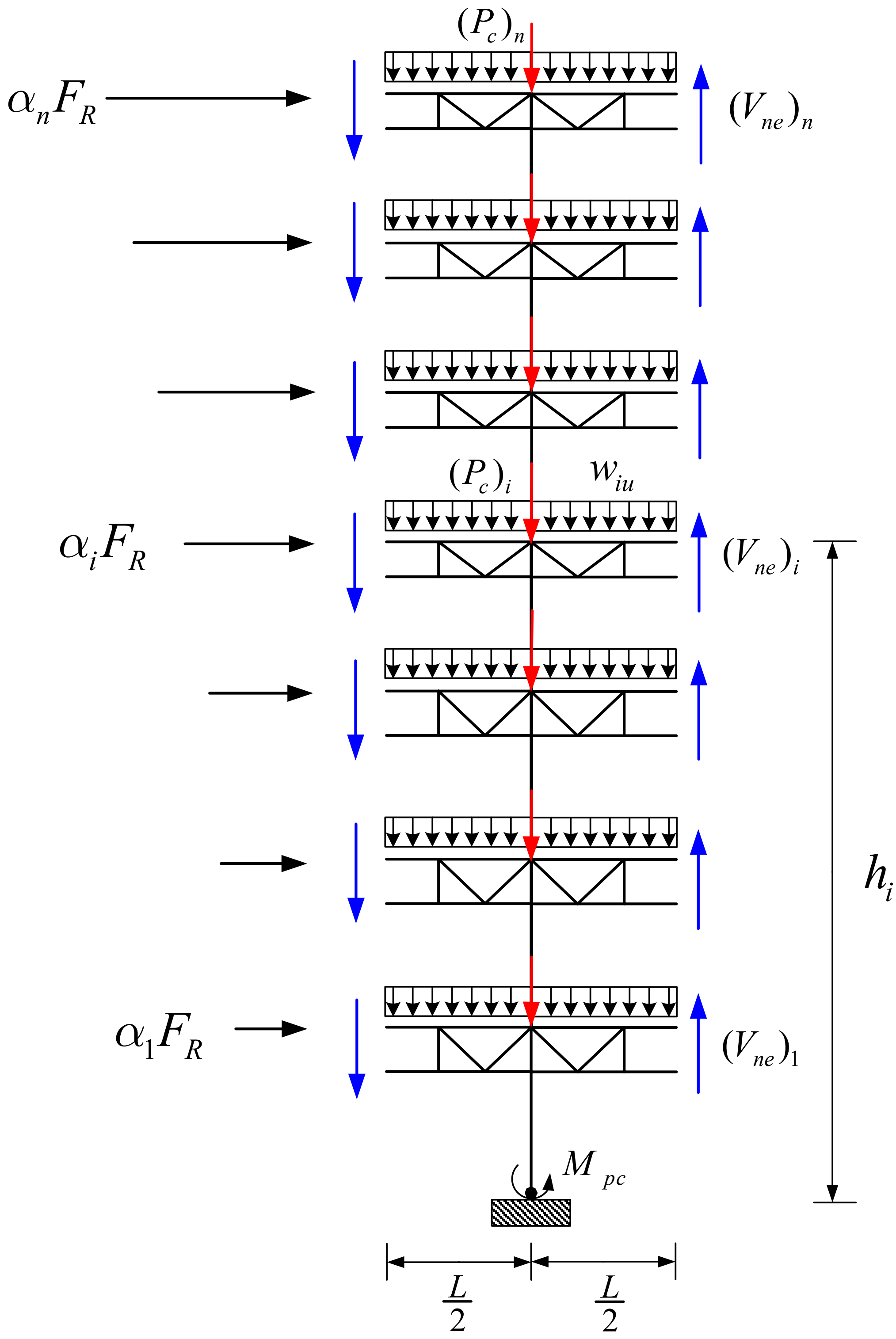

Figure 2.11 Free body diagram of an interior columns and associated truss girder branches subjected to lateral forces to right

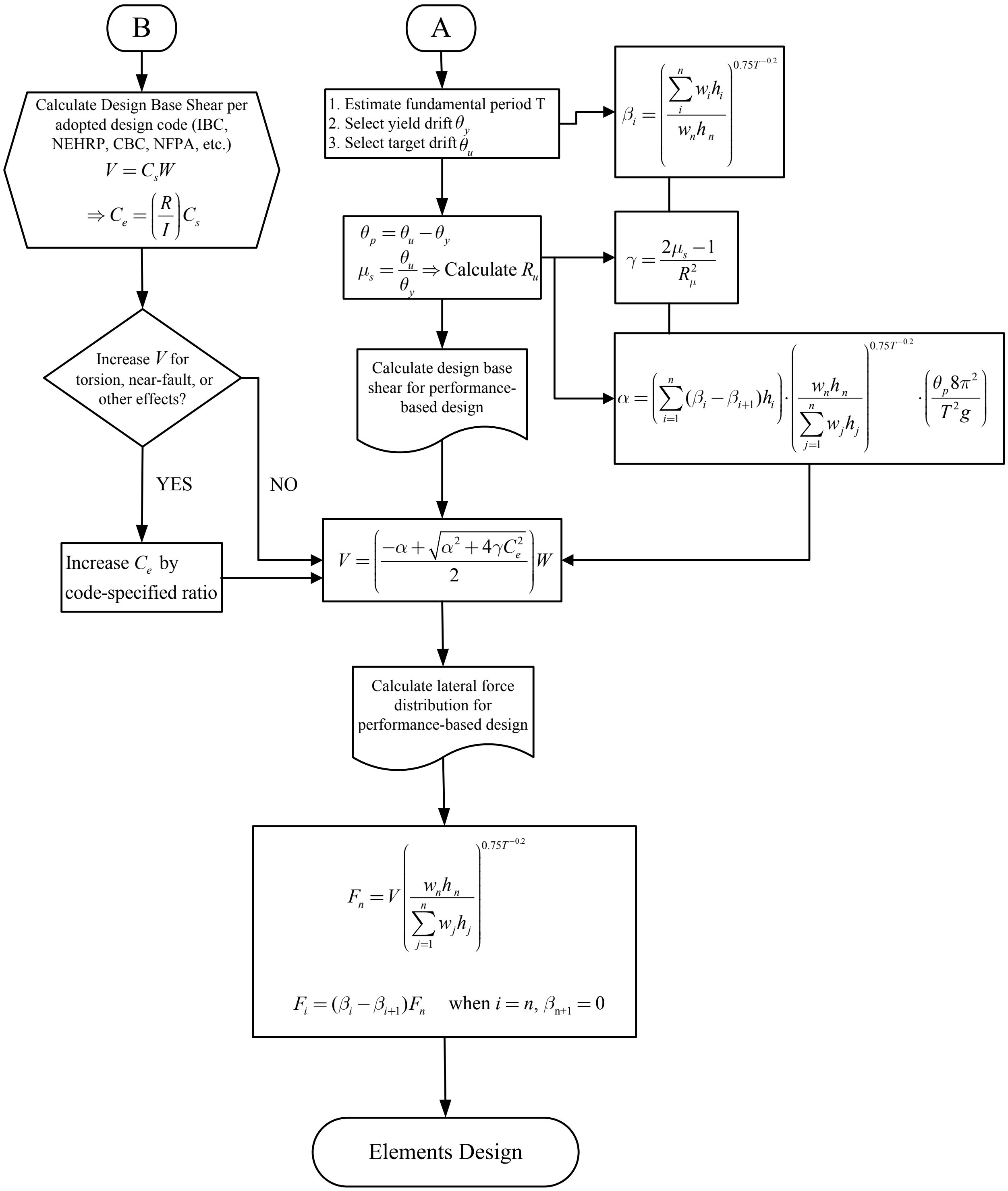

Figure 2.12 Performance-based plastic design flowchart for STMF: determine design base shear and lateral force distribution

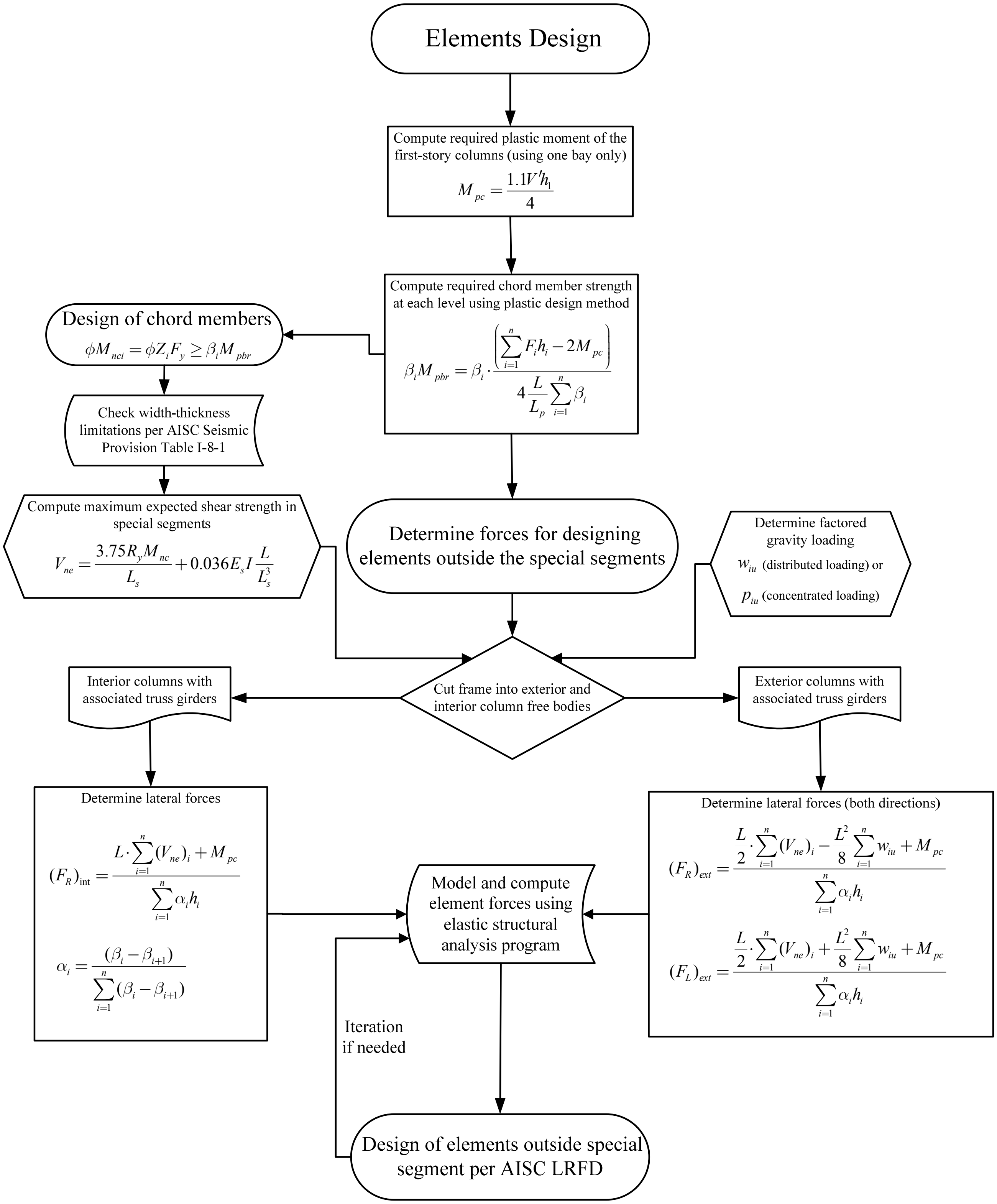

Figure 2.13 Performance-based plastic design flowchart for STMF: element design

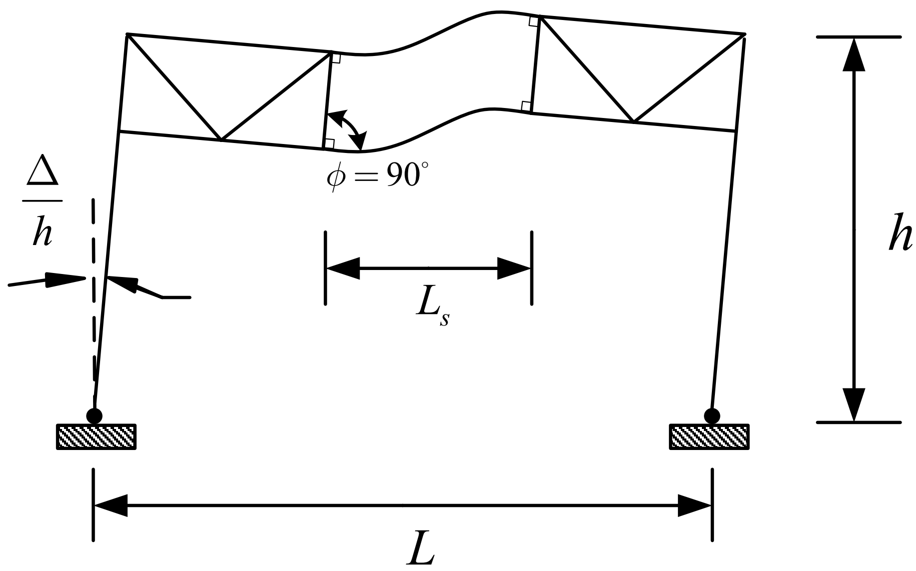

(a)

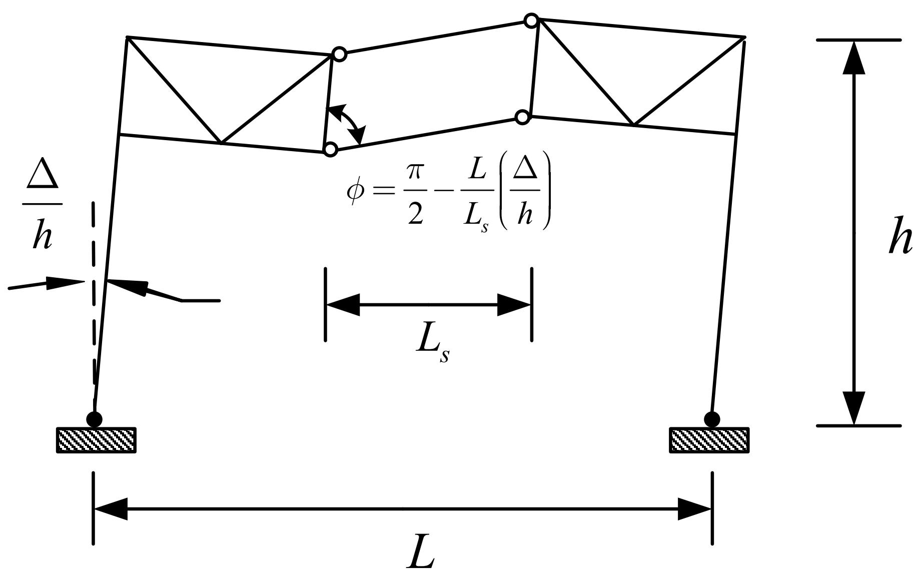

(b)

Figure 2.14 Deformation of in chord of the Vierendeel special segment: (a) no chord end rotation; (b) free chord end rotation

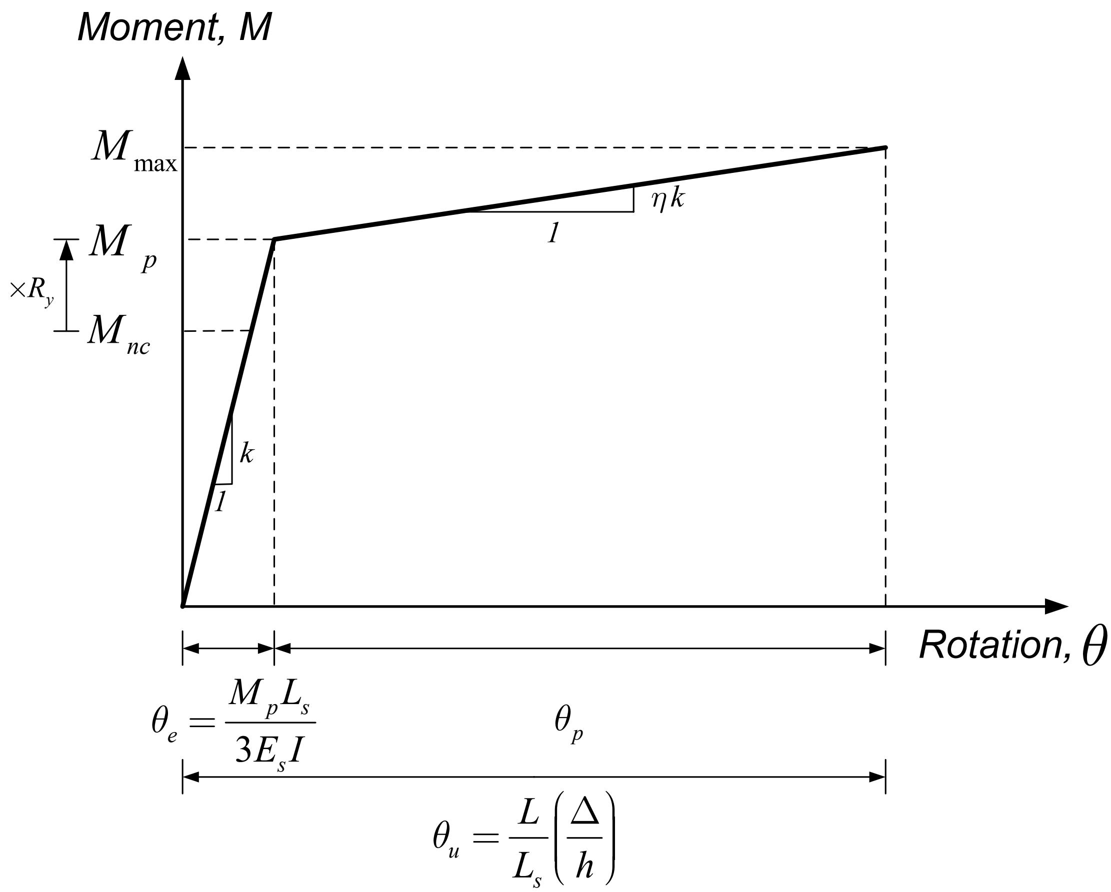

Figure 2.15 Moment-rotation relation of chord member

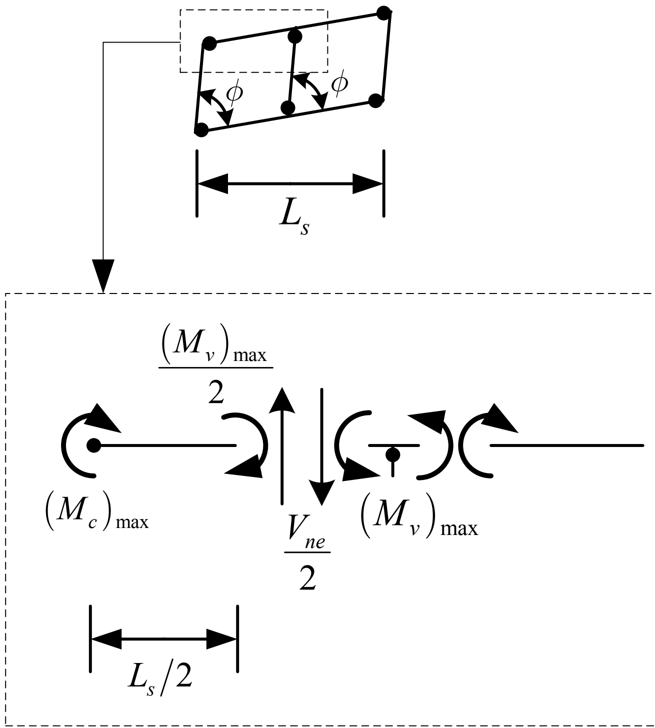

Figure 2.16 Calculation of V_{ne} for two Vierendeel panels

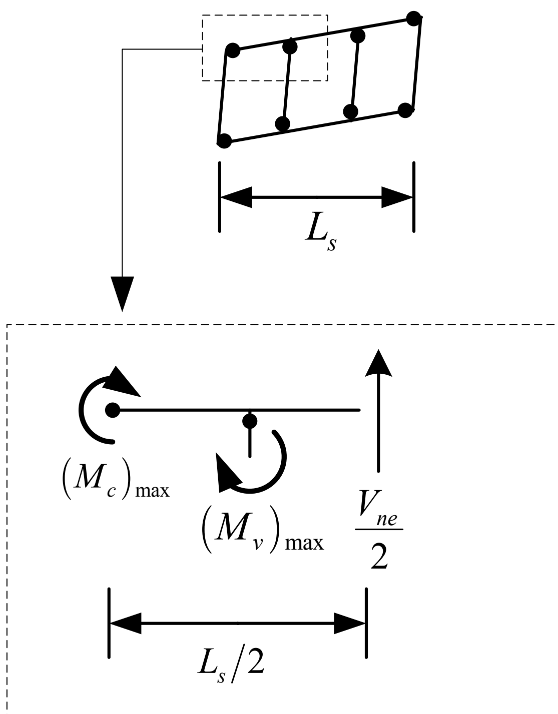

Figure 2.17 Calculation of V_{ne} for three Vierendeel panels

CHAPTER 3

Testing of Double Channel Built-Up Components under Reversed Cyclic Bending

[Condensed from reference paper by Parra-Montesinos, Goel, and Kim (2006)]

3.1 Introduction

Chord members of STMFs (See Figure 3.1) tested previously were built-up sections composed of double angles and plate (Itani and Goel, 1991; Basha and Goel, 1994) or T sections (Leelataviwat, Goel, and Stojadinović, 1998a). These built-up sections generally have smaller strength capacity. However, greater strength capacities are needed for taller STMFs subjected to strong seismic events, which are very likely to exceed the capacity of built-up double angle or T sections. In view of this, chord members composed of double channel sections may be more used for chord members of those STMFs. In order to investigate the feasibility of using double channel for chord members, double channel built-up component tests were conducted at the University of Michigan with various detailing configurations. Promising results were obtained and are presented in this chapter. More details of the test results and analysis can be found elsewhere (Kim et al., 2003; Parra et al., 2006). Based on the test results, a bilinear model for the moment-rotation relation of double channel chord members was developed for nonlinear analysis purposes.

3.2 Experimental Program

3.2.1 AISC-LRFD Provisions for Steel Channels

Chapter F of the AISC-LRFD Specification (AISC, 2001) includes provisions for maximum allowable unbraced length, L_{pd}, in the region adjacent to a plastic hinge for steel members designed by plastic analysis. For the case of doubly symmetric sections,

$$L_{pd} = \left[0.12 + 0.076 \left(\frac{M_1}{M_2} \right) \right] \left(\frac{E}{F_y} \right) r_y \qquad (3.1)$$

where M_1 and M_2 are the smaller and larger moments at the end of the unbraced segment of the member (positive M_1 / M_2 ratio implies double curvature), E and F_y are the modulus of elasticity and the specified yield strength, respectively, of the steel in the compression flange of the member, and r_y is the radius of gyration of the section about the weak (y) axis. Eq. (3.1) is intended to ensure a minimum rotational ductility capacity of 4.0 (AISC, 2001). However, such ductility capacity might not be adequate for chord members of STMF expected to sustain large displacement reversals, such as those induced by severe earthquakes. Thus, the commentary of the AISC-LRFD Specification gives a more stringent limit for the unbraced length, L_{pd}, in order to provide a rotational ductility capacity of at least 8.0, i.e.,

$$L_{pd} = 0.086 \left(\frac{E}{F_y} \right) r_y \tag{3.2}$$

Based on the above, satisfying Eq. (3.2) should lead to a member capable of reaching and maintaining its plastic moment strength when subjected to large reversals of rotation. In order to evaluate the validity of Eqs. (3.1) and (3.2) for double channel built-up members, a series of tests of double channels with various bracing conditions and stitch spacings under reversed cyclic bending was conducted.

3.2.2 Test Program

A total of seven cantilever double channel built-up members were tested under reversed cyclic bending. The specimen dimensions and test setup are shown in Figure 3.2. Except for Specimen C1, which used a double channel built-up member made of 2-C12x20.7 sections, all the other specimens (C2-C7) used 2-C10x25 sections. All channel sections satisfied the compactness requirements in AISC Seismic Provisions (AISC 2005). The double channels were welded to a gusset plate which in turn was welded to a base made of tube sections, as shown in Figure 3.2.

The loading protocol (lateral displacement history) applied to the specimens was selected based on the expected displacement demands that would be imposed on the chord members of a special truss girder in a prototype STMF. In the prototype structure, the special truss girders were designed with a Vierendeel special segment. The cantilever specimens would then represent the chord member between the ends of the special segment (fixed end in the test specimen) and midspan (point of inflection) of the special segment (free end in test specimen) (Figure 3.2(a)). The displacement demands were estimated for story drifts in the prototype structure ranging from 0.375% to 3.0%, which translated into specimen drifts ranging from 0.8% to 6.6%. Lateral displacements were applied at 60 in. above the base of the built-up component. The displacement history planned for these specimens consisted of six cycles at 0.375%, 0.5% and 0.75% story drift in the prototype structure, four cycles at 1.0% drift, and two cycles at 1.5%, 2.0% and 3.0% drift, as shown in Figure 3.3. After the planned displacement history was completed, the specimens were cycled to failure or significant load deterioration.

3.2.3 Test Specimens

Emphasis in the experimental program was placed on three parameters including location of lateral support, spacing of stitches in the built-up members, and member-to-gusset plate connection details. All channels were made of Grade 50 steel, while A36 steel was used for the gusset plates and stitch plates. Details of the test specimens, such as channel sections, stitch spacing, member unbraced length are summarized in Table 3.1. Configurations of Specimen C1 thru C6 are shown in Figures 3.4 thru 3.9. Stitch spacing and unbraced length in Specimen C1 were designed based on Eqs. (3.1) and (3.2), in an attempt to prevent lateral-torsional buckling of the individual channels as well as that of the overall member.

As will be explained later, the stitch spacing and lateral bracing provided in

Specimen C1 was not adequate to ensure a stable inelastic response. Thus, in Specimen C2, a different channel section and a reduced stitch spacing were used. Specimen C2 consisted of a 2-C10x25 built-up section. This specimen had a plastic moment capacity similar to that of the 2-C12x20.7 built-up section, but featured a thicker web. Also, the depth of the gusset plate above the base girder was increased to 8 in. for Specimen C2 and the brace location at the top of the specimen was slightly lowered as compared to Specimen C1, thus leading to a shorter unsupported length for the member (42 in.). The reason for providing a deeper gusset plate was to reduce the demands in the welds connecting the channels to the gusset plate and the base girder.

Specimen C3 was identical to Specimen C2, expect for a reduced stitch spacing of 9 in. provided in the region adjacent to the member plastic hinge. In order to evaluate the effect of lateral bracing of the plastic hinge region, Specimen 4 used the same details as in Specimen C3, but an additional lateral supported at the location of the first stitch was provided (Figure 3.7). The stitch spacing and lateral support locations were the same in Specimens 4 thru 6. However, in Specimens C5 and C6 refined connection details between the gusset plate and the steel channels were provided in order to reduce concentration of stresses near the extreme fibers of the channels.

Results from finite element analyses and testing of steel beam-column connections (Goel et al. 1997; Choi et al. 2003), indicate that the distribution of stresses over the beam depth near the connection region greatly differs from that predicted by using Bernoulli-Navier's beam theory (i.e. plane sections remain plane after bending), the larger shear stresses being concentrated near the beam flanges as opposed to the web region. In order to limit the shear force that would be transferred through the beam flanges in moment connections, Choi et al. (2003) proposed a moment connection with a strong and stiff web plate (free flange moment connection) that would attract most of the beam shear force, allowing the beam flanges to resist primarily normal stresses. In Specimens 5 and 6 of this investigation, a similar concept was applied, where the gusset plate would simulate the web plate in the free flange moment connections. Thus, the connection details included a rounded and trapezoid-shaped web cut-out for Specimens 5 and 6, respectively (Figures. 3.8 and 3.9). The cut-out also provided more welding area to relieve the stresses in the welds at flange-to-gusset plate. In addition, the flanges of the channels in Specimen 6 were reinforced with 0.5 in. thick plates in the connection region, in an attempt to achieve a more uniform distribution of strains in the critical region of the plastic hinge.

3.3 Experimental Results

3.3.1 Overall Behavior of Specimens C1 thru C6

The moment versus (member and prototype structure story) drift responses of Specimens C1 thru C6 are shown in Figure 3.10 (Parra et al., 2006). In general, all specimens exhibited a stable response up to failure. The calculated plastic moment capacity, M_p, based on nominal material properties, and the expected moment strength accounting for material overstrength and strain hardening, are also shown in Figure 3.10

for evaluation of moment capacity of the double channel members. The effect of material overstrength and strain-hardening on the expected moment strength was determined as recommended in the AISC Seismic Provisions (AISC, 2005) by scaling the moment strength using an R_y (1.1 for Grade 50 steel) and 1.1 factor, respectively. It is seen that the moment capacity could reach much higher values than the expected maximum strength, $1.1 R_y M_p$, especially for those specimens that were able to sustain greater rotations.

As can be observed in Figure 3.10, Specimen C1 showed a displacement capacity substantially smaller than that of Specimens C2 thru C6. Yielding of the channels in Specimen C1 was noticed at early stages of the test (about 0.5% prototype structure drift) and spread over approximately one member depth above the gusset plate during the later loading cycles. Lateral-torsional buckling of the individual channels, as well as of the overall member, was first noticed during the 1.0% drift cycles. This lateral-torsional buckling became severe during the cycles at 1.5% drift (Figure 3.11), which ultimately led to termination of the test. Since the stitches and lateral bracing were provided based on the requirements in the AISC LRFD Specifications for plastic design, it appears that these requirements for L_{pd} are not adequate to prevent lateral-torsional buckling of double channel built-up members subjected to large reversals of rotation.

The moment versus drift response for Specimen C2 is shown in Figure 3.10b. This specimen exhibited a much superior response compared to Specimen C1, with substantially larger displacement and energy dissipation capacity. Specimen C2 showed no significant deterioration of strength during the cycles up to 3.0% story drift (prototype structure). For the second cycle to 3.35% drift, the maximum lateral load dropped to about 75% of that at 3.0% story drift. Yielding in the channels of Specimen C2 was first noticed at approximately 0.5% drift and spread over approximately 1.5 times the channel depth above the gusset plate during subsequent cycles. At 2.0% drift, fracture in the region connecting the gusset plate and channels was first noticed. The fracture appeared to have begun in the channel flange region near the web, propagating towards the channel web and flange on further cycling of the specimen.

The reduction in stitch spacing from that in Specimen C1, and the use of a channel section with thicker web, led to a less severe lateral-torsional buckling in Specimen C2. The use of a stitch spacing of 13.75 in. seemed to be adequate to prevent lateral-torsional buckling of the individual channels. However, lateral-torsional buckling of the overall member was first noticed during the 1.5% story drift cycles, becoming significant during the 3.0% drift cycles (Figure 3.12b). Local buckling of the channel flanges was also noticed during the cycles to 3.0% and 3.35% drift (Figure 3.13a). The test was terminated due to complete fracture of one channel flange during the second cycle to 3.35% drift (Figure 3.13b).

Specimen C3 showed a very similar moment versus drift response compared to Specimen C2 (Figure 3.10c) with no deterioration of strength during the cycles up to 3.0% story drift. For the cycle to 3.5% drift, the peak moment dropped slightly from that at 3.0% story drift. The addition of a stitch at 7.5 in. from the top of the gusset plate did not prevent lateral-torsional buckling of the member and, compared to Specimen C2, it did not seem to provide a tangible improvement in the behavior (Figure 3.14). Local buckling of the channel flanges in Specimen C3 was noticed during the cycles at 3.0% and 3.5% drift. A crack was also observed in the gusset plate-channel connection (Figure 3.15a). The test was terminated due to fracture of one channel flange during the second leg of the cycle at 3.5% drift as shown in Figure 3.15b, which followed crack formation and propagation sequence similar to that in Specimen C2.

The fact that lateral-torsional buckling still occurred in Specimen C3 with a short stitch spacing of 9.0 in. indicates that there is need for additional lateral bracing to the built-up member near the plastic hinge region. Thus, the double channel member in Specimen C4 was laterally supported at the location of the first stitch, as shown in Figure 3.7. Note that the first stitch was welded to the double channel member but not to the accompanying lateral support system (two tubes on each side of the double channel member), which allowed the stitch move freely in-between the two tubes. As in Specimens C2 and C3, Specimen C4 showed no deterioration of strength up to the second cycle at 3.0% story drift (Figure 3.10d). At that stage, slight local buckling in the channel flanges was observed, and failure due to channel fracture occurred during the third cycle of 3.0% story drift (Figure 3.16). It was found that use of additional lateral support at the location of the first stitch was very effective in preventing lateral-torsional buckling of the member.

In Specimen C5, the effect of providing a rounded web cut-out to reduce concentration of stresses in the channel flanges, and thus to delay fracture was evaluated. Specimen C5 exhibited an almost identical behavior compared to Specimen C4 (Figure

3.10e), sustaining one additional cycle to 3.0% drift before failure of the specimen, which occurred during the fourth cycle of 3.0% story drift and was preceded by severe buckling of the channel flanges (Figure 3.17). In Specimen C6, a modified web cut-out detailing was used, and reinforcing plates were added to the channel flanges to strengthen the member in the connection region (Figure 3.9). The modification of the web cut-out consisted of a reduction in the cut size compared to that in Specimen C5, and using a trapezoid-shaped cut-out (Figure 3.9) in order to reduce concentration of stresses in that region. Specimen C6 was cycled five times at 3.0% drift with no decay in strength. Thus, additional cycles were applied at 3.5% drift, and failure occurred due to fracture of a channel flange, in the region where local buckling had concentrated during the second negative loading half-cycle at that drift level (Figure 3.18). Based on the results of Specimens C4 thru C6, it is clear that providing a lateral support at the end of the plastic hinge region is required in order to prevent lateral-torsional buckling of double channel built-up members subjected to large inelastic rotations. Further, for double channel members subjected to large reversals of rotation, a combination of a trapezoid-shaped web cut-out and plates reinforcing the channel section at the end of the gusset plate is an effective means to reduce concentration of stresses and prevent premature fracture in the member-to-gusset plate connection region.

3.3.2 Specimen C7 with Innovative Reinforcing Method

Specimen C7, having the same configuration as that of Specimen C6 (double channels $\mathrm{C}10\times25, F_y = 50\ \mathrm{ksi}$) but with an innovative reinforcing method, as discussed in Ekiz et al. (2004), is shown in Figure 3.19. As in Specimen C6, trapezoid-shaped cut-out in the webs of the double channels was used and the channels were welded to a $10'' \times 24'' \times 1\frac{1}{4}''$ gusset plate. Unlike Specimen C6, Specimens C7 was reinforced with four layers carbon fiber fabric (or CFRP) with an ultimate tensile strength of 550 ksi and ultimate strain of 0.015. The fabric was attached at the bottom portion of the channel flanges by epoxy in an attempt to prevent stress concentration in the welded area. The four layers of the carbon fabric had different lengths, thus smoothening the force transfer between steel and the fabric reinforcement. Epoxy was applied to each layer of the carbon fabric, rendering them firmly attached to the flanges. The details of the carbon fabric reinforcement are shown in Figure 3.19b.

Strain gauge data showed that the double channels and carbon fabric were essentially elastic before cyclic displacement reached 0.75% story drift. The epoxy at the location where the first layer of the fabric meets the channel flange started to peel off during the first cycle of 0.75% story drift. Yielding of the flanges developed outside the wrapped portion in the second cycle of 0.75 story drift. Following the spalling of epoxy, the fabric gradually debonded. The ends of the first layer debonded when the displacement reached the third cycle of 1% story drift. Yielding of the steel was shifted to the upper portion of the double channels, basically beyond the wrapped flange parts. However, after debonding of the fabric had started, yielding of the steel started to move down and extended into the lower portion of the specimen. The plastic hinge developed during 1.5% story drift at a distance about 10 inches from the bottom. Evident local buckling occurred after 3% story drift (Figure 3.20a). Channel flanges exhibited significant local bucking after the carbon fabric came off. Gusset plate did not show any yielding throughout the test.

The load-displacement (story drift) response of Specimen C7 is shown in Figure 3.21. As can be seen, the specimen exhibited stable hysteretic loops, signifying large energy dissipation. Moreover, it shows no deterioration of strength until the third cycle of 3.5% story drift. The wrapping in one flange totally came off during the third cycle of 3.5% drift (positive loading direction), resulting in loss of confinement. As a consequence, the flange without wrap fractured in the succeeding cycle (the third cycle of 3.5% drift, negative loading direction). It should be noted that no lateral torsional buckling occurred in this specimen.

3.3.3 Comparison between Specimens C5, C6, and C7

Specimen C5 has identical configuration with that of Specimen C6 and C7 except that no reinforcement was used on the channel flanges in the region of plastic hinge. Specimen C7 and C6 have identical configurations except the scenarios used for reinforcing the channel flanges in the plastic hinge and connection region. The comparison of load-displacement behavior between the three specimens is shown in Figure 3.22. It is noted that Specimen C5 failed due to fracture during the forth cycle of 3% story drift, whereas Specimen C7 did not fail until the third cycle of 3.5% story drift. Figure 3.22 shows that Specimens C6 and C7 had excellent and almost identical energy-dissipation capacity. Both specimens reached 3.5% story drift. As seen in Figure 3.23, Specimens C6 and C7 outperformed Specimen C5 in terms of the cumulative energy dissipation capacity.

3.4 Rotation Capacity and Design Recommendations

Table 3.2 gives the maximum achieved plastic rotations as well as the cumulative plastic rotations of all test seven specimens. The maximum plastic rotation was calculated by dividing the peak tip displacement before fracture by the distance from the loading point to the center of plastic hinge (it is approximately 56 in. for Specimen C1 and 52 in. for all the other specimens), minus the elastic rotation (which is approximately 0.015 rad.).

It is seen that reducing the stitch spacing and unbraced length (Specimens C2 and C3) significantly increased the rotation capacity as well as the cumulative plastic rotation, which eliminating lateral-torsional buckling of individual channels and delaying lateral-torsional buckling of the overall member. Member rotation capacity and cumulative plastic rotation was further enhanced by adding a lateral support in the plastic hinge region, which totally prevented lateral-torsional buckling of the member. Table 3.2 also gives the unsupported length, $L_b / \left(E / F_y\right) r_y$, for both individual channel and entire built-up member. Based on this observation, Parra et al. (2006) proposed a design equation for the unsupported length of individual channels of built-up members subjected to large reversals of rotations (*i.e.*, stitch spacing):

$$L_{pdi} = 0.04 \left(\frac{E}{F_y}\right) r_y \tag{3.3}$$

Note that for double channel built-up members requiring at least 0.06 rad plastic rotation capacity, a lateral support should also be provided in the region adjacent to the plastic hinge in order to prevent lateral-torsional buckling. Lateral bracing outside the plastic hinge region can be provided according to Eq. (3.1)

3.5 Modeling of The Moment-Rotation Relationship

In order to perform nonlinear static and dynamic analyses of STMF, the relationship of moment and rotation of the chord members is needed. Since all the hysteresis curves (Figure 3.10, Figure 3.21) show similar backbone curve, the backbone curve of moment-rotation relation of Specimen C6 was chosen for the model curve. As shown in Figure 3.24, a bilinear curve was adopted to represent the backbone curve. The first line extends up to the expected plastic moment, $R_y M_p$, and the second line, with a slope approximately 10% of the first line, accounts for strain-hardening. It is noted that the strain-hardening ratio, $\eta = 10\%$, is the same as that observed by Basha and Goel (1994) for double angle built-up members.

Table 3.1 Properties of test specimens

		Channel	**Stitch Spacing (in.)**	L_b **(member) (in.)**
Specimen	C1	2-C12x20.7	30	56
	C2	2-C10x25	13.75	42
	C3	2-C10x25	9	42
	C4	2-C10x25	9	7.5(in plastic hinge region)
	C5*	2-C10x25	9	7.5(in plastic hinge region)
	C6*,**	2-C10x25	9	7.5(in plastic hinge region)
	C7*,***	2-C10x25	9	7.5(in plastic hinge region)

*** With Web-cutting**

**** Flange reinforced with** $6''\times 5''\times 1/2''$ **plates in the plastic hinge region**

***** Flange reinforced with 4 layers of Carbon Woven Mesh plates in the plastic hinge region**

Table 3.2 Rotation capacity of test specimens

Specimen	$\dfrac{L_b(\text{channel})}{(E/F_y)r_y}$	$\dfrac{L_b(\text{member})}{(E/F_y)r_y}$	**Maximum Plastic Rotation (rad.)**	**Cumulative Plastic Rotation (rad.)**
C1	0.065	0.063	0.02	0.35
C2	0.035	0.051	0.05	1.10
C3	0.023	0.051	0.05	1.06
C4	0.023	0.009	0.06	1.14
C5	0.023	0.009	0.06	1.31
C6	0.023	0.009	0.07	1.83
C7	0.023	0.009	0.07	1.90

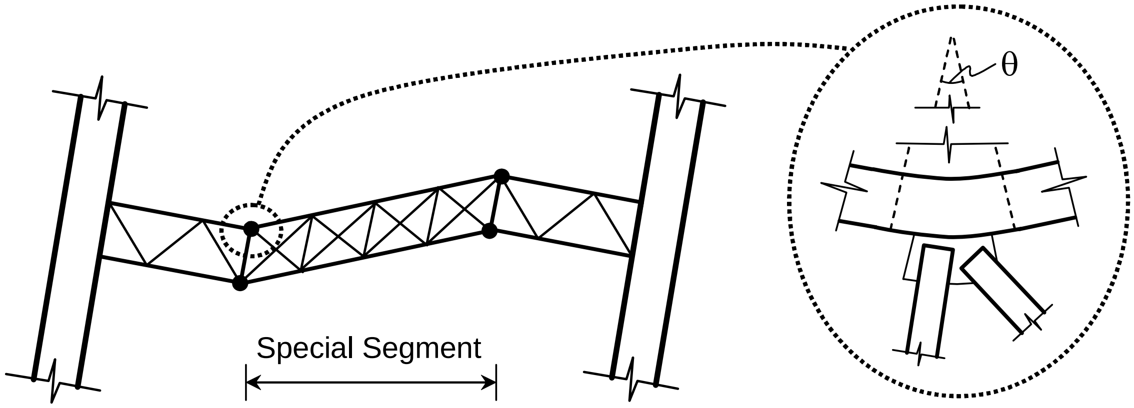

Figure 3.1 Plastic rotation in chords of special segments in STMFs (Parra et al., 2006)

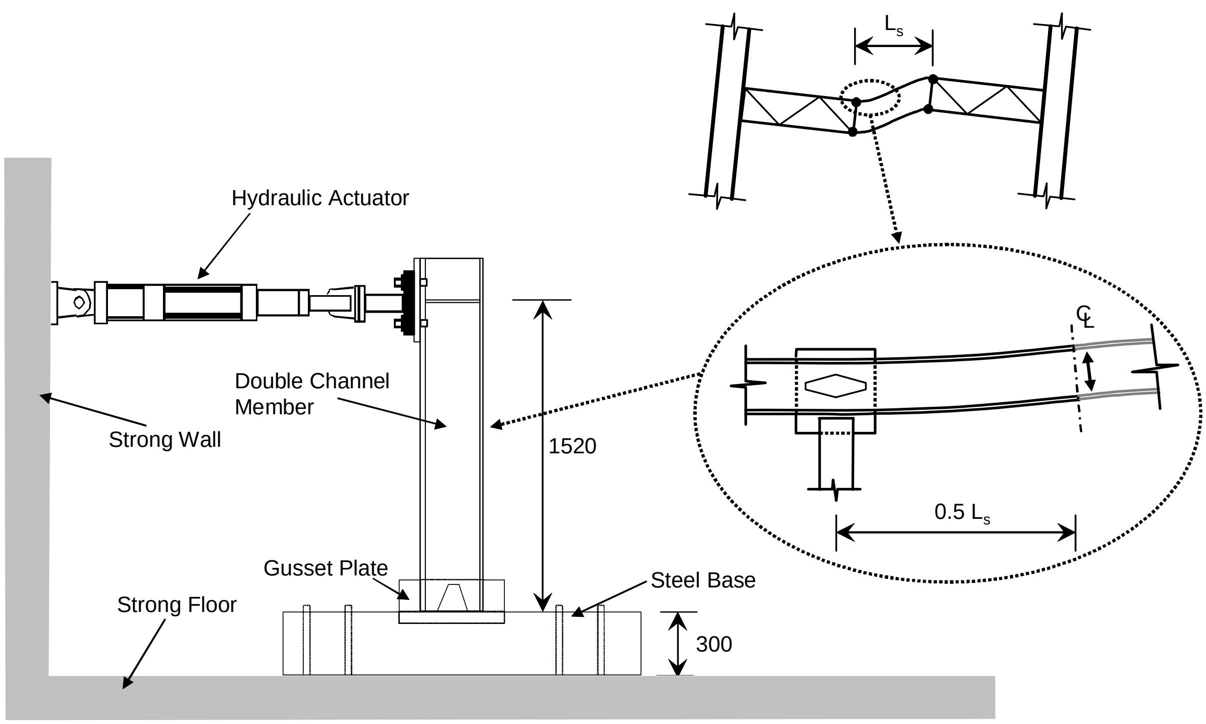

Unit: mm

Figure 3.2(a) Test setup (Parra et al., 2006)

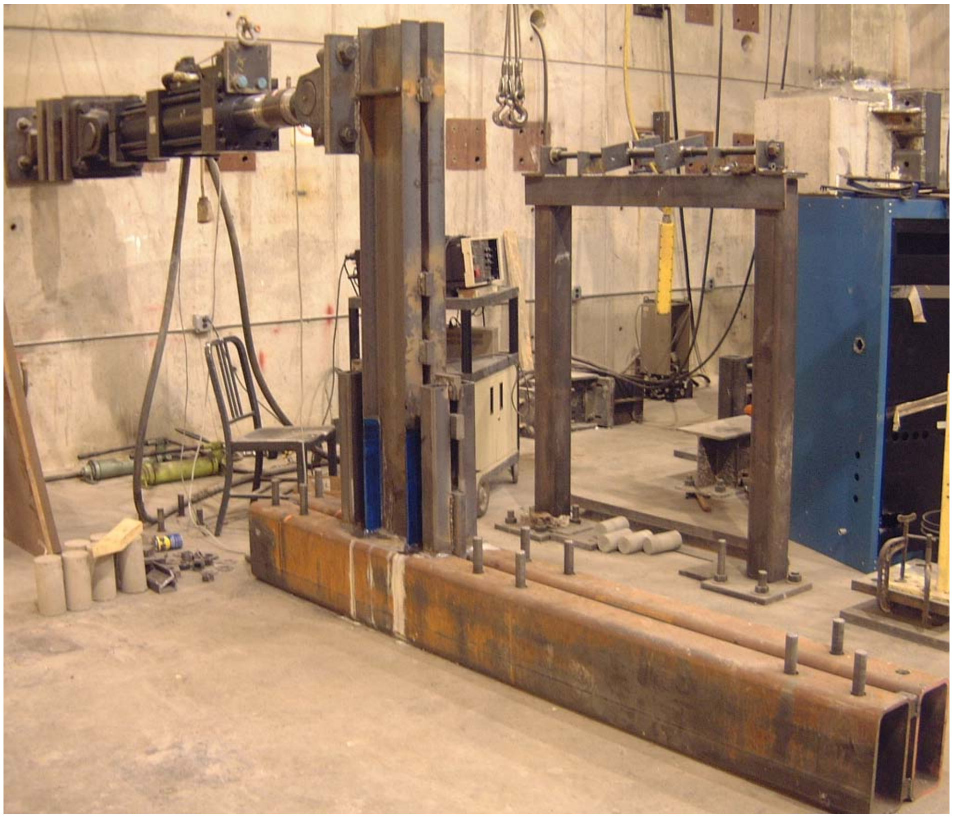

Figure 3.2(b) Overall view of test setup and test specimen

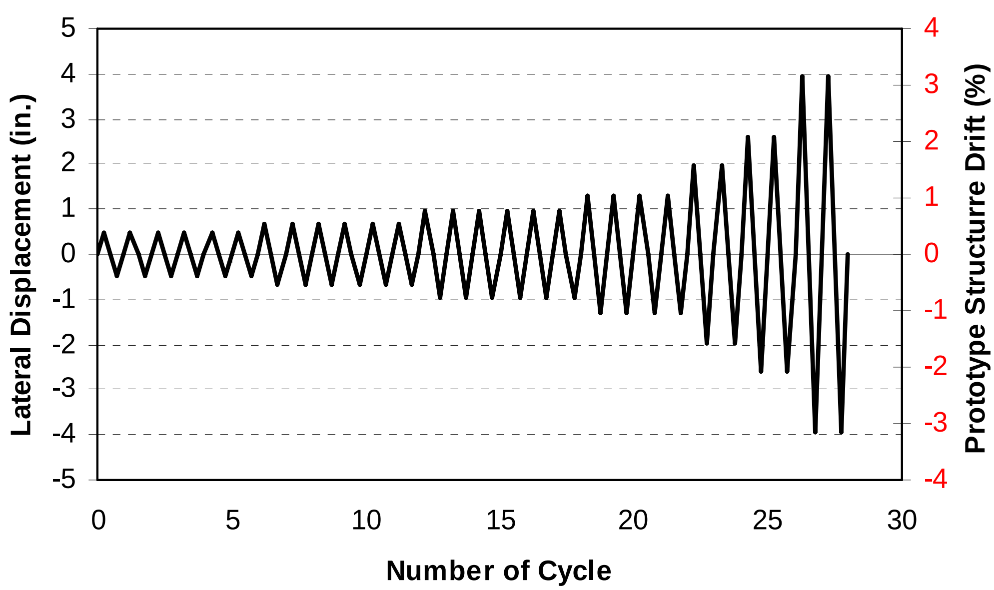

Figure 3.3 Loading protocol

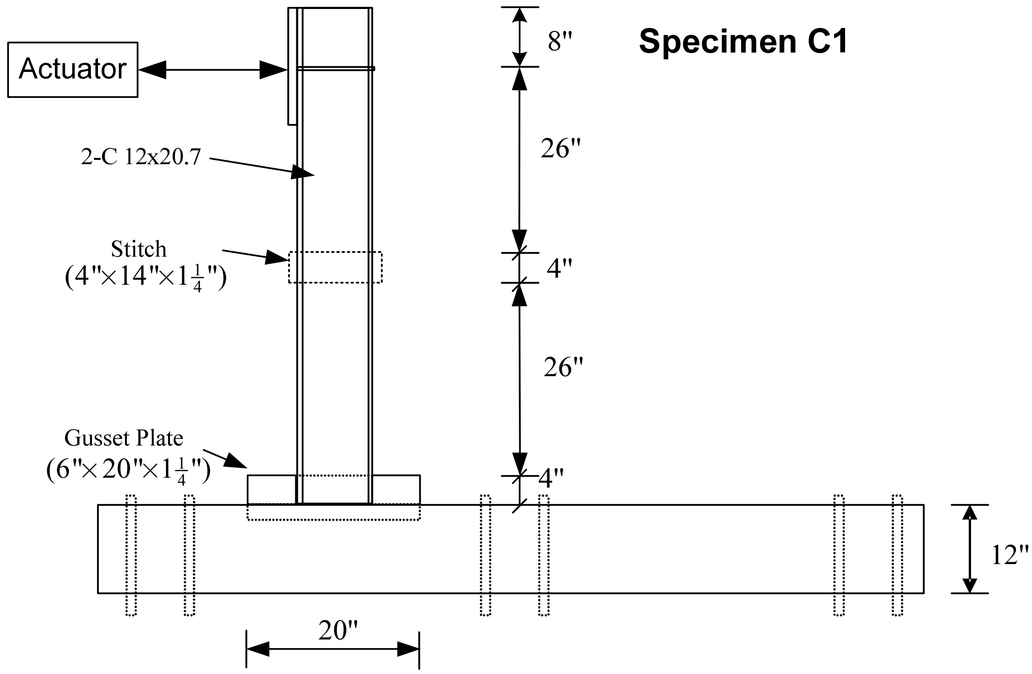

Figure 3.4 Detail of Specimen C1

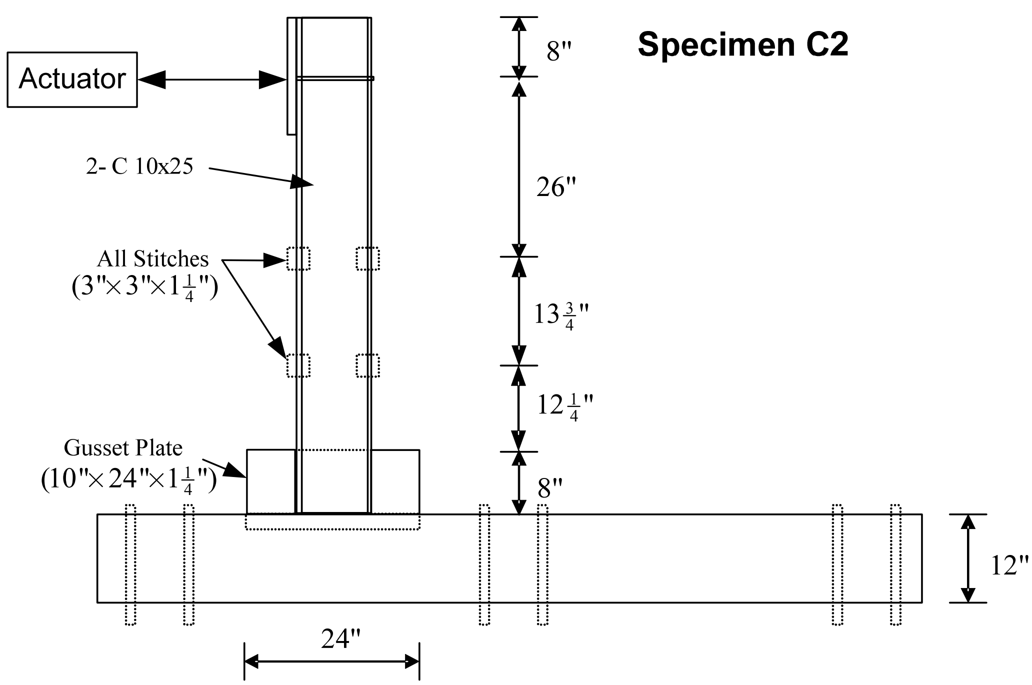

Figure 3.5 Detail of Specimen C2

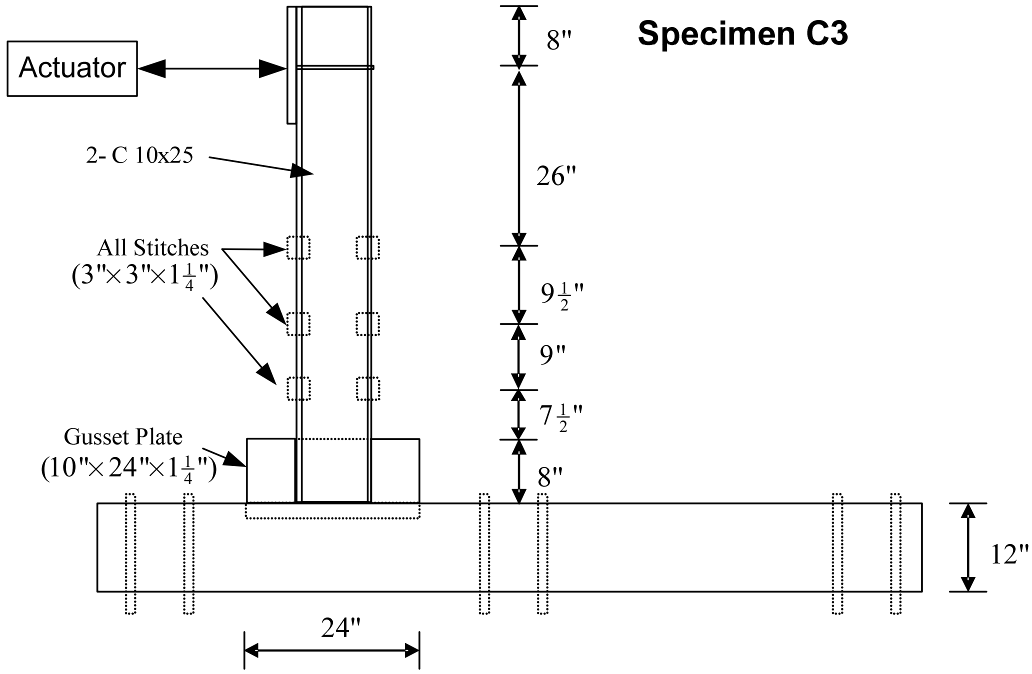

Figure 3.6 Detail of Specimen C3

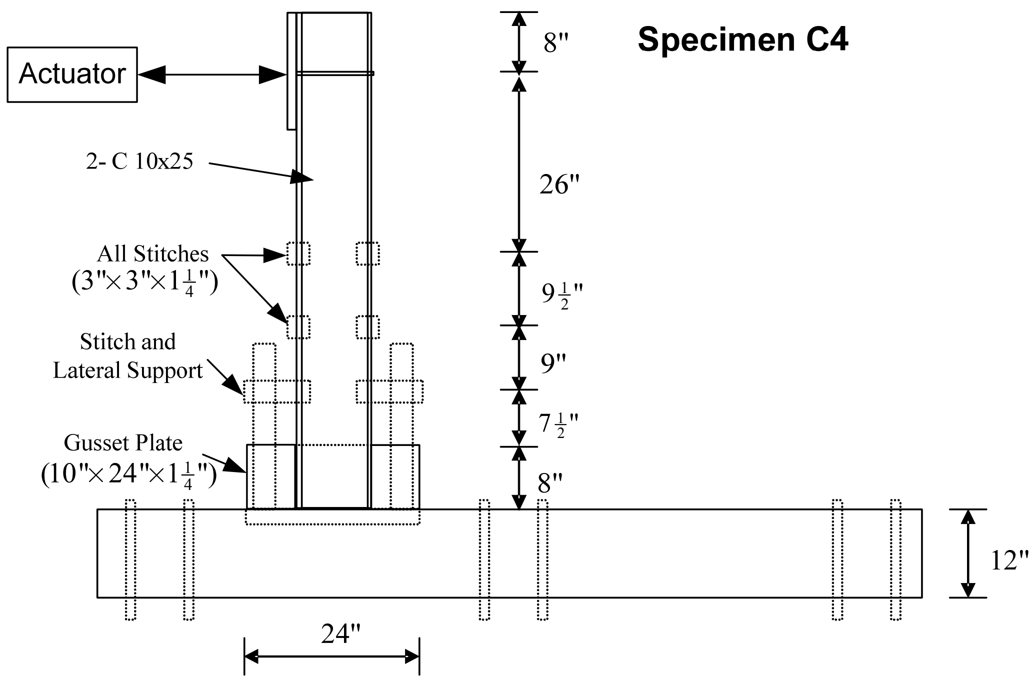

Figure 3.7 Detail of Specimen C4

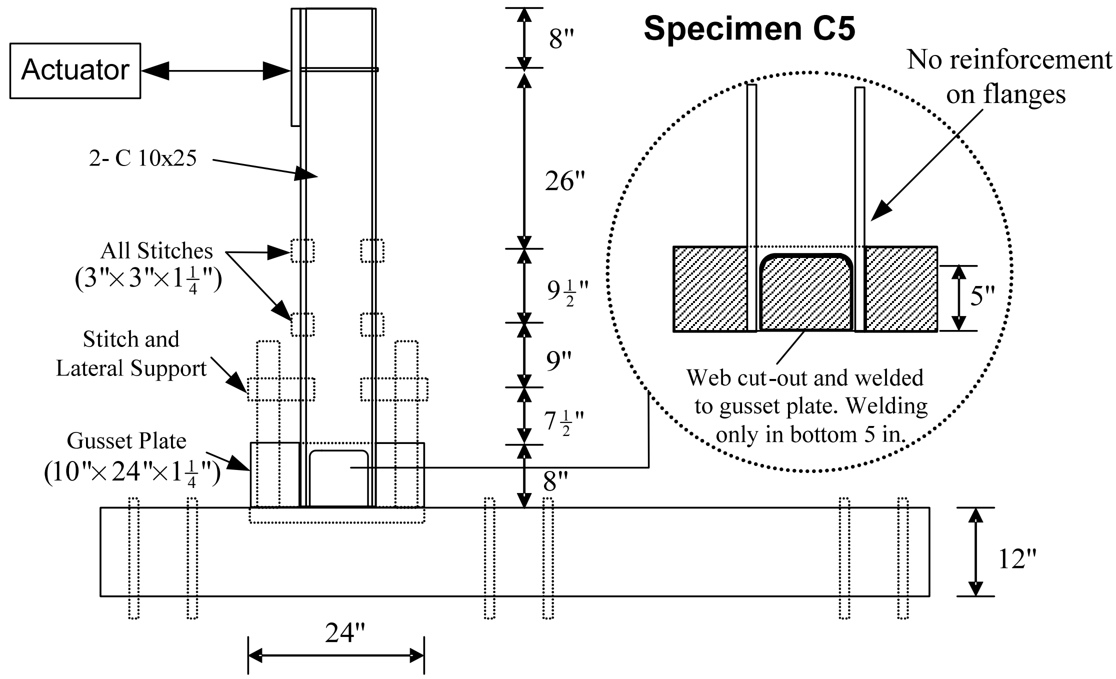

Figure 3.8 Detail of Specimen C5

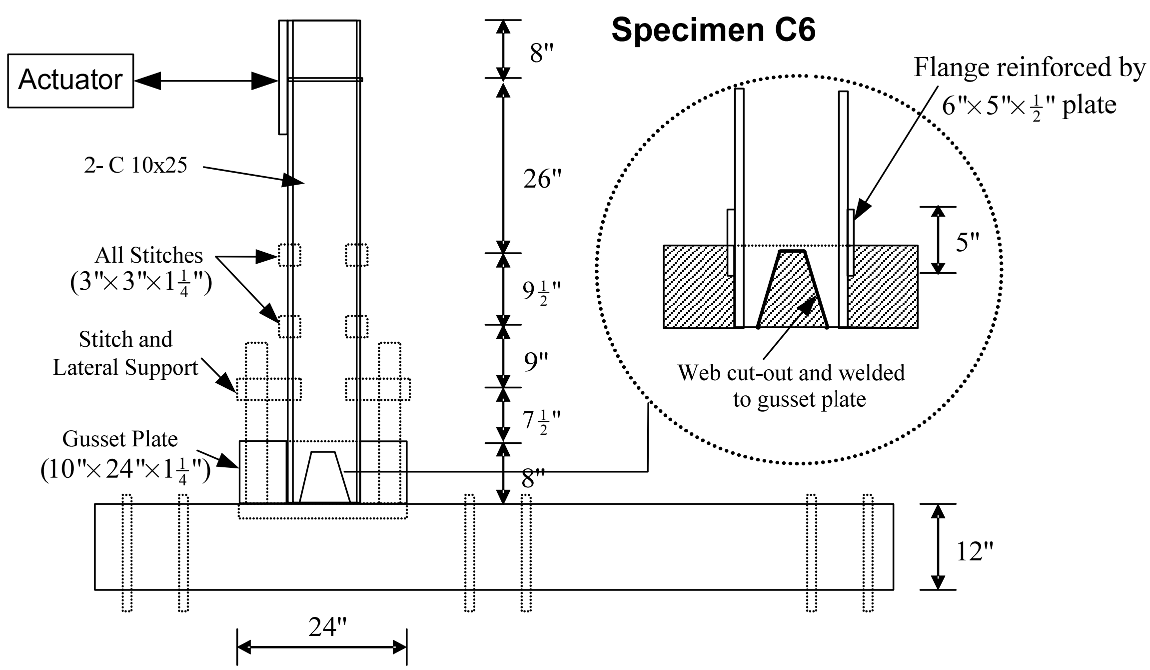

Figure 3.9(a) Detail of Specimen C6

Figure 3.9 (b) Welding detail of Specimen C6

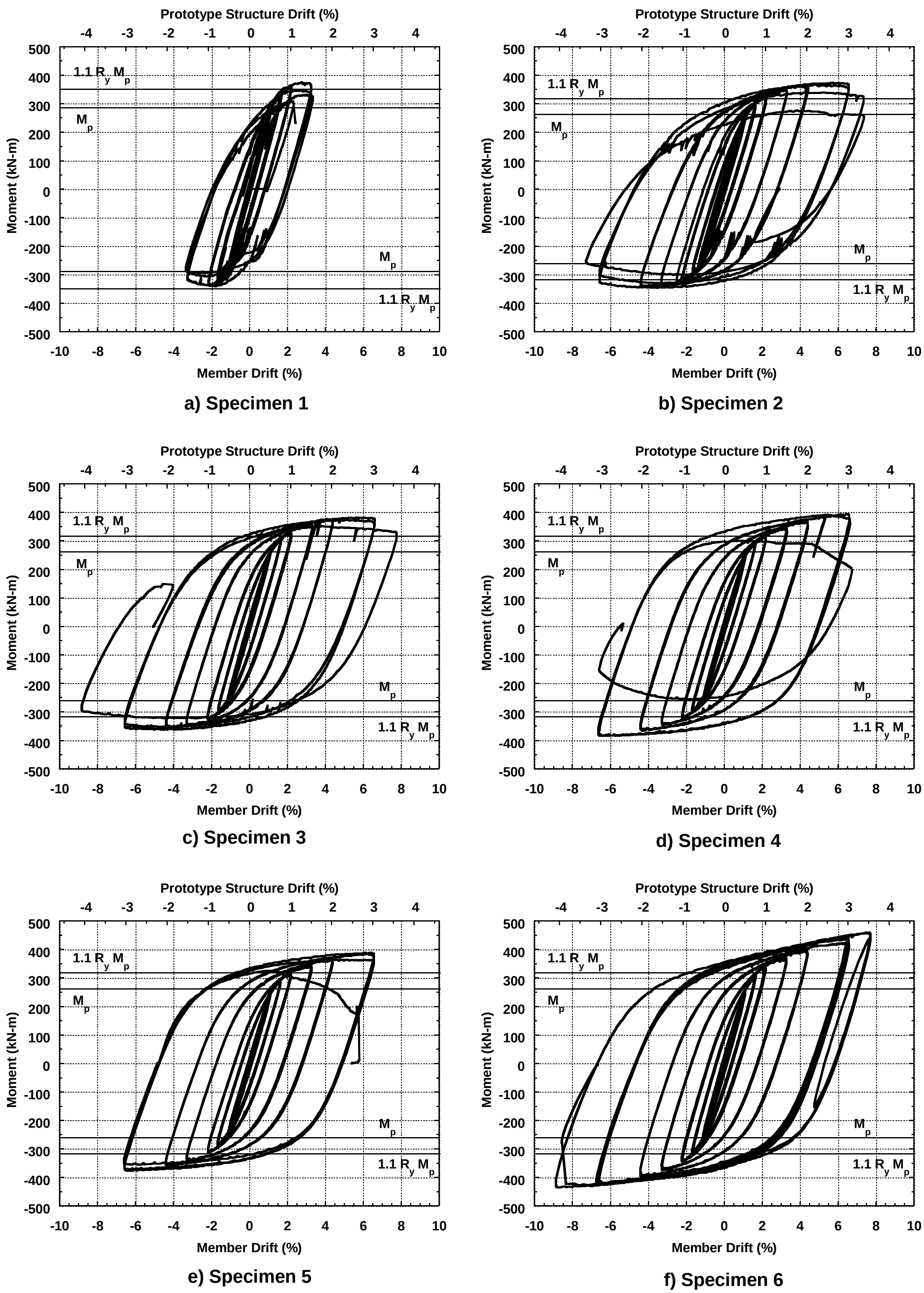

Figure 3.10 Moment versus drift response of Specimens C1-C6 (Parra et al., 2006)

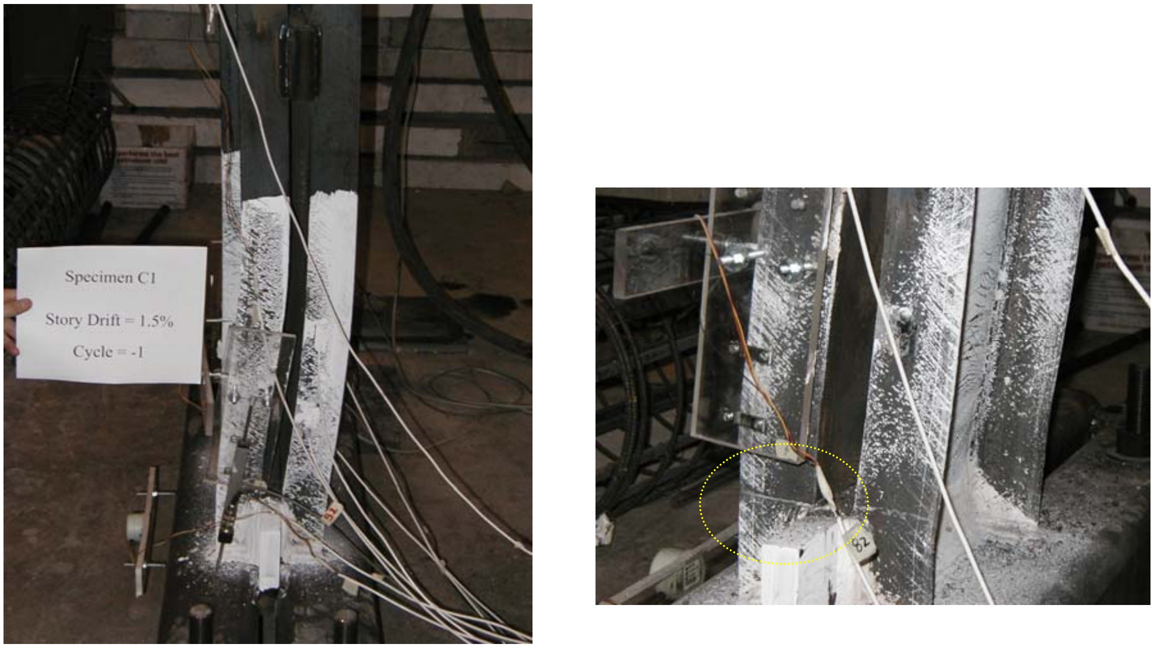

(a) (b)

Figure 3.11 (a) Lateral-torsional buckling in Specimens C1 at 1.5% story drift; (b) Fracture of the channel leg in Specimen C1

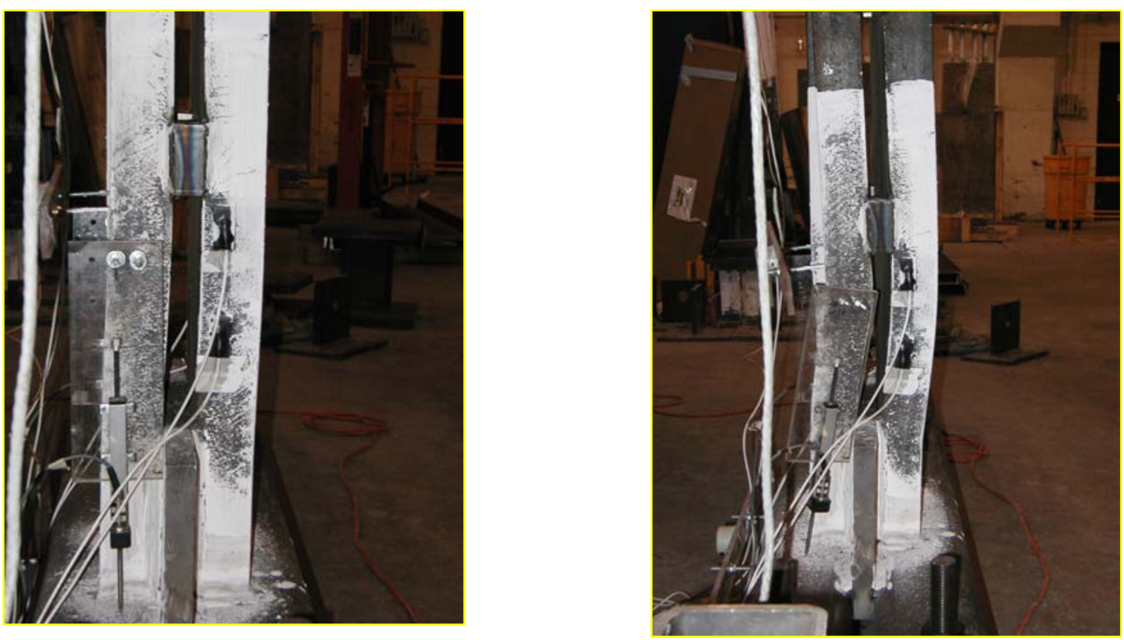

(a) (b)

Figure 3.12 Lateral-torsional buckling in Specimens C2 at (a) 1.5% story drift; (b) 3.0% story drift

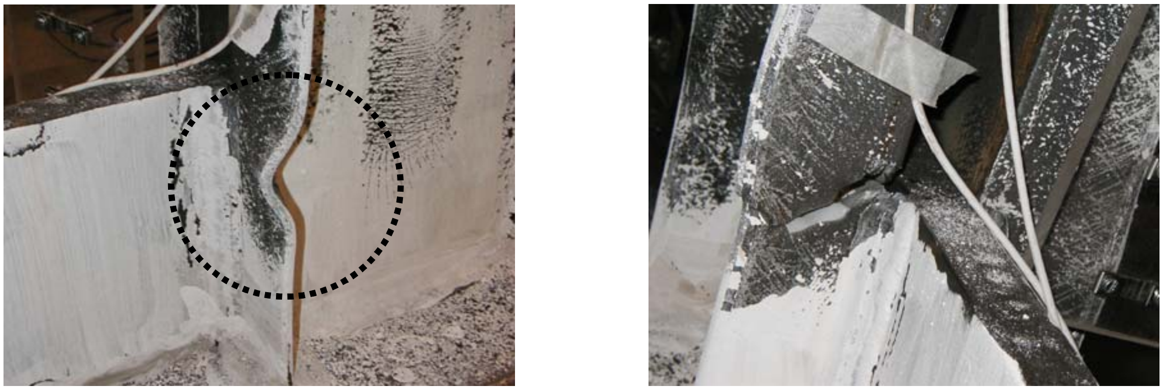

a) Channel Flange Local Buckling b) Channel Fracture

Figure 3.13 Local buckling and fracture in Specimen C2

(a) (b)

Figure 3.14 Lateral-torsional buckling in Specimens C3 at (a) 1.5% story drift; (b) 3.0% story drift

(a) (b)

Figure 3.15 (a) Cracking of gusset plate-channel connection and (b) fracture of channel in Specimen C3 during 3.5% story drift cycle

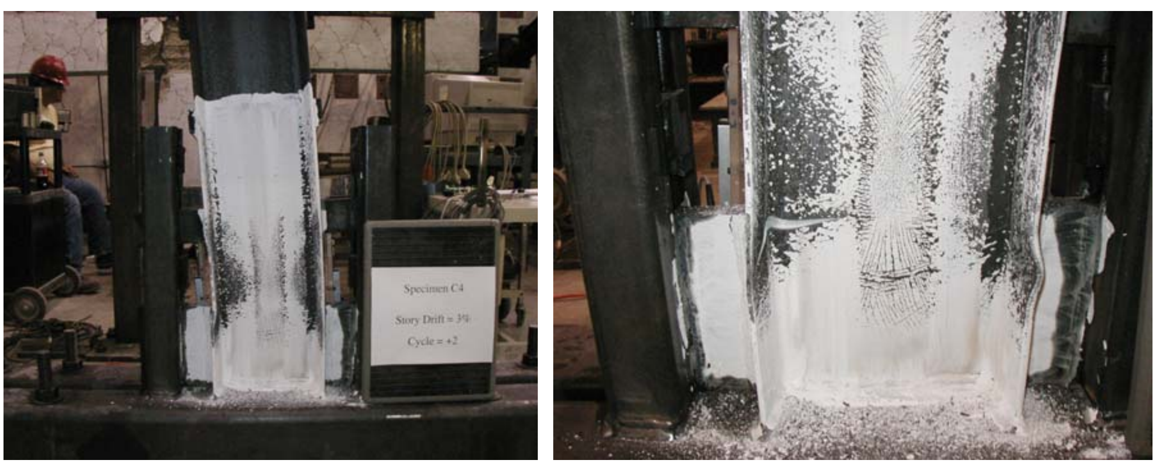

(a) (b)

Figure 3.16 Specimen C4: (a) Yielding pattern and local buckling at the second cycle of 3.0% story drift; (b) Fracture of channel during the third cycle to 3.0% story drift

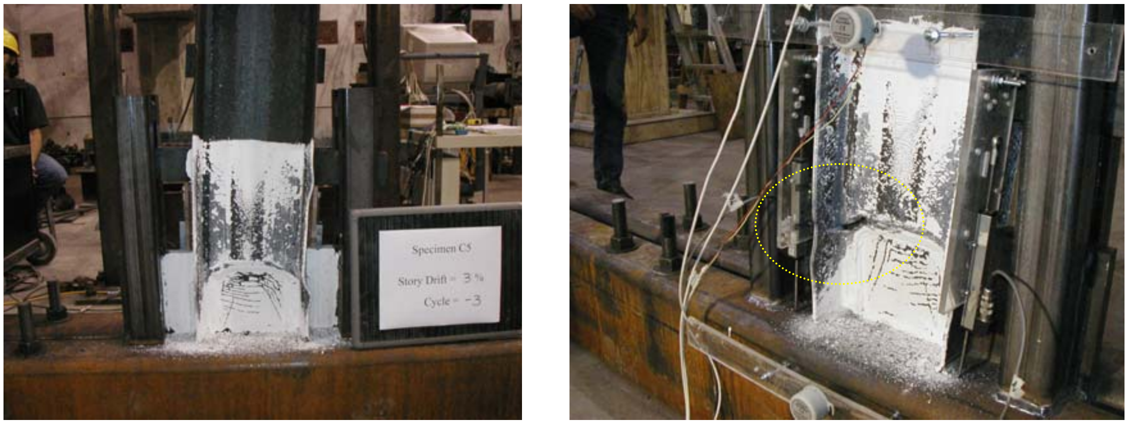

(a) (b)

Figure 3.17 Specimen C5: (a) Yielding pattern and local buckling at the third cycle of 3.0% story drift; (b) Fracture of channel during the fourth cycle to 3.0% story drift

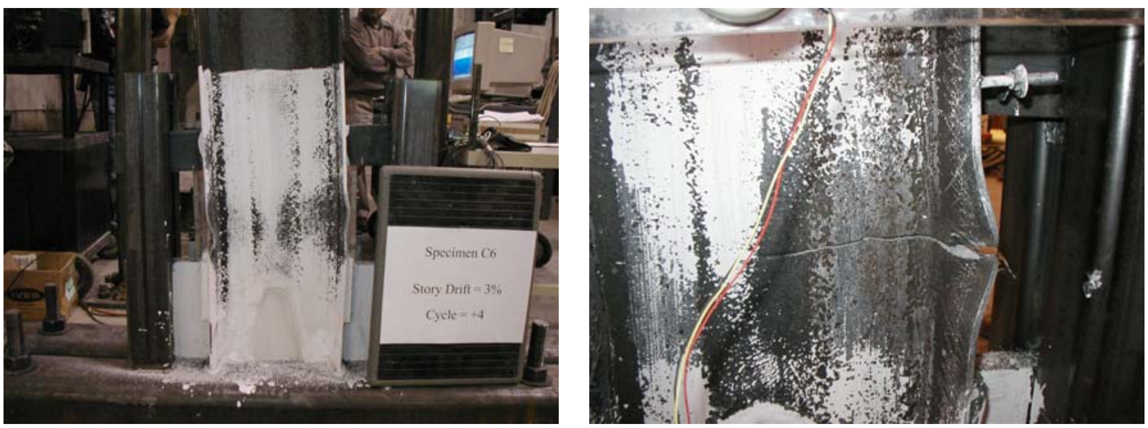

(a) (b)

Figure 3.18 Specimen C6: (a) Yielding pattern and local buckling at the fourth cycle of 3.0% story drift; (b) Fracture of channel during the second cycle to 3.5% story drift

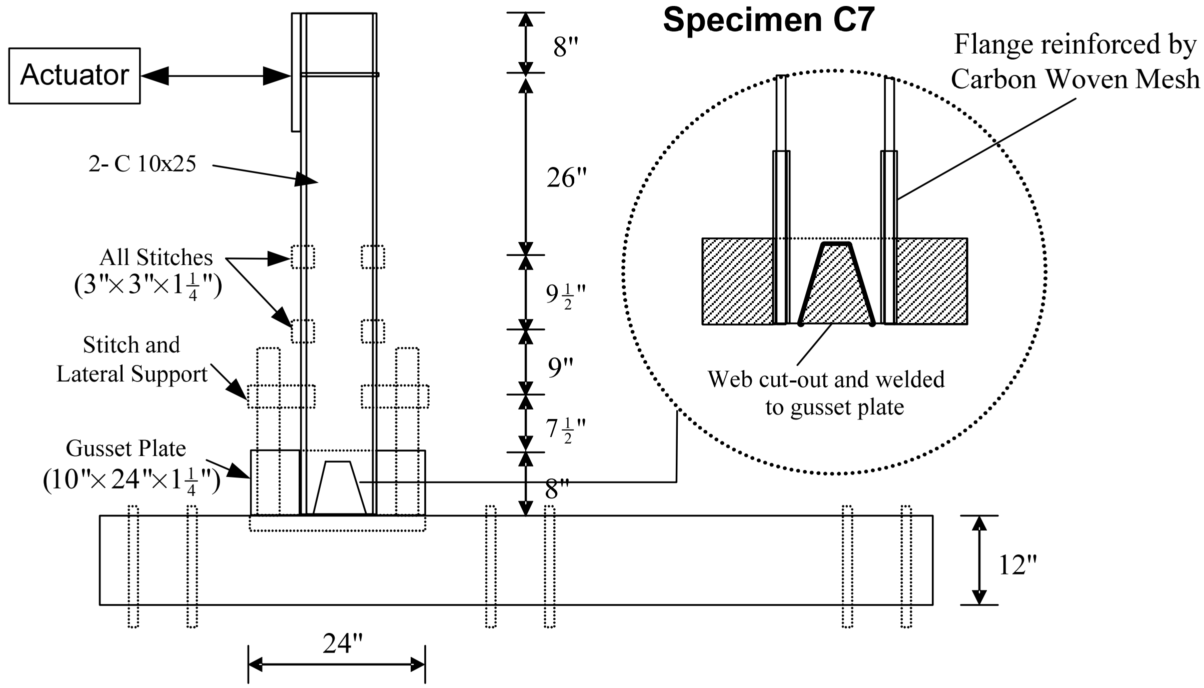

Figure 3.19 (a) Detail of Specimen C7

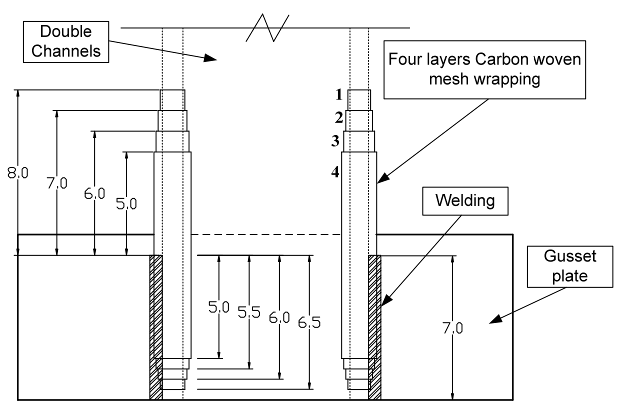

Figure 3.19 (b) Detail of the carbon woven mesh wrapping on Specimen C7 (unit: inches)

(a)

(b)

Figure 3.20 Specimen C7: (a) Yielding pattern and local buckling at the fourth cycle of 3.0% story drift; (b) Fracture of channel during the second cycle to 3.5% story drift

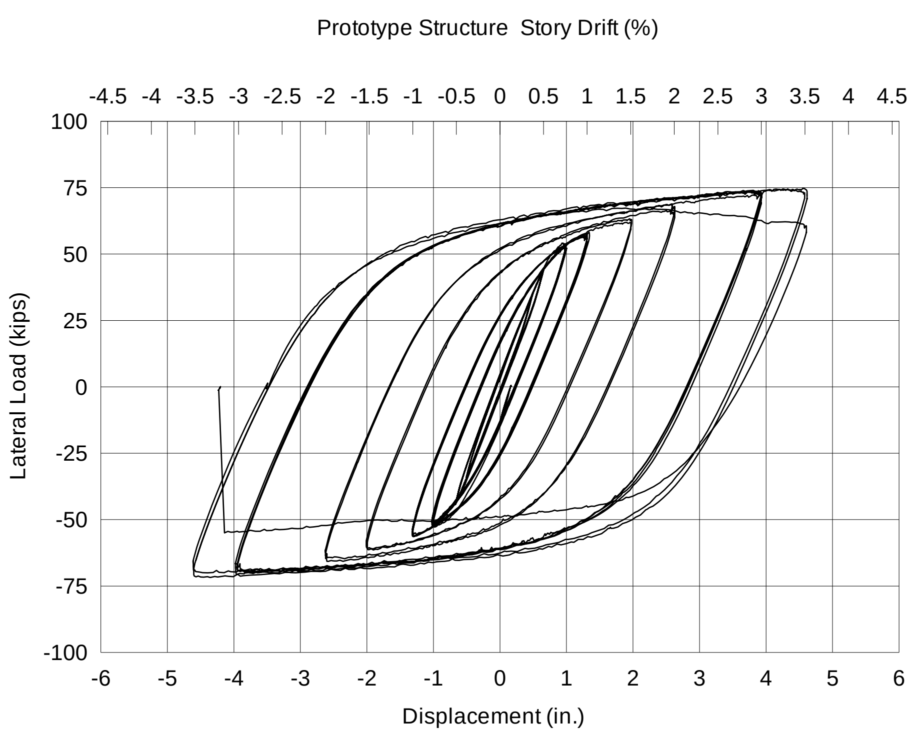

Figure 3.21 Lateral load versus story drift response of Specimen C7

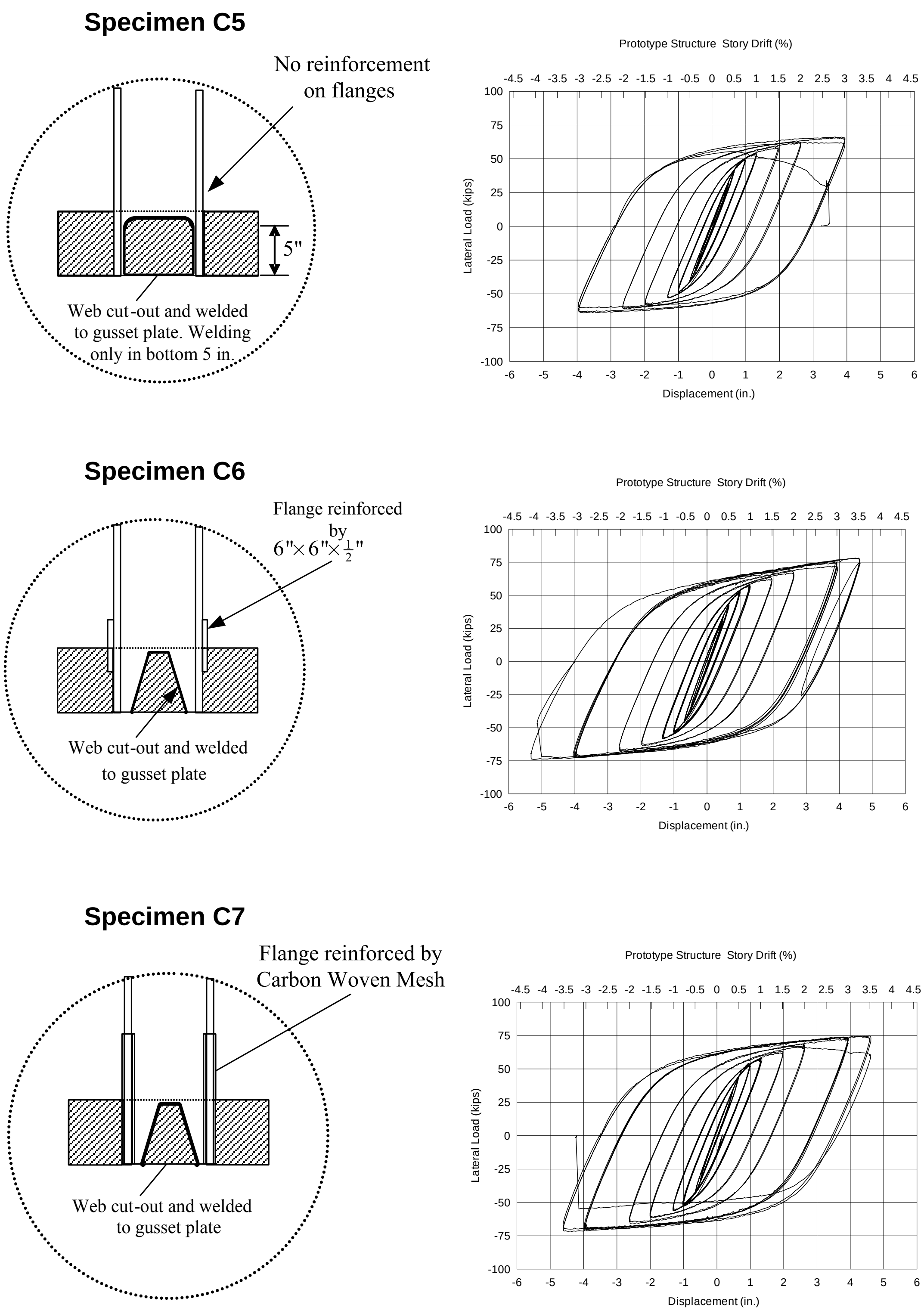

Figure 3.22 Comparison of the reinforcing details and overall cyclic performance in Specimens C5, C6, and C7

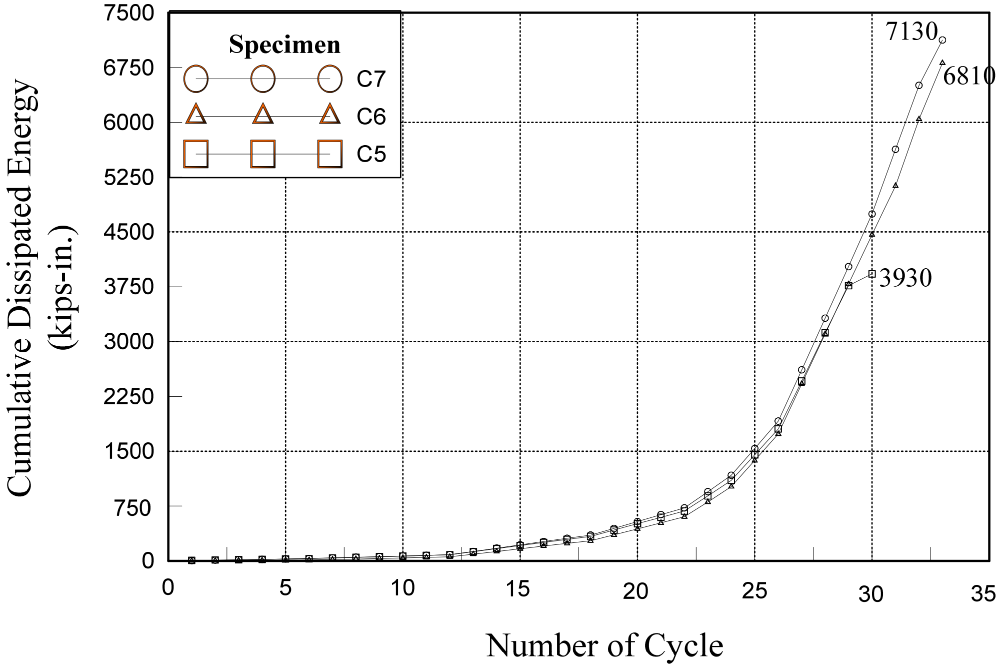

Figure 3.23 Comparison of dissipated energy in Specimens C5, C6, and C7

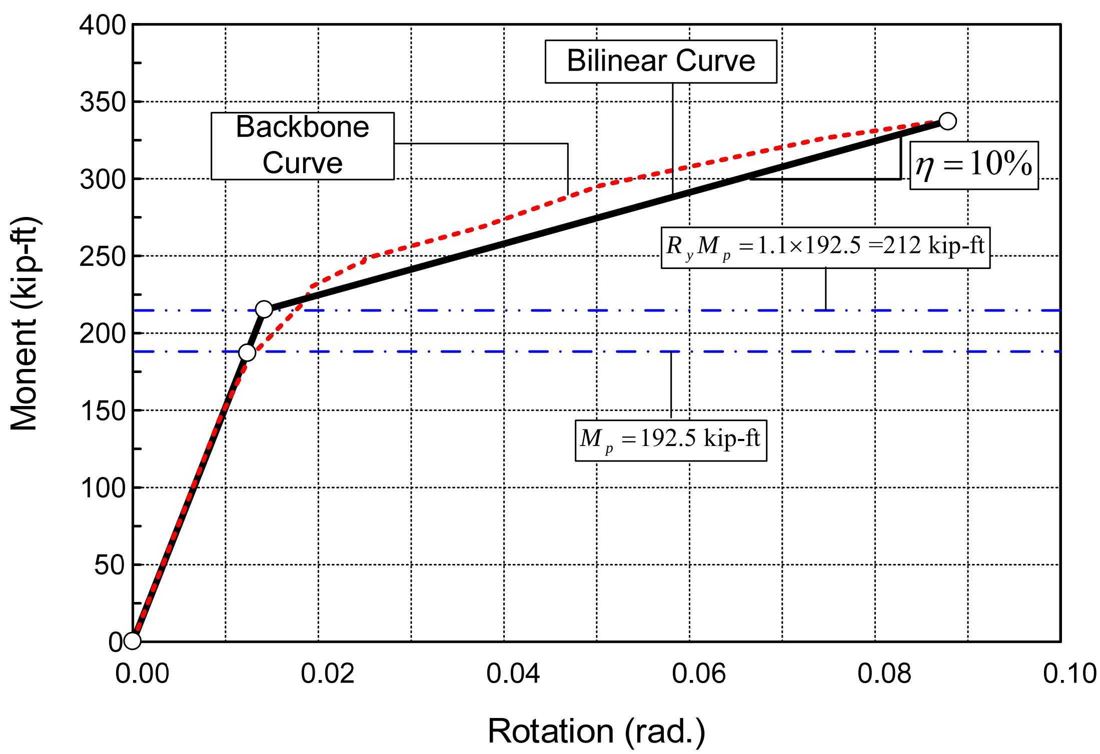

Figure 3.24 Modeling of the backbone curve of Specimen C6 using bilinear curve

CHAPTER 4

First Phase Investigation

4.1 Introduction

The first phase investigation focused on determining the design parameters for the proposed performance-based design methodology as described in Chapter 2. A 7-story STMF was selected and designed according to the proposed procedure. The structural performance under seismic excitation was evaluated through nonlinear static and dynamic analyses. Design parameters were then refined based on the results. The main issues investigated are:

1. Design yield drift ratio.
2. Maximum developed shears in the special segments.
3. Plastic hinge rotation demand in chord members.
4. Story drift ratio.
5. Lateral force distribution.
6. Axial forces in the chord members.

4.2 Prototype Structure

The prototype structure is a hospital building with perimeter STMFs as shown in

Figure 4.1. A Vierendeel special segment was used and typical truss elevation is shown in Figure 4.2. Figure 4.3 shows the overall profile of the study 7-story STMF. The bases are rotation fixed by providing grade beams. All truss members are double channels oriented back-to-back. Cover plates were used to increase the strength of the chord members outside the special segment in order to confine the inelastic activity within the special segment.

The first STMF (called STMF-1) was designed in accordance with California Building Code (CBC, 2001) design spectrum, which represents a maximum probable ground motion having a 10 percent probability of being exceeded in 50 years (statistical return period = 475 years). Corresponding floor weights and design parameters are summarized in Tables 4.1 and 4.2, respectively. It should be noted that since STMF system is inherently quite redundant (four plastic hinges in one truss girder), no redundancy factor was used to further increase the design force.

Concentrated gravity loads from cross beams are not permitted to be applied within the special segments. If needed, header beams can be used to transfer any such loads to the ends of special segments. Elements outside the special segments were designed to remain elastic for the combination of the factored gravity loads and lateral forces that are necessary to develop the maximum expected nominal shear strength of the special segment in a fully yielded and strain-hardened state (see Figures 2.9 thru 2.11). The factored gravity loads were determined by:

$$1.2DL+0.5LL \tag{4.1}$$

In this study (exterior truss loading condition):

Slab dead load = 100 psf$\times$ 6'(5'interior tributary and1'edge condition) = 0.6 klf

Slab live load = 100 psf$\times$ 6'(5'interior tributary and1'edge condition) = 0.6 klf

Curtain wall dead load = 75 psf (precast)$\times$16'= 1.2 klf

Therefore DL = 1.8 klf and LL = 0.6 klf,

The modified design base shear based on the proposed performance-based plastic design procedure, and the target drift of 2%, was obtained by following Eq. (2.14) and Figure 2.12. The corresponding design parameters are shown in Table 4.3. Table 4.4 gives the design lateral force at each level of the frame. It is noted that, in this initial study, the yield drift was assumed as 1% and the shear distribution factor , β_i , was the same (equal to 0.5) as the one previously derived for moment frames Lee and Goel, 2001). That is (see Eq. (2.1) for comparison):

$$\beta_i = \frac{V_i}{V_n} = \left(\frac{\sum_i^n w_i h_i}{w_n h_n} \right)^{0.5T^{-0.2}} \tag{4.2}$$

The expected maximum vertical nominal shear strength of the special segment V_{ne} used for design of elements outside the special segments according to AISC Seismic Provision (AISC, 2005) Eq. (12-1) is:

$$V_{ne} = \frac{3.75R_y M_{nc}}{L_s} + 0.075E_s I \frac{(L - L_s)}{L_s^3} + R_y (P_{nt} + 0.3P_{nc}) sin\alpha \tag{4.3}$$

The resulting sections for special segments, truss members and columns are shown in Figures 4.4 and 4.5.

4.3 Modeling for Nonlinear Analyses

In order to investigate the behavior of the study building under major earthquakes, nonlinear static push-over and time-history dynamic analyses were conducted by using Perform-2D (RAM, 2003) program. Selected SAC Los Angeles ground motions with 10 percent probability of exceedance in 50 years were used as the input earthquake records.

4.3.1 Modeling of STMF Components

4.3.1.1 Force-Deformation Relations and Component Models

In Perform-2D, the relation between moment and rotation of an element entering inelastic range is modeled by a rigid-plastic moment hinge, which is analogous to a friction hinge that rotates only after enough moment has been applied to overcome the friction between the hinge pin and the casing. Figure 4.6 shows a hinge and corresponding moment-rotation relationship. This hinge is initially rigid, and begins to rotate at the yield moment (M_y). The moment increases after yield moment is reached if strain-hardening is taken into account. The maximum moment which a rigid-plastic moment hinge can achieve is designated as M_u . All members were modeled as beam-columns and axial force-plastic moment surfaces are shown in Figure 4.7. For a typical I section, the *P-M* yield surface is close to the dashed curve shown in Figure 4.7 (Chen and Han, 1988). In this study, the double channel (back-to-back) sections were assumed to have *P-M* relations as for I sections. In general, the dashed curve shown in Figure 4.7 can be expressed as:

$$\left(\frac{P}{P_y}\right)^{\alpha} + \left(\frac{M}{M_p}\right)^{\beta} = 1.0 \tag{4.4}$$

where P = axial force, M = bending moment, P_y = yield force at $M = 0$, and M_p = yield moment at $P = 0$. Minimum values of $\alpha = 1.5$ and $\beta = 1.1$ suggested by Perform-2D (RAM, 2003) were used in this study for both I sections and double channel sections. It is noted that when $\alpha = 1.0$ and $\beta = 1.0$, the *P-M* relation will become linear as that for a sandwich section shown in Figure 4.7.

Grade 50 steel was used for all steel sections. Assuming that the nominal axial (P_n) and bending (M_n) strengths for a column are calculated in accordance with the AISC LRFD equations, the strengths used for the *P-M* interaction are given by:

$$P_y = R_y P_n; \quad P_u = 1.1 \cdot R_y P_n \tag{4.5}$$

$$M_y = R_y M_n; \quad M_u = 1.1 \cdot R_y M_n \tag{4.6}$$

where $R_y = 1.1$ for Grade 50 steel (AISC, 2005), and the factor of 1.1 in Eqs (4.5) and (4.6) represents the strain-hardening effect.

Figure 4.8 illustrates the column models, which consist of an elastic segment, two rigid-plastic moment hinges with *P-M* interaction, and stiff end zones if needed. These models are "lumped plasticity" models, since the plastic deformations are concentrated in zero-length plastic hinges. The stiffness of the elastic segment is the initial stiffness of the member. The deformation of this elastic segment accounts for the elastic part of the total deformation. The rigid-plastic moment hinge then accounts for the plastic part of the total deformation (RAM, 2003).

Lateral bracing within special segment for top and bottom chords of truss girder were assumed to be provided according to Section 12.6 in the AISC Seismic Provisions (AISC, 2005) and the spacing satisfied Eq. (3.3). Therefore, the response of chord members in the special segment was modeled based on test results shown in Figure 3.24 and their strength can be expressed by (assuming that a plastic hinge rotation of 0.07 rad. can be achieved):

$$P_y = R_y P_n; \quad P_u = 1.5 \cdot R_y P_n \tag{4.7}$$

$$M_y = R_y M_n; \quad M_u = 1.5 \cdot R_y M_n \tag{4.8}$$

Chord members were also modeled as beam-column elements. Figure 4.9 shows the chord member model, which has similar components as the column model. Figures 4.10

and 4.11 show the models for vertical and diagonal members in the truss girder, respectively. Both were modeled as beam-column elements with similar *P-M* curves as that of the chord members. It is noted that, since a capacity design approach was used, all elements except for chord members in the special segments would generally remain elastic when subjected to a major earthquake.

4.3.2 Gravity Loads and Seismic Masses

The design gravity loads were described in Section 4.2 and a load combination of 1.2DL+0.5LL was applied to the structure during nonlinear static push-over and time-history dynamic analyses. Both $P-\Delta$ and $P-\delta$ effects of the study frames were accounted for in the analysis. However, the “leaning columns” with vertical loading from gravity frames were not included in this study since the interstory drifts were not large enough to induce significant $P-\Delta$ effect. Also, the beneficial effect of the leaning columns to provide additional lateral strength, was ignored. The seismic masses were lumped at frame joints and obtained as:

$$\begin{aligned} &\mathrm{w} = 1287 \text{ kips / (2 trusses } \times \text{ 19 joints) = 33.9 kips / joint} \\ &\mathrm{m} = 33.9 / 386.4 = 0.088 \text{ kips-sec}^2 / \text{in.} \end{aligned} \tag{4.9}$$

4.3.3 Damping

In nonlinear dynamic analysis it is common practice to use some viscous damping to account for the energy dissipation in addition to hysteretic energy. Perform-2D uses the

" $\alpha M + \beta K$ " (Rayleigh damping) model, which assumes that the structure has a constant damping matrix, [C], given by:

$$[C] = \alpha[M] + \beta[K] \tag{4.10}$$

where [*M*] is the structure mass matrix, [*K*] is the initial elastic stiffness matrix; α and β are multiplying factors. By combining αM and βK damping it is possible to have essentially constant damping over a significant range of periods, as indicated in Figure 4.12. As a structure yields it usually softens, and its effective vibration period usually increases. By using this damping model, a constant elastic damping is maintained throughout the response. In this study, a 2% of critical viscous damping was assumed.

4.3.4 Earthquake Records

Six selected 10% in 50 years (return period 474 years) and SAC Los Angeles ground motions were used for the nonlinear time history analysis. Figure 4.13 shows the design spectrum according to CBC, as well as the response spectra of selected SAC earthquake records. More detailed description of the SAC ground motions used in this study is given in Chapter 5. It is noted that the SAC ground motions were already scaled (Somerville et al., 1997) hence no further scaling was used in this study.

The effect of floor deck was neglected in the dynamic analysis as suggested by Aslani (1998). This is because the composite action deteriorates very rapidly under cyclic loading and after a few cycles the effect of composite action almost vanishes.

4.4 Analysis Results of STMF-1

Nonlinear dynamic analyses were conducted using six SAC records (10% exceedance in 50 years). Important findings are given below:

1. As shown in Figure 4.14, the pushover response indicates that the yield drift of the study 7-story STMF (about 0.5%) is much smaller than that assumed in the design (1%).

2. Figure 4.15 shows that, when the study frame was statically pushed to 2% target drift, the maximum developed shear forces in the special segments were much less than the expected shear strength V_{ne} (see Table 4.4), which resulted in very conservative sections for the elements outside the special segments. Note that the code specified shear strength was based on 3% roof drift, thus resulting in much higher expected shear strength. This finding was further confirmed by non-linear dynamic analyses, which suggested that the code expected shear force is generally 1.5 times the actually developed shear force, as shown in Figure 4.16. It is noted that the shear force developed in each special segment of the same floor level is almost identical.

3. All inelastic activity was confined to the special segments only and the maximum plastic rotation experienced by the chord members in the special segments was 0.05 radian (note the plastic rotation capacity of the double channels achieved in the UM tests was 0.07 radian). Only minor yielding occurred in the vertical members (it was found almost unavoidable in the previous experiments, Basha and Goel, 1994) and

column bases (plastic rotation is in the range of 0.001 rad.), while all elements outside the special segments remained elastic. However, as can be seen in Figure 4.17, the lower floor special segments developed much larger plastic rotation than the upper floors. Upper floor special segments did not even yield during some ground motions. This indicates that the design strength distribution of each level was not quite close to the actual seismic demand distribution, which led to uneven plastic rotation distribution along the building height. The top floor special segments were generally not utilized to dissipate earthquake energy.

4. The above observation was further confirmed by examining the dissipated energy of all elements as well as the maximum interstory distribution, as shown in Figures 4.18 and 4.19, respectively. It was observed that the inelastic dissipated energy and maximum interstory drifts were somewhat unevenly distributed along the height of the frame in the special segments; that is, special segments in the second, third, and fourth floors dissipated most of the energy and had larger interstory drifts than the other floors.

5. The maximum interstory drifts were generally within the target drift, 2%, with one exception during the La09 ground motion (see Figure 4.19b). The maximum roof drift was about 1.5%.

6. The uneven distributions of plastic hinge rotation and maximum interstory drift can be attributed to the lateral force distribution used for design, which was derived and calibrated for a limited number of ground motions by Lee and Goel (2001). Figure

4.20 gives the relative story shear distributions based on Eq. (4.2), in which the story shear, V_i, in any story is the sum of the lateral forces above that story, V_n is the story shear in the top level. By comparing with the results obtained from nonlinear dynamic analyses, it is seen that Eq. (4.2) generally overestimates the story shear demand in upper stories, which in turn results in relatively larger plastic rotation and story drift in the lower stories. An accompanying plot is the relative story shear distribution obtained from CBC lateral design force distribution formulas:

$$F_i = \left(V - F_t\right)\frac{w_i h_i}{\sum_{j=1}^{n} w_j h_j} \tag{4.11}$$

with the exception that the force at the top floor computed from Eq. (4.11) is increased by an additional force,

$$F_t = 0.07TV \qquad \text{if } \; T > 0.7 \text{ sec.} \tag{4.12}$$

$$F_t = 0 \qquad \text{if } \; T \le 0.7 \text{ sec.} \tag{4.13}$$

where F_i is the lateral force applied at level i, F_t is the additional concentrated force applied at the top floor of the structure, and n is the number of stories. The force F_t is intended to account for higher mode effects.

It is seen that the CBC distribution overestimates the story shear demands in lower stories. Therefore, a more reasonable relative story shear distribution could be, for example, the one shown in Figure 4.20, that is:

$$\beta_i = \frac{V_i}{V_n} = \left(\frac{\sum_i^n w_i h_i}{w_n h_n} \right)^{0.75T^{-0.2}} \tag{4.14}$$

Actually, Eq. (4.14) was found to work very well for eccentrically braced frames also (Chao and Goel, 2005).

7. The axial forces in the chord members of the special segments are generally small and can be ignored when designing the special segments. As shown in Figure 4.21, the ratio of maximum axial force in the special segment of a particular floor to the nominal axial strength (either tension or compression) is in the range of 0.02~0.1 (Note: the maximum axial force ratio, 0.1, only occurred in the top chord members of the top floor.). As suggested by Driscoll et al. (1965), if the axial force demand is less than 15% of the yield load, the reduced plastic moment capacity due to axial load can be neglected.

It was found from this initial study that the proposed performance-based design approach can effectively confine the inelastic behavior in the special segments only. The maximum interstory drifts were generally within the limitation specified in CBC (2%). However, the proposed relative distribution of story shears did not result in evenly distributed inelastic energy dissipation among the floors. Therefore, the interstory drifts and plastic rotations were not quite uniformly distributed either. The next stage of this study was focused on modifying the relative story shear distribution in accordance with the maximum story shear distribution obtained from the nonlinear dynamic analyses, *i.e.*, Eq. (4.14).

4.5 Second Stage Study

In the second stage of the first phase study, with some adjustment of the design parameters, which included changing the yield drift from 1% to a more realistic value of 0.75 for STMF and lateral design force distribution using Eq. (4.14), the design base shear for the revised frame turned out to be *V=0.14W* (See Table 4.5), for which much lighter sections were needed as shown in Table 4.6 and Figure 4.22. It is noted that using a yield drift equal to 0.75% is more conservative than using 0.5% yield drift. This is because a lower yield drift leads to a larger $\theta_p \left(= \text{target drift} - \text{yield drift} = \theta_u - \theta_y\right)$, which in turn results in a lower design base shear (more ductility demand, θ_p) according to Eqs. (2.14) and (2.15).

For study purposes, except for the chord members of the special segment, all other elements were kept the same as in the previous design. The re-designed frame is denoted as “STMF-2”. Nonlinear dynamic analysis results from the same six ground motions as used previously showed that:

1. As compared to STMF-1 (see Figure 4.18), the dissipated inelastic energy in STMF-2

is more evenly distributed in the special segments among floors (including the top floor), as can be seen in Figure 4.23.

2. The maximum plastic rotation is also more uniformly distributed in STMF-2 compared to that in STMF-1, as shown in Figure 4.24 (also see Figure 4.17). Because the special segments in all the floors participated in energy dissipation activity, especially in the upper floors, the maximum plastic rotation in the chord members was also reduced from 0.05 radian to 0.037 radian (La09 ground motion).

3. The maximum interstory drifts in STMF-2 are not as concentrated in lower stories as in STMF-1 and they are generally more even along the height of the frame as shown in Figure 4.25. Although lighter sections were used, the maximum interstory drift in the revised frame decreased from 2.3% in the previous design to 1.87%. The maximum roof drift was reduced to 1.44%.

4.6 Third Stage Study

In order to obtain an improved lateral force distribution wherein the energy is more uniformly distributed among the floors, a third phase of the study was performed by using the same base shear ($V=0.14W$) but with plastic design procedure and three different lateral force distributions; that is, the previously proposed lateral force distribution (Eq. (4.2), Lee and Goel, 2001), the revised lateral force distribution used in the second phase (Eq. (4.14)), and the CBC lateral force distribution (Eq. (4.11)), as shown in Figure 4.20. Only the chord members in the special segments were re-designed and all the other elements outside the special segments were kept the same as in the first stage frame. Note that the frame designed based on Eq. (4.14) is the same as that in the second stage. All the sections are summarized in Table 4.6. Results from the nonlinear static and dynamic analyses are summarized as follows:

1. It can be seen from the pushover plots (Figure 4.26) that the frame designed based on CBC distribution (STMF-2-CBC) exhibited the least overstrength relative to the design base shear, followed by the frame (STMF-2) designed according to Eq. (4.14) and then Eq. (4.2) (STMF-2-SK, most overstrength).

2. The dissipated inelastic energy in STMF-2-SK was somewhat unevenly distributed in the special segments among the various floors for all the earthquake time histories used; it was found that most energy was dissipated at the second and third floors in most cases. The dissipated energy was more evenly distributed among the floors in the STMF-2-CBC for most time-histories except for two of the ground motions, wherein the upper floors dissipated majority of the energy. In contrast, as previously mentioned, STMF-2 which was designed by the Eq. (4-14) distribution resulted in most uniform distribution of inelastic energy in the frame during all the ground motions used.

3. The middle floors of the STMF-2-SK had larger interstory drifts for all the time histories. The STMF-2-CBC exhibited more uniform interstory drifts through the entire height, with somewhat larger interstory drifts in the upper stories (See Figure

4.27, in which the result from the first stage study is also included for comparison purposes). The maximum interstory drifts in STMF-2-SK and STMF-2-CBC were 2.05% and 1.88%, respectively. The maximum roof drifts in the STMF-2-SK and STMF-2-CBC were 1.46% and 1.41%, respectively.

4. In STMF-2 and STMF-2-CBC, the maximum plastic rotations in the chord members are more even through the entire frame, whereas STMF-2-SK had larger plastic rotations in the middle floors (See Figure 4.28, in which the result from first stage study is also presented). The maximum plastic rotations of the chord members in the STMF-2-SK and STMF-2-CBC were 0.044 radian and 0.038 radian, respectively.

4.7 Conclusions from the First Phase Study

In conclusion, the STMF designed by the proposed performance-based plastic approach can assure the desired global performance of the structure in terms of interstory drifts, plastic hinge rotations, and yield mechanism. Nonlinear analysis results obtained from the first phase study served as the basis for the design in the second phase and were included in the overall design procedure as presented in Chapter 2. Major findings are:

1. A yield drift of 0.75% is suggested for the design of STMFs.

2. The maximum developed shear in the special segment was much less than that

predicted by the AISC equation. In general, the code expected shear strength V_{ne} (AISC, 2005) in the special segments is about 1.5 times the actually developed shear forces, thereby resulting in overly conservative design for the elements outside the special segments. A more reasonable expression is proposed and given in Section 2.4.

3. The axial forces in chord members of the special segments are generally small and can be ignored when designing the special segments.

4. A lateral force distribution (Eq. (4.14)) which accounts for the inelastic state of the structure is proposed. The STMF designed by using this distribution experienced more uniform plastic hinge rotation, dissipated energy, and maximum interstory drift distributions along the height of the frame.

Table 4.1 Floor weights for the design of STMF

3 in. Metal Deck with 3-1/4 in. Light Weight Concrete Fill	48 psf
Ceiling/MEP	10 psf
Partitions	20 psf
Steel Framing	10 psf
Misc.	12 psf
Total Dead Load	100 psf
Live Load	100 psf

Table 4.2 Design parameters in accordance with CBC (2001)

Parameters	Value/Note
Building Height h_n	118 ft
$T_a = C_t \left(h_n\right)^{3/4}$ $C_t = 0.035$ (steel moment frame)	1.25 sec.
Importance Factor, I	1.5 (Hospital Occupancy)
R	6.5
N_a	1.0 (>10 km from type B fault)
N_v	1.0 (>10 km from type B fault)
C_a	0.44 (Z = 0.4, S_D soil)
C_v	0.64 (Z = 0.4, S_D soil)
$V_1 = \begin{cases} V_{\max} = 2.5 C_a I W / R \\ V_{\min} = 0.11 C_a I W \\ V_{\min} = 0.8 Z N_v I W / R \end{cases}$ $V_1 = 0.11W$ $V_{sc} = V_1\left(SR\right) = 0.11W \times 1.25 = 0.14W$	V_{sc} = scaled dynamic base shear used for design (CBC 2001) SR = Spectral ration (CBC 2001) Final design base shear was further increased 10% to account for accidental torsion
Design Base Shear V	1390 kips
Total Building Weight W	9009 kips
$C_s = \dfrac{V}{W}$	0.154

Table 4.3 Design parameters of proposed procedure for STMF-1

Parameters	Values
$C_e = \left(\frac{R}{I}\right) C_s = \left(\frac{6.5}{1.5}\right) \times 0.154$	0.667g
T	1.25 sec.
Yield Drift θ_y	1.0%
Target Drift θ_u	2.0%
$\mu_s = \frac{\theta_u}{\theta_y}$	2.0
R_μ	2.0
γ	0.75
α	1.551
$\frac{V}{W}$	0.192
Design Base Shear V	1727 kips

Table 4.4 Design parameters for STMF-1

Level	Floor Weight (kips)	Design Lateral Forces (kips) (Entire structure)	V_{ne} (kips)
7th FLR	1287	880	144
6th FLR	1287	305	188
5th FLR	1287	202	214
4th FLR	1287	144	259
3rd FLR	1287	101	259
2nd FLR	1287	64	279
1st FLR	1287	31	279

Table 4.5 Design parameters of proposed procedure for STMF-2

Parameters	Values
$C_e = \left(\frac{R}{I}\right) C_s = \left(\frac{6.5}{1.5}\right) \times 0.154$	0.667g
T	1.25 sec.
Yield Drift θ_y	0.75%
Target Drift θ_u	2.0%
$\mu_s = \frac{\theta_u}{\theta_y}$	2.67
R_μ	2.67
γ	0.61
α	1.801
$\frac{V}{W}$	0.140
Design Base Shear V	1260 kips

Table 4.6 Sections of chord members of the study STMFs

FLR	STMF-1	STMF-2	STMF-2-CBC	STMF-2-SK
7	10MC22	8C13.75	8C11.5	8MC18.7
6	12C25	8MC21.4	8MC18.7	9MC23.9
5	12C30	10C25	10C25	10MC25
4	12MC31	10MC28.5	10MC25	10MC28.5
3	12MC31	12C30	12C30	12C30
2	12MC35	12C30	12C30	12C30
1	12MC35	12C30	12C30	12C30

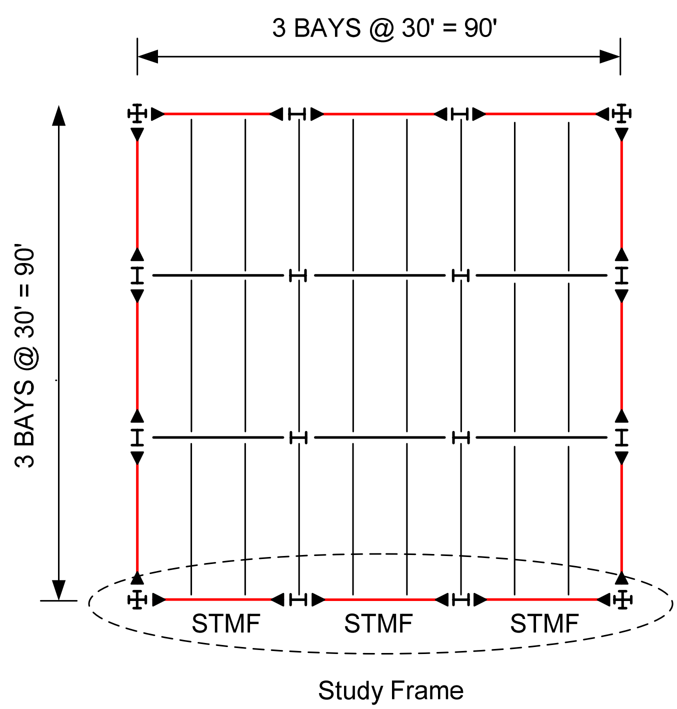

Figure 4.1 Study building layout and STMFs in the first phase investigation

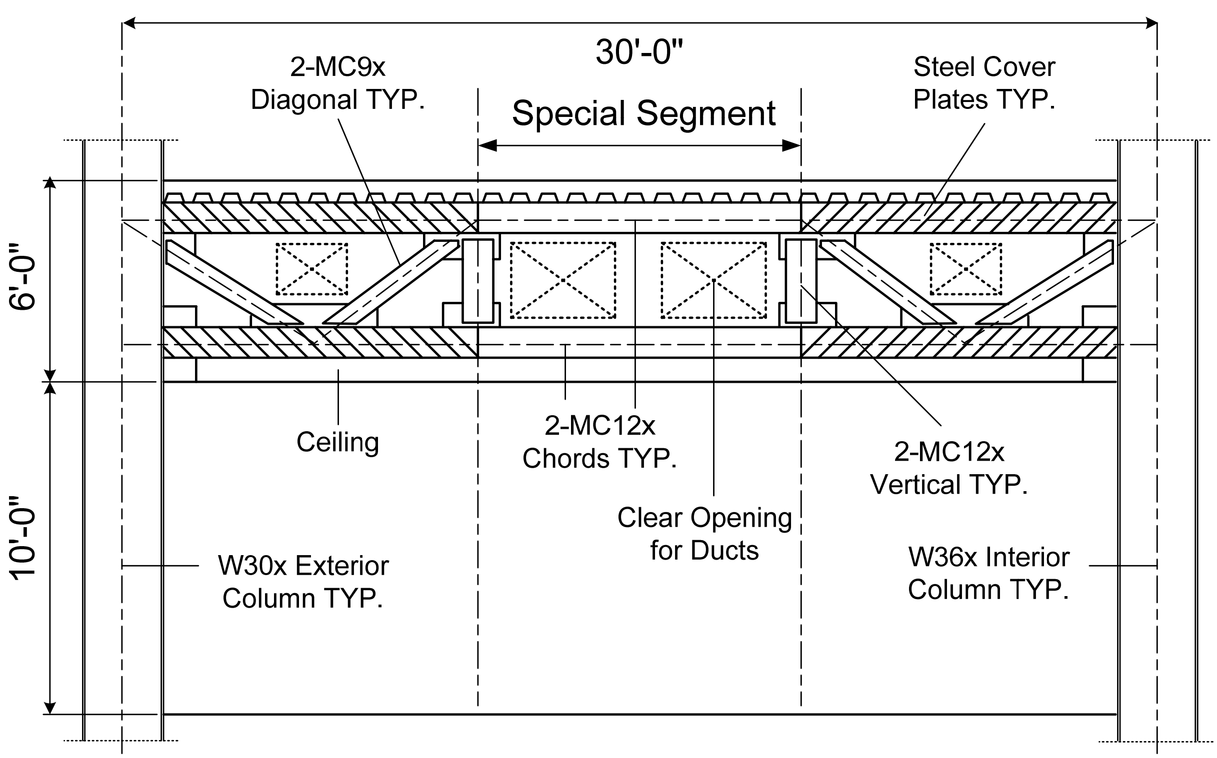

Figure 4.2 Typical truss elevation

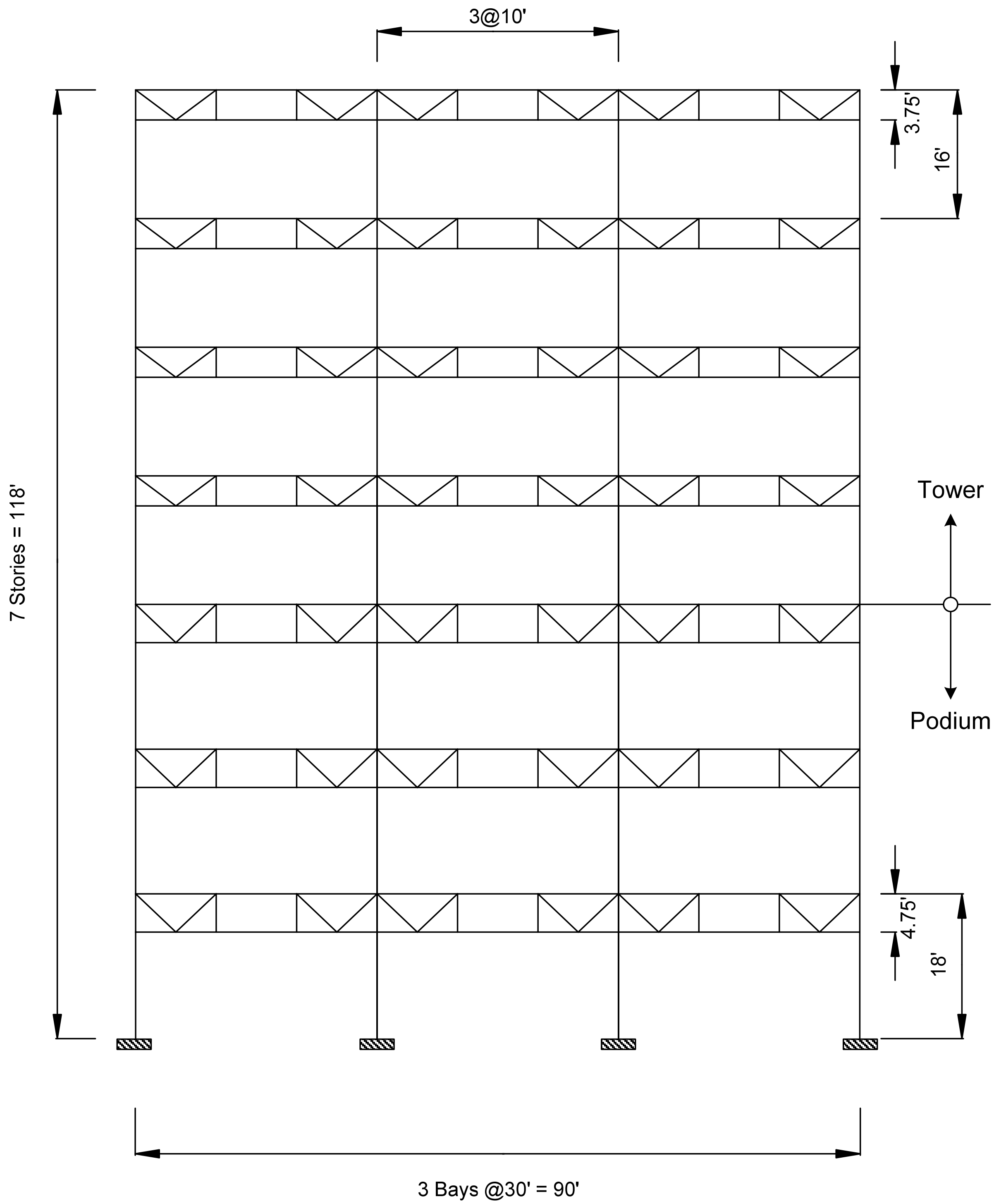

Figure 4.3 Profile of study STMF

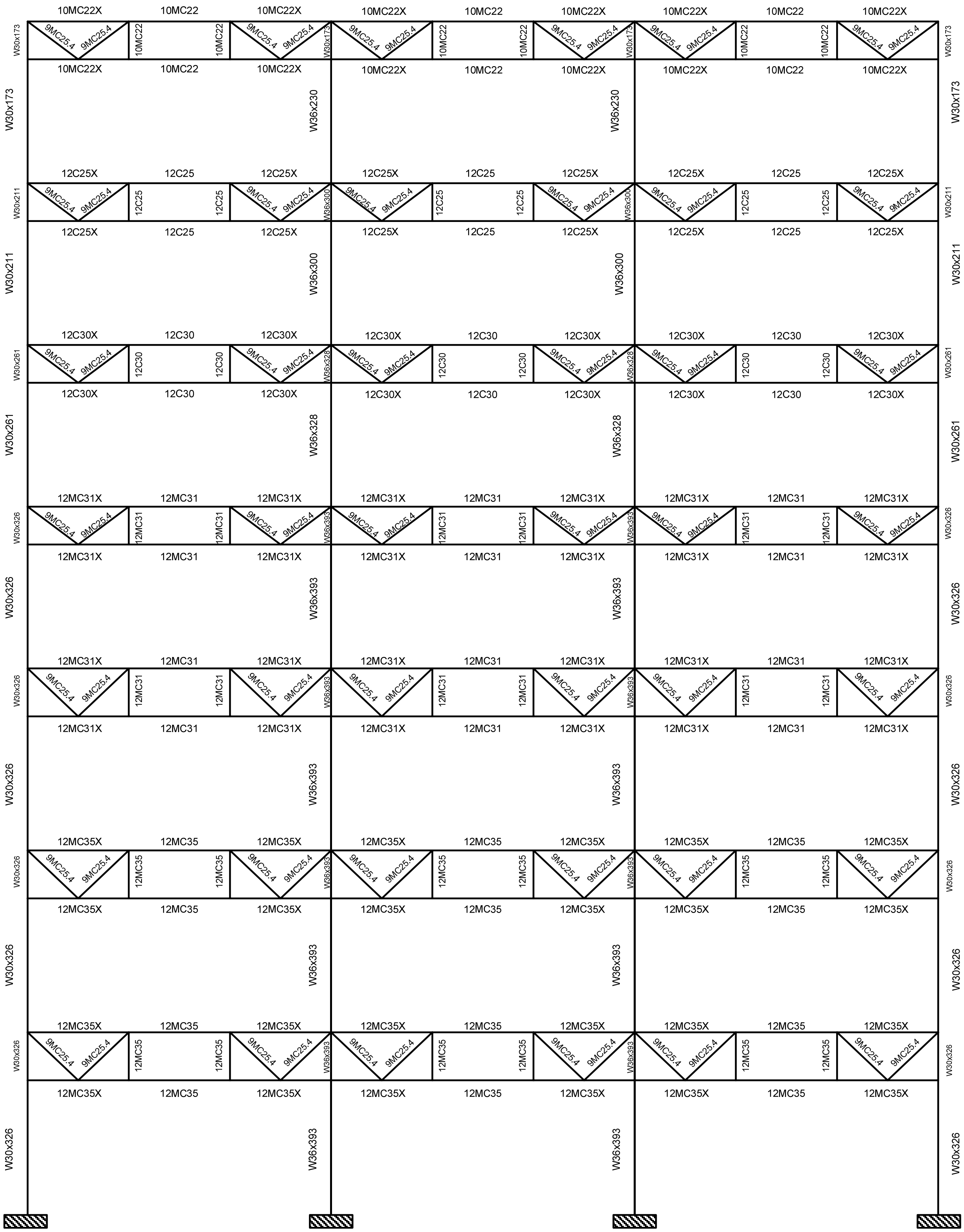

Figure 4.4 Sections of STMF-1

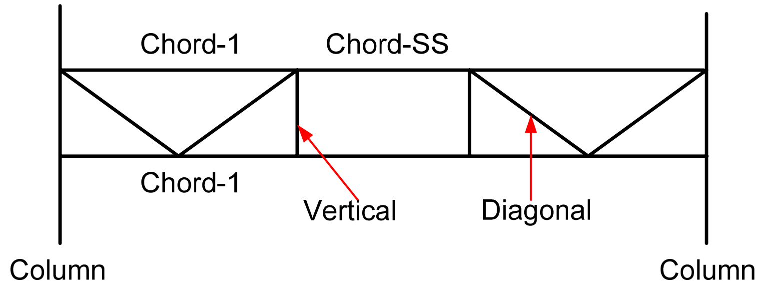

FLR	Chord-SS	Chord-1	Vertical	Diagonal	L (in.)*
7	10MC22	10MC22X (1 in. plate)	10MC22	9MC25.4	7.25
6	12C25	12C25X (1 in. plate)	12C25	9MC25.4	9.25
5	12C30	12C30X (1 in. plate)	12C30	9MC25.4	9.25
4	12MC31	12MC31X (1.5 in. plate)	12MC31	9MC25.4	9.25
3	12MC31	12MC31X (1.5 in. plate)	12MC31	9MC25.4	9.25
2	12MC35	12MC35X (1.5 in. plate)	12MC35	9MC25.4	9.25
1	12MC35	12MC35X (1.5 in. plate)	12MC35	9MC25.4	9.25

Note 1: All sections are double channels.
Note 2: Web plates are used for entire length of the cord member outside the special segment
***see figure below**

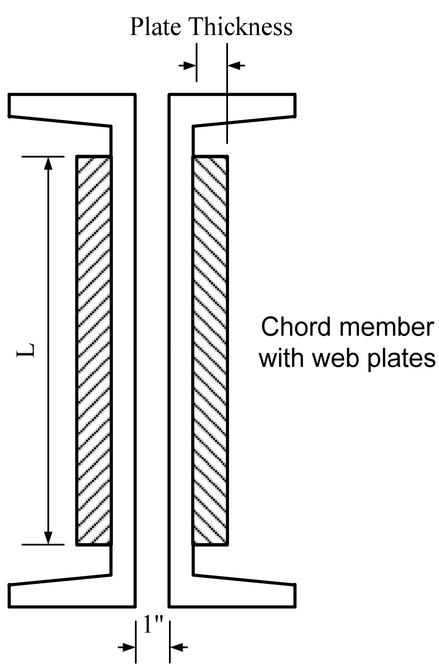

Figure 4.5 Design special segment and truss member sections for STMF-1

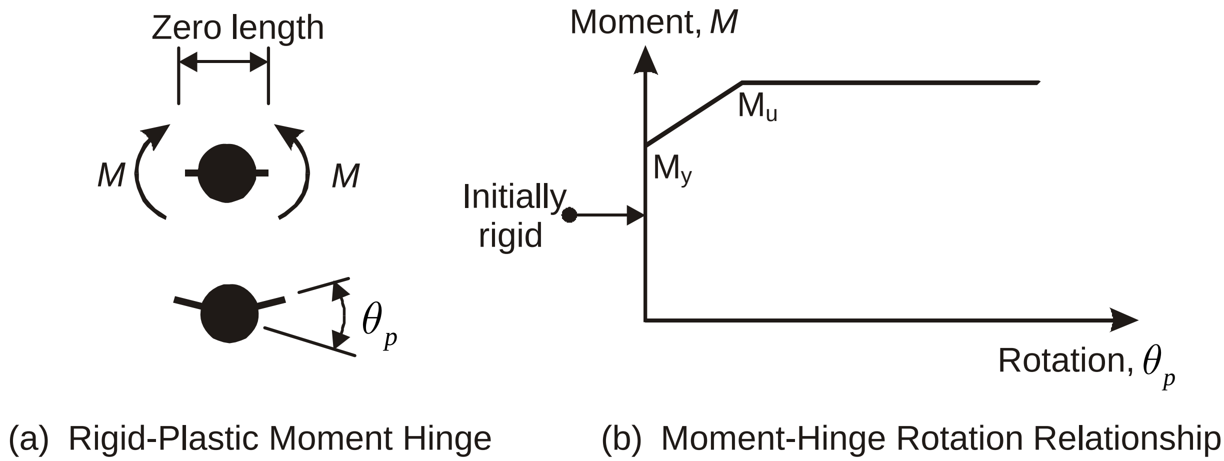

Figure 4.6 Rigid-plastic hinge model and corresponding moment-rotation relationship

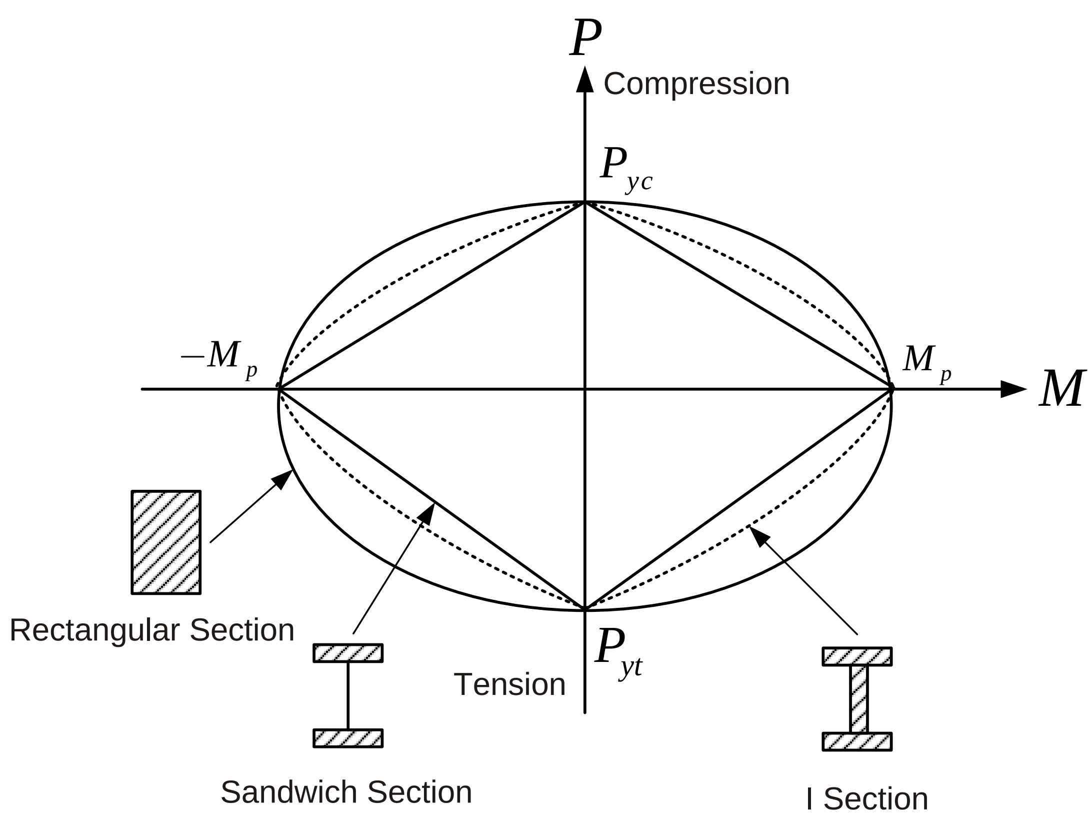

Figure 4.7 P-M interaction curves for Beam-Column elements

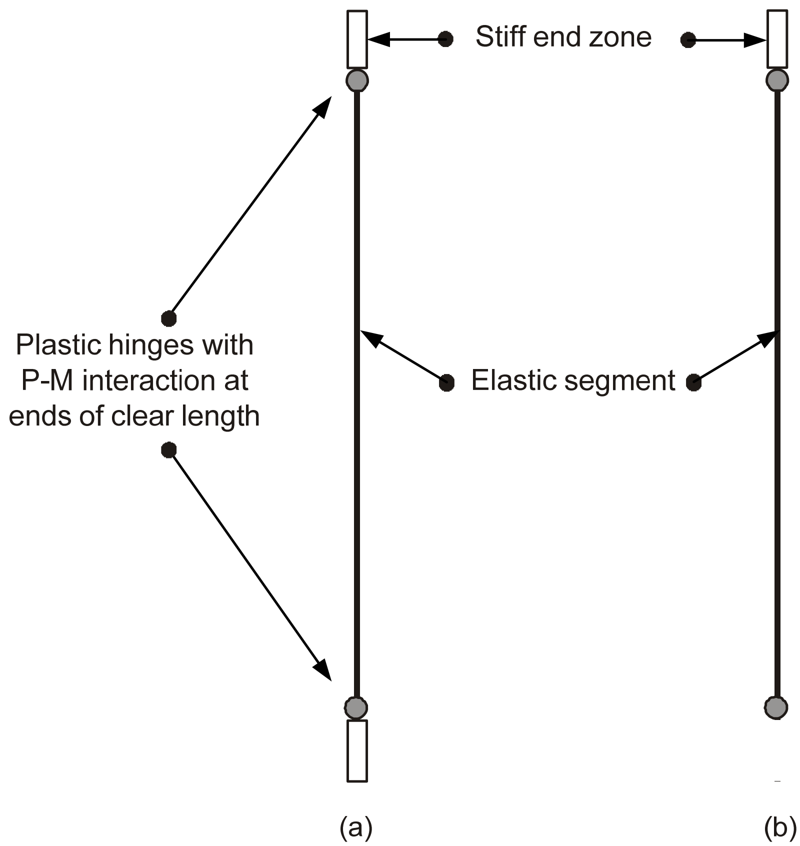

Figure 4.8 Column component model: (a) General floor columns; (b) First floor columns

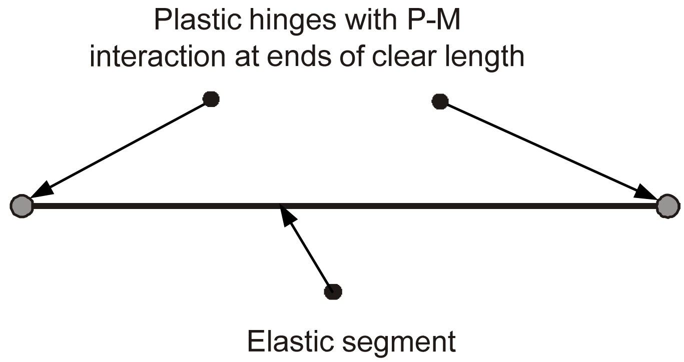

Figure 4.9 Component model for chord members

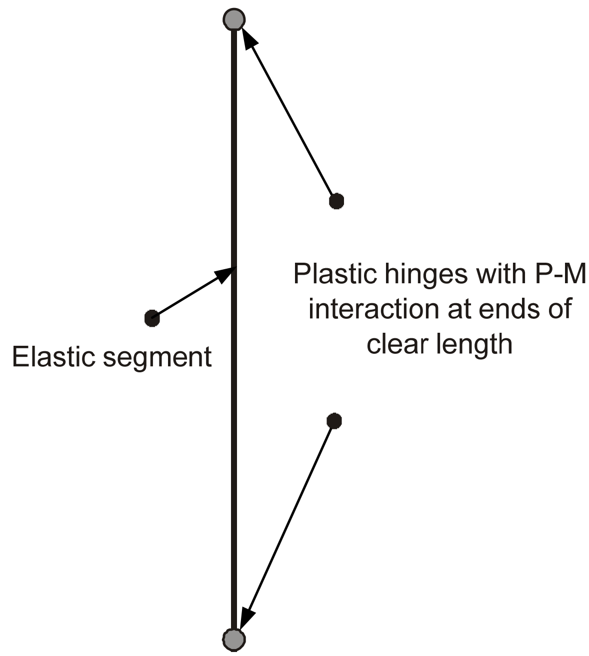

Figure 4.10 Component model for vertical members in a truss girder

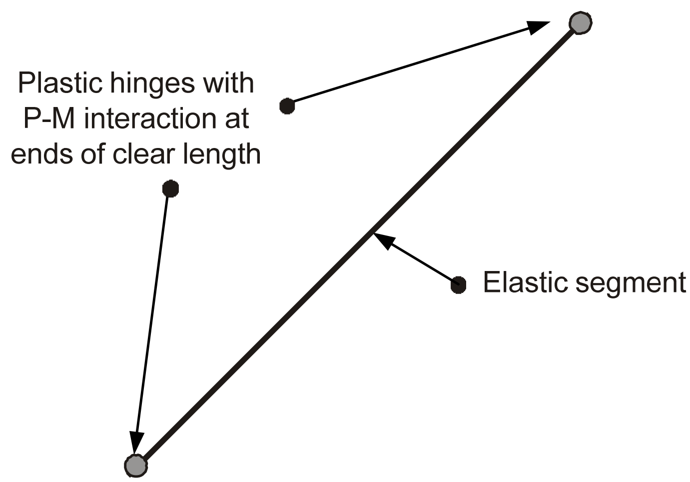

Figure 4.11 Component model for diagonal members in a truss girder

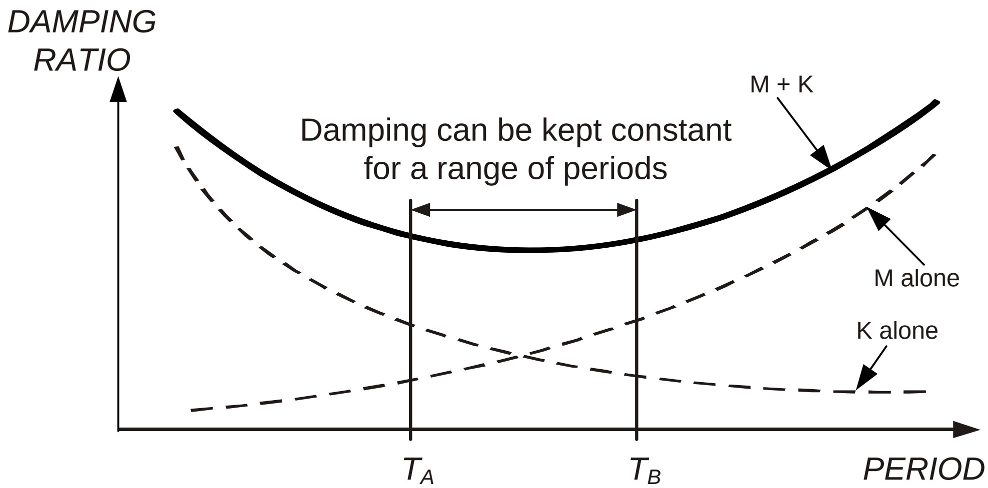

Figure 4.12 Variation of damping ratio with structural period

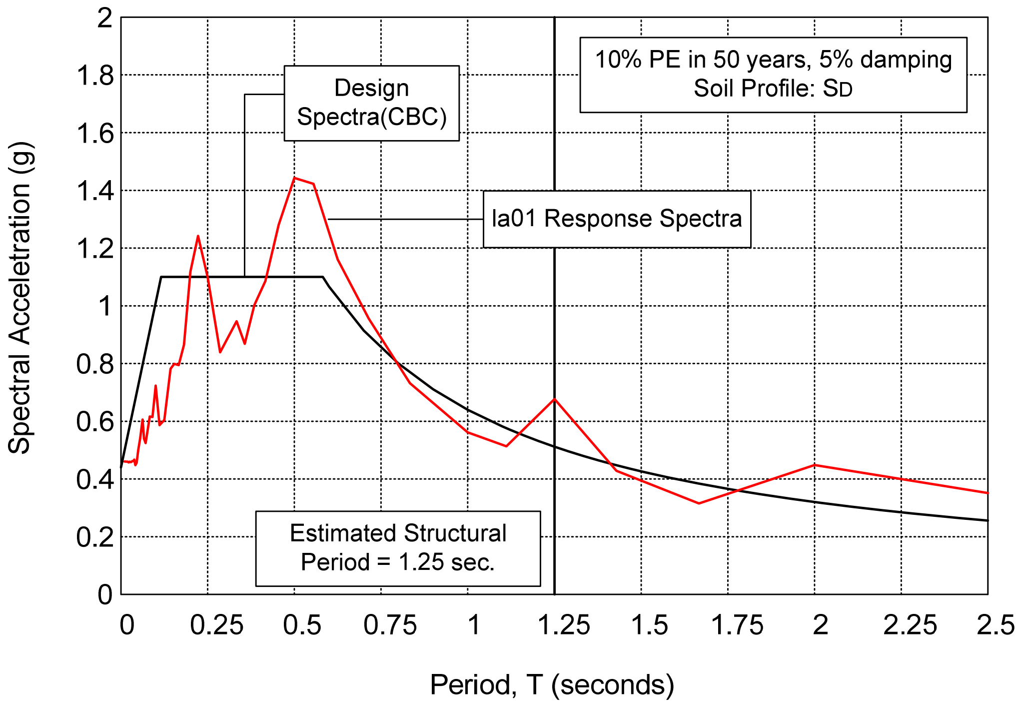

Figure 4.13 Design spectrum and LA 01 response spectra

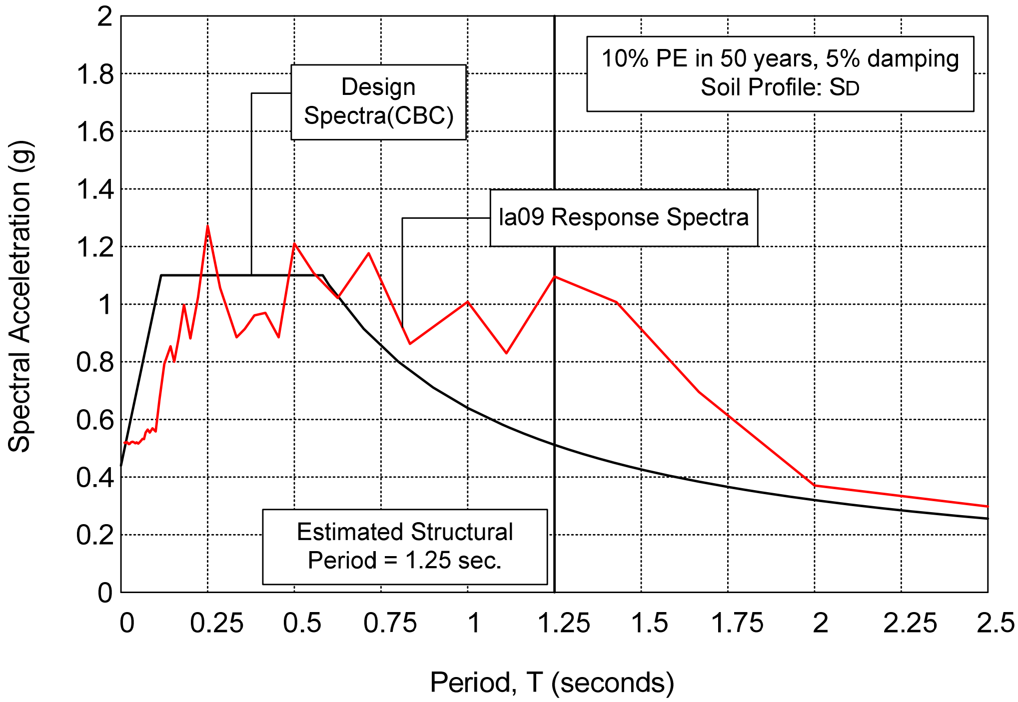

Figure 4.13 (Continued) Design spectrum and LA 09 response spectra

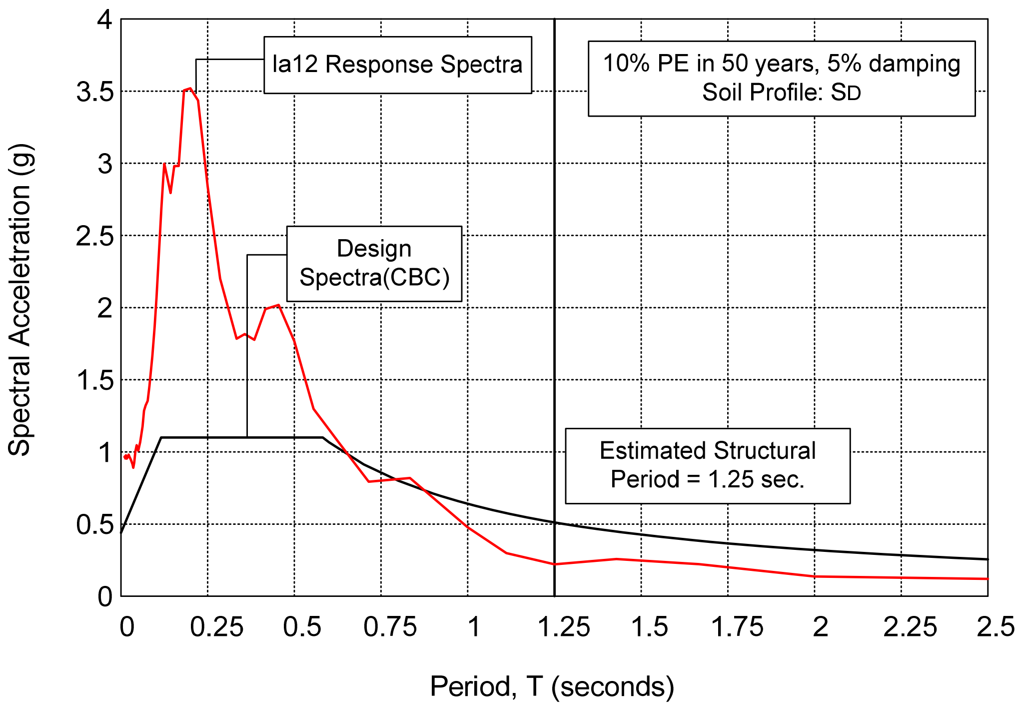

Figure 4.13 (Continued) Design spectrum and LA 12 response spectra

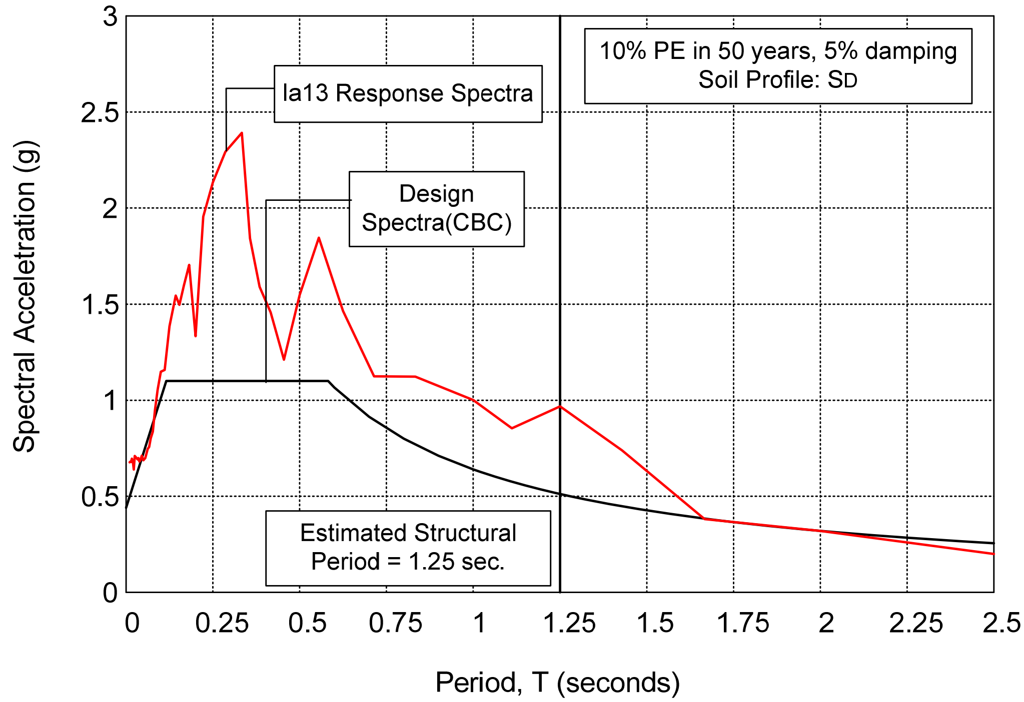

Figure 4.13 (Continued) Design spectrum and LA 13 response spectra

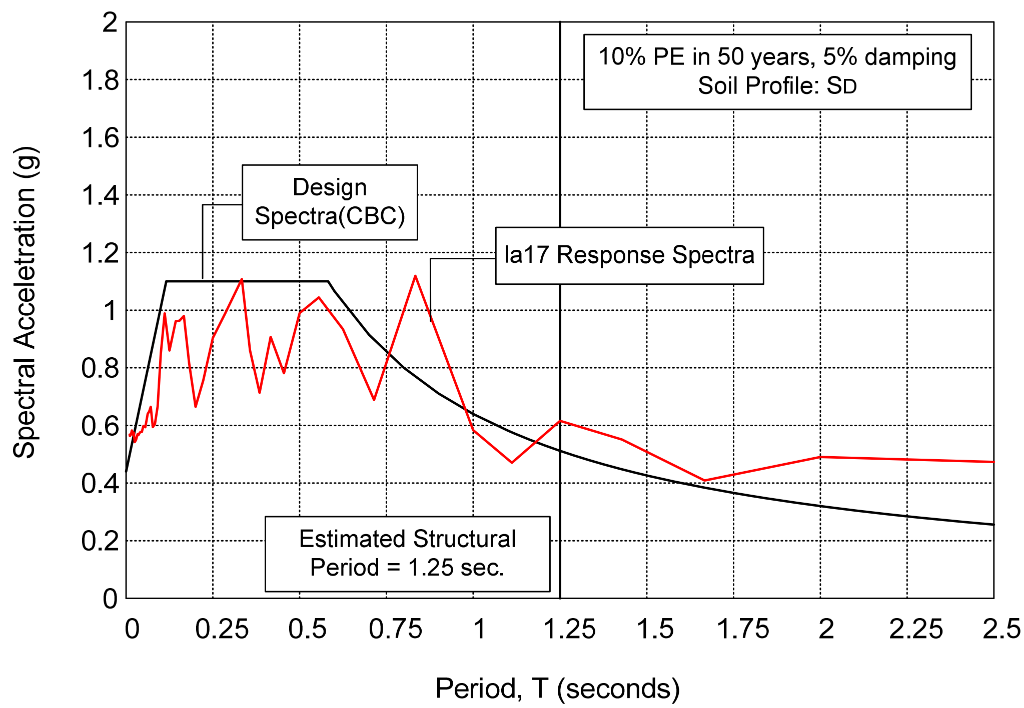

Figure 4.13 (Continued) Design spectrum and LA 17 response spectra

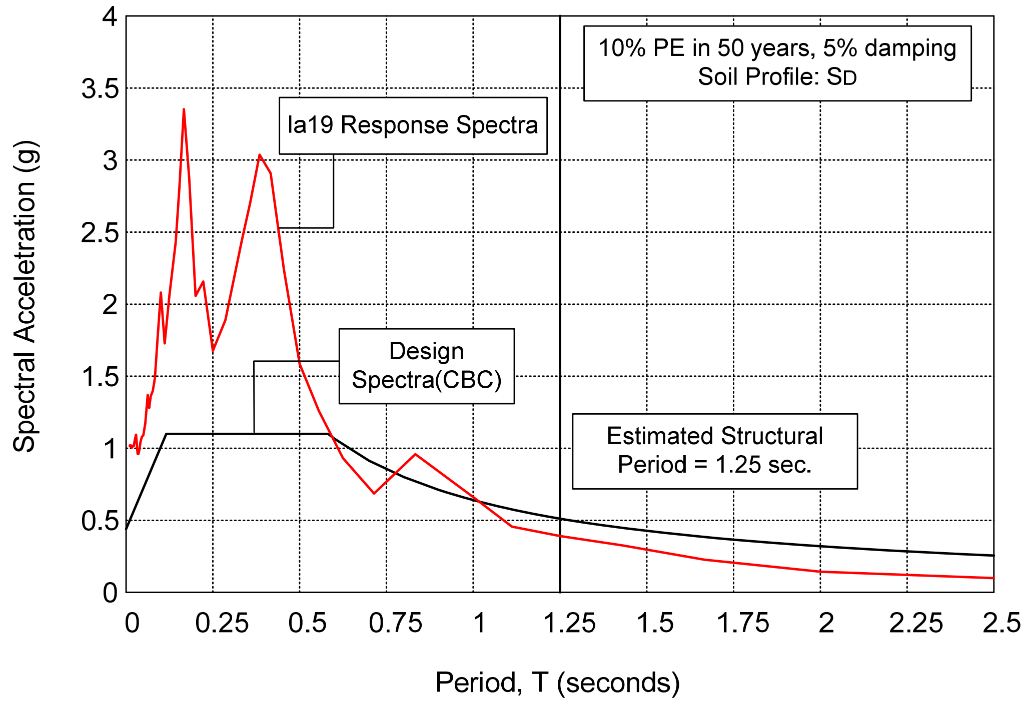

Figure 4.13 (Continued) Design spectrum and LA 19 response spectra

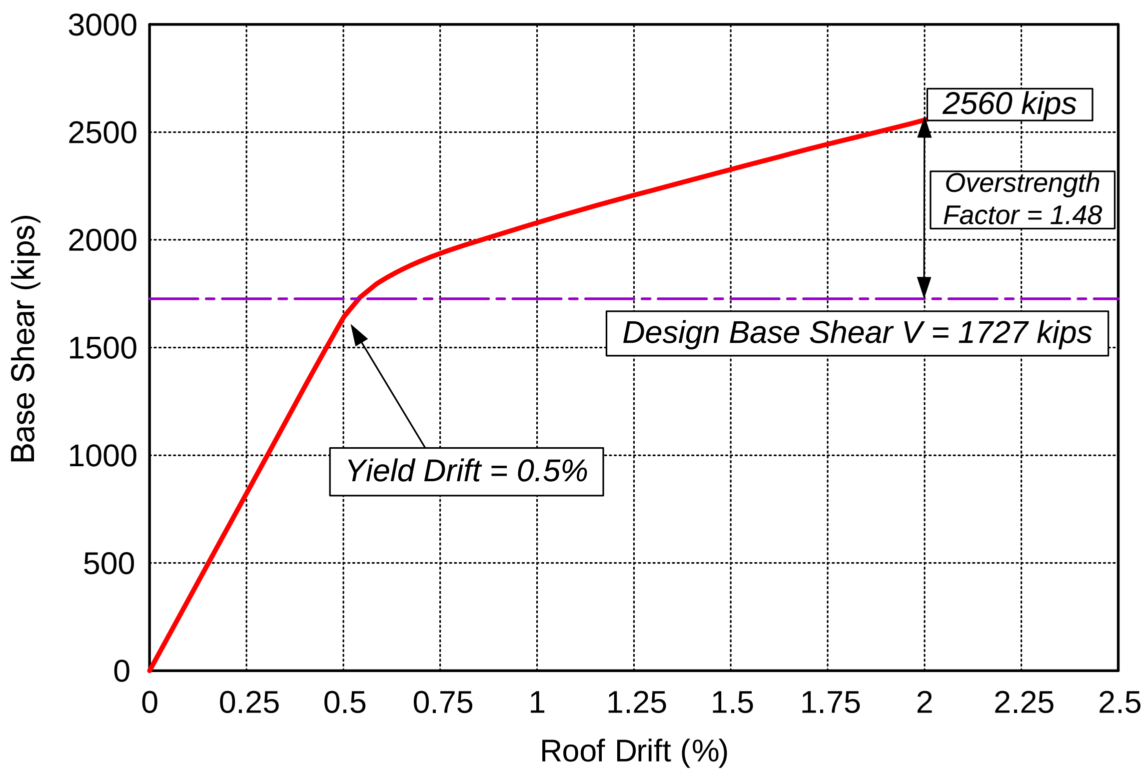

Figure 4.14 Pushover response of STMF-1

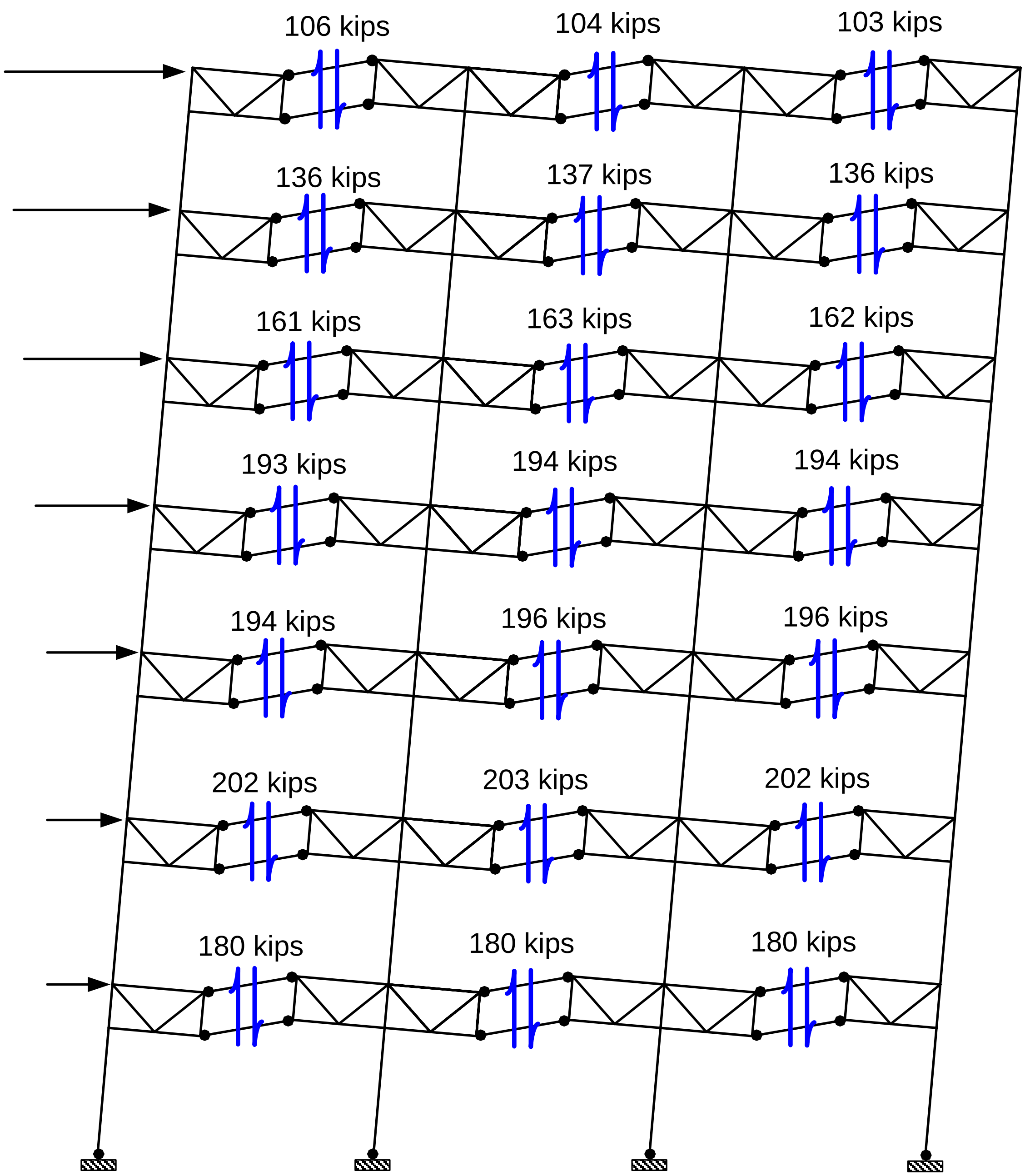

Figure 4.15 Maximum developed shears in special segments when STMF-1 was statically pushed to 2% roof drift

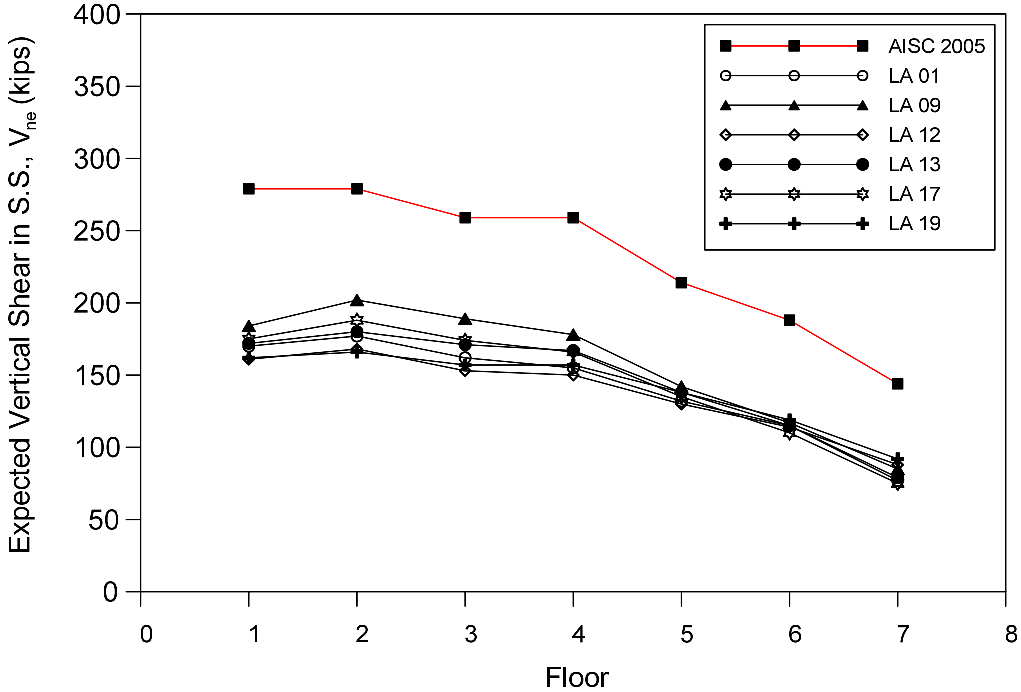

Figure 4.16 Maximum developed shears in special segments for various ground motions (STMF-1)

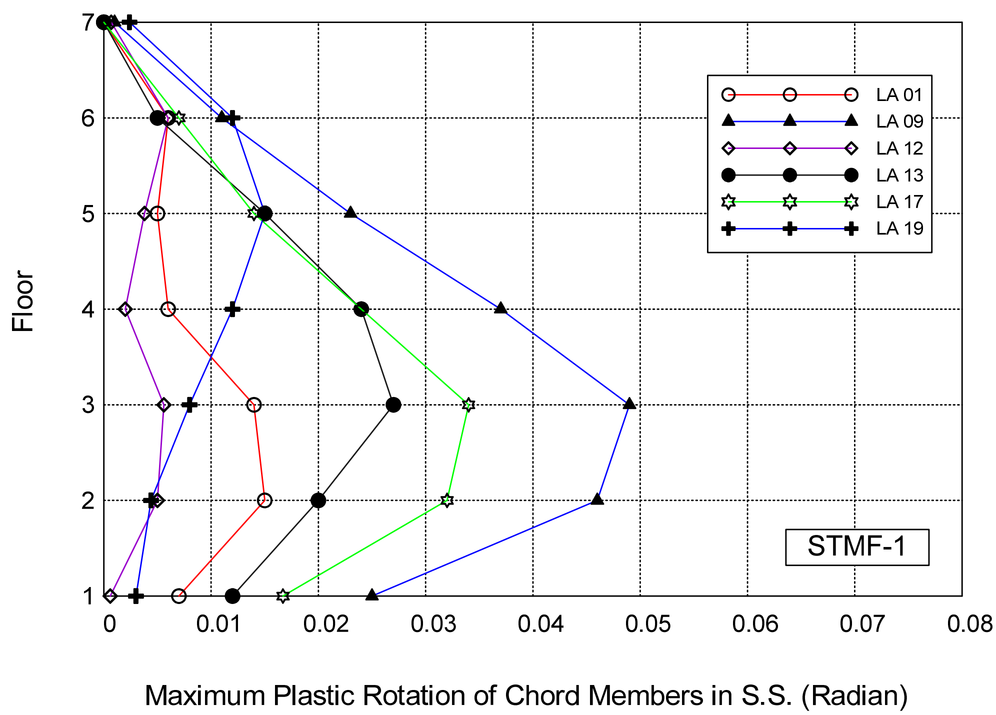

Figure 4.17 Maximum plastic hinge rotations in chord members (STMF-1)

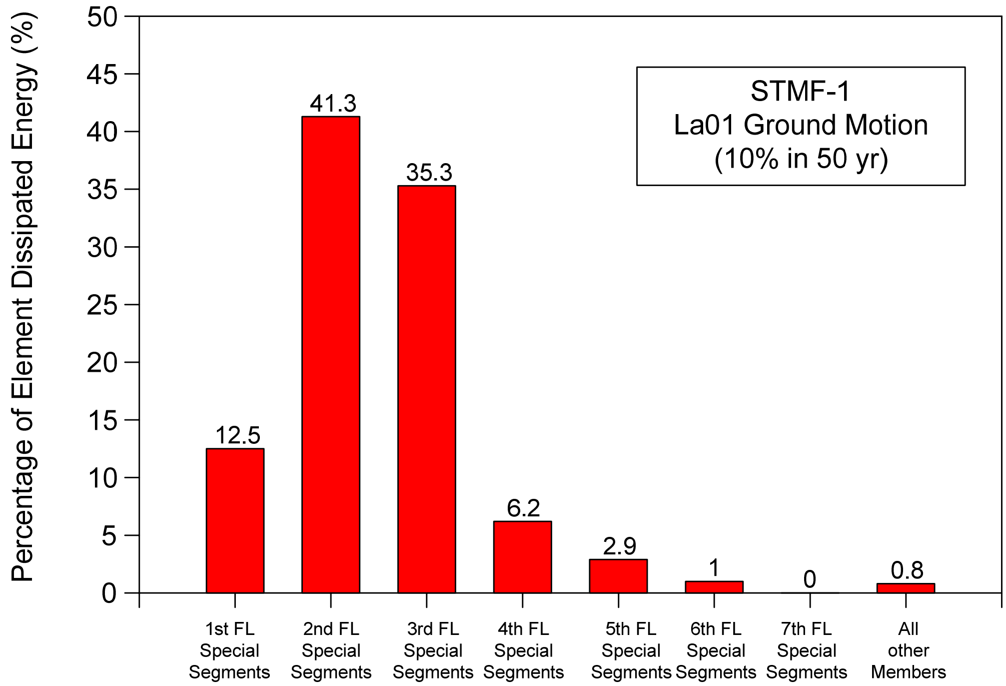

(a)

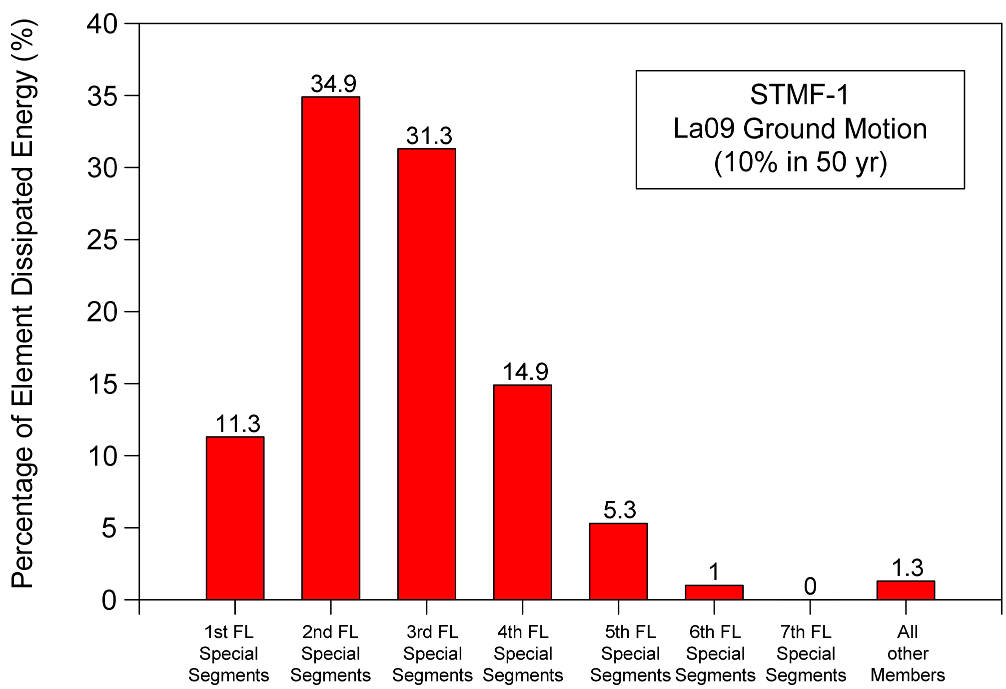

(b)

Figure 4.18 Percentage of dissipated hysteretic energy (STMF-1)

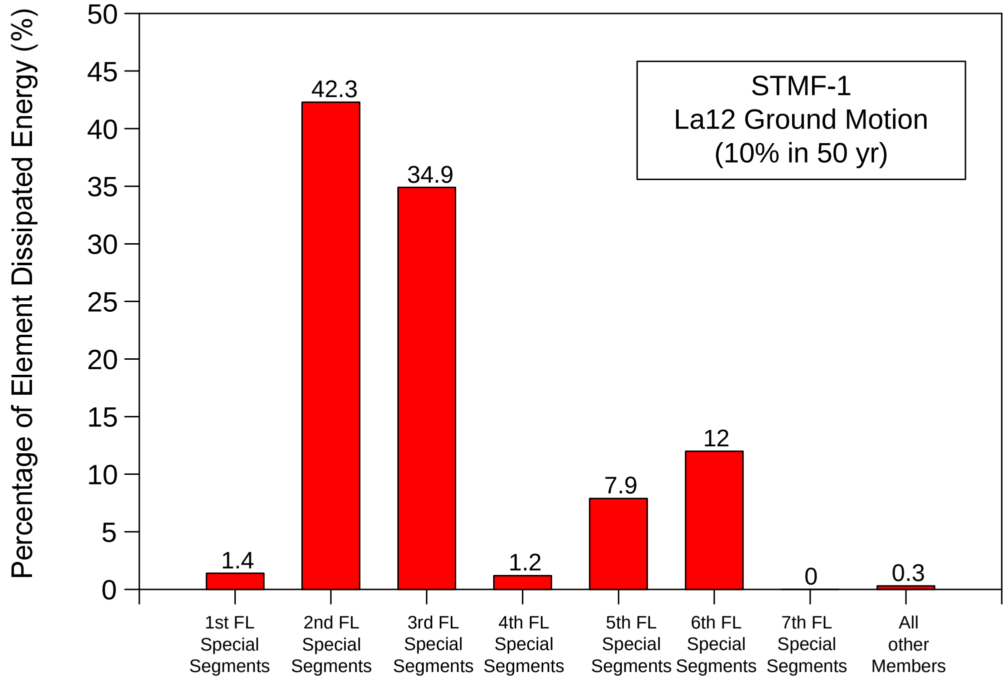

(c)

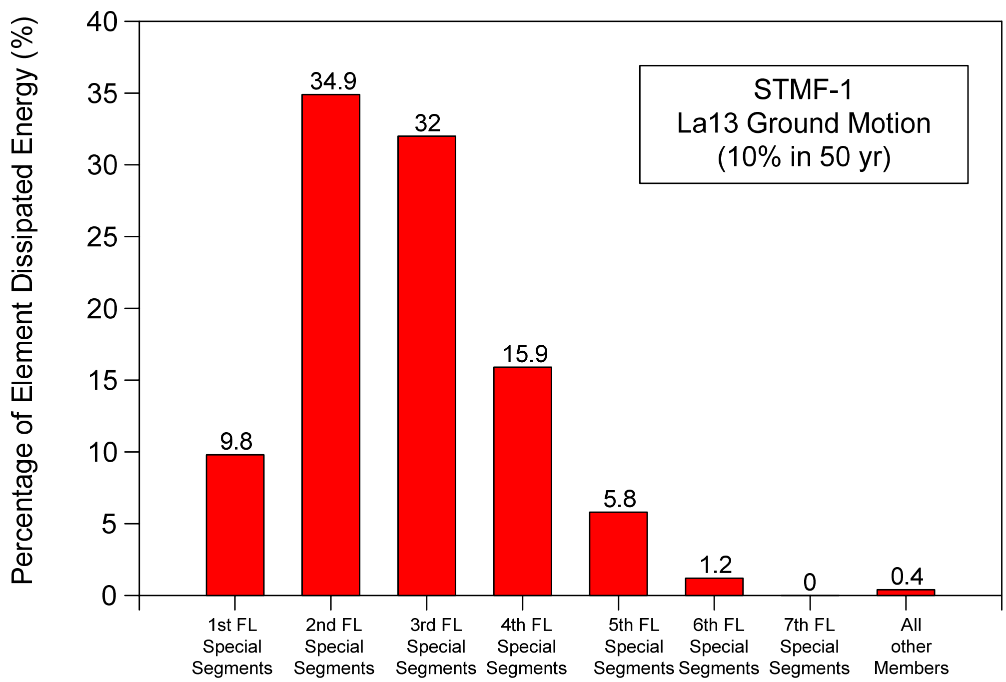

(d)

Figure 4.18 (Continued) Percentage of dissipated hysteretic energy (STMF-1)

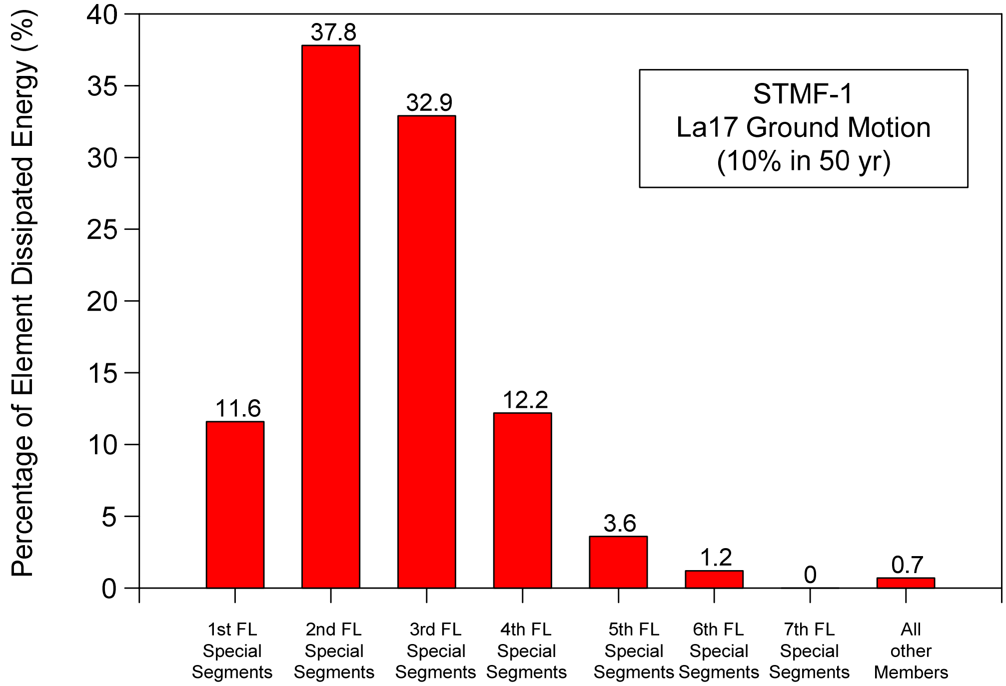

(e)

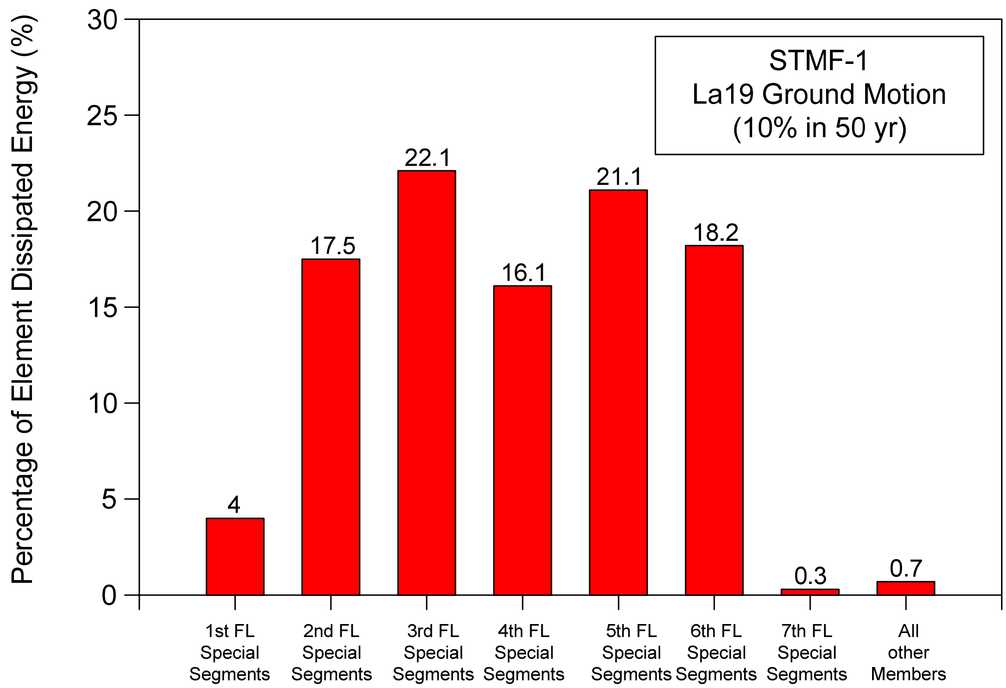

(f)

Figure 4.18 (Continued) Percentage of dissipated hysteretic energy (STMF-1)

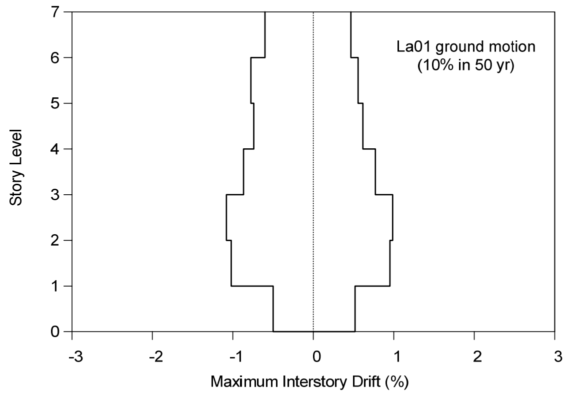

(a) La 01

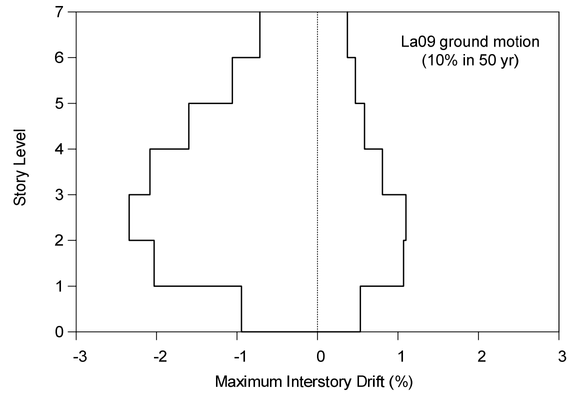

(b) La 09

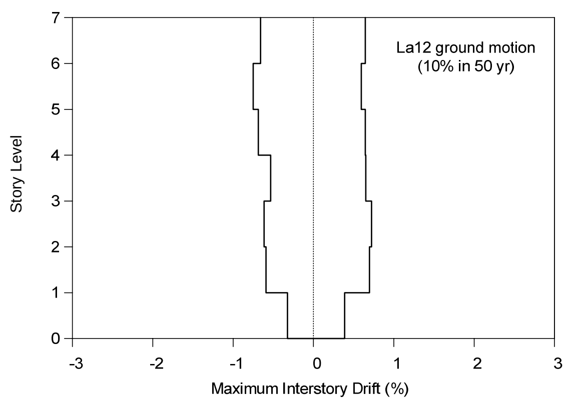

(c) La 12

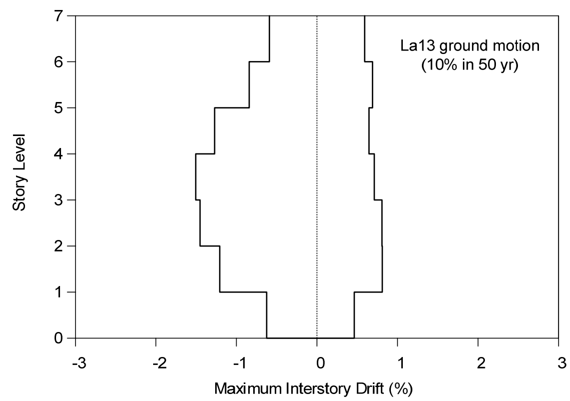

(d) La 13

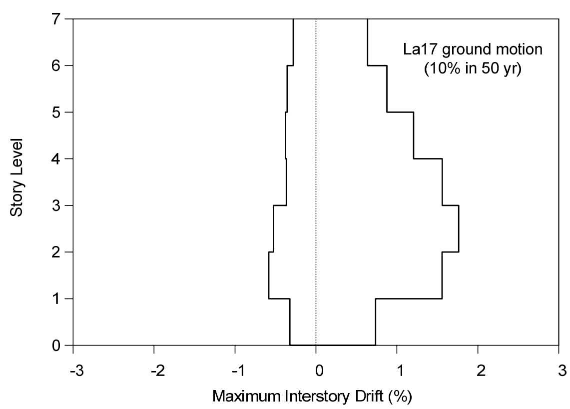

(e) La 17

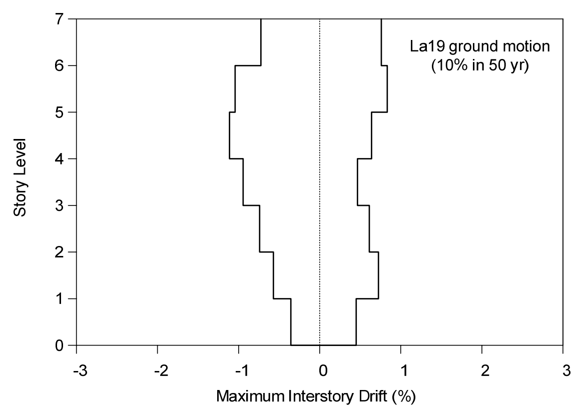

(f) La 19

Figure 4.19 Maximum interstory drift (STMF-1)

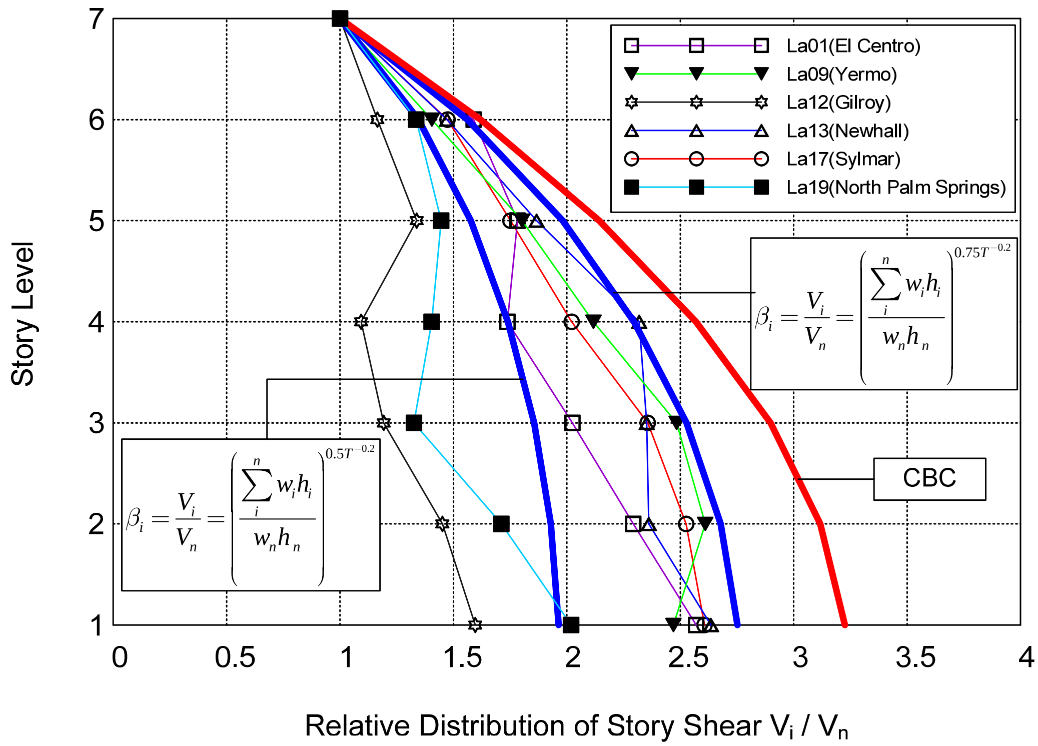

Figure 4.20 Relative distributions of story shears (STMF-1)

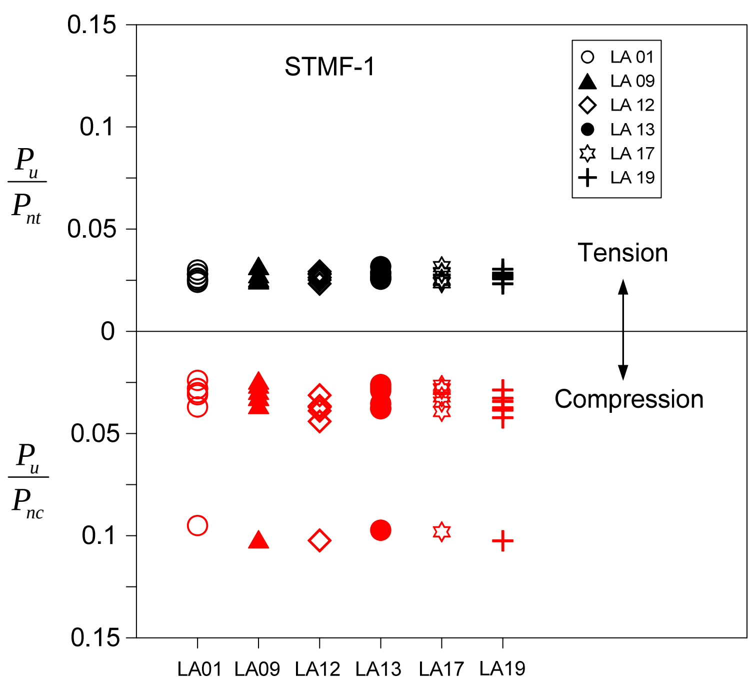

Figure 4.21 Axial force ratios in special segments for various ground motions (maximum value at each floor level was used to compare with nominal axial strength)

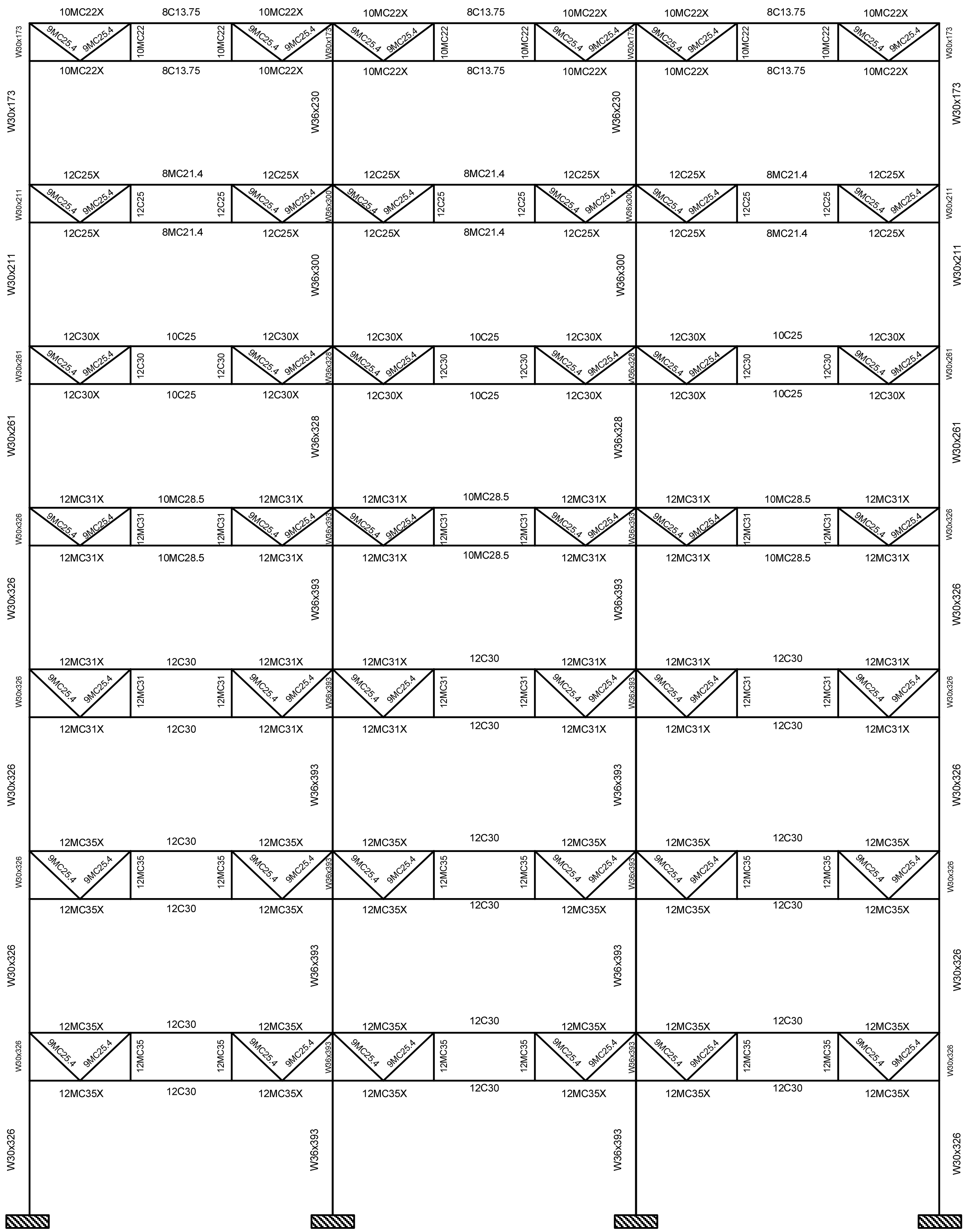

Figure 4.22 Sections of the STMF-2 designed in the second stage of the first phase study (Note for study purposes only chord members were redesigned)

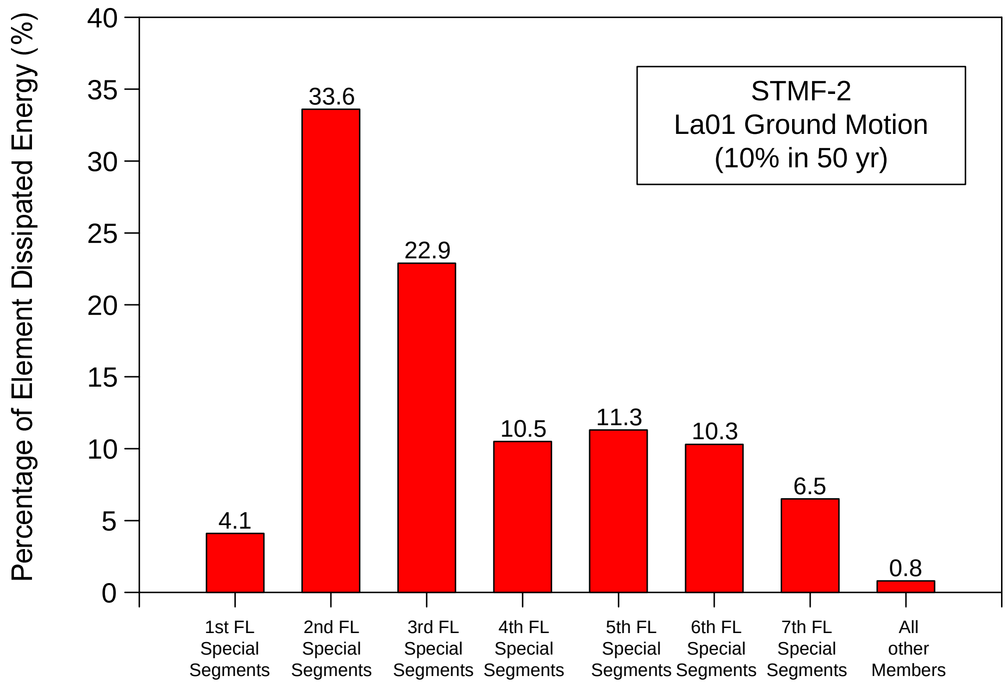

(a)

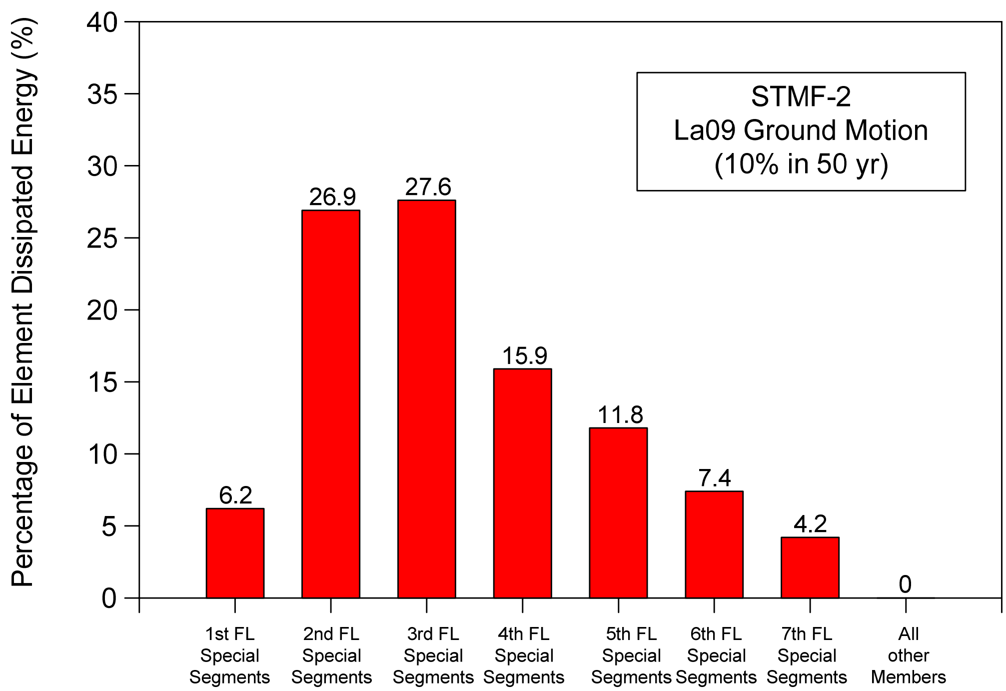

(b)

Figure 4.23 Percentage of dissipated hysteretic energy (STMF-2)

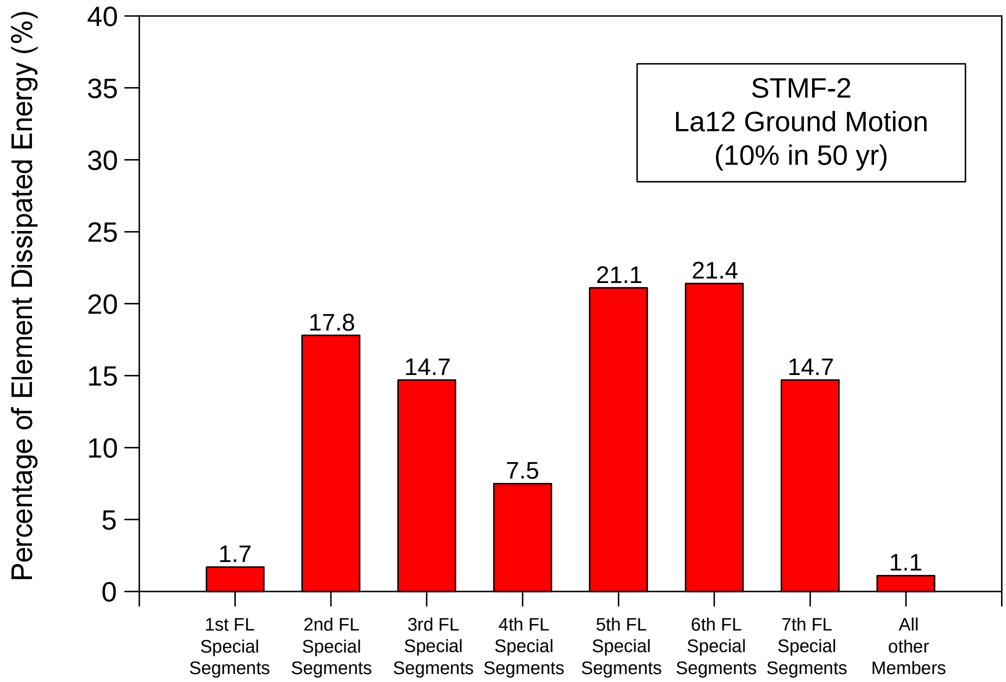

(c)

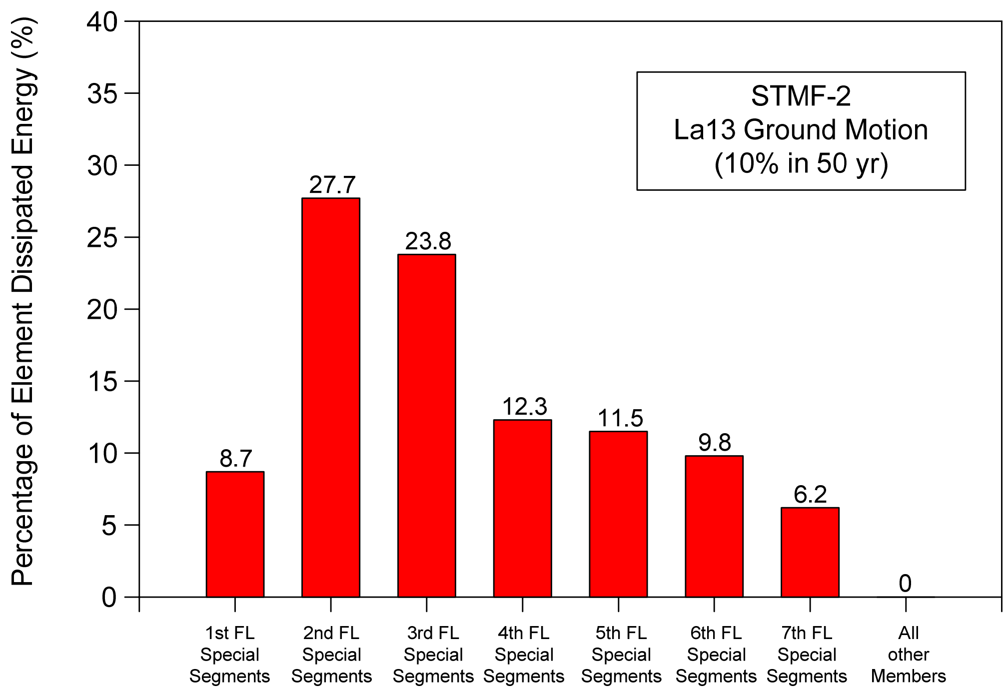

(d)

Figure 4.23 (Continued) Percentage of dissipated hysteretic energy (STMF-2)

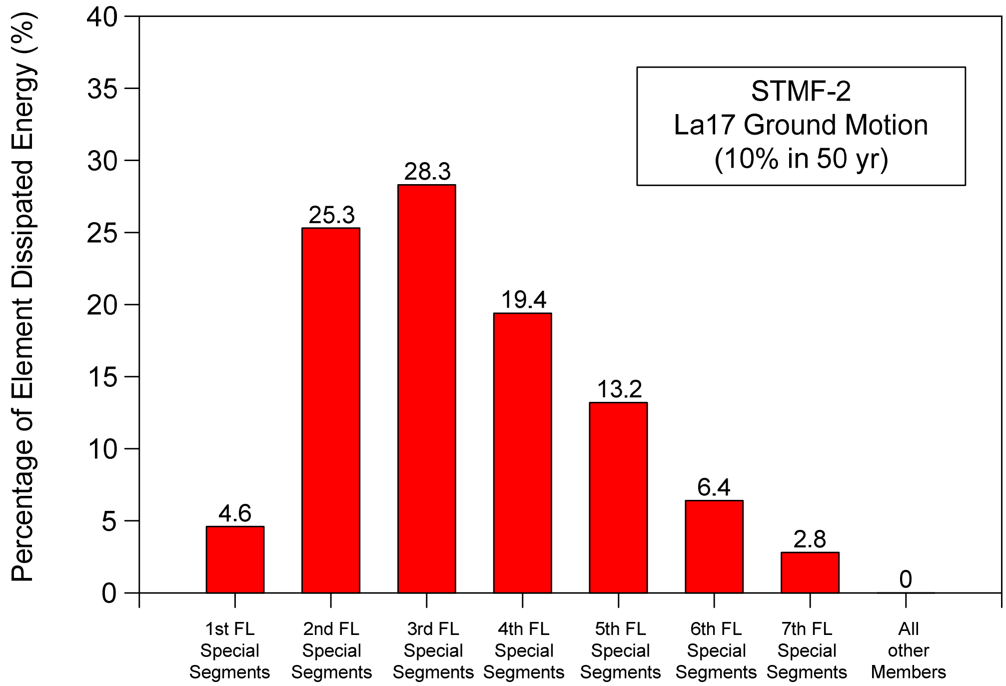

(e)

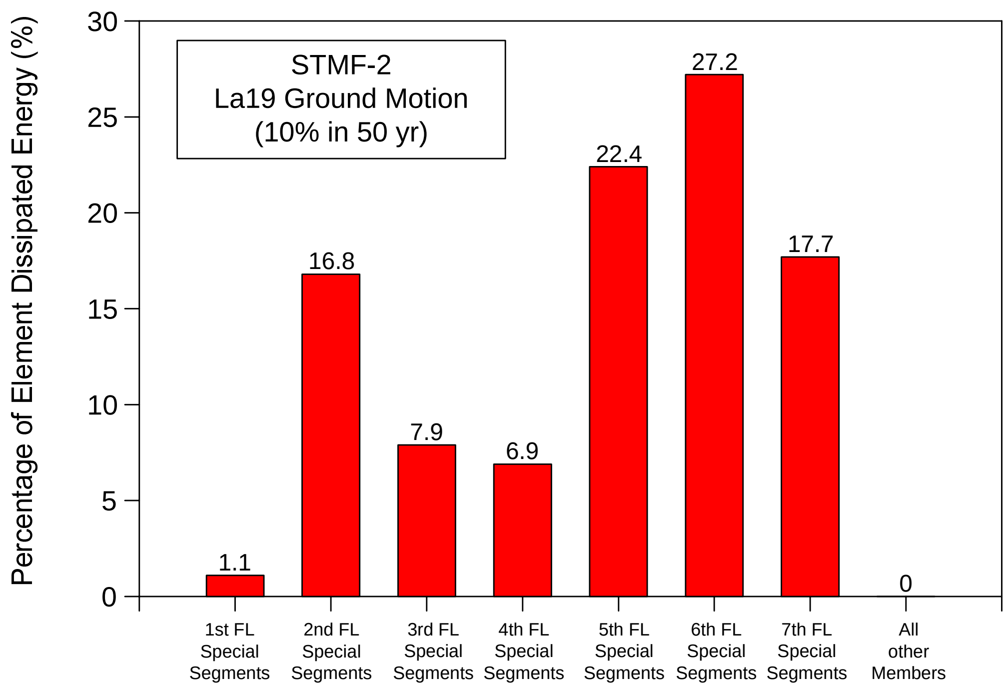

(f)

Figure 4.23 (Continued) Percentage of dissipated hysteretic energy (STMF-2)

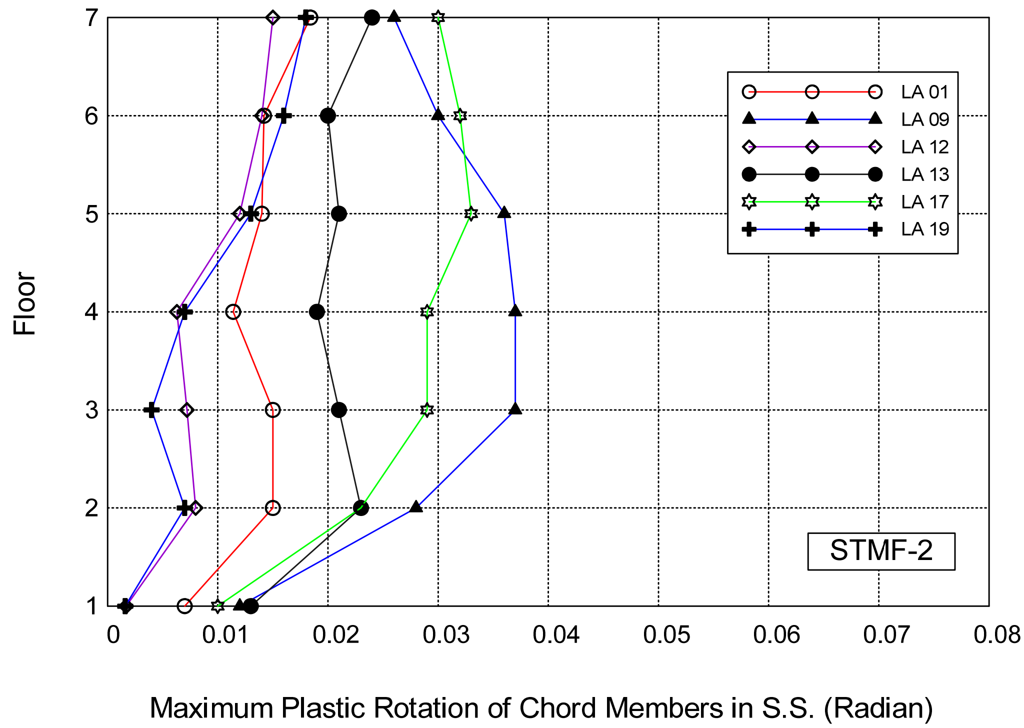

Figure 4.24 Maximum plastic hinge rotations in chord members (STMF-2)

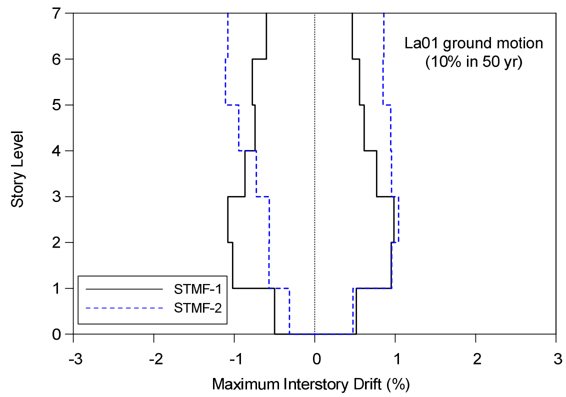

(a) La 01

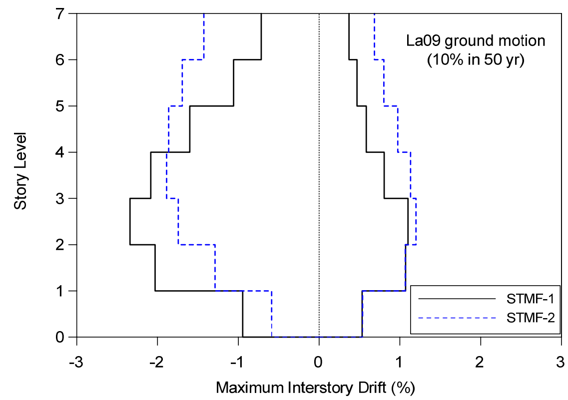

(b) La 09

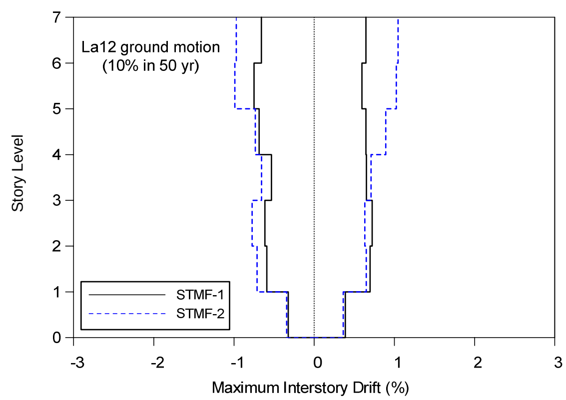

(c) La 12

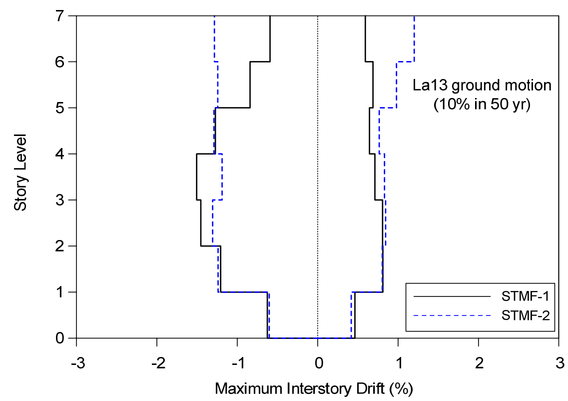

(d) La 13

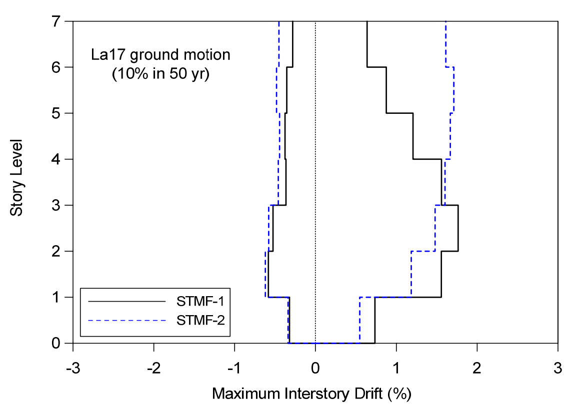

(e) La 17

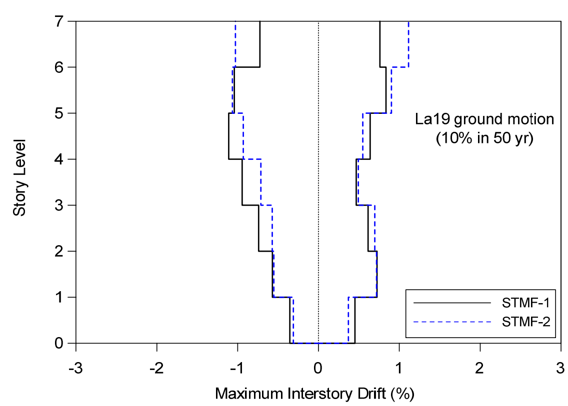

(f) La 19

Figure 4.25 Comparison of maximum interstory drift between STMF-1 and STMF-2

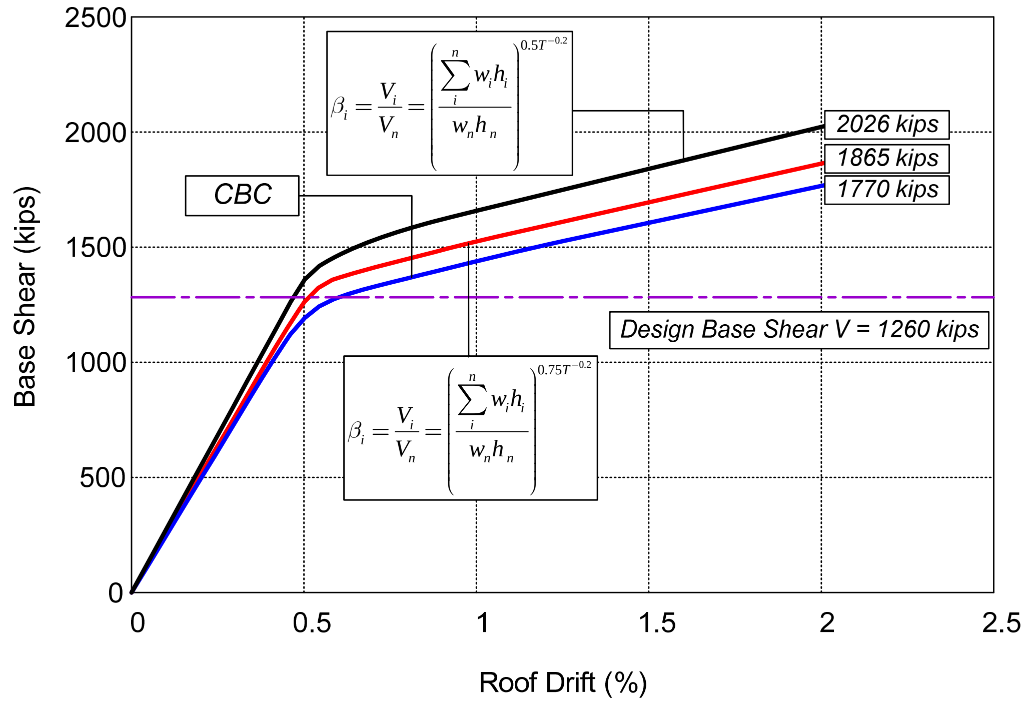

Figure 4.26 Pushover responses of three study frames designed by three different lateral force distributions in the third stage of the first phase study

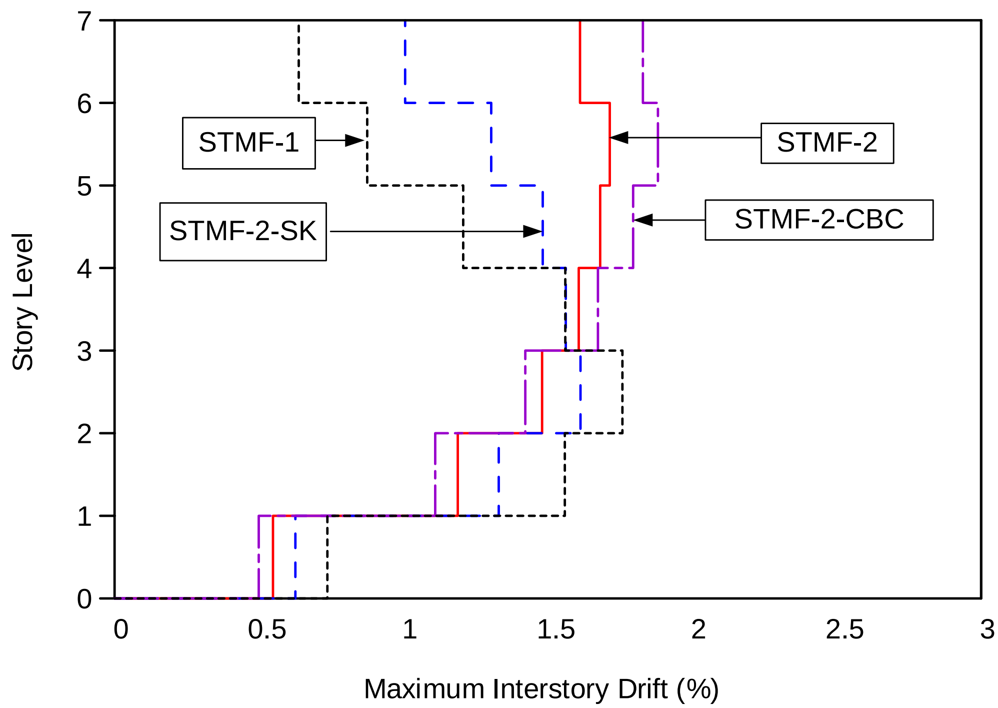

Figure 4.27 Maximum interstory drift of four study frames based on different lateral force distributions during La17 Northridge (Sylmar) ground motion

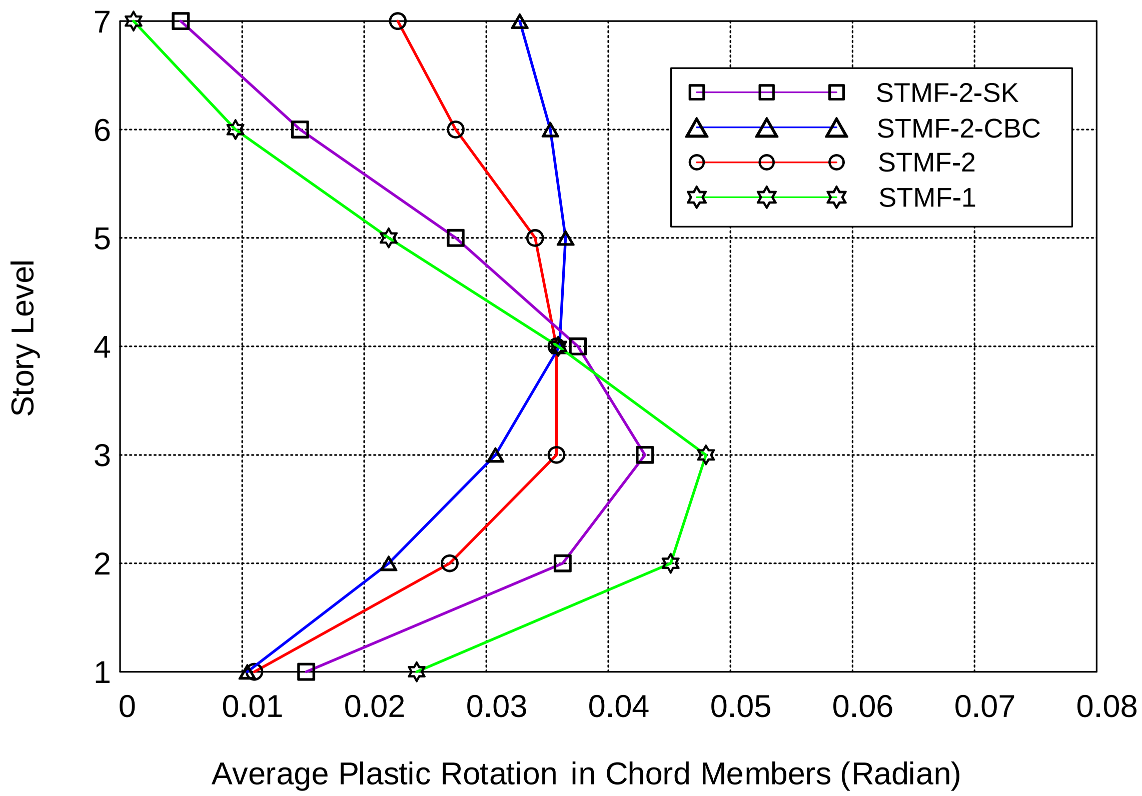

Figure 4-28 Average maximum plastic rotations of chord members in special segments at each floor during La09 Landers (Yermo) ground motion

CHAPTER 5

Second Phase Investigation

5.1 Introduction

Serious efforts have been undertaken to develop the framework for Performance-Based Earthquake Engineering (PBEE) in the United States after the 1994 Northridge Earthquake. Based on the requirement of PBEE, a structure should meet multiple performance objectives when subjected to earthquakes: *i.e.*, fully operational in a 72-year earthquake event (with 50% probability of exceedance in 50 years), and life safety in a 475-year event (10% in 50 years). This implies that the structural and nonstructural damage or performance need to be predictable with reasonable accuracy in order for owners or users to make appropriate decisions. In current practice, performance-based design is carried out in an indirect manner. It usually starts with an initial design according to conventional elastic design method based on applicable design codes, and then an assessment or evaluation analysis is performed. As a consequence, an iterative process between design and assessment is followed.

Two predominant methods, the Coefficient Method in FEMA 356 (ASCE, 2000) and Capacity-Spectrum Method in ATC-40 (ATC, 1996) are most often used in current U.S. practice. Both approaches use nonlinear static analysis (pushover analysis) to estimate the seismic demands. A target displacement, which is intended to represent the maximum displacement likely to be experienced during the design earthquake, is first calculated based on either coefficient method or capacity-spectrum method, then the structure is monotonically pushed by specified lateral forces until the target displacement is reached. If the performance indicated by the pushover analysis, such as interstory drift, member rotation angles, and ductility demands, do not meet the required objectives, the design is revised and the process is repeated until performance targets are met.

These performance-based design approaches, while practical, may have several problems:

1) A poor initial design may be improved eventually through many iterations, but it most likely will never become a good or optimal design (Krawinkler and Miranda, 2004).

2) Since a nonlinear static analysis is required, engineers need to deal with mathematical models which directly incorporate the nonlinear load-deformation characteristics of individual components and elements of the structure. Together with the iterative design process, the entire design is more time-consuming than the conventional ones.

3) The performance evaluations focus primarily on the demands and capacities of individual components, rather than the global structural behavior. Consequently, the overall structural performance will depend on the weakest or least ductile elements (Hamburger et al, 2004).

4) The nonlinear static procedures may not be reliable in predicting some demands as pointed out in FEMA 440 (ATC, 2004), such as maximum drifts at each level, story shear forces, etc. A direct nonlinear dynamic analysis, in many cases, gives better indications.

While future improvements are needed in the current performance-based design practice, this study proposes a direct design method which practically eliminates the need for any assessment after initial design. As described in Chapter 2, the proposed performance-based plastic design approach has the following features and advantages:

1) The work needed to push a structure monotonically up to the target drift is calculated based on the elastic design spectra given by the design codes. Then the design base shear is obtained by using an energy balance equation.

2) As shown in Chapter 2, the design proceeds with a pre-selected yield mechanism for the structure. The special segments at all levels are designed at the same time, as well as the elements outside the special segments. Thus, the designer is able to envision the targeted structural behavior.

3) It is a direct performance-based design method which basically requires no nonlinear static or dynamic assessment after initial design. That is the result of using pre-selected yield mechanism, pre-selected target drift, plastic design and capacity design approaches, and more rational story shear distribution.

4) The design procedure is easy to follow and can be easily computerized. In case where structural irregularities are present, the proposed design method will provide a good initial design, which reduces the amount of iteration.

In order to further validate the proposed performance-based design approach, the second phase study included buildings with two occupancy types—essential facilities (*i.e.*, hospital buildings) and ordinary office/residential buildings. The study parameters included: location of yielding, maximum plastic rotation in the truss girder chord members, maximum relative story shear distribution, maximum interstory drift, and peak floor acceleration.

A nine story building was selected for the study. The special segments are open Vierendeel type with chord members made of double-channel shapes as those in the first phase study. The special segments have lengths in the range of 20-25% of the truss span. The framing layout was designed to have configuration such that truss girders framing in the two directions of a column are avoided.

The performance-based plastic design procedure as proposed and used in the first phase study with some modifications according to the results in the first phase was used to design typical STMF for the study buildings. For ordinary buildings the target drifts of 2% and 3% for 10%/50 and 2%/50 design hazard levels, respectively, were chosen. The corresponding numbers for essential buildings are 1.5% and 2.25%. Design spectral values were based on NEHRP Provisions (FEMA, 2001) for the San Francisco site.

After the final design work was completed, inelastic pushover and dynamic analyses were conducted to study the response and ductility demands of the frames. Both 10% in 50 years and 2% in 50 years SAC Los Angeles region ground motions to represent the two design hazard levels were employed for the nonlinear dynamic analyses. The results of the analyses were studied to validate the design procedure, and to compare the ductility demands with the capacities as determined from the testing work (Chapter 3).

5.2 Description of the Structure

The nine-story structure is 150 ft by 150 ft in span, and 130 ft in elevation, as shown in Figure 5.1. The bays are 30 ft on center, in both directions, with five bays each in the north-south (N-S) and east-west (E-W) directions. The building's lateral load resisting system is comprised of steel perimeter special truss moment frames (STMFs). The interior bays of the structure consist of simple framing with composite floors.

The columns are 50 ksi steel and wide-flange sections. The levels of the 9-story building are numbered with respect to the ground level (see Figure 5.2). The ninth level is the roof. The building has a basement level denoted B-1. Typical floor-to-floor heights (for analysis purposes measured from center-of-top chord to center-of-top chord) are 14 ft. The floor-to-floor height of the basement level is 14 ft and for the first floor is 18 ft.

In this study, the column sizes were changed at every floor for study purposes. In practice, column sizes can be changed every two or three floors instead of every floor as done in this study. This would somewhat increase the material weight but reduce the fabrication cost such as column splices. The column bases were modeled as pinned and secured to the ground (at the B-1 level). Concrete foundation walls and surrounding soil are assumed to restrain the structure at the ground level from horizontal displacement.

Each frame resists one half of the seismic mass associated with the entire structure. The seismic mass is due to various components of the structure, including steel framing, floor slabs, ceiling/flooring, mechanical/electrical, partitions, roofing and a penthouse located on the roof. The seismic mass at the ground level is 66.0 kips-sec^2/ft, for the first level is 69.0 kips-sec^2/ft, for the second through eight levels is 67.7 kips-sec^2/ft and for the ninth level is 73.2 kips-sec^2/ft. The seismic mass of the entire structure above the ground level is 616 kips-sec^2/ft.

5.3 NEHRP 2000 Provisions

5.3.1 Background

The Maximum Considered Earthquake (MCE) is defined as the ground shaking for a 2%/50 year earthquake at a site (i.e. 2475 year mean recurrence interval). It is the largest earthquake that can be generated by known seismic sources. In the 1997 UBC or earlier NEHRP Provisions, the design ground motions were based on a 90 percent probability of not being exceeded in 50 years. However, it is recognized that larger ground motions are possible and they could occur at any time. **The Design Earthquake**

in the NEHRP 2000 is taken as two-thirds of the MCE in order to have some "seismic margin" against larger, less probable ground motions.

5.3.2 Design Base Shear and Lateral Force Distribution

The procedure for determining the design base shear in accordance with NEHRP 2000 Provisions (FEMA, 2001) is briefly described as follows:

(1) The maximum considered earthquake spectral response acceleration (used to construct the response spectra) at short periods, S_S, and at 1-second period, S_1, can be determined from Map 1 through 24 of the NEHRP Provisions, or directly from the USGS maps from their website by specifying the latitude and longitude of the site.

(2) Modifying S_S and S_1 for the soil conditions at the site:

$$S_{MS} = F_a S_S \tag{5.1}$$

$$S_{M1} = F_v S_1 \tag{5.2}$$

where F_a, F_v are site coefficients defined in NEHRP 2000 Tables 4.1.2a and 4.1.2b based on different site classes.

(3) Design spectral response acceleration parameters (two-thirds of MCE):

$$S_{DS} = \frac{2}{3} S_{MS} \tag{5.3}$$

$$S_{D1} = \frac{2}{3} S_{M1} \tag{5.4}$$

(4) Determine Seismic Use Group (NEHRP Section 1-3) and Occupancy Importance Factors (I) according to NEHRP 2000 Table 1.4 (I = 1.0, 1.25, or 1.5).

(5) Determine Seismic Design Category (A~F) according to NEHRP 2000 Table 5.2.5.1.

(6) Determine approximate building fundamental period T_a (sec.):

$$T_a = C_r h_n^x \tag{5.5}$$

where h_n is the height (ft) above the base to the highest level of the structure and C_r and x are to be determined from NEHRP 2000 Table 5.4.2.1. The calculated period (T) for design:

$$T \le C_u \times T_a \tag{5.6}$$

The coefficient C_u can be obtained from NEHRP 2000 Table 5.4.2.

(7) Seismic design base shear:

$$V = C_s W \tag{5.7}$$

where $C_s = \dfrac{V}{W}$ is the seismic response coefficient which is determined by:

$$C_s = \frac{S_{DS}}{(R/I)} \le \frac{S_{D1}}{(R/I)T}$$

$$\ge 0.044 S_{DS} I \tag{5.8}$$

$$\ge \frac{0.5 S_1}{(R/I)}$$

The last inequality applies to the Seismic Design Categories E and F. *R* is the response modification factor obtained from NEHRP 2000 Table 5.2.2 (= 7.0 for STMF).

(8) Vertical distribution of seismic forces:

$$F_x = C_{vx} V \tag{5.9}$$

$$C_{vx} = \frac{w_x h_x^k}{\sum_{i=1}^{n} w_i h_i^k} \tag{5.10}$$

$$\begin{aligned} &T \le 0.5 \text{ sec} \Rightarrow k = 1 \\ &T \ge 2.5 \text{ sec} \Rightarrow k = 2 \\ &0.5 < T < 2.5 \Rightarrow \text{ linear interpolation of } k \end{aligned}$$

5.4 NEHRP Design Response Spectrum and SAC Earthquake Records

Nine 10% in 50 years (return period 475 years) and five 2% in 50 years (return period 2,475 years) SAC Los Angeles ground motions were selected for the nonlinear time history analysis as shown in Figures 5.3 and 5.4, respectively. These time histories were plotted by SeismoSignal (SeismoSoft, 2004). In addition to the acceleration time histories, the companion velocity time histories as shown in Figures 5.3 and 5.4 are good indication of near-fault type ground motion in which high velocity pulse is observed (Bolt, 2004). Figure 5.5 gives the 5% damped design response spectrum based on NEHRP 2000 Provisions. Figure 5.6 shows the design spectrum as well as the response spectra of selected SAC earthquake records. Note that the SAC ground motions were already scaled (Somerville et al., 1997), hence no further scaling factor was used in this study.

5.5 Design of 9-story Ordinary STMF

5.5.1 Design Base Shear and Lateral Force Distribution

The 9-story ordinary STMF (Figure 5.2) was designed by the proposed performance-based design procedure with revised expected nominal shear strength of the special segments, V_{ne} (See Section 2.4 Eq. (2.44)). The proposed expression for V_{ne} is more rational as compared with the equation given in current AISC Seismic Provisions (AISC, 2005) which may be overly conservative, especially for heavier chord members.

The frame design procedure is briefly described as follows.

Design parameters given by NEHRP Provisions (FEMA, 2001) for the standard occupancy (Importance Factor I = 1.0) 9-story STMF are listed in Table 5.1. The fundamental period of the building, *T*, is calculated as:

$$T_a = 0.028(130)^{0.8} = 1.375\,\text{sec.} \tag{5.11}$$

$$T = C_u \times T_a = 1.4 \times T_a = 1.925\,\text{sec.} \tag{5.12}$$

The design base shear was determined for two level performance criteria: 1) A 2% maximum story drift for a ground motion hazard with 10% probability of exceedance in 50 years (10/50 and 2/3MCE); 2) 3% maximum story drift for 2/50 event (MCE).

The Seismic Response Coefficient, C_s, for the first hazard level (2/3MCE) is determined as:

$$C_s = \frac{S_{DS}}{(R/I)} = \frac{1.0}{(7/1)} = 0.143 \tag{5.13}$$

C_s need not exceed the following:

$$\frac{S_{D1}}{(R/I)T} = \frac{0.68}{(7/1)\cdot(1.925)} = 0.05 \tag{5.14}$$

and not be less than:

$$0.044 S_{DS} I = 0.044(1.0)(1.0) = 0.044 \tag{5.15}$$

For structures in Seismic Design Categories E and F, C_s not to be taken less than:

$$\frac{0.5 S_1}{(R/I)} = \frac{(0.5)(0.78)}{(7/1)} = 0.0557 \tag{5.16}$$

Thus,

$$C_s = 0.0557 \tag{5.17}$$

The design pseudo-acceleration coefficient, C_e , for the proposed method is calculated as:

$$C_e = C_s \cdot \left(\frac{R}{I}\right) = 0.0557 \cdot \left(\frac{7}{1}\right) = 0.39 \tag{5.18}$$

Seismic Response Coefficient for the second hazard level (MCE) can be calculated similarly by using Eqs. (5.13) thru (5.16) and replacing S_{DS} and S_{D1} with S_{MS} and S_{M1}, respectively. The following value of C_s was calculated:

$$C_s = 0.075 \tag{5.19}$$

Therefore,

$$C_e = C_s \cdot \left(\frac{R}{I}\right) = 0.525 \tag{5.20}$$

By following the flowchart for the STMF design procedure (see Figure 2.12), all the corresponding parameters are calculated and listed in Tables 5.2 and 5.3. It can be seen from Table 5.2 that the base shear for the first hazard level (2/3 MCE) governs the design, that is,

$$V = 0.099W = 1956.1 \ \text{ kips} \tag{5.21}$$

Design lateral force at each floor level is then calculated and given in Table 5.4.

5.5.2 Design of Chord Members in Special Segments

The required plastic moment of the first-story columns is computed as:

$$M_{pc} = \frac{1.1V'h_1}{4} = \frac{1.1 \times \frac{1956.1}{(2)(5)} \times 18}{4} = 968.3 \ \text{ kips-ft} \tag{5.22}$$

Note that V' is the base shear for one bay (in each direction of the building there are two STMFs and each STMF has five bays). Then the required chord member strength at each level is determined as:

$$\beta_i M_{pbr} = \beta_i \cdot \frac{\left(\sum_{i=1}^{n} F_i h_i - 2M_{pc} \right)}{4 \frac{L}{L_p} \sum_{i=1}^{n} \beta_i} \tag{5.23}$$

Here $L_s = 8$ ft is used to replace L_p so that no L_p needs to be estimated. Also the calculated values are more conservative. The selected chord sections for each level are given in Table 5.5 and compactness check is shown in Table 5.6.

5.5.3 Design of Members outside Special Segments

Design of members (chords, verticals, diagonals, and columns) outside the special segment is based on the capacity design approach (see Figure 2.13 for design flowchart). It should be noted that the lateral forces at each level are those needed to develop the expected ultimate strength of the special segments, i.e., V_{ne}. The applied forces on the interior and exterior column free bodies are shown in Table 5.7. Figure 5.7 shows the forces acting on the interior column free body. The required moment and axial force for each element can be easily obtained by using a computer program such as RISA-3D (RISA, 2001). All the elements are designed as beam-column elements, according to LRFD Equation (H1-1a) or (H1-1b) (AISC, 2001). Several key design issues are noted as following:

1) Double channels were used for all truss members. For chord members outside the special segment, web plates are added to provide the needed strength. $F_y = 50$ ksi was used for all sections including side plates.

2) Vertical members adjacent to the special segments have the same section as chord members in the special segments.

3) To avoid biaxial bending in the exterior columns, the lower chord member adjacent to the exterior column bending about the weak axis is not connected to the column (see Figure 5.8a). Note that the exterior columns are originally designed according the approach stated above, in which the exterior columns bend about the strong axis and both the upper and lower chords are connected to the columns. Then the same column sections are used at the other end of the five-bay frame but oriented in weak direction and lower chords not connected to them.

4) For simplicity, the effective length factor K for all the columns is assumed as 1.0. The reason is that, due to the presence of the truss girder, the stiffness of an STMF is somewhat in-between a moment frame and a braced frame. Further, the alignment chart used to calculate K in LRFD Eq. (C-C2-2) is based on purely elastic behavior. However, columns are generally loaded into inelastic range of column behavior which leads to smaller K factors (AISC, 2001). Nonlinear analyses (static as well as dynamic) including $P-\Delta$ effect showed that the columns designed with K=1.0 had adequate strength.

The final member sections for the 9-story STMF are shown in Figure 5.8.

5.6 Performance Evaluation of the 9-Story Ordinary STMF

The performance of the 9-story ordinary STMF design by the proposed procedure was evaluated through nonlinear static and dynamic analyses using a commercial program, Perform-2D (RAM, 2003). Nine 10% in 50 year and five 2% in 50 year SAC LA region ground motion time histories were employed for the nonlinear dynamic analyses. The study parameters included: location of plastic hinges, plastic hinge rotation, V_{ne}, interstory drift, and peak floor acceleration.

It has been seen in past earthquakes that seismic performance of nonstructural components has significant influence on the overall performance of a building. It is estimated that approximately 70% to 80% of the cost of a building goes into nonstructural components. This suggests that majority of the damage and potential economic losses come from the damage to nonstructural components (Villaverde, 2004). Generally, nonstructural components can be categorized into two types (FEMA 356, 2000): acceleration-sensitive components (such as mechanical equipments, piping systems, and storage vessels), and deformation-sensitive components (such as cladding, partitions, interior veneers, and glazing systems). The seismic performance of the former is directly related to the floor accelerations and that of the latter to interstory drifts. The maximum interstory drift is pre-selected in the beginning of the proposed design method, thus the performance of deformation-sensitive components can be assured. The seismic performance of acceleration-sensitive components can be assured by keeping the floor accelerations within acceptable limits such as code-specified values. A trapezoidal distribution of allowable floor accelerations is used in the NEHRP Provisions (FEMA, 2001):

$$(A_F)_i = 0.4 S_{DS}\left(1 + 2\frac{z}{h}\right) \qquad (5.24)$$

where z is the height of the point of attachment of the component in the structure; h is the average roof height of the structure from the ground level. Assuming the point of attachment is the floor, the design floor accelerations vary linearly from $0.4S_{DS}$ to $1.2S_{DS}$.

The analytical results and conclusions are summarized as follows:

1) Figure 5.9 shows the pushover response of the 9-story STMF. It can be seen that the yield drift is about 0.65%, close to the assumed 0.75% yield drift.

2) As shown in Figure 5.10, based on the 14 time-history nonlinear dynamic analyses, the proposed design story shear distribution represents the envelope story shear distribution of the structure very well. Relative story shear distributions according to NEHRP and CBC expressions are also plotted. It is seen while the NEHRP distribution shows significant deviation from those obtained from nonlinear dynamic analyses, the CBC distribution gives better prediction. This resulted from the additional concentrated force applied at the top floor by using the CBC expression (see Eq. (4.11)).

3) The plastic hinges occurred mainly at the ends of the chord members in the special

segments. As can be seen in Figure 5.11, the maximum plastic hinge rotation is about 0.04 rad when subjected to 10% in 50 year ground motions and 0.08 rad. when subjected to 2% in 50 year ground motions (Note that the maximum plastic rotation capacity of the double channel specimens achieved in the UM tests was 0.07 rad., see Table 3.2). Some minor yielding also occurred at the column bases and vertical members adjacent to the special segments, under some ground motions. It is also noticed that the plastic rotation demand of the special segment in the bay where the lower chord is not connected to the column is about 1/3 of that in the other bays. However, minor yielding occurred in the diagonals, and top chords connecting to the column.

4) The yielding was generally limited to the special segments only, while the other elements remained essentially elastic. This shows that the proposed expression for V_{ne} is quite adequate to ensure elastic performance of the elements outside the special segments. Figures 5.12a and 5.12b show the maximum developed shears in the special segment when the frame was subjected to 10% in 50 years and 2% in 50% years ground motions, respectively. It is seen that the AISC equation significantly overestimates the expected shear strength, which would lead to undue over design of elements outside the special segments. On the other hand, the proposed expression (Eq. (2.44)/(2.45)) is closer to the actual developed shears while maintaining some safety margin. It is worth mentioning that where the lower chords were not connected to the exterior columns it resulted in smaller demand on those columns, without yielding even though they were subjected to weak axis bending.

5) Figures 5.13a and 5.13b show maximum interstory drifts resulting from 10% in 50 year and 2% in 50 year ground motions, respectively. The mean value of maximum story drifts and corresponding target drifts are shown in Figure 5.14. It is seen that all the interstory drifts are within the 2% target drift for the 2/3 MCE ground motions (first level hazard). Only one of the MCE ground motions (LA30) resulted in interstory drift slightly exceeding the 3% target drift (second level hazard). This suggests that the seismic performance of the deformation-sensitive components can be controlled by the proposed design procedure.

6) Figure 5.15 shows somewhat uniform distribution of floor accelerations, which is quite different from the code-specified floor acceleration pattern. Except for a few lower levels, the absolute peak floor accelerations are well below the design values, indicating that the seismic performance of the acceleration-sensitive components can also be expected to be satisfactory.

5.7 Design of the 9-story Essential STMF

5.7.1 Design Base Shear and Lateral Force Distribution

The 9-story essential STMF has the same frame layout as the 9-story ordinary STMF and was designed based on the proposed performance-based design procedure with revised expected nominal shear strength of the special segments, V_{ne}. Except for the target drift, all the design parameters are the same for the two frames. The frame design procedure is briefly described as follows.

Design parameters given by NEHRP Provisions (FEMA, 2001) for the 9-story STMF with occupancy importance factor I = 1.5 (for essential buildings) are listed in Table 5.8. The fundamental period of the building used for the design is 1.925 sec., same as for the ordinary 9-story STMF.

The design base shear was determined for two level performance criteria: 1) 1.5% maximum story drift for a ground motion hazard with 10% probability of exceedance in 50 years (10/50 and 2/3MCE); 2) 2.25% maximum story drift for 2/50 event (MCE).

The Seismic Response Coefficient, C_s , for the first hazard level (2/3MCE) is determined as:

$$C_s = \frac{S_{DS}}{(R/I)} = \frac{1.0}{(7/1.5)} = 0.2143 \tag{5.25}$$

C_s need not exceed the following:

$$\frac{S_{D1}}{(R/I)T} = \frac{0.68}{(7/1.5)\cdot(1.925)} = 0.076 \tag{5.26}$$

and not be less than:

$$0.044 S_{DS} I = 0.044(1.0)(1.5) = 0.066 \tag{5.27}$$

For structures in Seismic Design Categories E and F, C_s shall not be taken less than:

$$\frac{0.5S_1}{(R/I)} = \frac{(0.5)(0.78)}{(7/1.5)} = 0.084 \tag{5.28}$$

Thus,

$$C_s = 0.084 \tag{5.29}$$

The elastic pseudo-acceleration coefficient, C_e , for the proposed method is calculated as:

$$C_e = C_s \cdot \left(\frac{R}{I}\right) = 0.084 \cdot \left(\frac{7}{1.5}\right) = 0.39 \tag{5.30}$$

The Seismic Response Coefficient for the second hazard level (MCE) can be calculated similarly by using Eqs. (5.26) - (5.28) and replacing S_{DS} and S_{D1} with S_{MS} and S_{M1}, respectively. Thus,

$$C_s = 0.113 \tag{5.31}$$

Therefore,

$$C_e = C_s \cdot \left(\frac{R}{I}\right) = 0.525 \tag{5.32}$$

By following the flowchart in the STMF design procedure (see Figure 2.12), all the corresponding parameters were calculated and are listed in Tables 5.9 and 5.10. It can be seen that the base shear for the first hazard level (2/3 MCE) governs the design, that is,

$$V = 0.169W = 3357.4 \ \text{ kips} \tag{5.33}$$

Design lateral force at each level is calculated as shown in Table 5.11.

5.7.2 Design of Chord Members in the Special Segments

The required plastic moment of the first-story columns is computed as:

$$M_{pc} = \frac{1.1V'h_1}{4} = \frac{1.1\times\frac{3357.4}{(2)(5)}\times 18}{4} = 1662 \ \text{ kips} \tag{5.34}$$

Note that V' is the base shear for one bay (in each direction of the building there are two STMFs and each STMF has five bays). Then the required chord member strength at each level is determined as:

$$\beta_i M_{pbr} = \beta_i \cdot \frac{\left(\sum_{i=1}^{n} F_i h_i - 2M_{pc}\right)}{4\frac{L}{L_p}\sum_{i=1}^{n}\beta_i} \tag{5.35}$$

Here $L_s = 8$ ft is used for L_p, which is somewhat on the conservative side. The selected chord sections at each level are given in Table 5.12 and compactness check is shown in

Table 5.13.

5.7.3 Design of Members outside the Special Segments

Design of members outside the special segments (chords, verticals, diagonals, and columns) is based on the capacity design approach. It should be noted that the lateral forces at each level are those needed to develop the expected ultimate strength of the special segments, i.e., V_{ne}. The applied forces on the interior and exterior column free bodies are shown in Table 5.14. The required moment and axial force in each element can be easily obtained by using an elastic structural analysis program such as RISA-3D (RISA, 2001). All the elements are designed as beam-column elements, according to LRFD Equation (H1-1a) or (H1-1b) (AISC, 2001).

The final member sections for the 9-story essential STMF are shown in Figures 5.16a and 5.16b. Note that in order to reduce the thickness of the side plates; they were connected to flanges of double channel chord members (providing more depth) rather than to the webs as was done in the design of the ordinary STMF.

5.8 Performance Evaluation of the 9-Story Essential STMF

The performance of the 9-story essential STMF design by the proposed PBPD method was evaluated through nonlinear static and dynamic analyses using the program Perform-2D (RAM, 2003) Nine 10% in 50 year and five 2% in 50 year SAC LA region ground motion time histories were employed for the nonlinear dynamic analyses. The study parameters included: location of plastic hinges, plastic hinge rotation, V_{ne}, inter story drift, peak floor acceleration, and residual displacement.

The analytical results and conclusions are summarized as follows:

1) Figure 5.17 shows the pushover response of the 9-story essential STMF. It can be seen that the yield drift is about 0.6%, slightly smaller than that of the ordinary STMF. This arises from heavier and stiffer sections needed for the essential STMF. The overall elastic stiffness of the essential STMF is about 1.8 times of that of the ordinary STMF.

2) As shown in Figure 5.18a, based on the 14 time-history nonlinear dynamic analyses, the proposed design story shear distribution represents the envelope story shear distribution of the structure very well. It is noted that, the proposed story shear distribution accounts for the effect of inelastic behavior of the structure, as well as the higher mode effect. To illustrate the differences of relative story shear distribution between inelastic and elastic response, elastic dynamic analyses were performed for the 9-story ordinary STMF using the same ground motions. The LA 12 and LA 19 ground motions were not included since the maximum plastic chord rotations were rather small, 0.007 and 0.01 for LA 12 and LA 19 ground motions, respectively. The overall behavior from inelastic and elastic dynamic analyses has only slight changes because most members of the ordinary STMF remained elastic when subjected to these two ground motions.

A notable feature observed in Figures 5.18b and 5.18c is that, for elastic dynamic analysis plots, 10 out of 12 relative story shear plots shifted to the right and are closer to the NEHRP 2000 distribution. This indicated that the NEHRP lateral force distribution is more representative of elastic response. On the other hand, the proposed distribution captures the realistic behavior as the structures experience significant inelastic activity when subjected to major earthquakes.

3) The plastic hinges occurred mainly at the ends of the chord members in the special segments. As can be seen in Figure 5.19, the maximum plastic hinge rotation is about 0.04 rad. when subjected to 10% in 50 year ground motions and 0.06 rad. when subjected to 2% in 50 year ground motions (Note that the maximum plastic rotation capacity of the double channel specimens achieved in the UM tests was 0.07 rad., see Table 3.2). Some very minor yielding also occurred at the column bases and in the vertical members adjacent to the special segments, due to some ground motions. It is also noticed that the plastic rotation demand of the special segment in the bay where the lower chord is not connected to the column is about 1/3 of that in the other bays.

4) The yielding was generally limited to the special segments only, while the other elements remained essentially elastic. This shows that the proposed expression for V_{ne} is adequate to ensure elastic behavior of the elements outside the special segments. Figures 5.20a and 5.20b show the maximum developed shears in the special segment when the frame was subjected to 10% in 50 years and 2% in 50% years ground motions, respectively. It is seen that the AISC equation generally significantly overestimates the expected shear strength, which leads to over design of

elements outside the special segments. On the other hand, the proposed expression (Eq. (2.44)/(2.45)) is closer to the actual developed shears while maintaining some safety margin. It is also worth mentioning that, as also observed in the 9-story ordinary frame, where the lower chords were not connected to the exterior columns that resulted in smaller demand on those columns, and no yielding was observed even though they were subjected to weak axis bending.

5) Figures 5.21a and 5.21b show maximum interstory drifts resulting from 10% in 50 year and 2% in 50 year ground motions, respectively. The mean value of maximum story drifts and corresponding target drifts are shown in Figure 5.22. It can be seen that generally all the interstory drifts are within 1.5% target drift when the structure is subjected to the 2/3 MCE ground motions (first level hazard); and are within 2.25% target drift when the structure is subjected to the MCE ground motions (second level hazard). A few interstory drifts slightly exceeded the 1.5% target drift when subjected to LA 09 ground motion due to specific characteristics of this ground motion as explained below.

While the design fundamental period is 1.925 sec in accordance with NEHRP, the fundamental periods based on dynamic analysis are 2.2 sec and 1.6 sec for the ordinary and essential STMF, respectively. Referring to Figure 5.6, it is seen that the design spectrum and the response spectrum of LA 09 ground motion have similar accelerations around T = 1.925 ~ 2.2 sec, but the spectrum acceleration of LA 09 ground motion around T = 1.6 sec is almost twice of that in the design spectrum around T = 1.925 sec. Note that the SAC ground motions have been already scaled

(Somerville et al., 1997) hence no further scaling factor was used in this study. Nonetheless, most analyses showed that the proposed design method is very effective in keeping the story drifts within the pre-selected target drift. This suggests that the seismic performance of the deformation-sensitive non-structural components can be controlled by the proposed design procedure.

6) Figure 5.23 presents the distribution of floor accelerations, which is different from the floor acceleration pattern obtained in the ordinary STMF. Higher floor accelerations in the essential STMF are primarily the result of higher stiffness of the essential STMF, which in turn causes greater floor accelerations (Mayes et al., 2004). Nonetheless, except for a few lower levels, the absolute peak floor accelerations are below the code design values, indicating that the seismic performance of the acceleration-sensitive components can also be expected to be satisfactory.

7) Excessive residual displacement of a structure after a major earthquake could result in the operational problems of some equipment such as elevators. Therefore, control of the residual displacement is another goal of performance-based design, especially for important facilities. The roof drift (displacement) time histories of the ordinary and essential STMF subjected to three selected ground motions are shown in Figure 5.24. It is evident that the study STMFs have acceptable residual displacements even when subjected to severe ground motions.

8) The weight of steel for both frames is calculated and listed in Tables 5.15 and 5.16. It is seen that the material weight (cost) for the essential STMF is about 1.5 times of

that for the ordinary STMF.

5.9 Additional Note on The Design of STMFs

In the PBPD procedure proposed in this study, the target building drift is selected before the design is carried out. The target building drift may be determined based on considerations, such as damage tolerance of structural and non-structural elements. Therefore, plastic rotation capacity of chord members used for the special segments can be one of those considerations. If the plastic rotation capacity of the chord members is known from test results, the maximum allowable story drift can be conservatively estimated from the following expression:

$$\theta_p = \frac{L}{L_s} \cdot (\text{story drift}) - 0.015 \ (\text{rad.}) \tag{5.36}$$

where L = span length of the truss girder; L_s = length of the special segment; θ_p is the plastic rotation capacity of the chord member. Eq. (5.36) is derived based on Eq. (2.39) and the experimental results shown in Figure 3.24, where the elastic rotation is about 0.015 rad. Some typical values according to Eq. (5.36), assuming $L/L_s = 30$ ft/8 ft = 3.75 (as the 9-story STMF), are listed in Table 5.17.

Table 5.1 Design Parameters for 9-story ordinary STMF calculated according to NEHRP 2000

Parameters	9-story STMF
S_S	1.50 g
S_1	0.78 g
S_{MS}	1.50 g
S_{M1}	1.01 g
F_a	1.000
F_v	1.3
S_{DS}	1.00 g
S_{D1}	0.68 g
Site Class	C
Occupancy Importance Factor	I = 1.0 (Ordinary Building)
Seismic Design Category	E
Building Height	130 ft (above the base)
T_a	1.375 sec.
C_U	1.4
T	1.925 sec.
Response Modification Factor	R= 7
Total Building Weight W	19839 kips
$C_s = \frac{V}{W}$	0.056

Table 5.2 Design Parameters for the proposed procedure

Parameters	10% in 50 year Hazard	2% in 50 year Hazard
C_e	0.39g	0.525g
T	1.925	1.925
Yield Drift θ_y	0.75%	0.75%
Target Drift θ_u	2%	3%
Inelastic Drift θ_p	1.25%	2.25%
$\mu_s = \frac{\theta_u}{\theta_y}$	2.67	4
R_μ	2.67	4
γ	0.609	0.438
α	0.841	1.515
$\frac{V}{W}$	0.099	0.076
Design Base Shear V	1956.1 kips	1504.3 kips

Table 5.3 Distribution of Shear Proportioning Factor for the 9-Story ordinary STMF

Floor	h_i (ft.)	w_i (kips)	$w_i h_i$ (kip-ft)	$\sum_i^n w_i h_i$	β_i (=V_i / V_n)	$(\beta_i - \beta_{i+1})h_i$
9	130	2357	306410	306410	1.000	130.00
8	116	2180	252880	559290	1.486	56.34
7	102	2180	222360	781650	1.852	37.34
6	88	2180	191840	973490	2.139	25.31
5	74	2180	161320	1134810	2.367	16.80
4	60	2180	130800	1265610	2.543	10.57
3	46	2180	100280	1365890	2.673	6.02
2	32	2180	69760	1435650	2.762	2.85
1	18	2222	39996	1475646	2.813	0.91

Table 5.4 Design Lateral Forces for the 9-Story ordinary STMF (for two frames)

Floor	$\beta_i - \beta_{i+1}$	F_i (kips)
9	1.000	695.43
8	0.486	337.78
7	0.366	254.55
6	0.288	200.05
5	0.227	157.92
4	0.176	122.46
3	0.131	90.97
2	0.089	61.94
1	0.050	35.05

Table 5.5 Required Chord Member Strength and Selected Chord Member Sections

Floor	Require moment strength $\beta_i M_{pbr}$ (kip-ft)	Required Z (in^3)	Section (Double channels)	Z (in^3)	M_{nc} (kip-in)	I_x (in^4)
9	61.0	16.3	**7C12.25**	16.92	846	48.4
8	90.6	24.2	**8C18.75**	27.8	1390	87.8
7	112.9	30.1	**9C20**	33.8	1690	121.8
6	130.5	34.8	**10C20**	38.8	1940	157.8
5	144.3	38.5	**10C25**	46.2	2310	182.2
4	155.1	41.4	**10C25**	46.2	2310	182.2
3	163.0	43.5	**10C25**	46.2	2310	182.2
2	168.5	44.9	**10C30**	53.4	2670	206
1	171.6	45.7	**10C30**	53.4	2670	206

Table 5.6 Compactness Check for Chord Member Sections per AISC Seismic Provision Table I-8-1

Floor	Width Thickness Ratio $\frac{b_f}{t_f}$	Limiting With Thickness Ratio $0.3\sqrt{E_s/F_y}$	Width Thickness Ratio $\frac{d}{t_w}$	Limiting With Thickness Ratio* $1.12\sqrt{\frac{E_s}{F_y}}\left(2.33-\frac{P_u}{\phi_b P_y}\right)$
9	5.98	7.22	22.3	35.87
8	6.49	7.22	16.4	35.87
7	6.42	7.22	20.1	35.87
6	6.28	7.22	26.4	35.87
5	6.63	7.22	19.0	35.87
4	6.63	7.22	19.0	35.87
3	6.63	7.22	19.0	35.87
2	6.95	7.22	14.9	35.87
1	6.95	7.22	14.9	35.87

***Note: Conservatively $P_u = \phi_b P_y$ was assumed even though the chord members in the special segment are generally subjected to small axial forces.**

Table 5.7 Design Forces for Elements outside Special Segments

Floor	$(V_{ne})_i$ (kips)	Concentrated Factored Gravity Loading @ 10 ft spacing in each bay (kips)	Lateral Forces at Ultimate Drift Level for Exterior Column Free Body (kips)		Lateral Forces at Ultimate Drift Level for Interior Column Free Body (kips)
			$\alpha_i F_R$	$\alpha_i F_L$	F_i
9	57.0	16	70.1	79.6	146.3
8	97.0	15	34.0	38.7	71.1
7	124.4	15	25.7	29.1	53.6
6	150.4	15	20.2	22.9	42.1
5	176.6	15	15.9	18.1	33.2
4	176.6	15	12.3	14.0	25.8
3	176.6	15	9.2	10.4	19.1
2	202.2	15	6.2	7.1	13.0
1	202.2	15	3.5	4.0	7.4

Table 5.8 Design Parameters for 9-story essential STMF calculated according to NEHRP 2000

Parameters	9-story STMF
S_S	1.50 g
S_1	0.78 g
S_{MS}	1.50 g
S_{M1}	1.01 g
F_a	1.000
F_v	1.3
S_{DS}	1.00 g
S_{D1}	0.68 g
Site Class	C
Occupancy Importance Factor	I = 1.5 (Essential Building)
Seismic Design Category	E
Building Height	130 ft (above the base)
T_a	1.375 sec.
C_U	1.4
T	1.925 sec.
Response Modification Factor	$R = 7$
Total Building Weight W	19839 kips
$C_s = \frac{V}{W}$	0.084

Table 5.9 Design Parameters for the proposed procedure

Parameters	10% in 50 year Hazard	2% in 50 year Hazard
C_e	0.39g	0.525g
T	1.925	1.925
Yield Drift θ_y	0.75%	0.75%
Target Drift θ_u	1.5%	2.25%
Inelastic Drift θ_p	0.75%	1.5%
$\mu_s = \frac{\theta_u}{\theta_y}$	2	3
R_μ	2	2
γ	0.75	0.556
α	0.505	1.01
$\frac{V}{W}$	0.169	0.134
Design Base Shear V	3357.4 kips	2656.4 kips

Table 5.10 Distribution of Shear Proportioning Factor for the 9-Story essential STMF

Floor	h_i (ft.)	w_i (kips)	$w_i h_i$ (kip-ft)	$\sum_i^n w_i h_i$	β_i (= V_i / V_n)	$(\beta_i - \beta_{i+1})h_i$
9	130	2357	306410	306410	1.000	130.00
8	116	2180	252880	559290	1.486	56.34
7	102	2180	222360	781650	1.852	37.34
6	88	2180	191840	973490	2.139	25.31
5	74	2180	161320	1134810	2.367	16.80
4	60	2180	130800	1265610	2.543	10.57
3	46	2180	100280	1365890	2.673	6.02
2	32	2180	69760	1435650	2.762	2.85
1	18	2222	39996	1475646	2.813	0.91

Table 5.11 Design Lateral Forces for the 9-Story essential STMF (for two frames)

Floor	$\beta_i - \beta_{i+1}$	F_i (kips)
9	1.000	1193.58
8	0.486	579.75
7	0.366	436.89
6	0.288	343.35
5	0.227	271.05
4	0.176	210.18
3	0.131	156.13
2	0.089	106.31
1	0.050	60.15

Table 5.12 Required Chord Member Strength and Selected Chord Member Sections

Floor	Require moment strength $\beta_i M_{pbr}$ (kip-ft)	Required Z (in^3)	Section (Double channels)	Z (in^3)	M_{nc} (kip-in)	I_x (in^4)
9	104.7	27.9	**9C20**	33.8	1690	121.8
8	155.5	41.5	**10C25**	46.2	2310	182.2
7	193.8	51.7	**10C30**	53.4	2670	206
6	223.9	59.7	**12C30**	67.6	3380	324
5	247.7	66.1	**12C30**	67.6	3380	324
4	266.1	71.0	**12MC31**	79.4	3970	404
3	279.8	74.6	**12MC31**	79.4	3970	404
2	289.2	77.1	**12MC35**	86.4	4320	432
1	294.4	78.5	**12MC35**	86.4	4320	432

Table 5.13 Compactness Check for Chord Member Sections per AISC Seismic Provision Table I-8-1

Floor	Width Thickness Ratio $\frac{b_f}{t_f}$	Limiting With Thickness Ratio $0.3\sqrt{E_s/F_y}$	Width Thickness Ratio $\frac{d}{t_w}$	Limiting With Thickness Ratio* $1.12\sqrt{\frac{E_s}{F_y}}\left(2.33-\frac{P_u}{\phi_b P_y}\right)$
9	6.42	7.22	20.1	35.87
8	6.63	7.22	19.0	35.87
7	6.95	7.22	14.9	35.87
6	6.33	7.22	23.5	35.87
5	6.33	7.22	23.5	35.87
4	5.24	7.22	32.4	35.87
3	5.24	7.22	32.4	35.87
2	5.39	7.22	25.7	35.87
1	5.39	7.22	25.7	35.87

***Note: Conservatively $P_u = \phi_b P_y$ was assumed even though the chord members in the special segment are generally subjected to small axial forces.**

Table 5.14 Design Forces for Elements outside Special Segments (for one frame only)

Floor	$(V_{ne})_i$ (kips)	Concentrated Factored Gravity Loading @ 10 ft spacing in each bay (kips)	Lateral Forces at Ultimate Drift Level for Exterior Column Free Body (kips)		Lateral Forces at Ultimate Drift Level for Interior Column Free Body (kips)
			$\alpha_i F_R$	$\alpha_i F_L$	F_i
9	124.4	16	131.7	141.2	267.0
8	176.7	15	64.0	68.6	129.7
7	202.2	15	48.2	51.7	97.7
6	282.9	15	37.9	40.6	76.8
5	282.9	15	29.9	32.1	60.6
4	342.2	15	23.2	24.9	47.0
3	342.2	15	17.2	18.5	34.9
2	369.1	15	11.7	12.6	23.8
1	369.1	15	6.6	7.1	13.5

Table 5.15 Steel weight calculation of ordinary STMF (one frame only)

Ordinary 9-story STMF									
Truss member—Double Channel (not including side plates)									
Floor	Chord	lb/ft	Vertical-SS	lb/ft	Vertical-1	lb/ft	Diagonal	lb/ft	Total
Basement	10C30	30	10C30	30	6MC16.3	16.3	10MC25	25	28504
1st FL	10C30	30	10C30	30	6MC16.3	16.3	10MC25	25	28504
2nd FL	10C30	30	10C30	30	6MC16.3	16.3	10MC25	25	28504
3rd FL	10C25	25	10C25	25	6MC12	12	9MC25.4	25.4	24868.8
4th FL	10C25	25	10C25	25	6MC12	12	9MC25.4	25.4	24868.8
5th FL	10C25	25	10C25	25	6MC12	12	9MC25.4	25.4	24868.8
6th FL	10C20	20	10C20	20	6MC12	12	7MC22.7	22.7	20734.4
7th FL	9C20	20	9C20	20	6MC12	12	7MC22.7	22.7	20734.4
8th FL	8C18.75	18.75	8C18.75	18.75	6MC12	12	6MC16.3	16.3	18143.6
9th FL	7C12.25	12.25	7C12.25	12.25	6MC12	12	6MC12	12	12554
								SUM	**232284**

Column									
Floor	Interior	lb/ft	Amount	Length(ft)	Exterior	lb/ft	Amount	Length(ft)	Total
Basement	W30X357	357	4	18	W30X292	292	2	18	36216
1st FL	W30X357	357	4	18	W30X292	292	2	18	36216
2nd FL	W30X326	326	4	14	W30X261	261	2	14	25564
3rd FL	W30X292	292	4	14	W30X235	235	2	14	22932
4th FL	W30X292	292	4	14	W30X211	211	2	14	22260
5th FL	W30X261	261	4	14	W30X191	191	2	14	19964
6th FL	W30X211	211	4	14	W30X148	148	2	14	15960
7th FL	W30X173	173	4	14	W30X132	132	2	14	13384
8th FL	W30X148	148	4	14	W30X108	108	2	14	11312
9th FL	W30X108	108	4	14	W24X84	84	2	14	8400
								SUM	**212208**
					Total Weight of frame(kips) =				**444.5**

Table 5.16 Steel weight calculation of essential STMF (one frame only)

Essential 9-story STMF									
Truss member—Double Channel (not including side plates)									
Floor	Chord	lb/ft	Vertical-SS	lb/ft	Vertical-1	lb/ft	Diagonal	lb/ft	Total
Basement	12MC35	35	12MC35	35	8MC22.8	22.8	10MC41.1	41.1	36803.2
1st FL	12MC35	35	12MC35	35	8MC22.8	22.8	10MC41.1	41.1	36803.2
2nd FL	12MC35	35	12MC35	35	7MC22.7	22.7	10MC41.1	41.1	36795.2
3rd FL	12MC31	31	12MC31	31	7MC22.7	22.7	10MC41.1	41.1	34075.2
4th FL	12MC31	31	12MC31	31	7MC22.7	22.7	10MC41.1	41.1	34075.2
5th FL	12C30	30	12C30	30	7MC22.7	22.7	10MC41.1	41.1	33395.2
6th FL	12C30	30	12C30	30	6MC12	12	10MC41.1	41.1	32539.2
7th FL	10C30	30	10C30	30	6MC12	12	9MC25.4	25.4	28268.8
8th FL	10C25	25	10C25	25	6MC12	12	9MC25.4	25.4	24868.8
9th FL	9C20	20	9C20	20	6MC12	12	9MC25.4	25.4	21468.8
								SUM	**319092**

Column									
Floor	Interior	lb/ft	Amount	Length(ft)	Exterior	lb/ft	Amount	Length(ft)	Total
Basement	W36X650	650	4	18	W36X527	527	2	18	65772
1st FL	W36X650	650	4	18	W36X527	527	2	18	65772
2nd FL	W36X527	527	4	14	W36X439	439	2	14	41804
3rd FL	W36X527	527	4	14	W36X359	359	2	14	39564
4th FL	W36X439	439	4	14	W36X300	300	2	14	32984
5th FL	W36X359	350	4	14	W36X256	256	2	14	26768
6th FL	W36X328	328	4	14	W36X232	232	2	14	24864
7th FL	W36X256	256	4	14	W36X182	182	2	14	19432
8th FL	W36X245	245	4	14	W36X160	160	2	14	18200
9th FL	W36X194	194	4	14	W36X135	135	2	14	14644
								SUM	**349804**
					Total Weight of frame(kips) =				**668.9**

Table 5.17 Relation between plastic rotation of chord members and story drift ratio of a typical STMF (Note: assuming the ratio of truss girder span to the length of special segment is 3.75)

Story Drift Ratio (%)	Plastic Rotation θ_p (rad.)
0.50	0.00
0.75	0.01
1.00	0.02
1.25	0.03
1.50	0.04
1.75	0.05
2.00	0.06
2.25	0.07
2.50	0.08
2.75	0.09
3.00	0.10

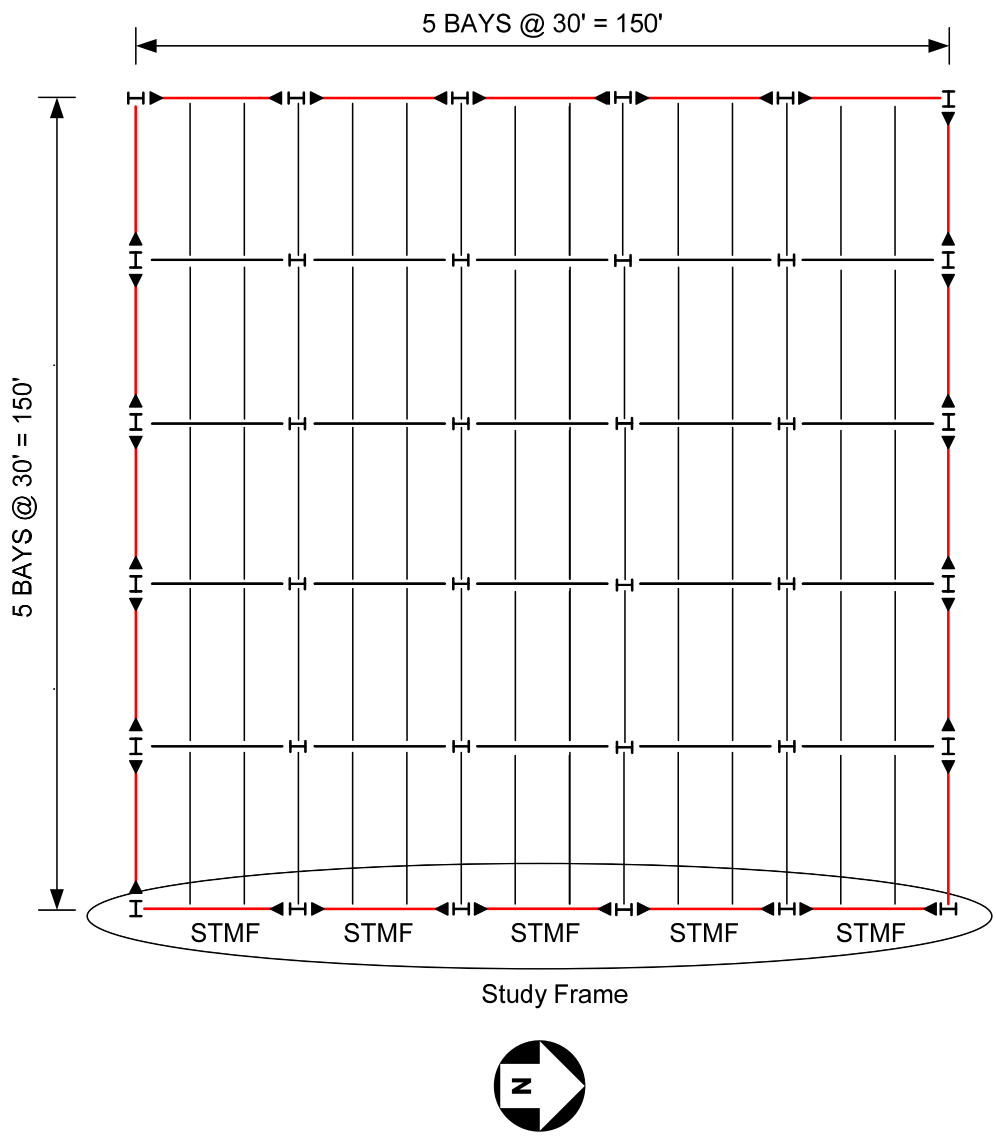

Figure 5.1 Building plan and STMFs in the second phase investigation

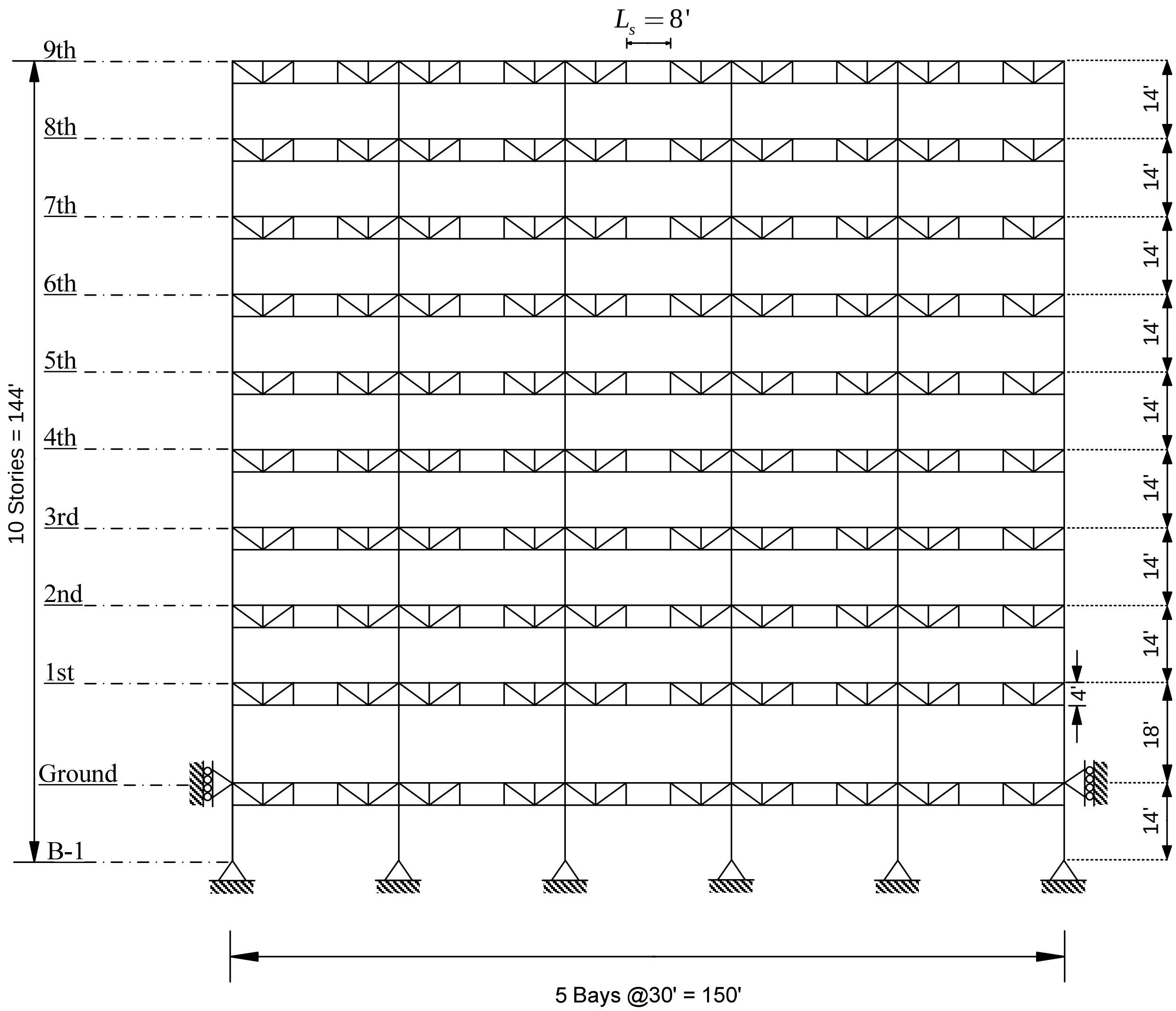

Figure 5.2 Elevation of study STMFs in the second phase investigation

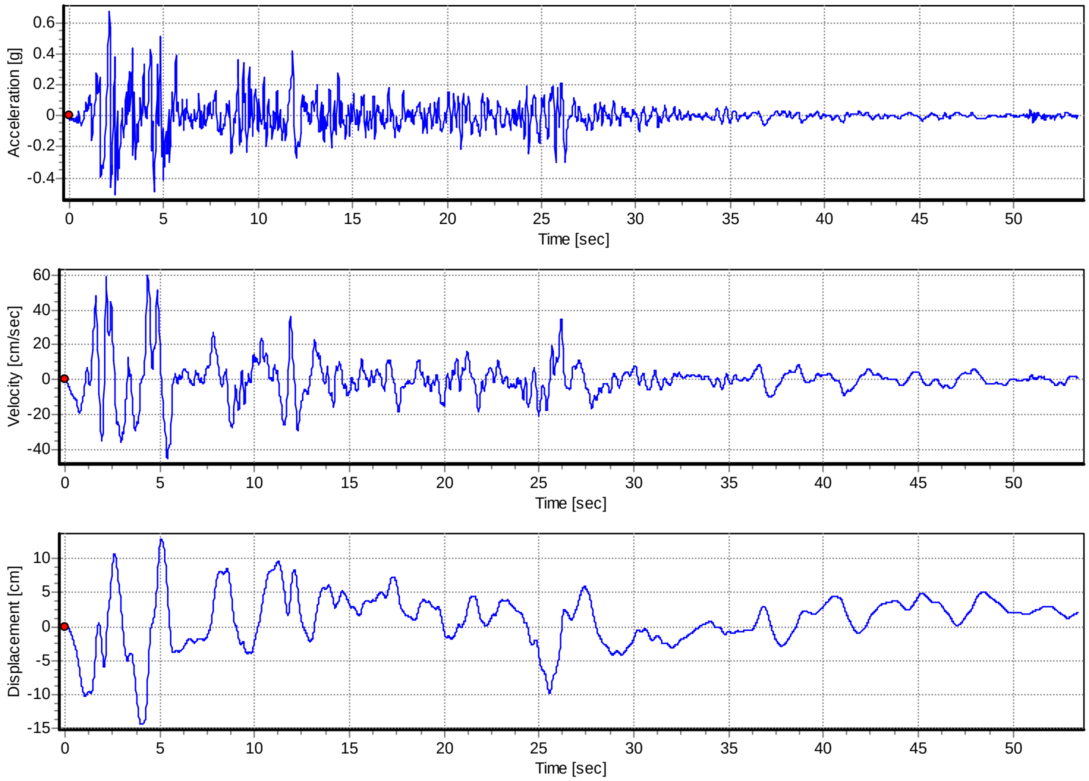

LA 02 (Imperial Valley, 1940, El Centro)

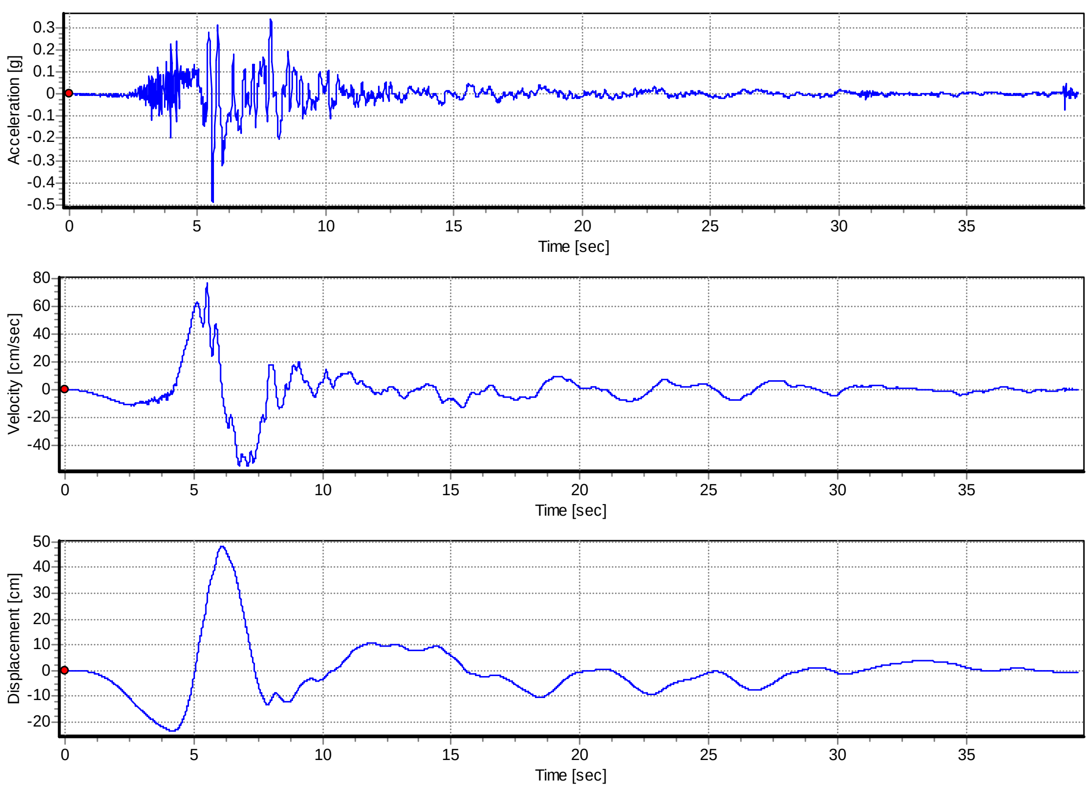

LA 04 (Imperial Valley, 1979, Array #05)

Figure 5.3 Acceleration, velocity, and displacement time histories of 10/50 SAC records

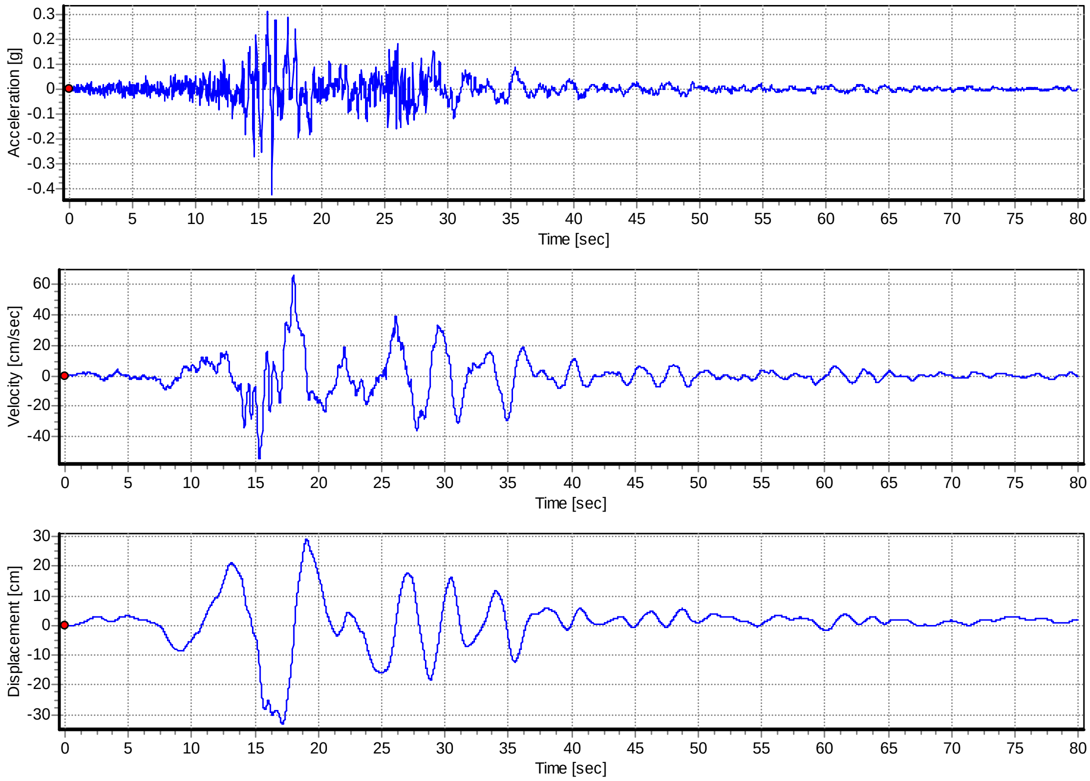

LA 07 (Landers, 1992, Barstow)

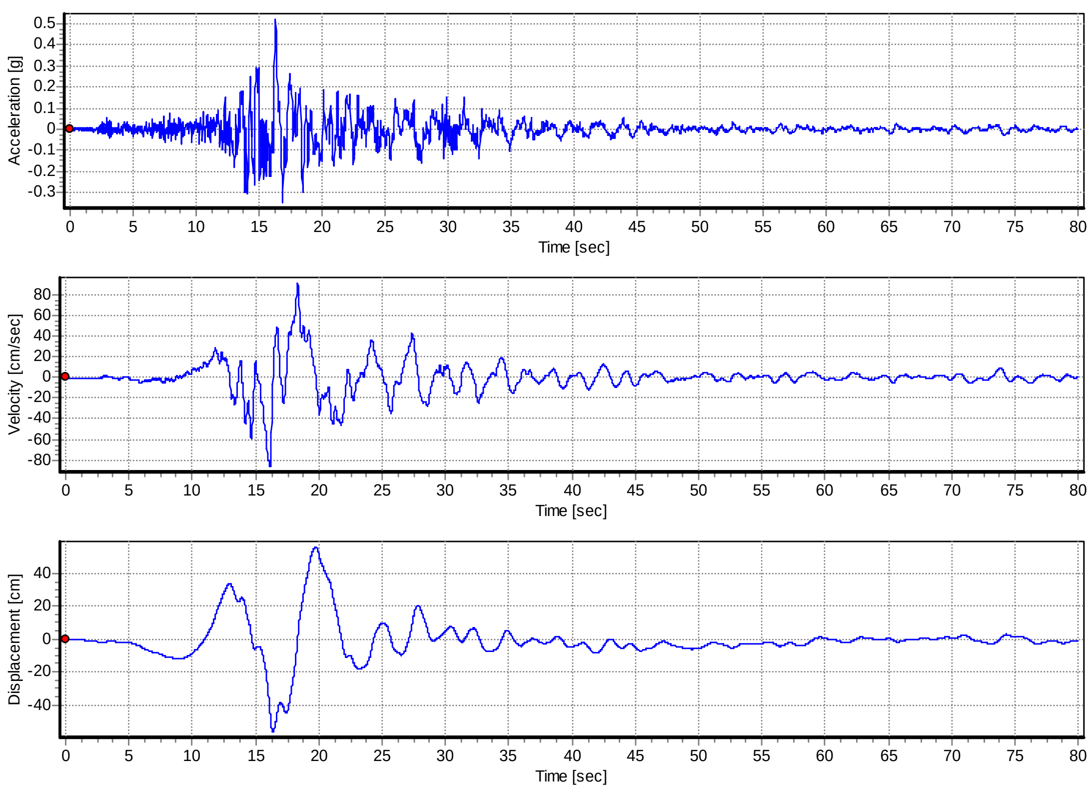

LA 09 (Landers, 1992, Yermo)

Figure 5.3 (Continued) Acceleration, velocity, and displacement time histories of 10/50 SAC records

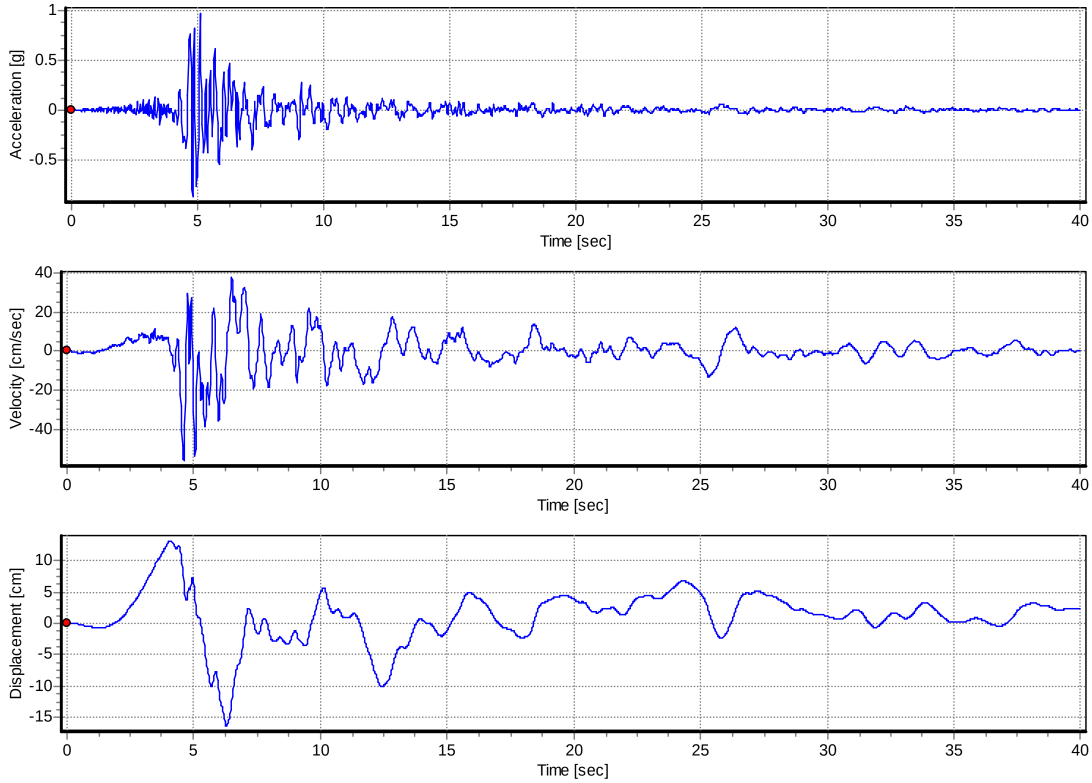

LA 12 (Loma Prieta, 1989, Gilroy)

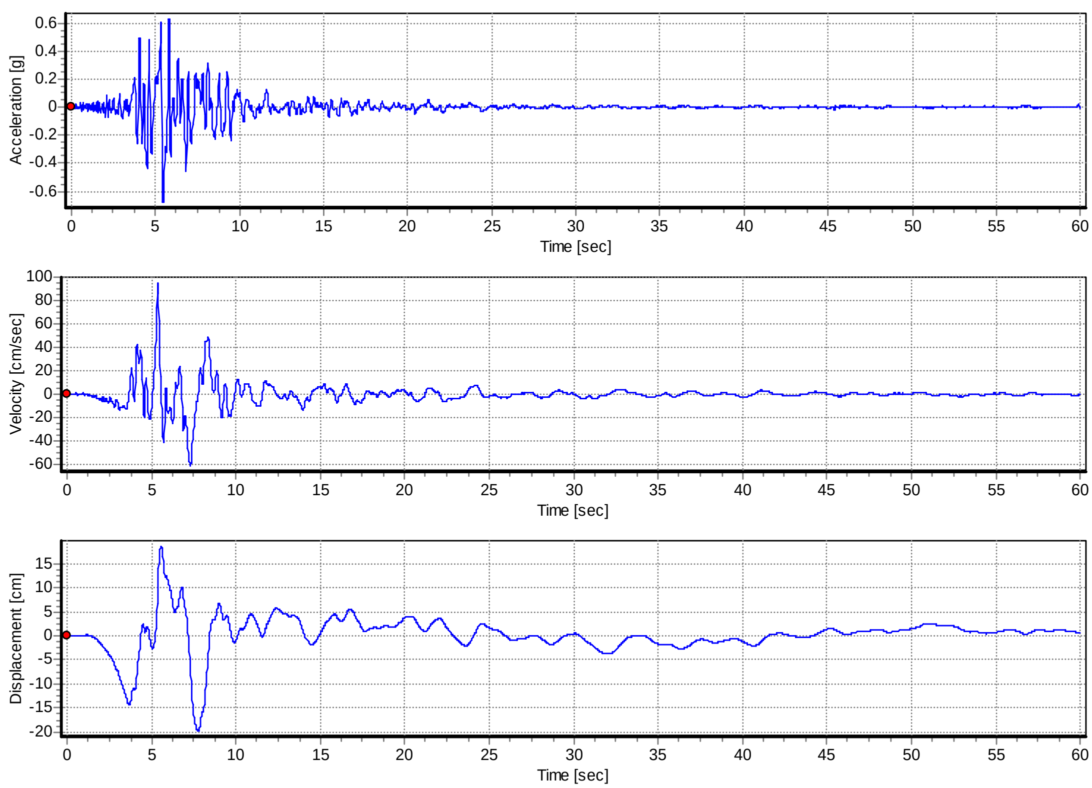

LA 13 (Northridge, 1994, Newhall)

Figure 5.3 (Continued) Acceleration, velocity, and displacement time histories of 10/50 SAC records

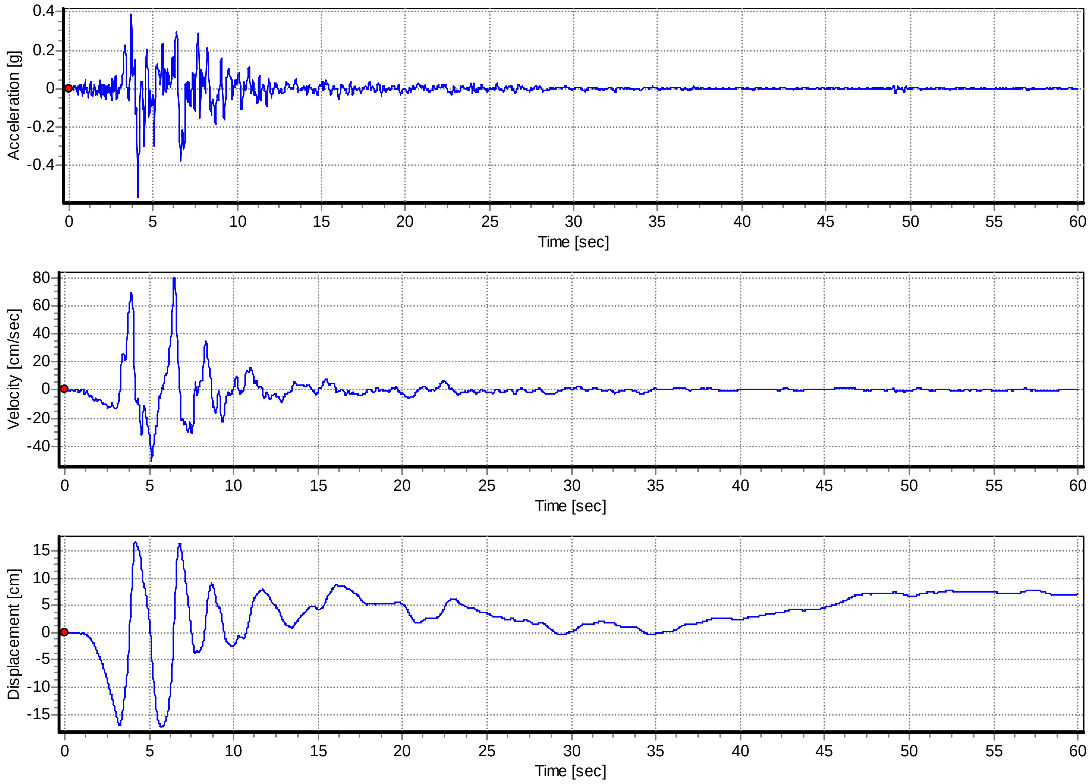

LA 17 (Northridge, 1994, Sylmar)

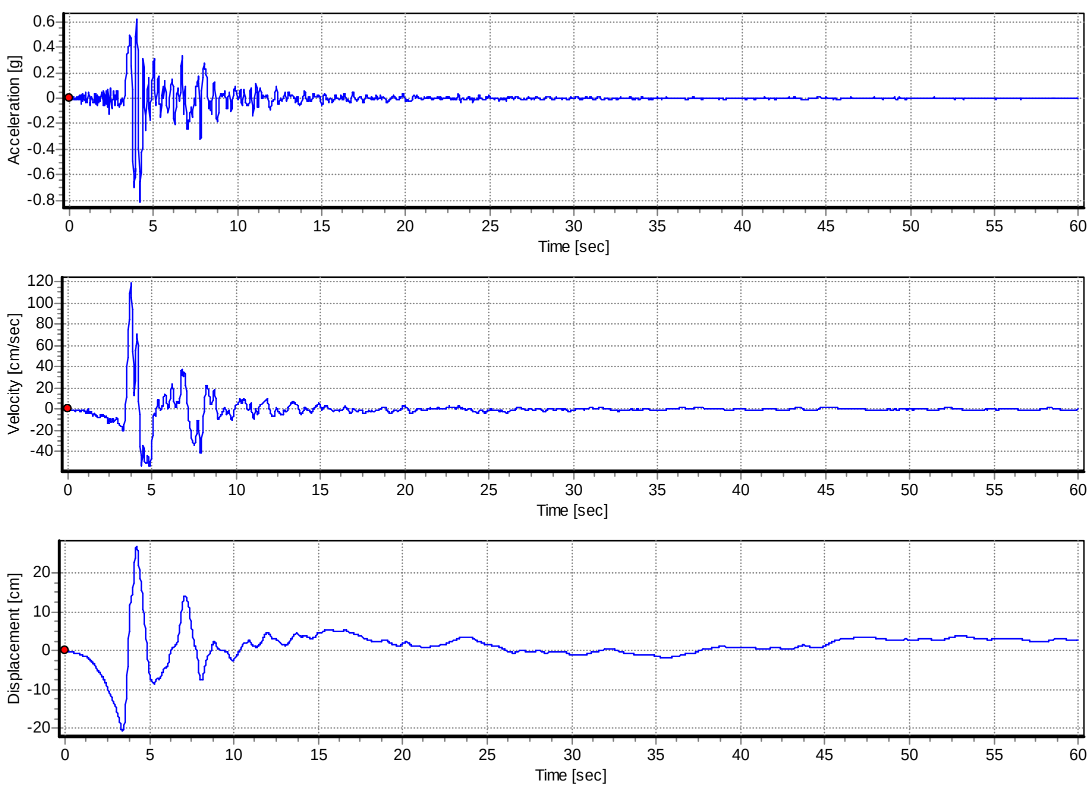

LA 18 (Northridge, 1994, Sylmar-2)

Figure 5.3 (Continued) Acceleration, velocity, and displacement time histories of 10/50 SAC records

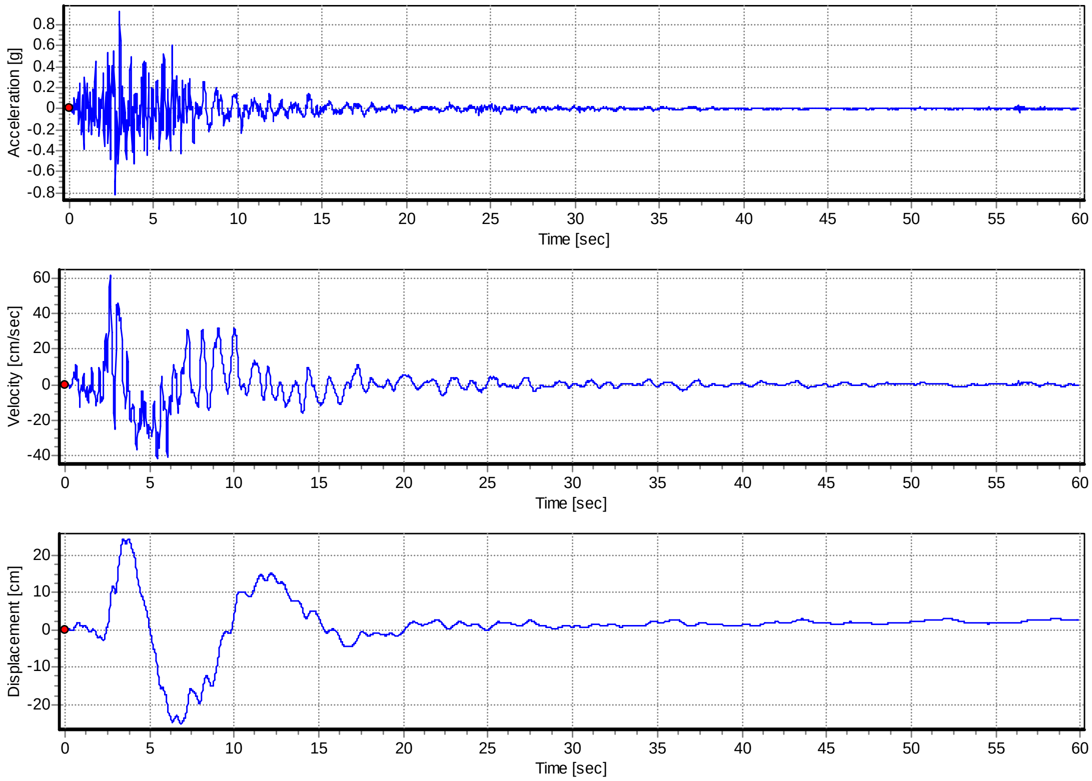

LA 19 (North Palm Springs, 1986)

Figure 5.3 (Continued) Acceleration, velocity, and displacement time histories of 10/50 SAC records

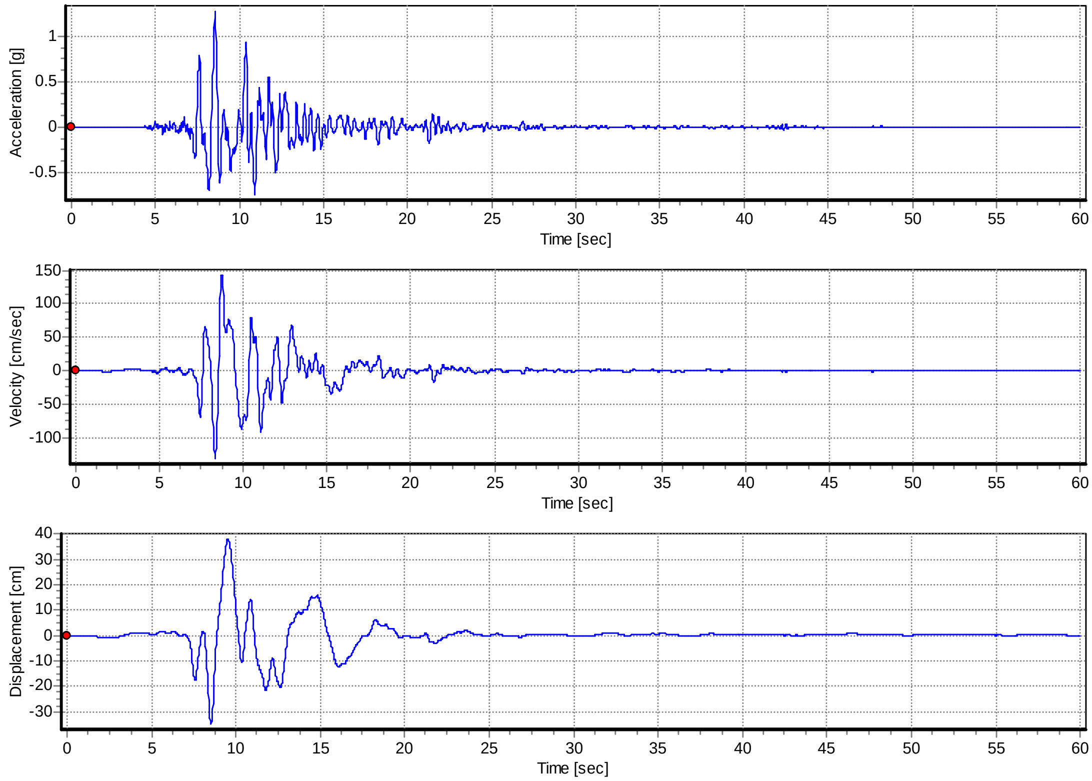

LA 21 (1995 Kobe)

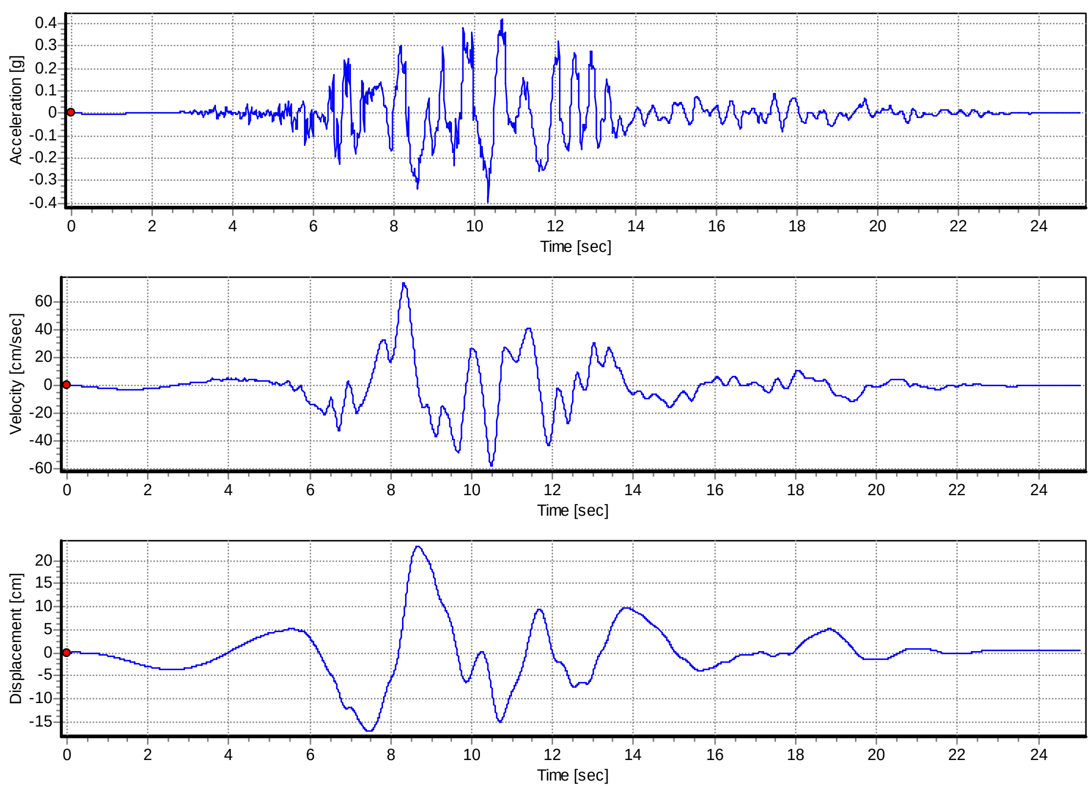

LA 23 (1989 Loma Prieta)

Figure 5.4 Acceleration, velocity, and displacement time histories of 2/50 SAC records

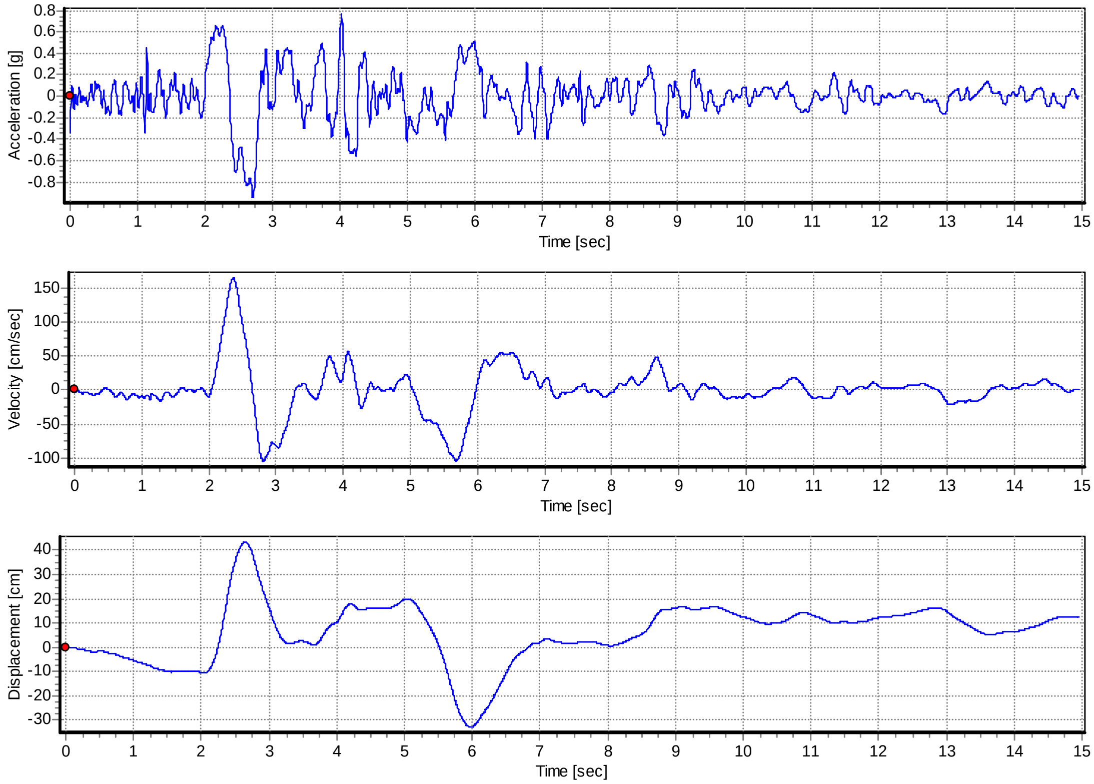

LA 26 (1994 Northridge)

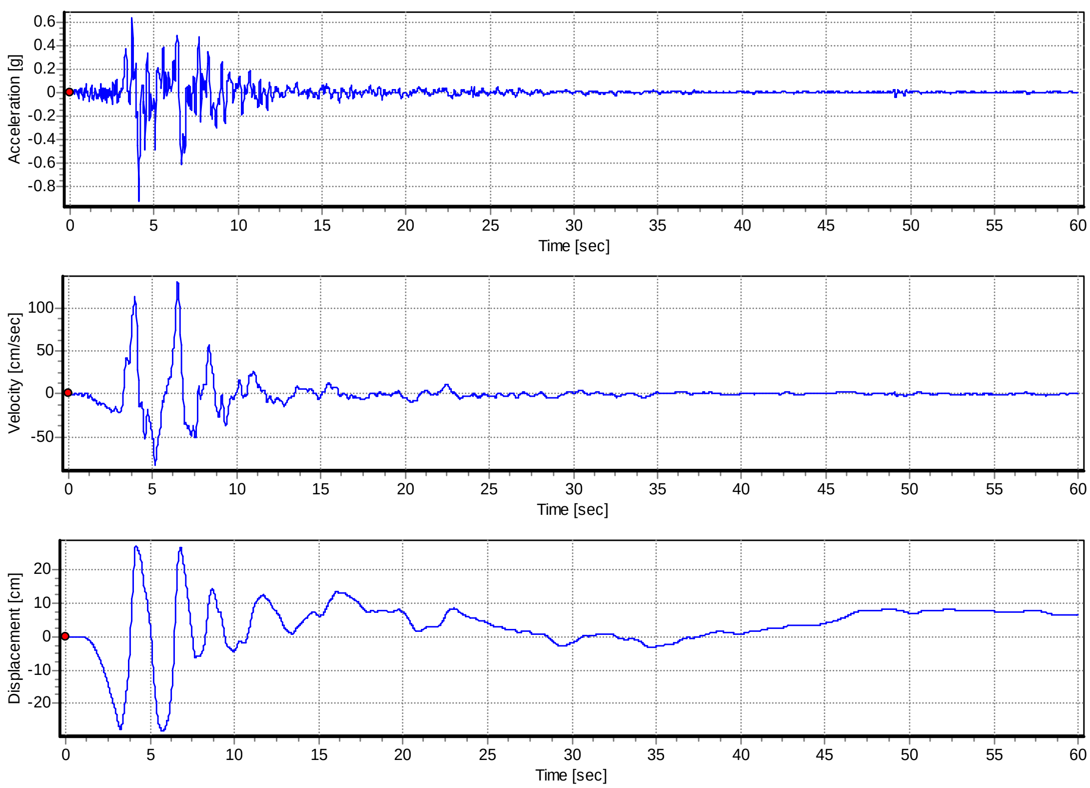

LA 27 (1994 Northridge-2)

Figure 5.4 (Continued) Acceleration, velocity, and displacement time histories of 2/50 SAC records

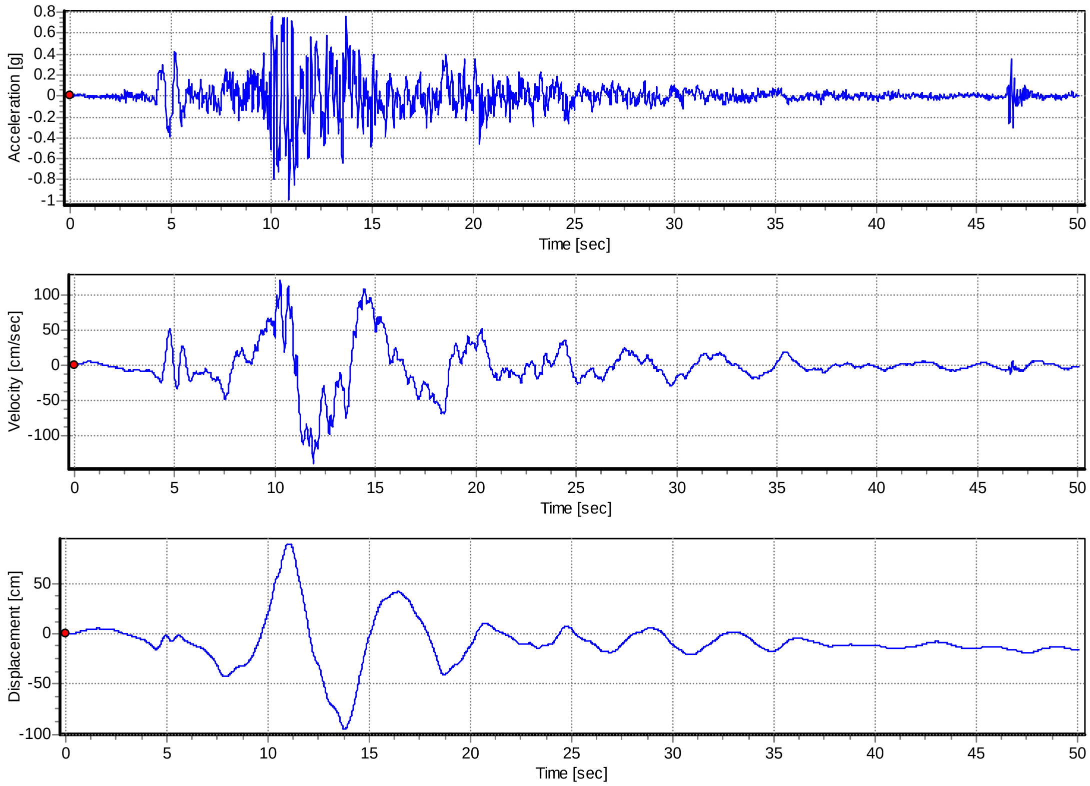

LA 30 (1974 Tabas)

Figure 5.4 (Continued) Acceleration, velocity, and displacement time histories of 2/50 SAC records

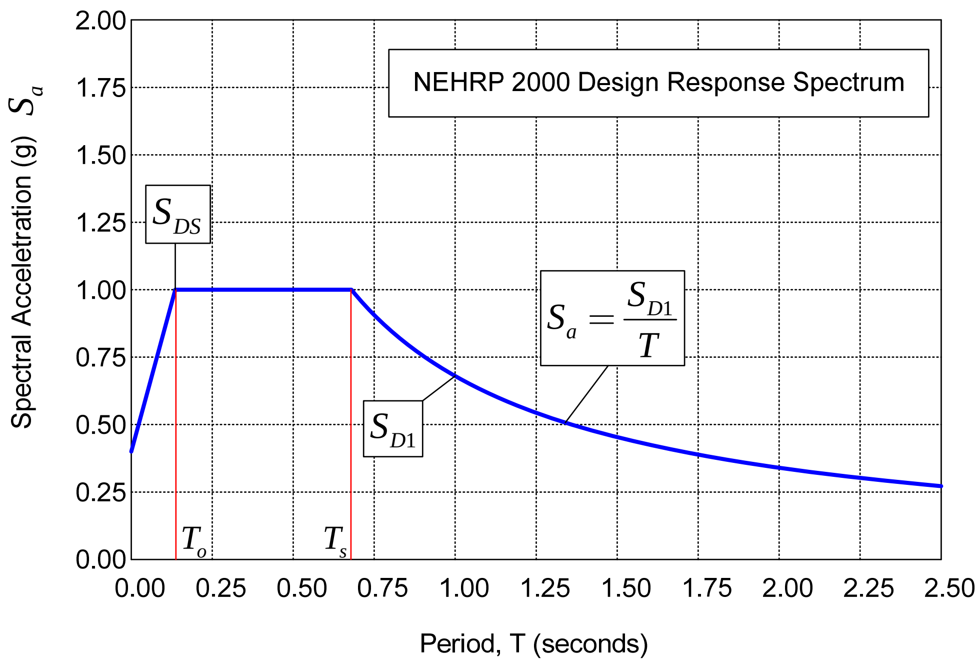

Figure 5.5 NEHRP 2000 design response spectrum

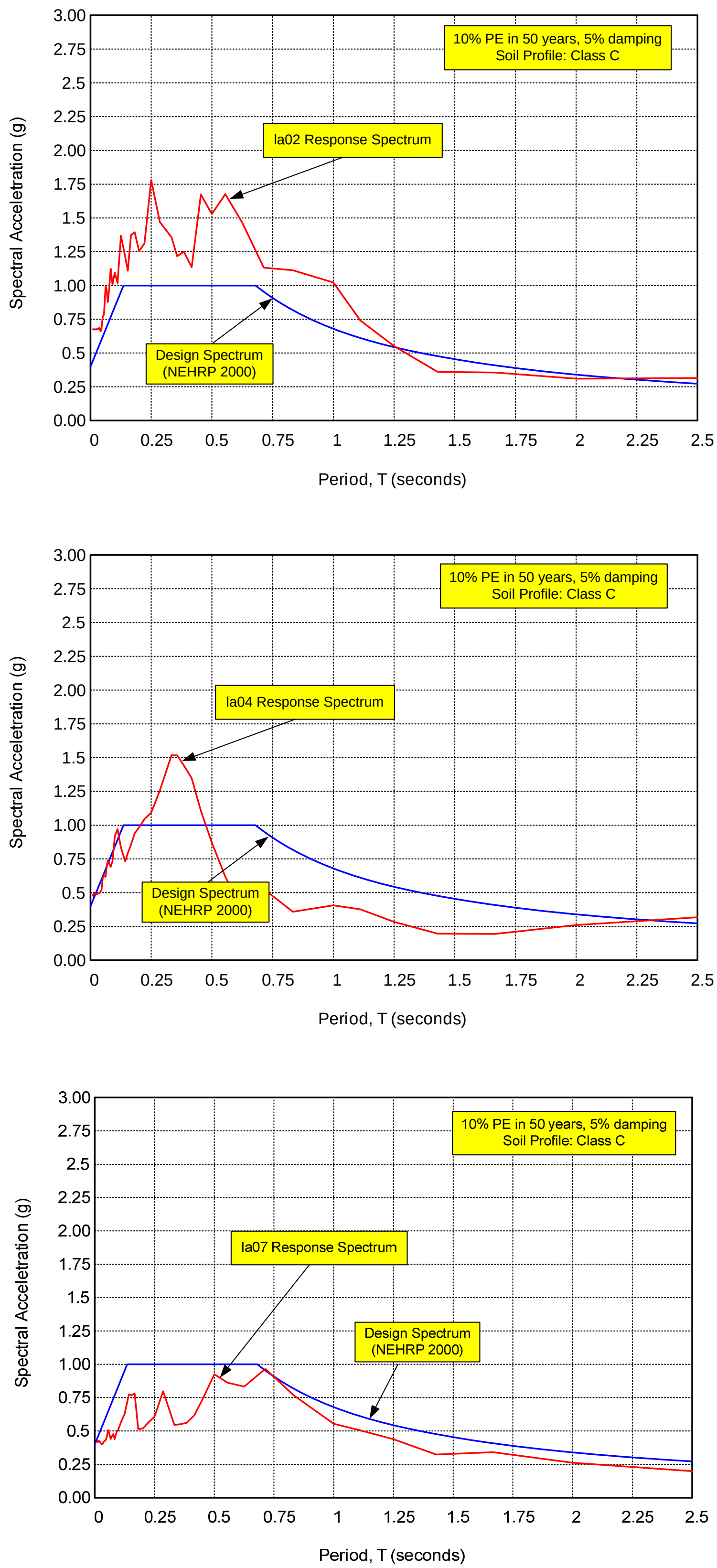

Figure 5.6 Design spectrum and response spectra of SAC ground motions (LA Region)

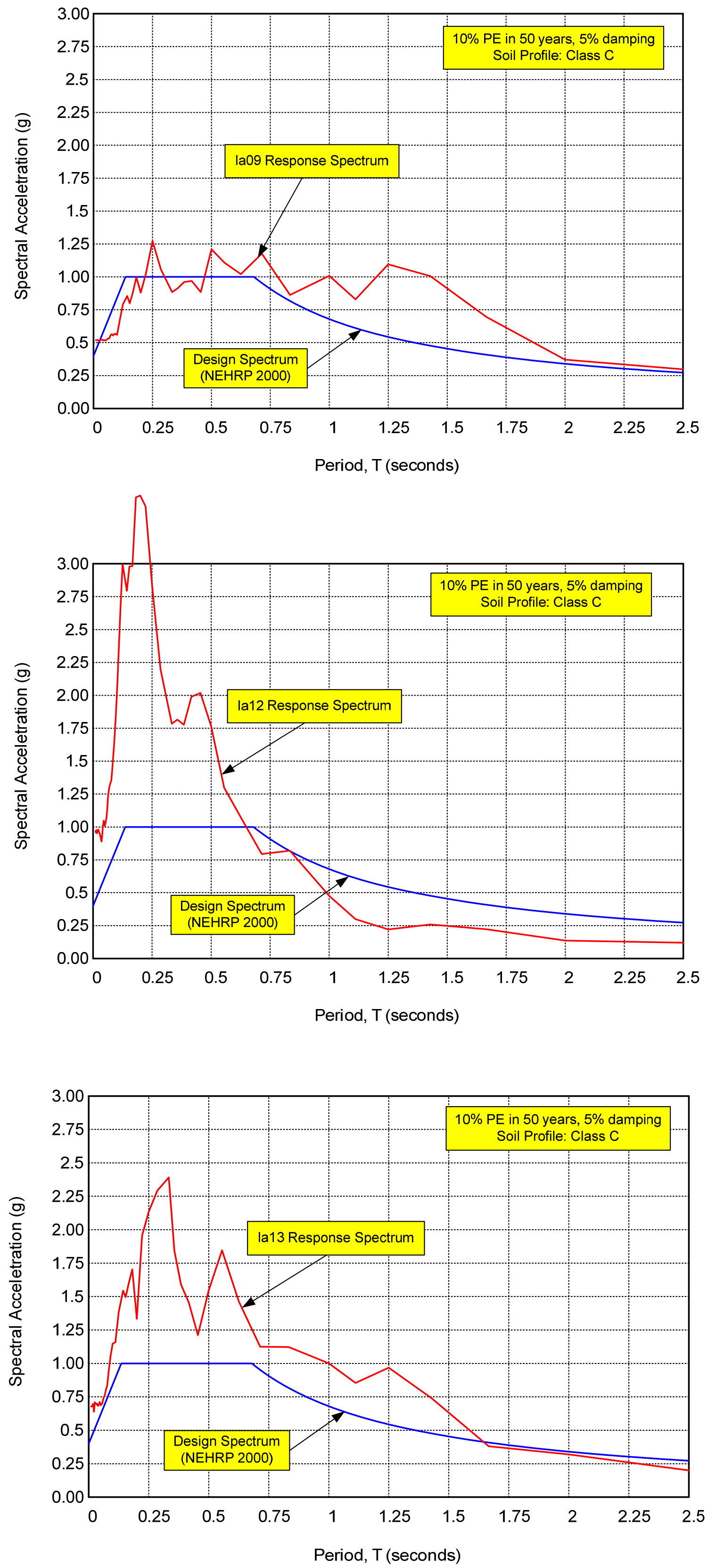

Figure 5.6 (Continued) Design spectrum and response spectra of SAC ground motions (LA Region)

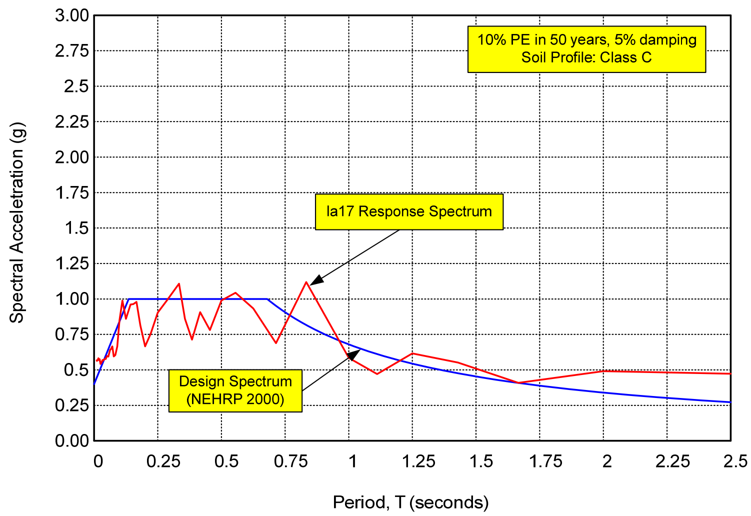

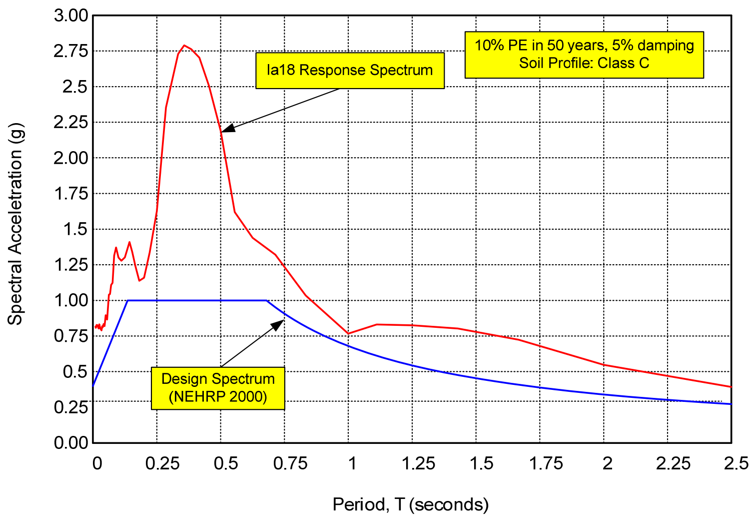

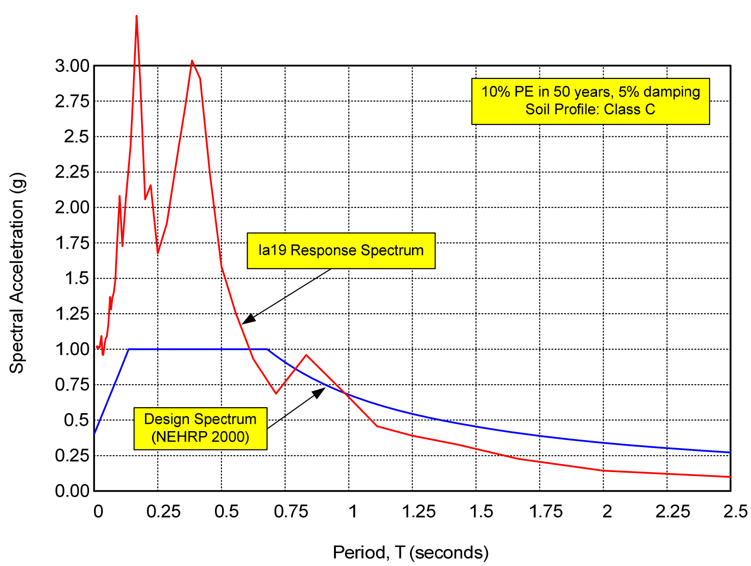

Figure 5.6 (Continued) Design spectrum and response spectra of SAC ground motions (LA Region)

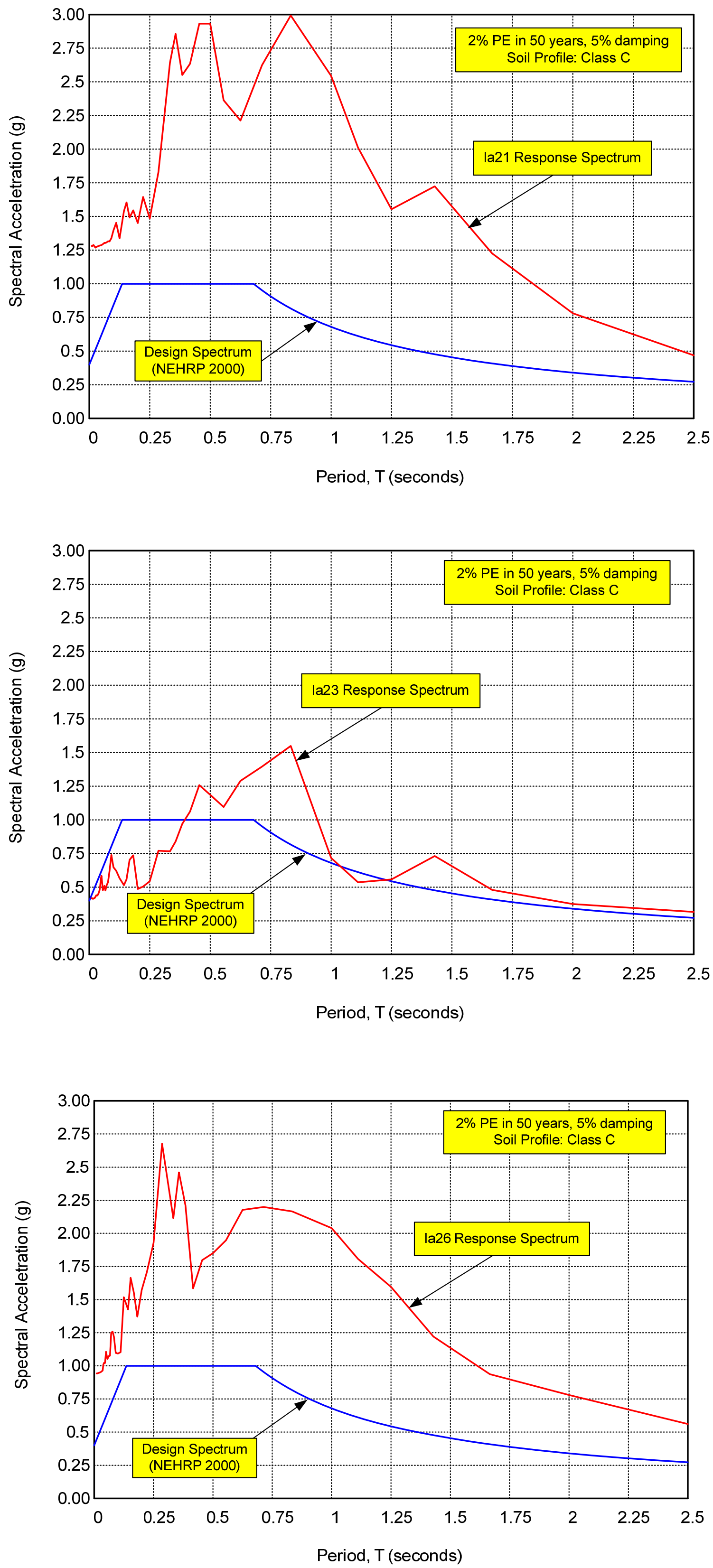

Figure 5.6 (Continued) Design spectrum and response spectra of SAC ground motions (LA Region)

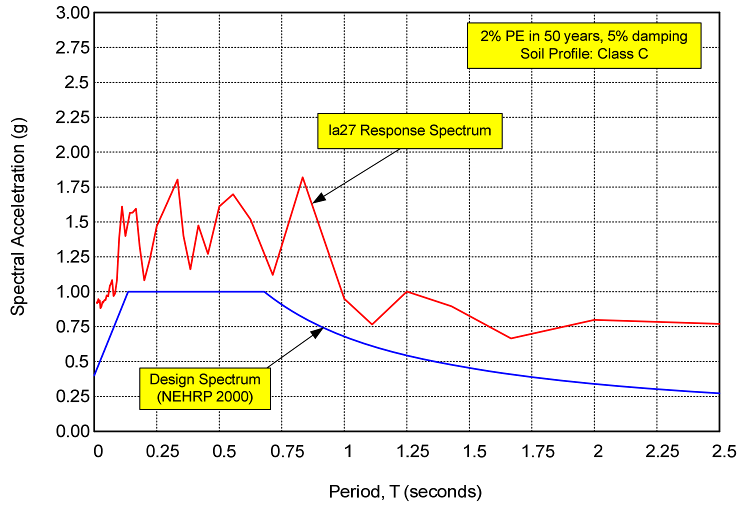

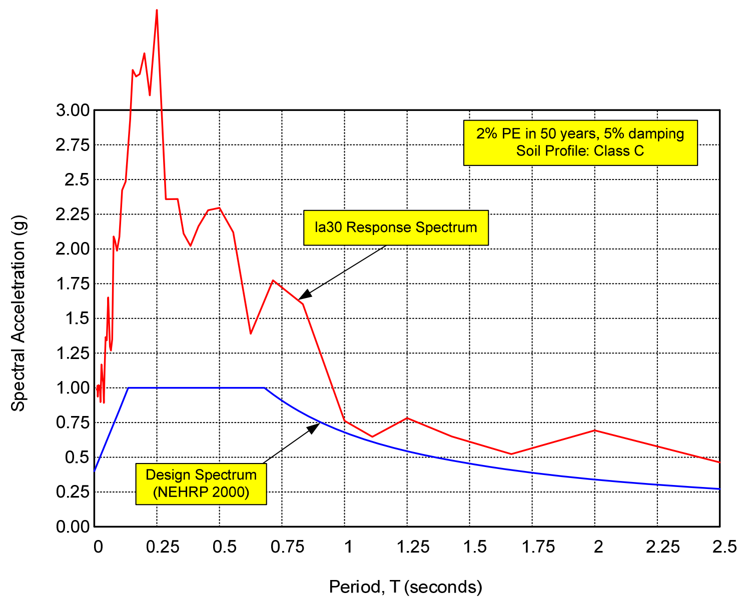

Figure 5.6 (Continued) Design spectrum and response spectra of SAC ground motions (LA Region)

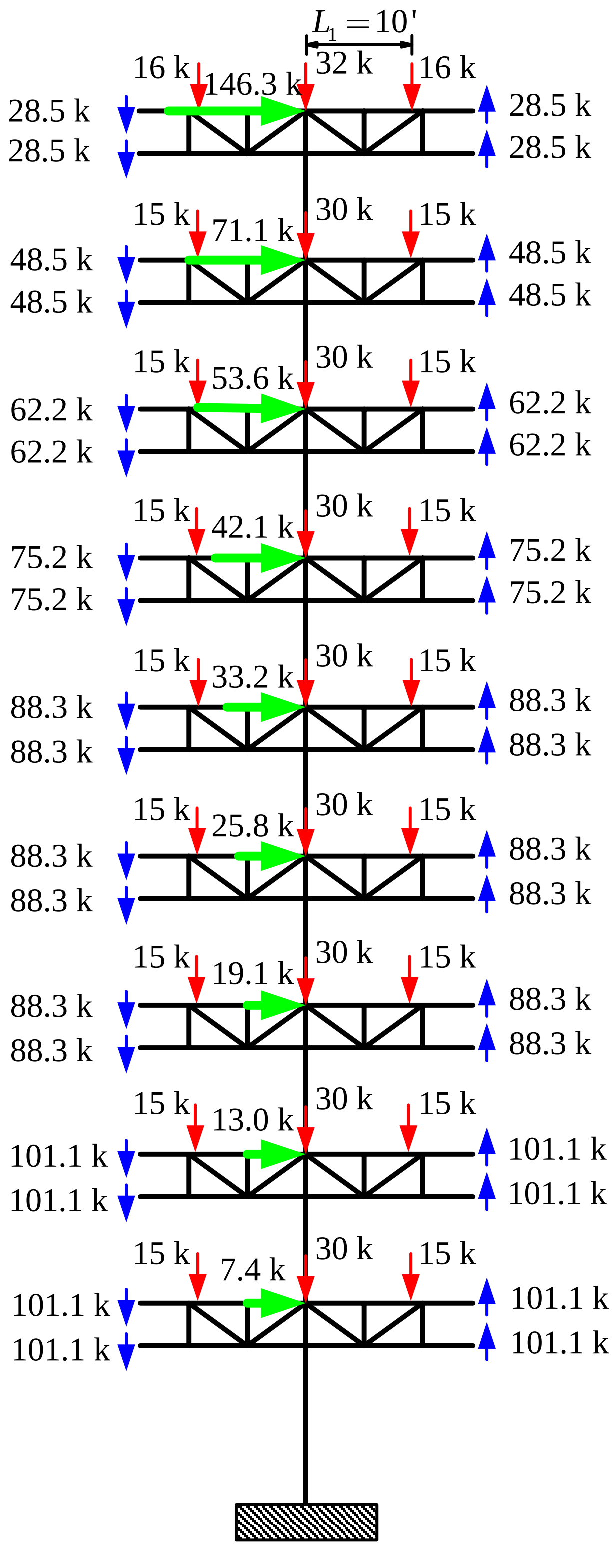

Figure 5.7 Forces acting on the interior column free body (9-story ordinary STMF)

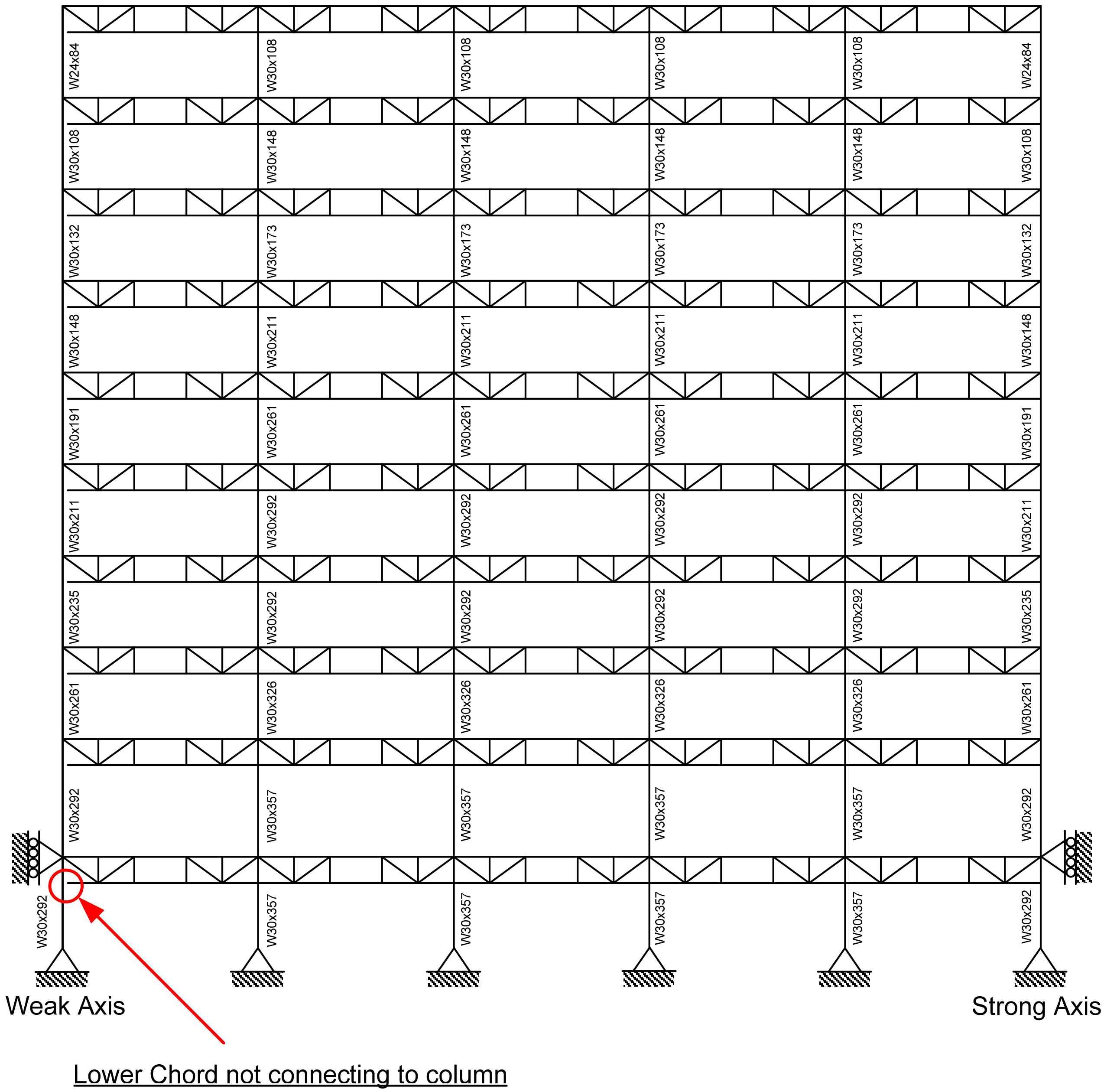

Figure 5.8a Design Column Sections for the 9-story ordinary STMF

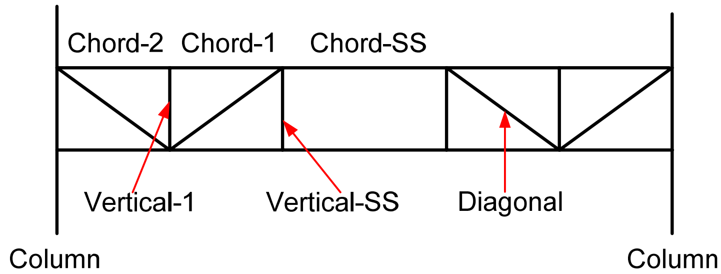

FLR	Chord-SS	Chord-1	Chord-2	Vertical-SS	Vertical-1	Diagonal
9	7C12.25	7C12.25	7C12.25X (0.25" plate)	7C12.25	6MC12	6MC12
8	8C18.75	8C18.75	8C18.75X (0.5" plate)	8C18.75	6MC12	6MC16.3
7	9C20	9C20	9C20X (0.75" plate)	9C20	6MC12	7MC22.7
6	10C20	10C20	10C20X (1.0" plate)	10C20	6MC12	7MC22.7
5	10C25	10C25	10C25X (1.25" plate)	10C25	6MC12	9MC25.4
4	10C25	10C25	10C25X (1.25" plate)	10C25	6MC12	9MC25.4
3	10C25	10C25	10C25X (1.25" plate)	10C25	6MC12	9MC25.4
2	10C30	10C30	10C30X (1.5" plate)	10C30	6MC16.3	10MC25
1	10C30	10C30	10C30X (1.5" plate)	10C30	6MC16.3	10MC25
B-1	10C30	10C30	10C30X (1.5" plate)	10C30	6MC16.3	10MC25

Note 1: All sections are double channels.
Note 2: B-1 Level uses the same sections as at Level 1.
Note 3: Web plates are extended over the whole length of the corresponding panel, *i.e.*, 5.5 ft.

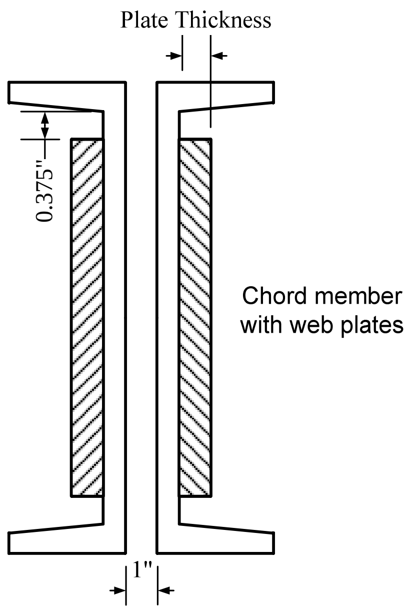

Figure 5.8b Design Special Segment and Truss Member Sections for the 9-story ordinary STMF

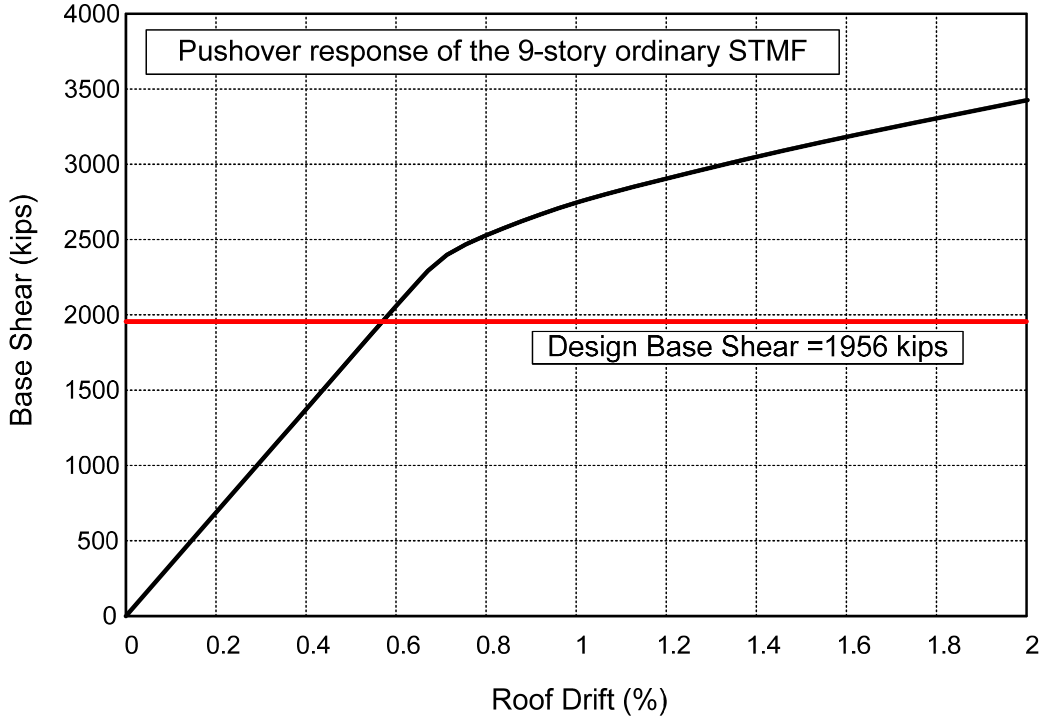

Figure 5.9 Nonlinear Static Pushover Response of the 9-Story ordinary STMF

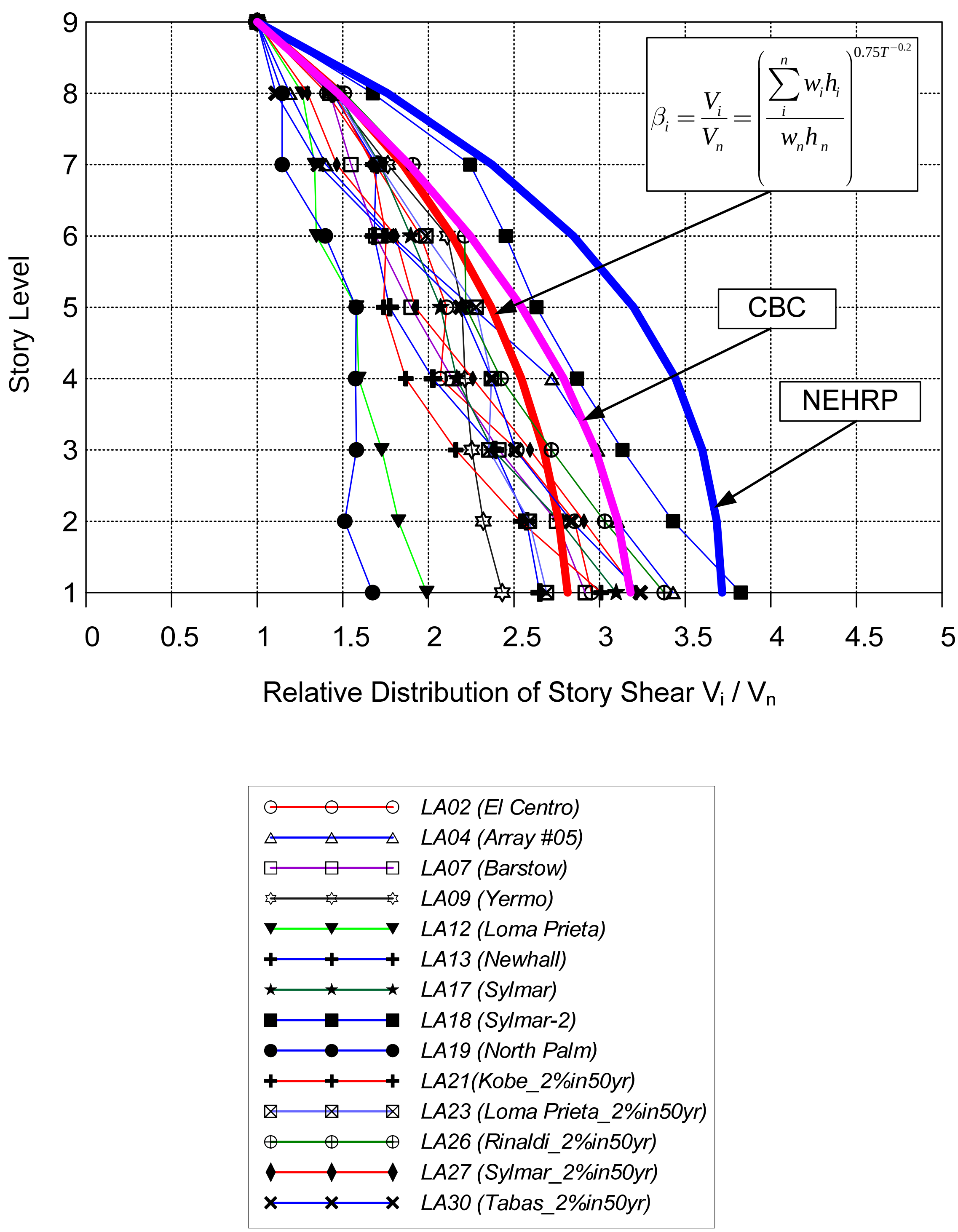

Figure 5.10 Relative Story Shear Distributions obtained from Nonlinear Dynamic Analyses (9-story ordinary STMF)

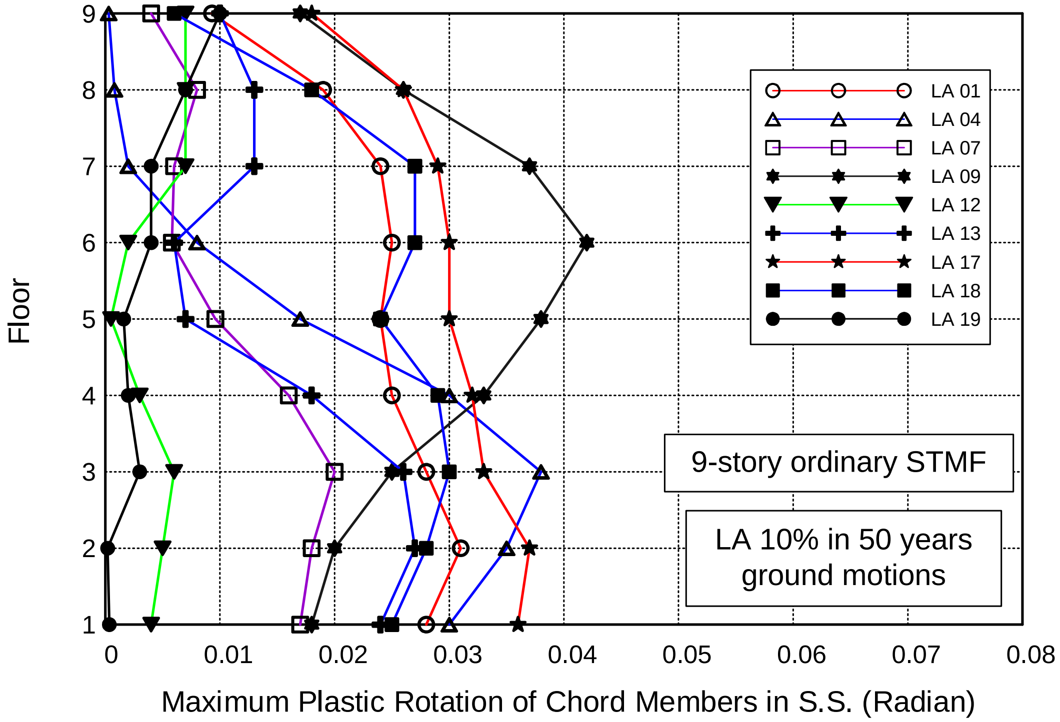

(a)

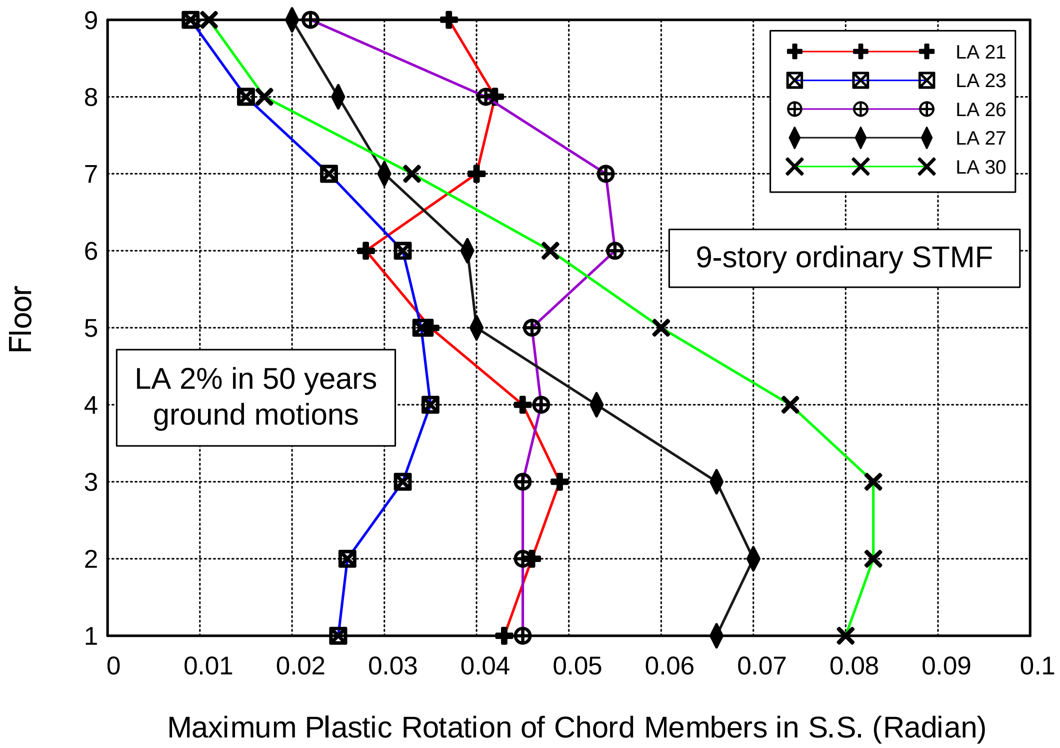

(b)

Figure 5.11 Maximum plastic hinge rotations in chord members for 9-story ordinary STMF subjected to 10%/50 and 2%/50 ground motions

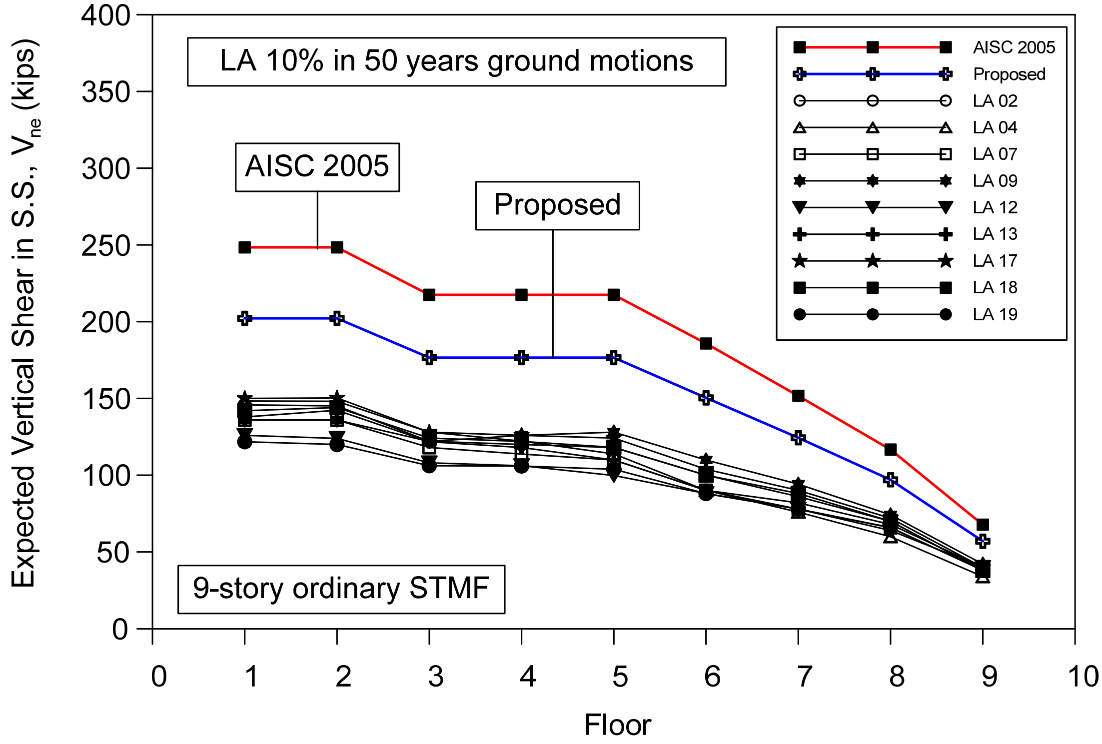

(a)

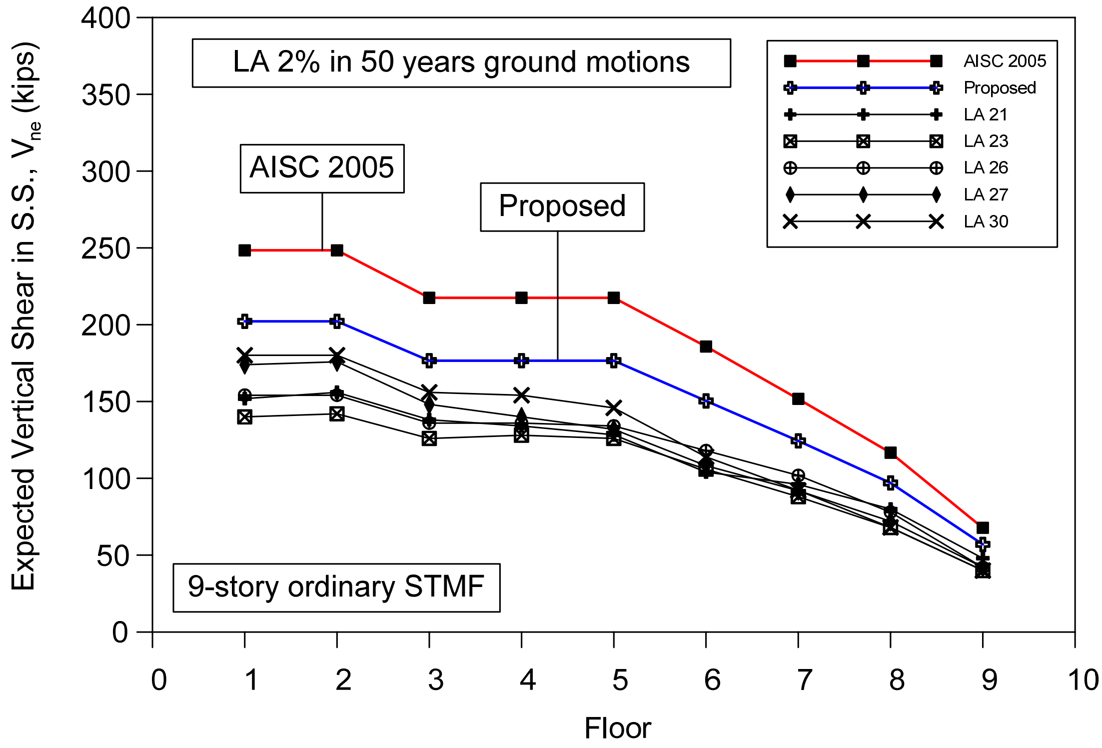

(b)

Figure 5.12 Maximum developed shears in special segments in the 9-story ordinary STMF subjected to 10%/50 and 2%/50 ground motions

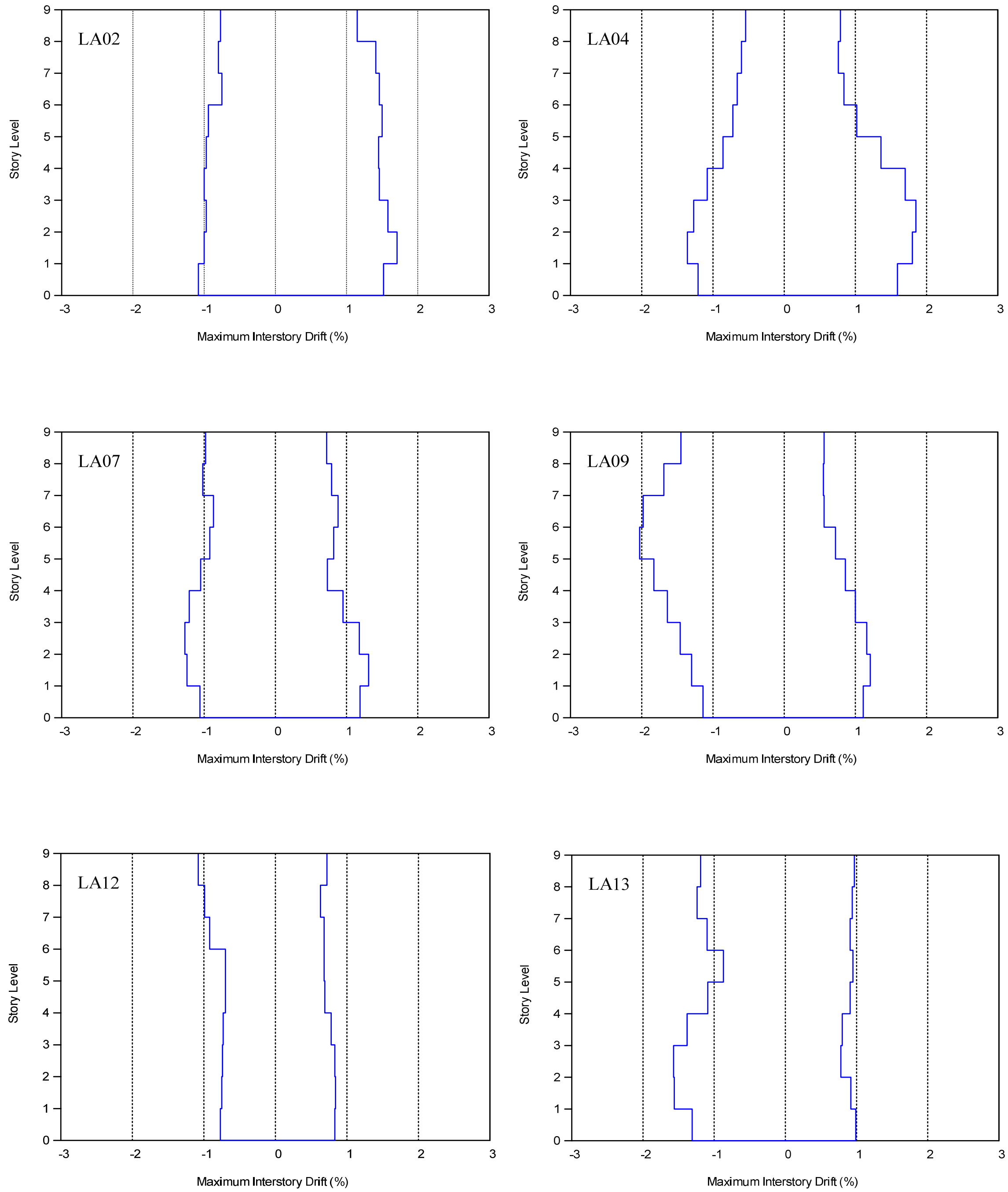

Figure 5.13 (a) Maximum interstory drift distributions of the 9-Story ordinary STMF subjected to 10% in 50 year SAC earthquake records (LA Region)

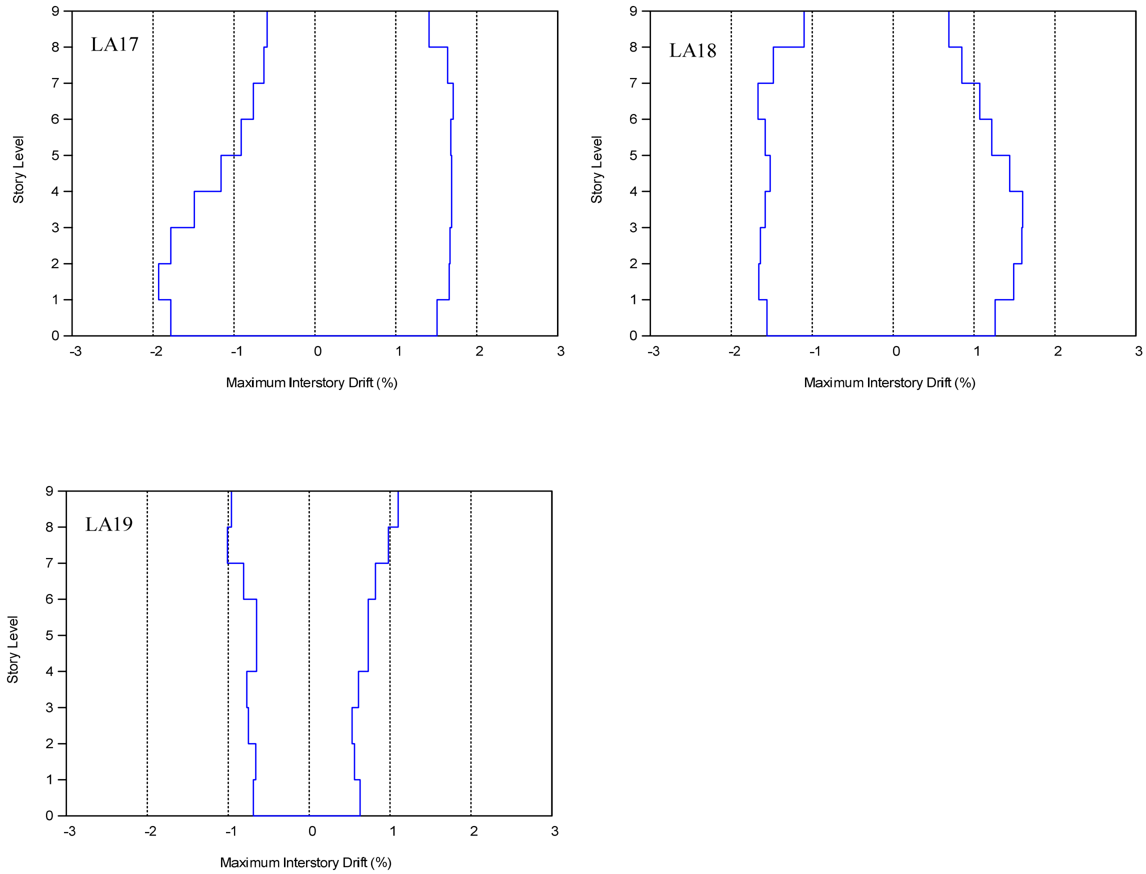

Figure 5.13 (a) (Continued) Maximum interstory drift distributions of the 9-Story ordinary STMF subjected to 10% in 50 year SAC earthquake records (LA Region)

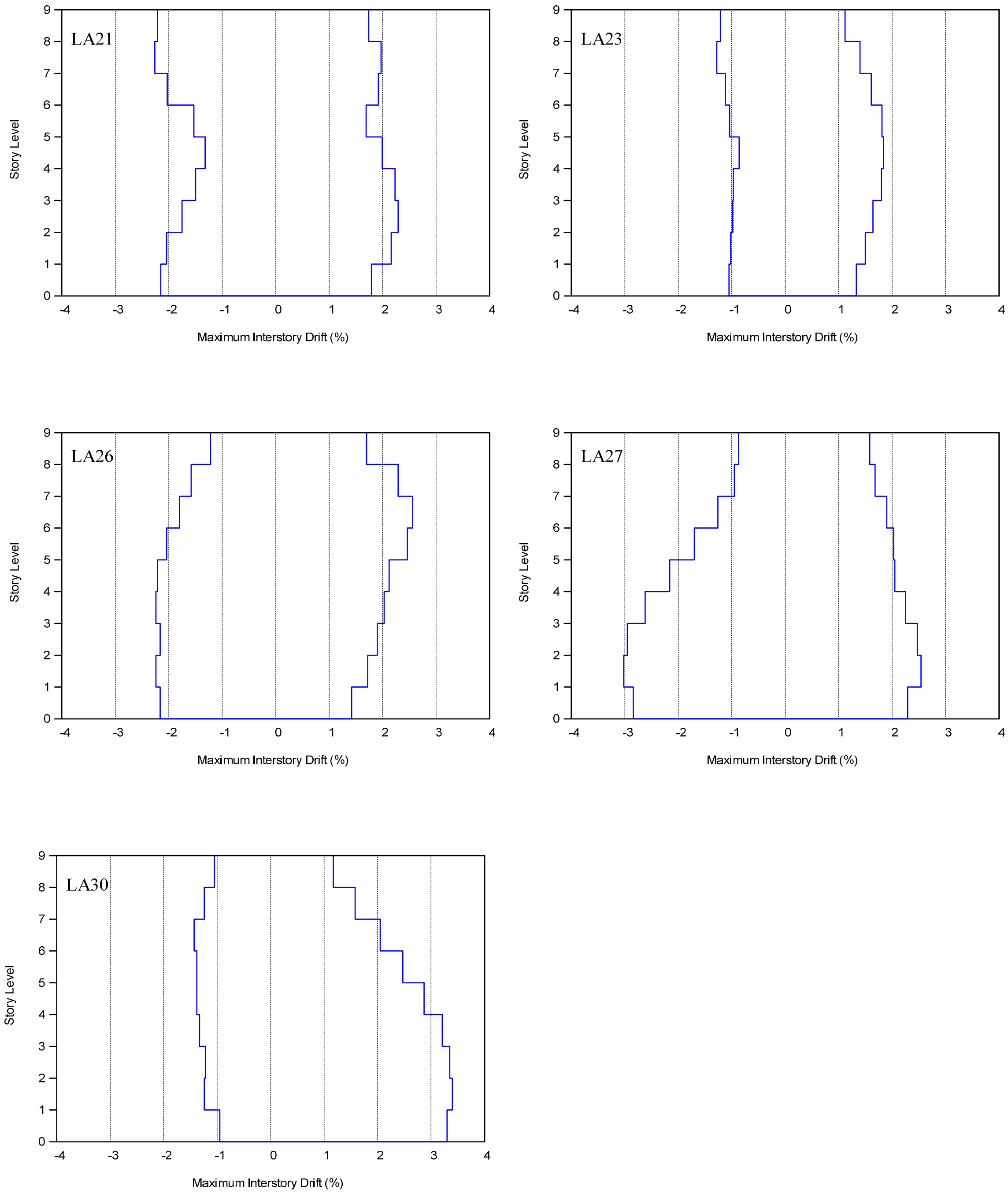

Figure 5.13 (b) Maximum interstory drift distributions of the 9-Story ordinary STMF subjected to 2% in 50 year SAC earthquake records (LA Region)

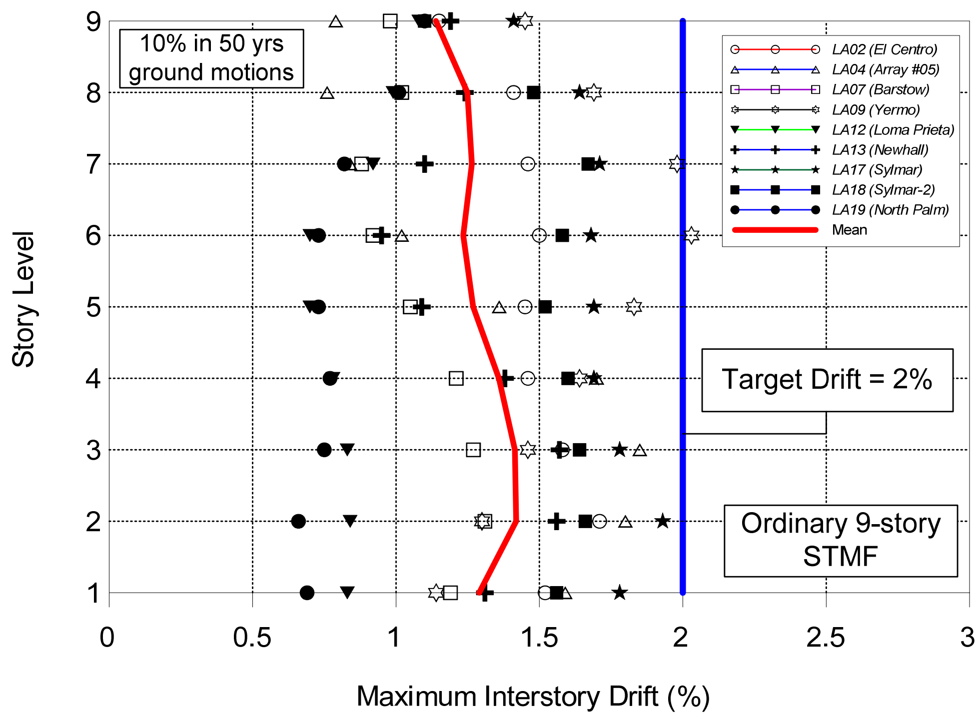

(a)

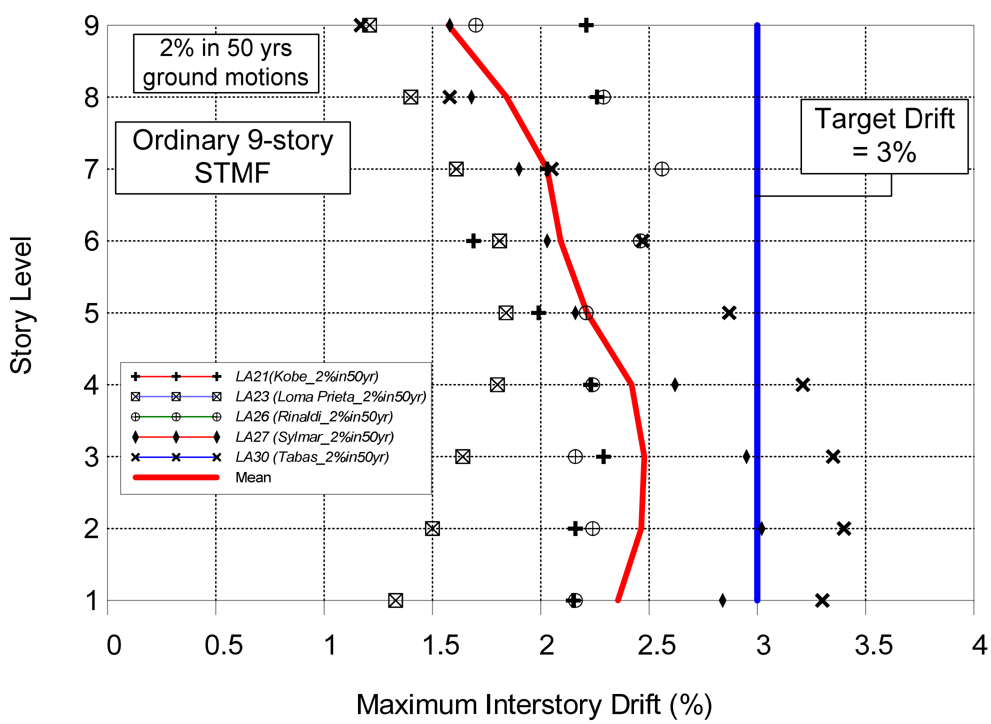

(b)

Figure 5.14 Mean value of maximum interstory drifts and corresponding target drifts for the 9-Story ordinary STMF

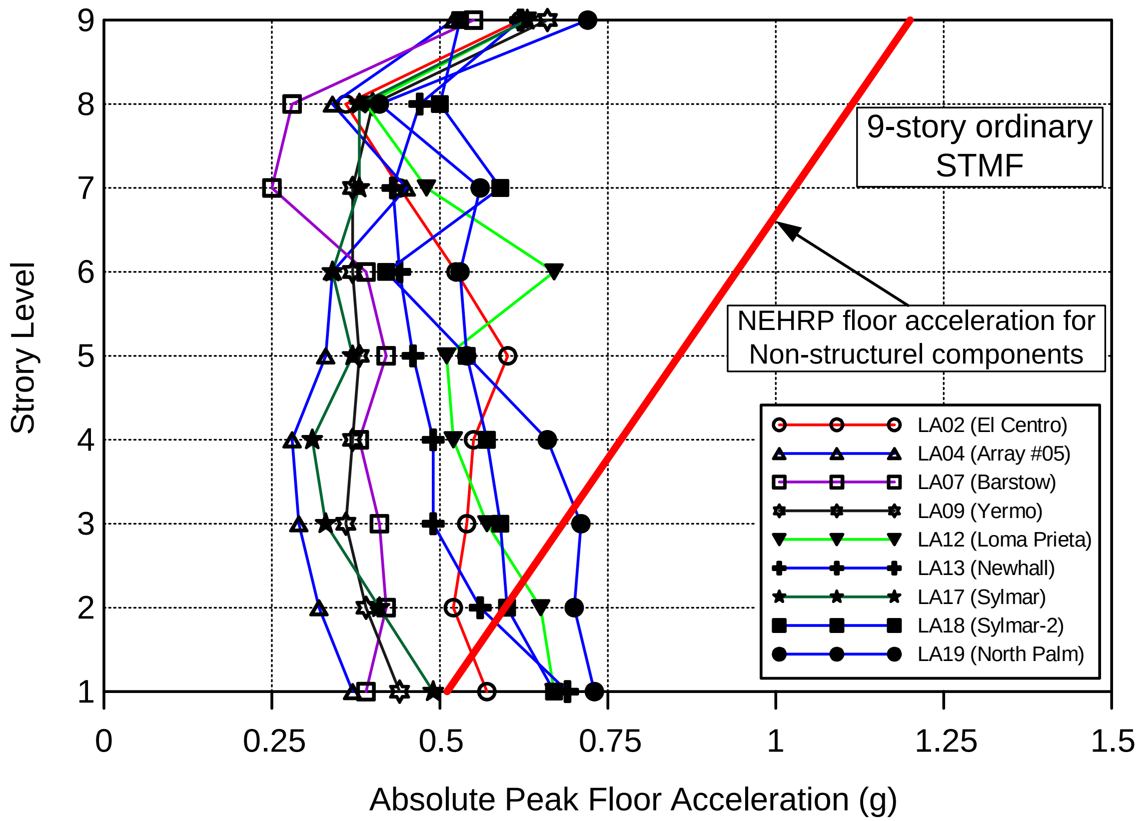

Figure 5.15 Peak Floor Accelerations (10% in 50 year) and the NEHRP-specified Design Acceleration for Acceleration-Sensitive nonstructural components

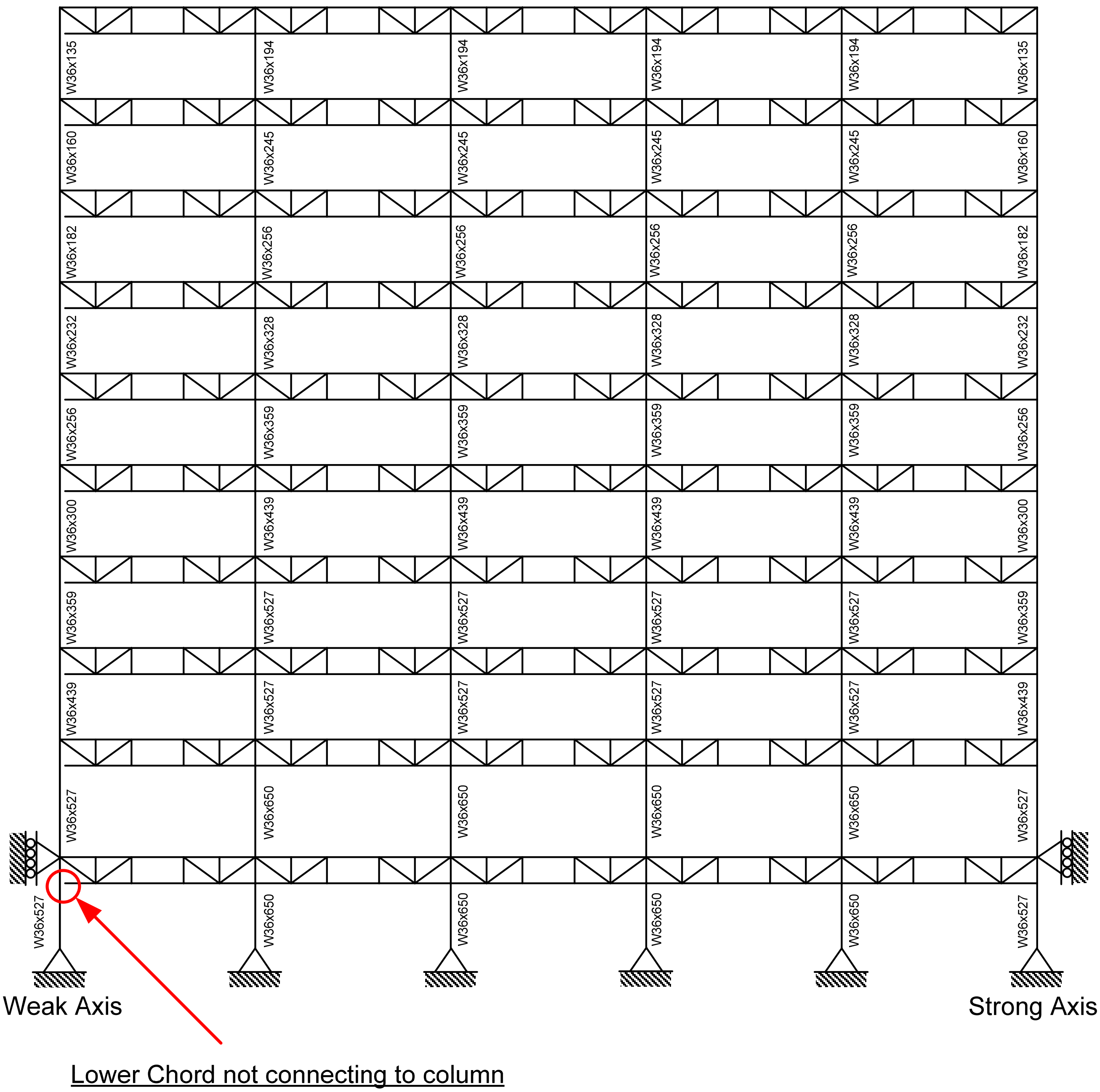

Figure 5.16a Design Column Sections for the 9-story essential STMF

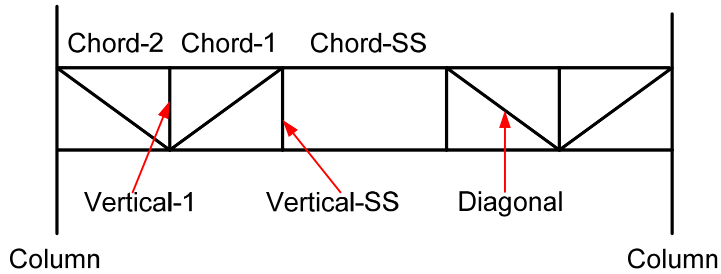

FLR	Chord-SS	Chord-1	Chord-2	Vertical-SS	Vertical-1	Diagonal
9	9C20	9C20	9C20 X (0.25" plate)	9C20	6MC12	9MC25.4
8	10C25	10C25	10C25 X (0.5" plate)	10C25	6MC12	9MC25.4
7	10C30	10C30	10C30 X (0.75" plate)	10C30	6MC12	9MC25.4
6	12C30	12C30 X (0.25" plate)	12C30 X (1.0" plate)	12C30	6MC12	10MC41.1
5	12C30	12C30 X (0.25" plate)	12C30 X (1.0" plate)	12C30	7MC22.7	10MC41.1
4	12MC31	12MC31 X (0.25" plate)	12MC31 X (1.25" plate)	12MC31	7MC22.7	10MC41.1
3	12MC31	12MC31 X (0.25" plate)	12MC31 X (1.25" plate)	12MC31	7MC22.7	10MC41.1
2	12MC35	12MC35 X (0.25" plate)	12MC35 X (1.5" plate)	12MC35	7MC22.7	10MC41.1
1	12MC35	12MC35 X (0.25" plate)	12MC35 X (2.0" plate)	12MC35	8MC22.8	10MC41.1
B-1	12MC35	12MC35 X (0.25" plate)	12MC35 X (2.0" plate)	12MC35	8MC22.8	10MC41.1

Note 1: All sections are double channels.
Note 2: B-1 Level uses the same sections as at Level 1.
Note 3: Web plates are extended over the whole length of the corresponding panel, *i.e.*, 5.5 ft.

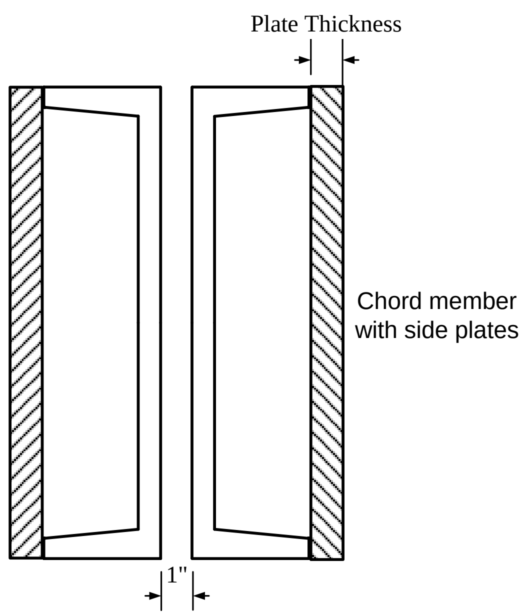

Figure 5.16b Design Special Segment and Truss Member Sections for the 9-story essential STMF

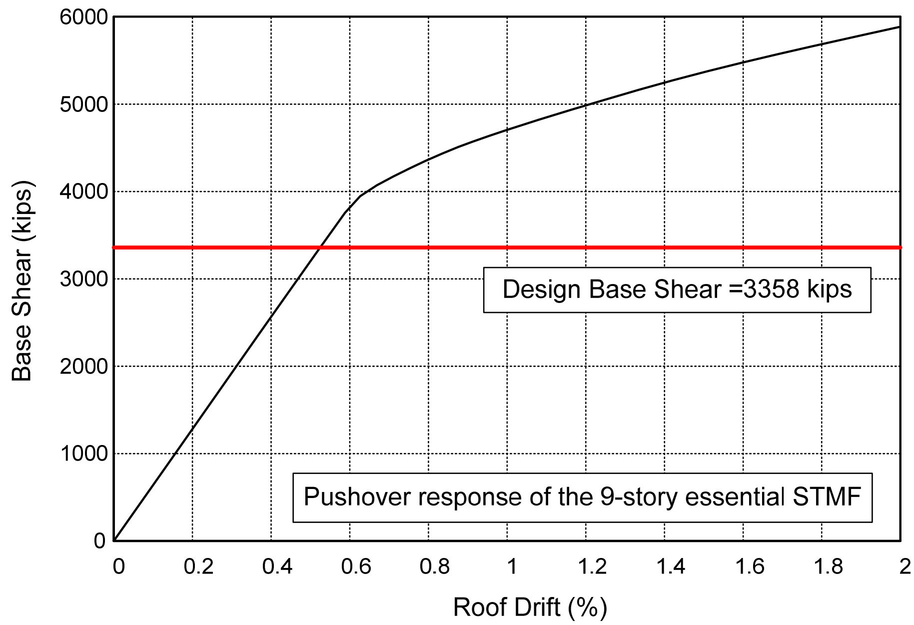

Figure 5.17 Nonlinear Static Pushover Response of the 9-Story Essential STMF

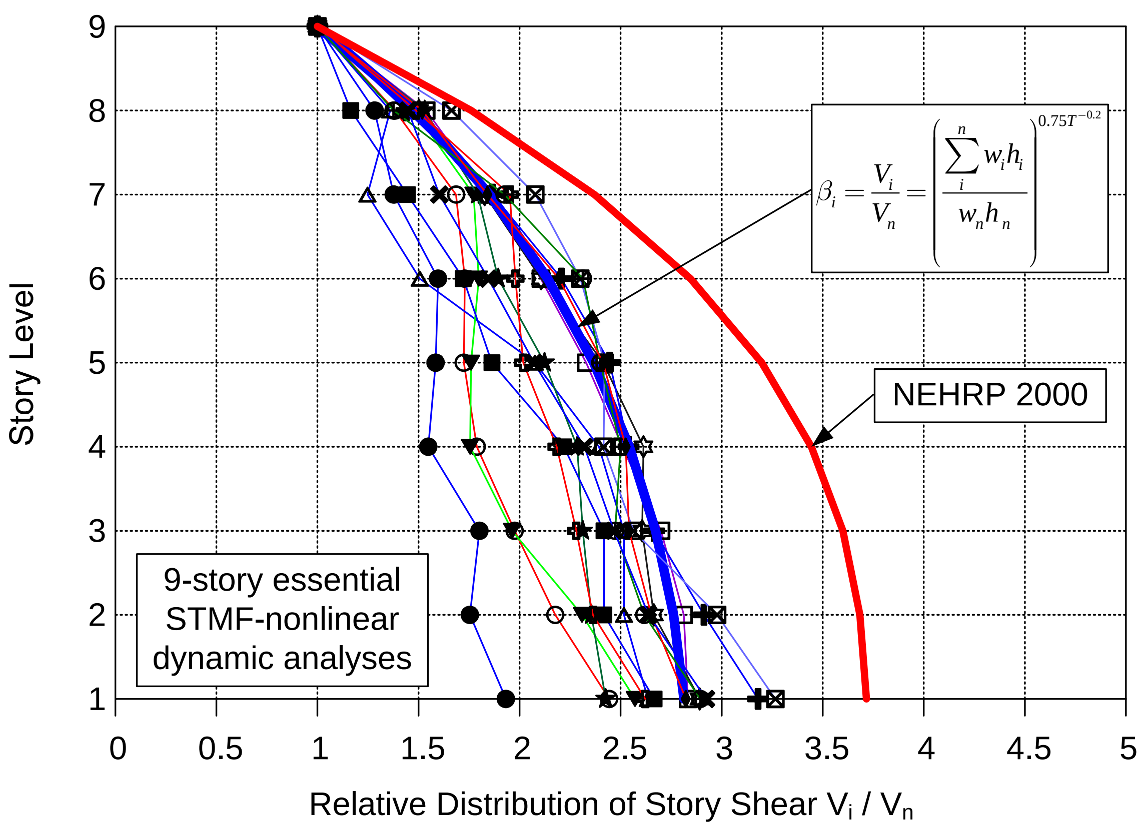

(a)

Figure 5.18 Relative Story Shear Distributions obtained from: (a) Nonlinear Dynamic Analyses of the 9-story essential STMF

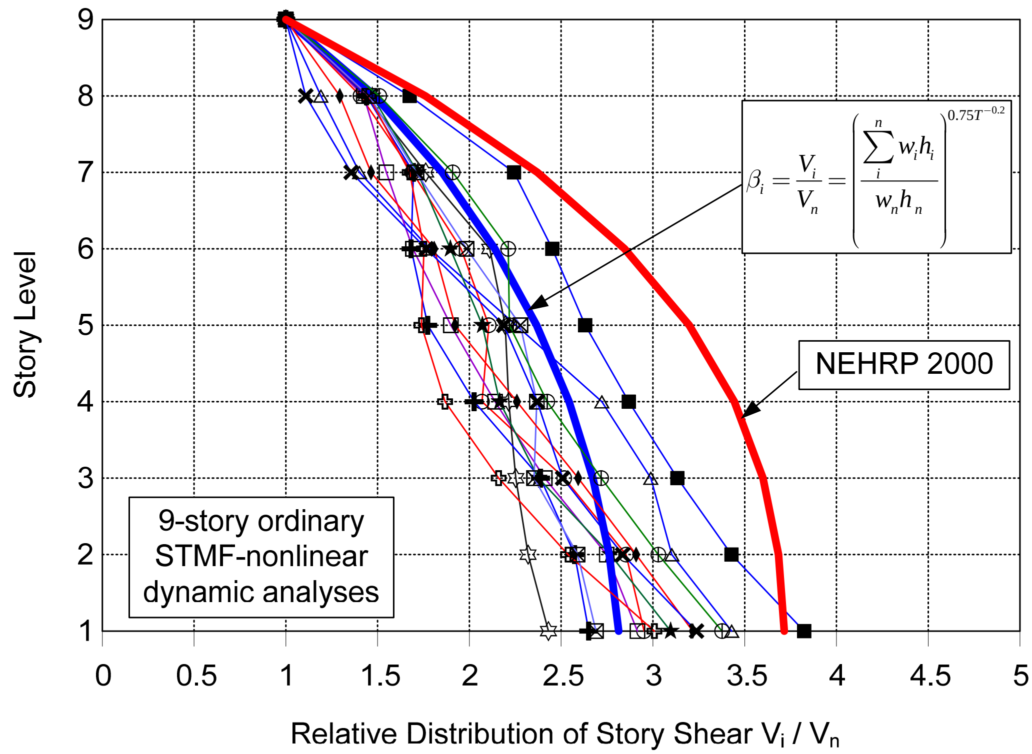

(b)

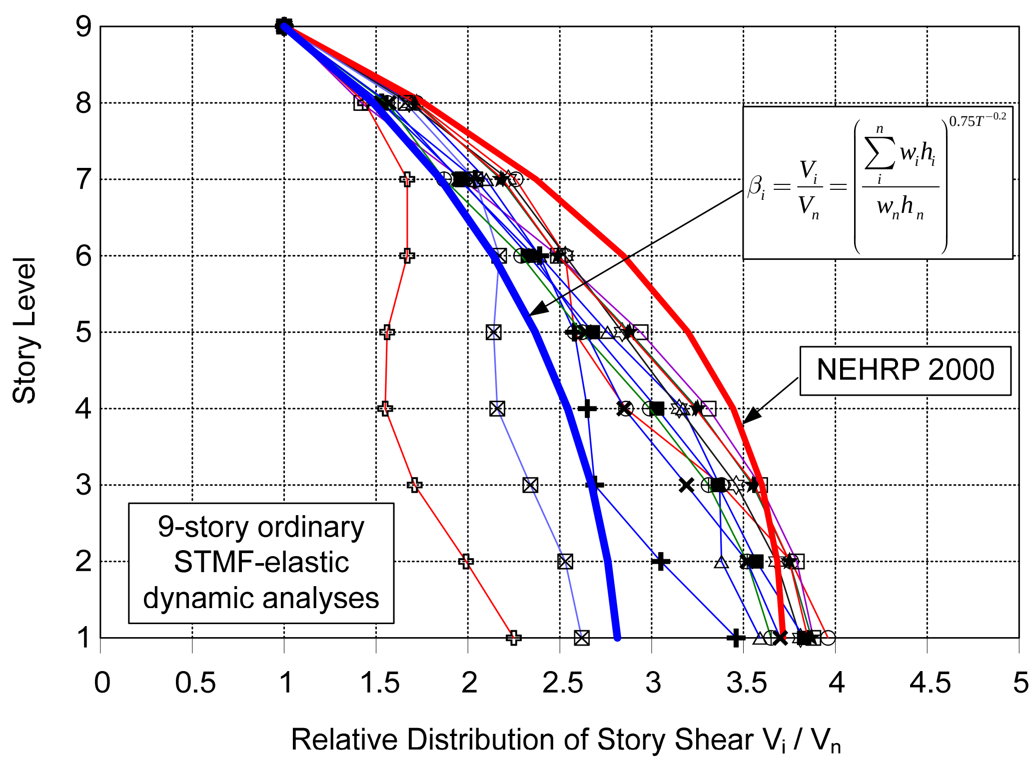

(c)

Figure 5.18 (Continued) Relative Story Shear Distributions obtained from: (b) Nonlinear Dynamic Analyses of the 9-story ordinary STMF; (c) Elastic Dynamic Analyses of the 9-story ordinary STMF

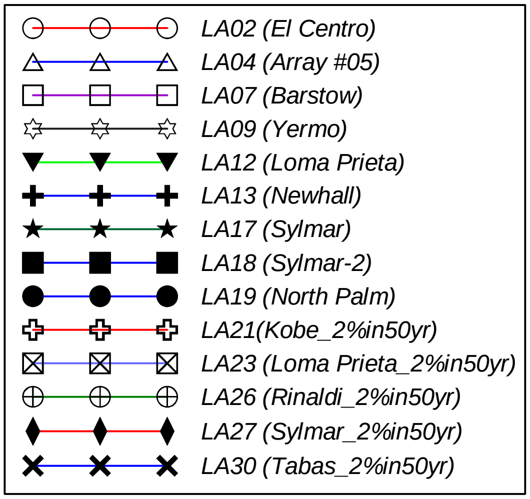

(d)

Figure 5.18 (Continued) Relative Story Shear Distributions: (d) Legend

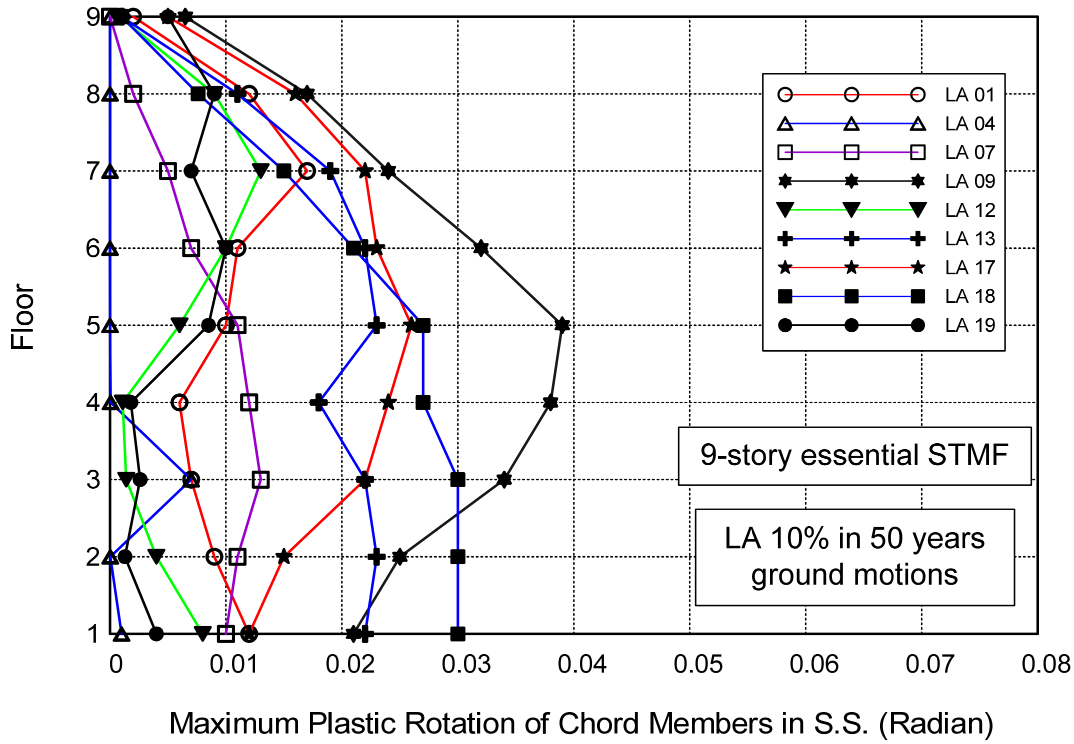

(a)

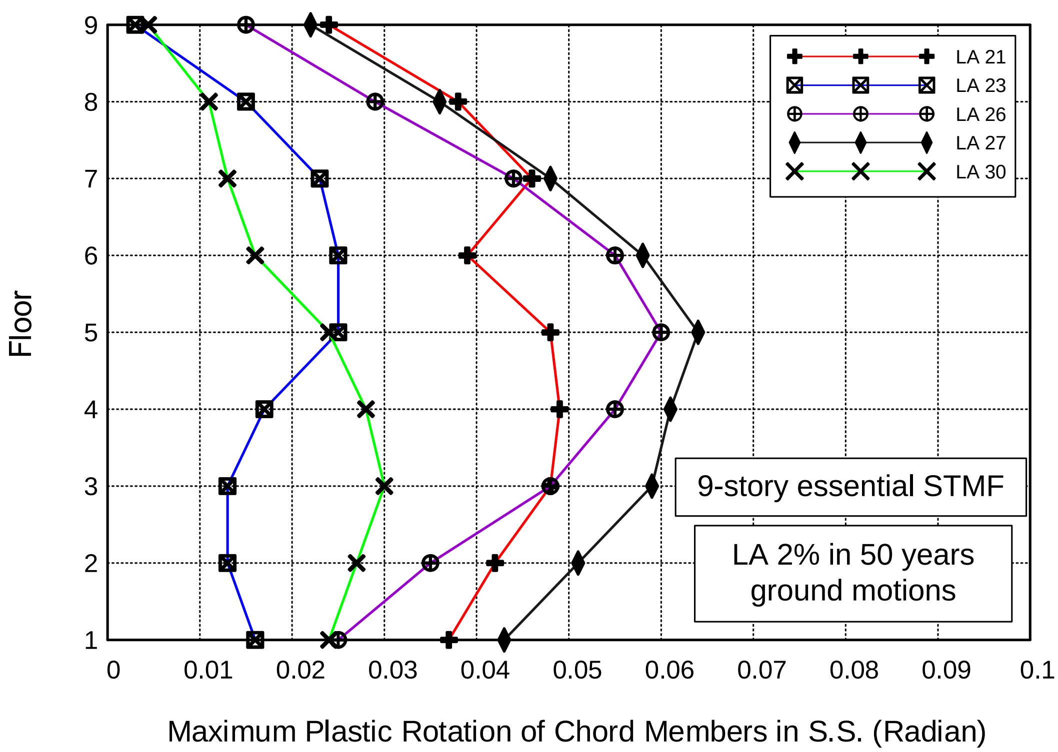

(b)

Figure 5.19 Maximum plastic hinge rotations in chord members for 9-story essential STMF subjected to 10%/50 and 2%/50 ground motions

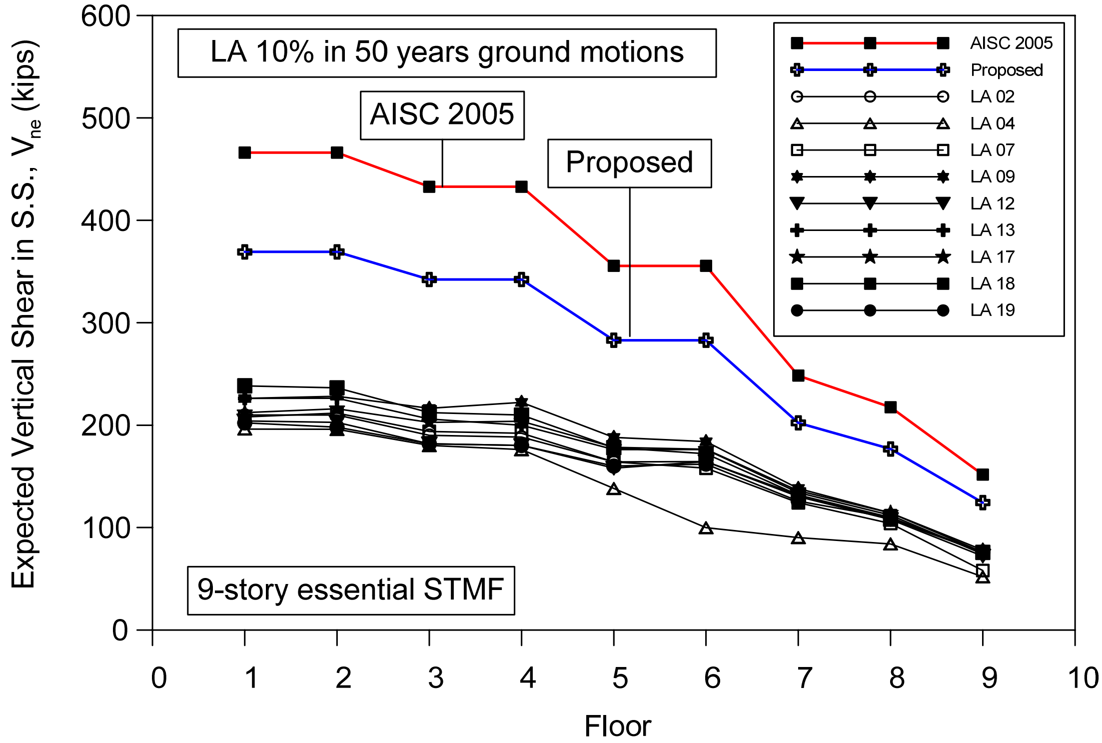

(a)

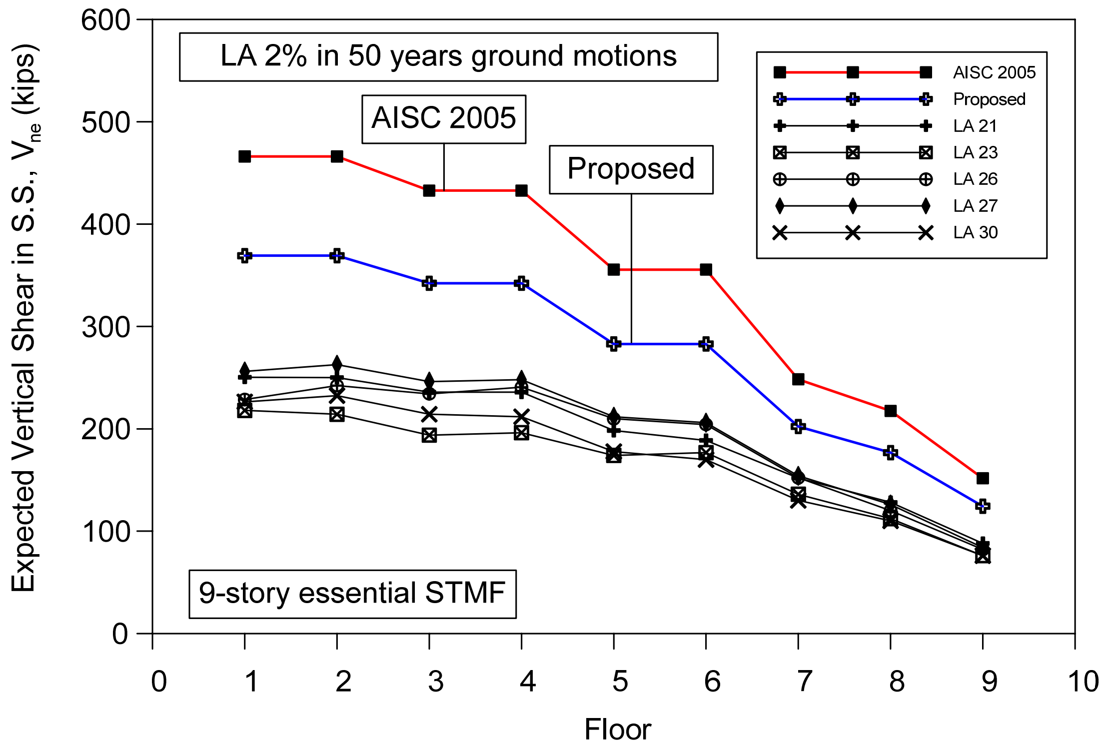

(b)

Figure 5.20 Maximum developed shears in special segments in the 9-story essential STMF subjected to 10%/50 and 2%/50 ground motions

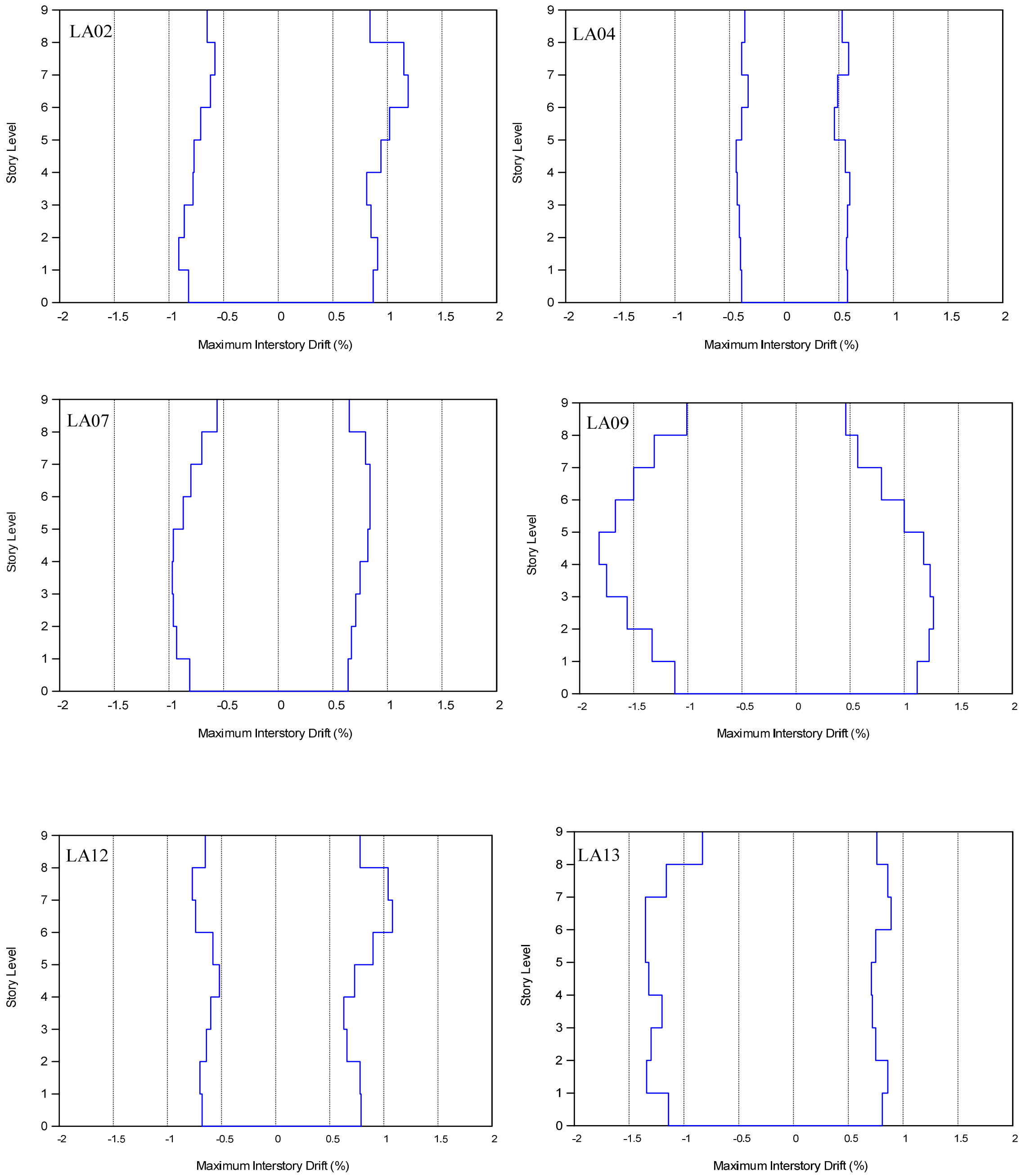

Figure 5.21 (a) Maximum interstory drift distributions of the 9-Story essential STMF subjected to 10% in 50 year SAC earthquake records (LA Region)

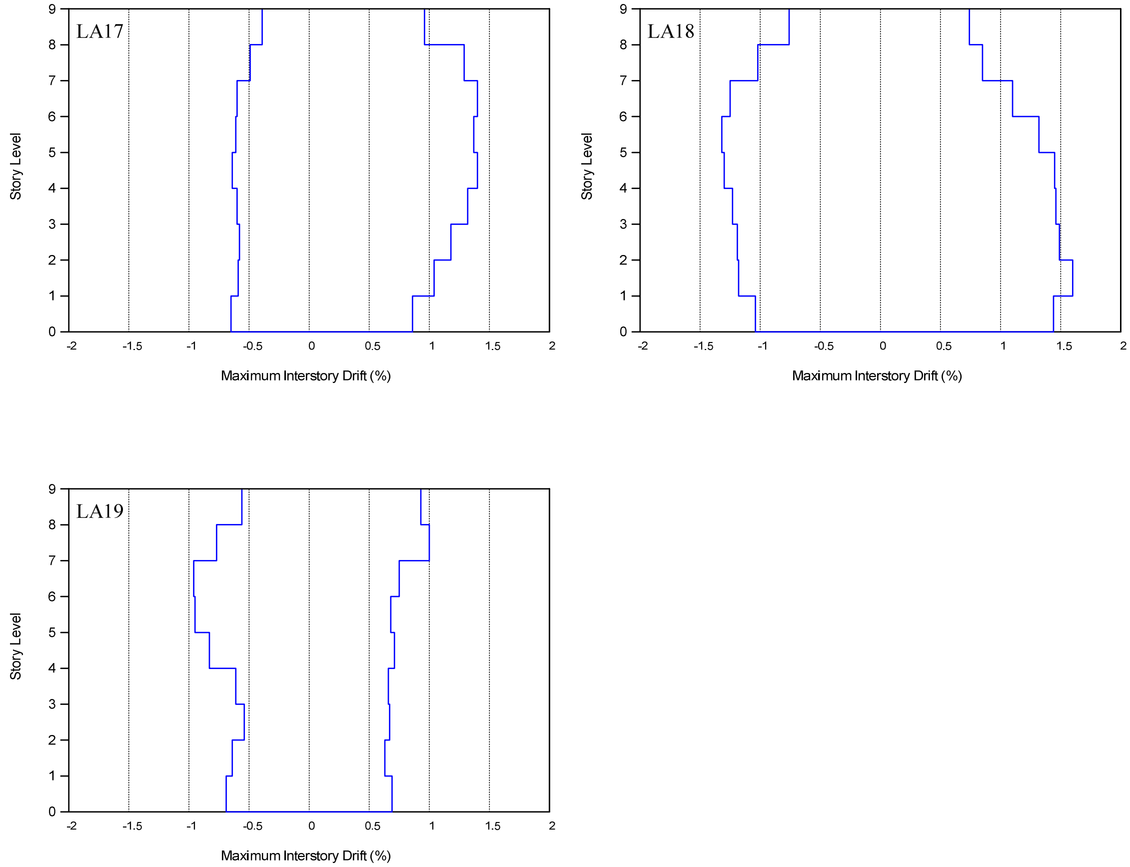

Figure 5.21 (a) (Continued) Maximum interstory drift distributions of the 9-Story essential STMF subjected to 10% in 50 year SAC earthquake records (LA Region)

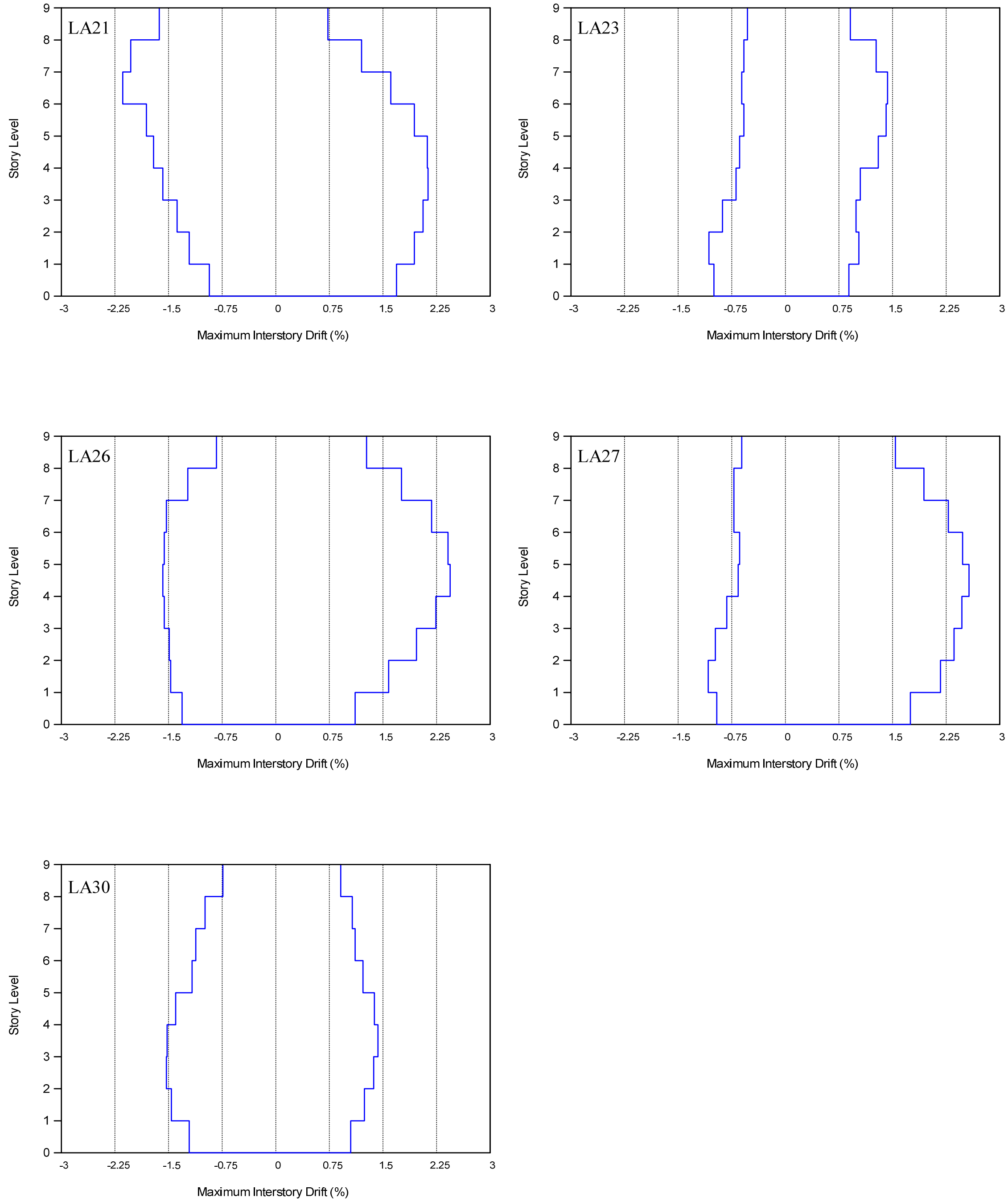

Figure 5.21 (b) Maximum interstory drift distributions of the 9-Story essential STMF subjected to 2% in 50 year SAC earthquake records (LA Region)

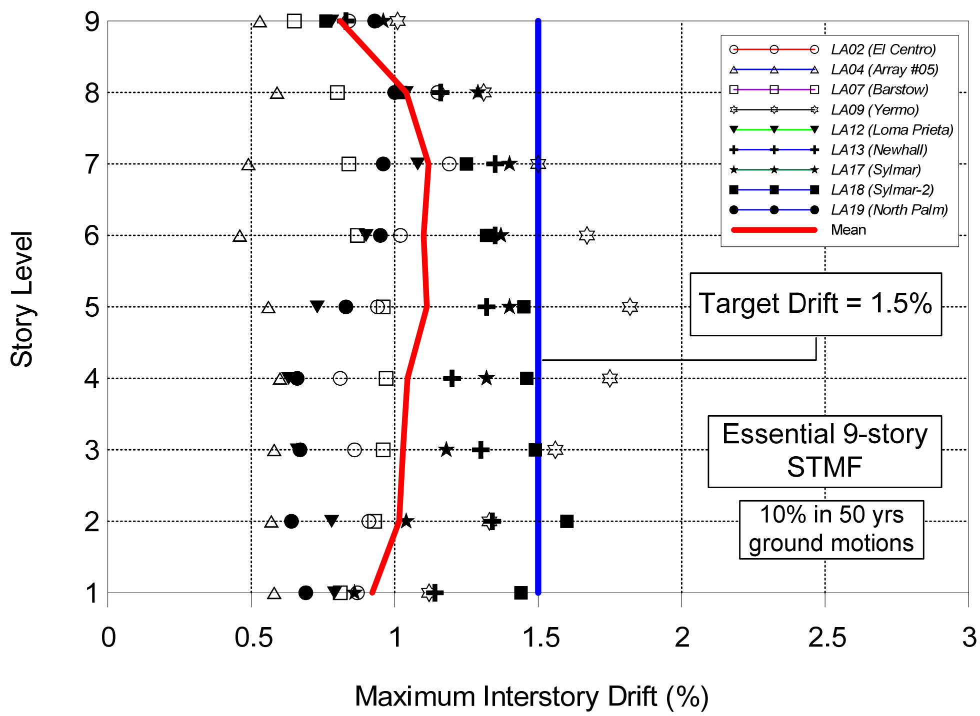

(a)

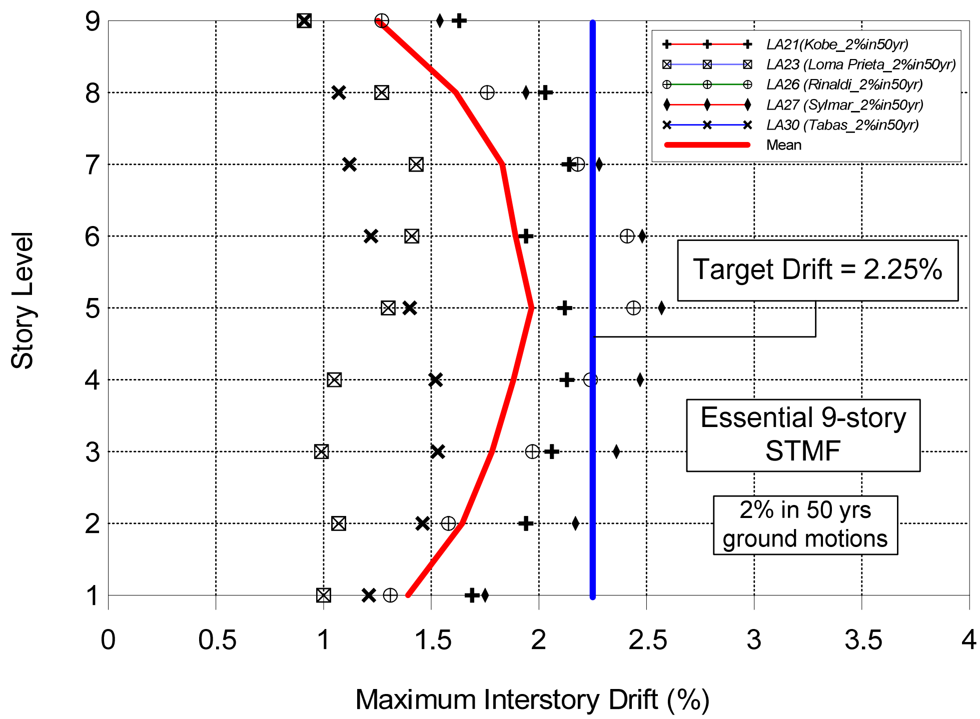

(b)

Figure 5.22 Mean value of maximum interstory drifts and corresponding target drifts for the 9-Story essential STMF

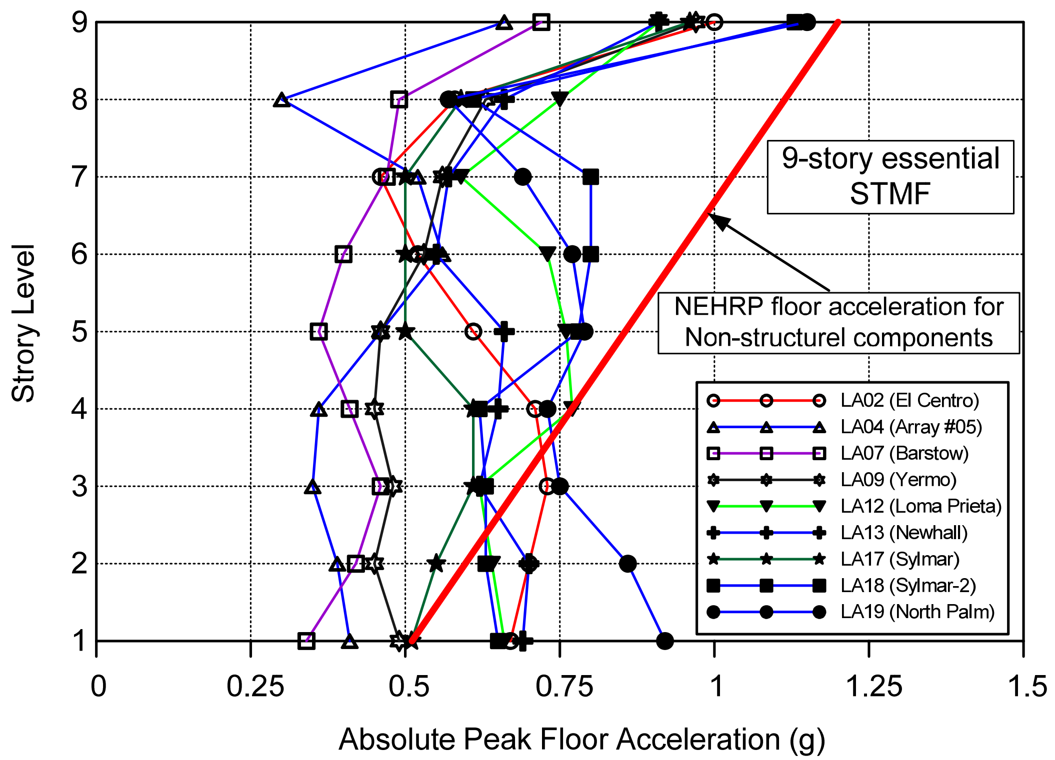

Figure 5.23 Peak Floor Accelerations (10% in 50 year) and the NEHRP-specified Design Acceleration for Acceleration-Sensitive nonstructural components

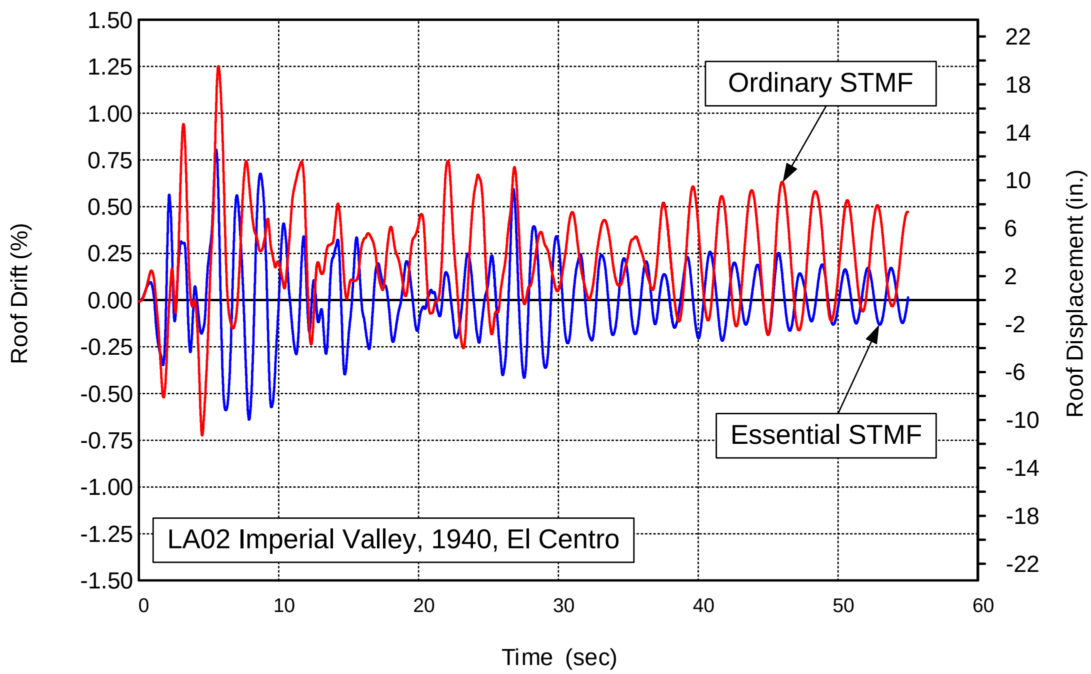

(a)

Figure 5.24 Comparison of the residual roof drifts (displacements) between 9-story ordinary and essential STMFs

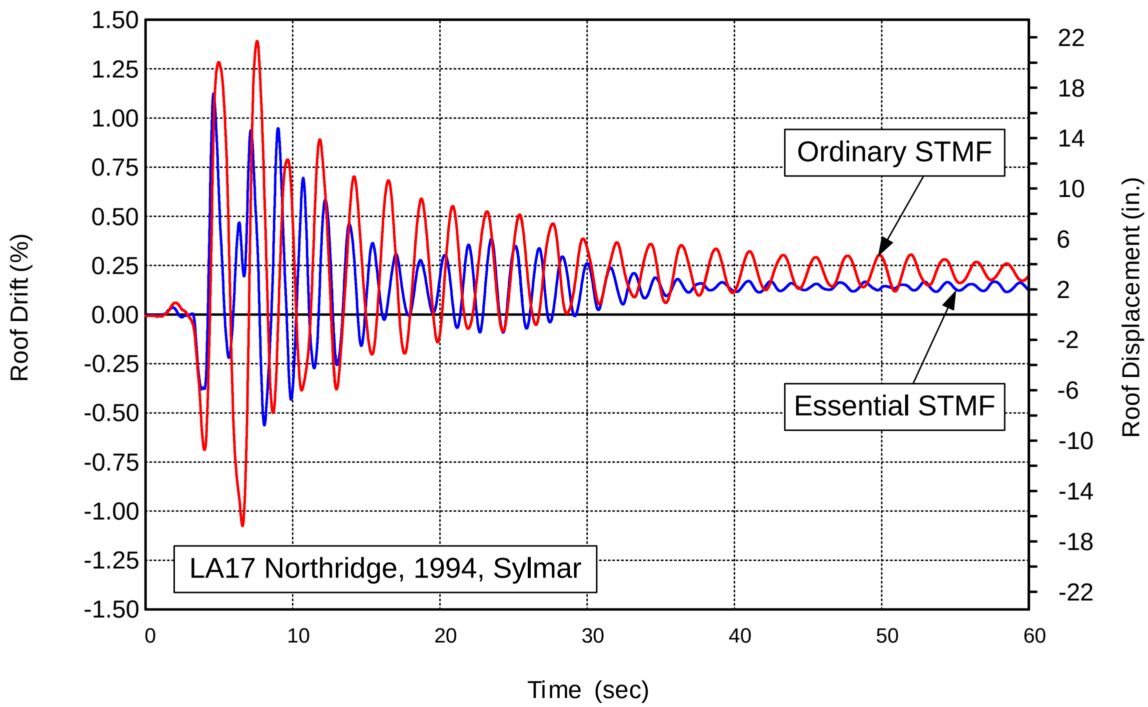

(b)

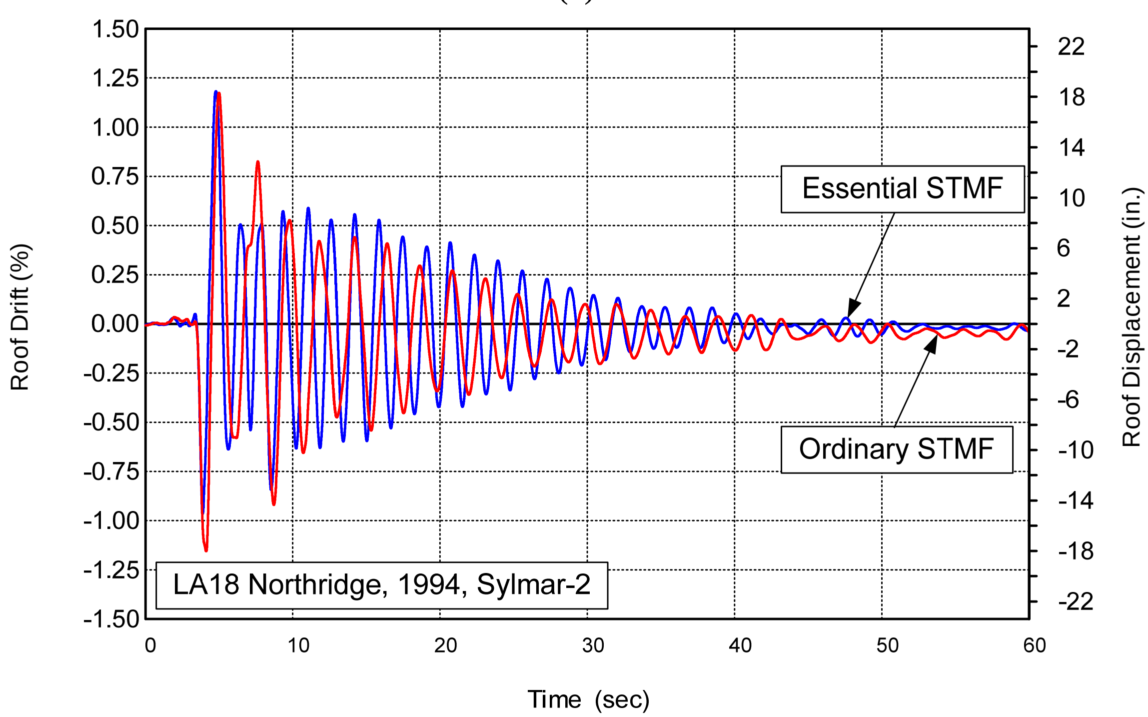

(c)

Figure 5.24 (Continued) Comparison of the residual roof drifts (displacements) between 9-story ordinary and essential STMFs

CHAPTER 6

Summary and Conclusions

6.1 Summary

Two investigations were carried out in this study: (1) an experimental program focusing on the cyclic flexural behavior of built-up double channel members; (2) an analytical program to develop the Performance-Based Plastic Design (PBPD) method for STMFs.

The experimental program was conducted to investigate the ductility and plastic rotation capacity of chord members consisting of double channel sections. The need and motivation came from the fact that previous testing work on STMF at the University of Michigan used double angle sections for the chords and no prior test results on double channel members were available in the literature. A total of seven specimens were tested under reversed cyclic bending. These specimens represented half length of a chord member of open Vierendeel special segment of an STMF. The testing was undertaken to determine the influence of some detailing parameters, such as compactness, stitch spacing, lateral supports and end connections, on the ductility and hysteretic behavior.

In the current practice, performance-based seismic design for new structures is carried out in a somewhat indirect manner. It usually starts with an initial design according to conventional elastic design procedure using applicable design codes, followed by a nonlinear static (pushover) assessment analysis. Usually, iterative process between design and assessment is followed. Moreover, as mentioned in FEMA 440, this procedure still has difficulty in predicting reasonably accurate structural behavior during a major earthquake when compared with the results from a nonlinear dynamic analysis.

While further improvement is needed in the current practice to move toward a more reliable performance-based design philosophy, this study proposes a direct performance-based design approach for STMFs, which basically requires no assessment such as nonlinear static or dynamic analysis after initial design. Based on energy concept, the proposed approach gives design base shear by using the code-specified elastic design spectral value for a given hazard level, a pre-selected global structural yield mechanism, and a pre-designated target drift. In addition, the design lateral force distribution employed in the proposed method is based on nonlinear dynamic analysis results for a number of SAC ground motions. The chord members in the special segments are designed according to plastic design method, while the members outside the links are designed by using capacity design approach. A complete detailed design procedure was developed and the design steps were summarized in a flowchart. The entire design procedure can be easily computerized.

The analytical study was carried out in two phases. The first phase investigation focused on determining the design parameters for the proposed performance-based design methodology. A 7-story STMF was selected and designed according to the proposed procedure. The structural performance under seismic excitation was evaluated through nonlinear static and dynamic analyses using SAC Los Angeles region ground motions. Design parameters were then refined based on the findings. The main issues for investigation included: design yield drift, shear force in the special segments, plastic hinge rotation demand in chord members, story drift, lateral force distribution, and axial force in the chord members.

The second phase of the analytical program included two 9-story STMFs, representing the class of essential facilities (i.e., hospital buildings) as well as ordinary office/residential occupancy type. The performance-based plastic design (PBPD) procedure, as proposed and used in the first phase study with some modifications indicated by the results in that phase, was used to design these two frames. For ordinary building type the target drifts of 2% and 3% for 10%/50 and 2%/50 design hazard levels, respectively, were chosen. The corresponding numbers for the essential building type were 1.5% and 2.25%. Design spectral values were based on NEHRP Provisions for the San Francisco site. After the final design work was completed, inelastic pushover and dynamic analyses were conducted to study the response and ductility demands of the frames. Nine 10% in 50 years and five 2% in 50 years SAC Los Angeles region ground motions representing the two design hazard levels were used for the nonlinear dynamic analyses. The results of the analyses were studied to validate the design procedure, and to compare the chord member ductility demands with the capacities as determined from the testing work on built-up double channel specimens. The study parameters included: location of yielding, maximum plastic rotation in chord members, maximum relative story shear distribution, maximum interstory drift, and peak floor accelerations.

6.2 Conclusions

The following conclusions and recommendations are drawn from the study:

1) The test results of double channel members showed that the stitch spacing and lateral support requirements in the current LRFD Provisions (AISC, 2001) do not ensure adequate ductility under severe seismic loading. However, compactness provisions for channel sections as given in the AISC Seismic provisions are adequate.

2) A design equation of the unsupported length for individual channels of built-up members (*i.e.*, stitch spacing) when subjected to large reversed cyclic bending is proposed to ensure adequate ductility. It was also found that lateral support at the location of first stitch is very effective to mitigate lateral-torsional deformation in the plastic hinge region. Welding of the channel webs to the end gusset plates with a trapezoid shaped cut-out, and reinforcement of the channel flanges in the connection region are very helpful to mitigate stress-strain concentration and early fractures.

3) A 0.75% yield drift for STMFs appears reasonable for use in the proposed design method.

4) The axial forces in the chord members of the special segments are generally very small and can be neglected for designing the special segments.

5) Based on 14 time-history nonlinear dynamic analyses, the suggested design story shear distribution (lateral force distribution) represents the envelope story shear distributions of the structure very well because it is based on inelastic behavior. On the contrary, the NEHRP force distribution does not represent realistic maximum story shear distribution during strong earthquakes. The CBC (or UBC 97) expression, by providing an additional force at top level, gave more realistic relative story shear distribution than the NEHRP expression.

6) A revised equation for maximum expected vertical shear strength, V_{ne}, was derived by using a more realistic assumption and validated by experimental results. Based on extensive nonlinear dynamic analyses, it was found that the current code equation for V_{ne} in the special segments significantly overestimates the expected shear strength, which leads to over design of elements outside the special segments. The values given by the proposed equation were closer to the actual developed shears while maintaining some safety margin. A design equation of V_{ne} for STMF using multiple Vierendeel panels in the special segments was also proposed.

7) The inelastic activity was generally limited to the special segments only, while the other elements remained essentially elastic; that is, STMFs designed by the proposed performance-based plastic design (PBPD) method resulted in the formation of mechanism as intended.

8) The maximum plastic hinge rotation of chord members in the study frames were within the rotation capacity for all 10% in 50 years ground motions used in this study. Moreover, the study frames generally showed quite uniformly distributed plastic rotations along the height, due to the use of the proposed lateral force distribution. This also leads to more evenly distributed dissipated energy among floors.

9) It was observed that all interstory drifts of the study frames were within 1.5% and 2% pre-selected target drift when the structure was subjected to the 2/3 MCE ground motions (first level hazard) for the ordinary and essential buildings, respectively. Also, most interstory drifts were within 2.25% and 3% pre-selected target drift when the structure was subjected to

the MCE ground motions (second level hazard) for the ordinary and essential buildings, respectively. This suggests that satisfactory seismic performance of the deformation-sensitive non-structural components can also be achieved by the proposed design procedure.

10) The maximum floor accelerations were generally within the code-specified values, suggesting that the seismic performance of the acceleration-sensitive components can also be assumed to be satisfactory.

11) It was clearly shown that the proposed procedure can be easily used to achieve the multilevel design goals as currently envisioned in PBEE design philosophy.

BIBLIOGRAPHY

AISC. (2001), “Load and Resistance Factor Design Specification for Structural Steel Buildings,” 3rd edition, American Institute of Steel Construction, Chicago, Illinois.

AISC. (2005), “Seismic Provisions for Structural Steel Building,” AISC-341-05, American Institute of Steel Construction, Chicago, Illinois.

Akiyama, H. (1985), “Earthquake-Resistant Limit-State Design of Buildings.” University of Tokyo Press, Japan.

ASCE. (2000), “Prestandard and Commentary for the Seismic Rehabilitation of Buildings,” FEMA 356 Report, prepared by the American Society of Civil Engineers, published by Federal Emergency Management Agency, Washington, D. C.

Aslani, H, O, (1998), “Special Truss Moment Frames (STMF) under Combined Gravity and Lateral Loads,” Ph. D. Thesis, Department of Civil and Environmental Engineering, University of Michigan, Ann Arbor, MI.

ATC. (1996), “Seismic Evaluation and Retrofit of Concrete Buildings,” ATC-40 Report, Vol. 1&2, Applied Technology Council, Redwood City, California.

ATC. (2004), “Improvement of Nonlinear Static Seismic Analysis Procedures (Draft),” FEMA 440 Report, Applied Technology Council, Redwood City, California and Federal Emergency Management Agency, Washington, D. C.

Basha, H., and Goel, S. C. (1994), “Seismic Resistant Truss Moment Frames with Ductile Vierendeel Segment,” *Report No. UMCEE 94-29*, Dept. of Civ. & Env. Engrg., Univ. of Michigan, Ann Arbor, Michigan.

Bolt, B. A. (2004), “Engineering Seismology,” Earthquake Engineering—from engineering seismology to performance-based engineering, Bozorgni, Y., and Bertero, V. V. ed., CRC Press, Bruneau, M., Uang, C. -M., and Whittaker, A. (1998), "Ductile Design of Steel Structures", McGraw-Hill.

CBC (2001), California Building Code.

Chao, S. H. and Goel, S. C. (2005), "Performance-Based Seismic Design of EBF Using Target Drift and Yield Mechanism as Performance Criteria," *Report No. UMCEE 05-05*, Department of Civil and Environmental Engineering, University of Michigan, Ann Arbor, MI.

Chen, W. F. and Han, D. J. (1988), "Plasticity for Structural Engineers." Springer, 606 pp.

Choi, J., Stojadinovic, B., and Goel, S. C. (2003). "Design of Free Flange Moment Connection," Engineering Journal, AISC, Vol. 39, No. 1, pp. 25-41.

Driscoll, G. C., et al. (1965), "Plastic Design of Multi-Story Frames: Design Aids," Fritz Engineering Laboratory, Lehigh University, Department of Civil Engineering, *Report No. 273.24*, Summer.

Ekiz, E., El-Tawil, S., Parra-Montesinos, G. J., and Goel, S. C. (2004), "Strengthening of Steel Moment Connections using CFRP Shells," Proceedings of the 13th World Conference on Earthquake Engineering, Vancouver, BC, Canada.

Engelhardt, M. D. and Popov, E. P. (1989), "Behavior of Long Links in Eccentrically Braced Frames," *Report No. UCB/EERC-89/01*, Earthquake Engineering Research Center, University of California at Berkeley.

Englekirk, R. (1994), "Steel Structures, Controlling Behavior Through Design," John Wiley & Sons.

FEMA. (2000), "Recommended Seismic Design Criteria for New Stell Moment-Frame Buildings," FEMA 350.

FEMA. (2000), "State of the Art Report on Past Performance of Steel Moment-Frame Buildings in Earthquakes," FEMA 355E.

Goel, S. C., Stojadinovic, B., and Lee, K. H. (1997). “Truss Analogy for Steel Moment Connections,” Engineering Journal, AISC, Vol. 33, No. 2, pp. 43-53.

Goel, S. C., and Leelataviwat, S. (1998), “Seismic Design by Plastic Method,” Engineering Structures, Elsevier Science, 20 (4-6), 465-471.

Hamburger, R., Rojahn, C., Moehle, J., Bachman, R., Comartin, C., and Whittaker, A. (2004), “The ATC-58 Project: Development of Next-Generation Performance-Based Earthquake Engineering Design Criteria for Buildings,” 13th World Conference on Earthquake Engineering, Paper No. 1819, Vancouver, B. C., Canada.

Hassan, O. and Goel, S. C. (1991), “Seismic Behavior and Design of Concentrically Braced Steel Structures,” *Report No. UMCEE 91-1*, Department of Civil and Environmental Engineering, University of Michigan, Ann Arbor, MI.

Ireland, R. C. (1997), “Special Truss Moment Frames in Low to Moderate Seismic Regions with Wind,” *Ph. D. Thesis*, Department of Civil and Environmental Engineering, University of Michigan, Ann Arbor, MI.

Itani, A. M., and Goel, S. C. (1991), “Earthquake Resistance of Open Web Framing Systems,” *Report No. UMCEE 91-21*, Department of Civil and Environmental Engineering, University of Michigan, Ann Arbor, MI.

Kim, K. Y., Parra-Montesinos, G. J., Goel, S. C., and Nuttal B. (2003). “Behavior of Double Channel Built-Up Members Subjected to Reversed Cyclic Bending,” SSRC, 2003 Annual Technical Session Proceedings.

Krawinkler, H. and Miranda, E. (2004), “Performance-Based Earthquake Engineering,” Earthquake Engineering—from Engineering Seismology to Performance-Based Engineering, Edited by Bozorgnia, Y. and Bertero, V. V., CRC Press.

Lee, H. S. (1996), “Revised Rule for Concept of Strong-Column Weak-Girder Design,” Journal of Structural Engineering, ASCE, 122 (4), 359-364.

Lee, S. S. and Goel, S. C. (2001), “Performance-Based Design of Steel Moment Frames

Using Target Drift and Yield Mechanism," *Report No. UMCEE 01-17*, Department of Civil and Environmental Engineering, University of Michigan, Ann Arbor, MI.

Lee, S. S., Goel, S. C., and Chao, S. H. (2004), "Performance-Based Design of Steel Moment Frames Using Target Drift and Yield Mechanism," Proceedings, 13th World Conference on Earthquake Engineering, Paper No. 266, Vancouver, B. C., Canada.

Leelataviwat, S., Goel, S. C., and Stojadinović, B. (1998a), "Drift and Yield Mechanism Based Seismic Design and Upgrading of Steel Moment Frames," *Report No. UMCEE 98-29*, Department of Civil and Environmental Engineering, University of Michigan, Ann Arbor, MI.

Leelataviwat, S., Goel, S. C., and Stojadinović, B. (1998b), "Seismic design by plastic method," Engineering Structures, v 20 n 4-6 Apr-Jun, 465-471

Leelataviwat, S., Goel, S. C., and Stojadinović, B. (1999), "Toward Performance-Based Seismic Design of Structures," Earthquake Spectra, Vol. 15, No. 3, 435-461.

Mayes, R. L., Goings, C., Naguib, W. Harris, S., Lovejoy, J., Fanucci, J. P., Bystricky, P., and Hayes, J. R. (2004), "Comparative Performance of Buckling-Restrained Braces and Moment Frames," Proceedings, 13th World Conference on Earthquake Engineering, Paper No. 2887, Vancouver, B. C., Canada.

Miranda, E. and Bertero, V. V. (1994), "Evaluation of Strength Reduction Factors for Earthquake-Resistant Design," Earthquake Spectra, Vol. 10, No. 2, 357-379.

Naeim, F. (1995), "On Seismic Design Implication of the 1994 Northridge Earthquake Records," Earthquake Spectra, EERI, 11 (1), 91-109.

NEHRP (2001), "Recommended Provisions for the Development of Seismic Regulations for New Buildings (FEMA 368)," Federal Emergency Management Agency, Washington, D. C.

NEHRP (2001), "Commentary on Recommended Provisions for the Development of Seismic Regulations for New Buildings (FEMA 369)," Federal Emergency Management Agency, Washington, D. C.

Parra-Montesinos, G. J., Goel, S. C., and Kim, K. Y. (2006). "Behavior of Steel Double Channel Built-Up Members Under Large Reversed Cyclic Bending," Journal of Structural Engineering, ASCE, September, 2006.

Paulay, T. and Priestley, M. J. N. (1992), "Seismic design of reinforced concrete and masonry buildings," Wiley, New York.

Rai, D. C., Basha, H., and Goel, S. C. (1998), "Special truss moment frames (STMF): design guide," *Report No. UMCEE 98-44*, Department of Civil and Environmental Engineering, University of Michigan, Ann Arbor, MI.

Rai, D. C. (2000), "Future Trends in Earthquake-Resistant Design of Structures," special section: seismology, Current Science, Vol. 79, No. 9, 10 Nov. 1291-1300.

RAM International. (2003), "Perform-2D User's Guide."

RISA Technologies. (2001), "RISA-3D Version 4.5 User's Guide."

Roeder, C. W., Foutch, D. A., and Goel, S. C. (1987), "Seismic Testing of Full-Scale Steel Building—Part II," Journal of Structural Engineering, ASCE, 113 (11), 2130-2145.

Schneider, S. P., Roeder, C. W., and Carpenter, J. E. (1993), "Seismic Behavior of Moment-Resisting Steel Frames: Experimental Study," Journal of Structural Engineering, ASCE, 119 (6), 1885-1902.

SEAOC (1999), "Recommended Lateral Force Requirements and Commentary," Seismology Committee of Structural Engineers Association of California, Sacramento, California, Seventh Edition.

SEAOC (2000), "Seismic Design Manual—Building Design Examples: Steel, Concrete, and Cladding," Volume III, Seismology Committee of Structural Engineers Association of California, Sacramento, California.

SeismoSoft (2004), "SeismoSignal - A computer program for signal processing of strong motion data," [online]. Available from URL: http://www.seismosoft.com.

Somerville, P. G., Smith, M., Punyamurthula, S., and Sun, J. (1997), "Development of Ground Motion Time Histories for Phase 2 of the FEMA/SAC Steel Project, Report No. SAC/BD-97/04, SAC Joint Venture, Sacramento, CA.

Uang, C.-M. and Bertero, V. V. (1988), "Use of Energy as a Design Criterion in Earthquake-Reistant Design." *Report No. UCB/EERC-88/18*, Earthquake Engrg. Res. Ctr., University of California, Berkeley, CA, USA.

Uang, C. -M., Bruneau, M., Whittaker, A. S., and Tsai, K. C. (2001), "Seismic Design of Steel Structures," The Seismic Design Handbook, 2nd edition, Kluwer Academic Publishers, 409-462.

Valley, M. and Hooper, J. (2002), "Issues in The Design of Special Truss Moment Frames in High-Seismic Regions," Proceedings, 7th U.S. National Conference on Earthquake Engineering Boston, Massachusetts, July 21-25, 2002, pp. 1177-1185.

Viest, I. M., Colaco, J. P., Furlong, R. W., Griffis, L. G., Leon, R. T., and Wyllie, L. A. (1997), "Composite Consstruction Design for Buildings," ASCE & McGraw-Hill Publication.

Villaverde, R. (2004), "Seismic Analysis and Design of Nonstructural Elements," Earthquake Engineering—from Engineering Seismology to Performance-Based Engineering, Edited by Bozorgnia, Y. and Bertero, V. V., CRC Press.